

PhD Thesis

Power Frequency Electric and Magnetic Fields: Worst-Case
Calculation and Optimisation Through Optimal Conductor
Arrangement



Institute of Electrical Power Systems
Graz University of Technology

1st Reviewer:

Univ.-Prof. DI Dr.techn. Lothar Fickert

2nd Reviewer:

Ao.Univ.Prof.i.R. DI Dr.techn. Wolfgang Hadrian

Supervisor:

Dr.techn. Ernst Schmutzner

Author:

DI Katrin Friedl

Head of Institute: Univ.-Prof. DI Dr.techn. Lothar Fickert

A - 8010 Graz, Inffeldgasse 18-I

tel.: +43 316 873 - 7551

fax: +43 316 873 - 7553

www.ifea.tugraz.at

www.tugraz.at

Graz / April 2012



Acknowledgements

Completing a PhD-Thesis is a long way, and I would not have been able to complete this journey without the aid and support of countless people over the past five years. I must first express my gratitude towards Prof. Lothar Fickert. He was not only supervising my thesis with great effort of patience and knowledge, but was further my leader and mentor through my time at Graz University of Technology.

Further I would like to thank Prof. Hadrian, who accepted to review my thesis.

In the various projects I have been aided by Dr. Schmautzer, who made it possible for me to work in the field of low frequency electromagnetic fields. Thank you for the main idea to this work, the practical input, the continuous guidance and the generous access to your enormous practical experience. Only due to your incredible gift to acquire projects it was possible for me to be a part of the team.

Prof. Renner has offered much advice and insight to many theoretical aspects about electrical power systems and had always an open ear to scientific questions. Thanks a lot for many ideas, your contribution to my technical education and the support to finish my work.

I also thank some of my fellow colleagues, at the begin Beti Trajanoska. Thank you so much for being such a good friend and my lovely room mate. Thank you, René Braunstein for being a perfect discussion partner. Thanks to Georg Rechberger and Alexander Gaun, who gave me a perfect start at the institute and formed some kind of labour union. I would also like to thank Maria Aigner and Gerald Propst, who had to take over the majority of my project work. Also many thanks to Herbert Gößler, who was never tired to take care for my computer. Many thanks to all others, not named colleagues and students, it was a great time with you all, thanks for the fruitful discussions and support.

Finally, I thank my family and especially my beloved husband Christof for the moral support and the confidence in me that I will bring this thesis to an end.

Abstract

Electromagnetic fields in vicinity of electrical power systems and their impact on health of people is a widely discussed topic. This thesis provides a contribution to this topic in form of evaluation of the actual electric and magnetic fields under worst case conditions of overhead lines, underground cables as well as electric railways. The main parameter of these three types of electrical power systems for the field evaluations are discussed in detail and methods concerning a fast and effective worst case estimation are introduced. Further, the conductor arrangement of these power systems are modified using optimisation algorithms. The goal therefore was to manipulate the configuration in such a way, that they lead under certain conditions to the lowest possible electrical and / or magnetic fields. For this task, general models are developed and the effects of various constraints and objective functions on the resulting objective function are investigated.

Keywords: electromagnetic fields, consideration of harmonics, overhead lines, underground cables, exposure evaluation, phase shifts and unbalances, interference of cardiac pacemakers, conductor arrangement optimisation

Kurzfassung

Elektromagnetische Felder in der Nähe von elektrischen Anlagen und deren Auswirkungen auf die Gesundheit von Menschen ist ein viel diskutiertes Thema. Die vorliegende Arbeit stellt einen Beitrag zu diesem Thema in Form der Auswertung der tatsächlichen elektrischen und magnetischen Feldern unter ungünstigsten Bedingungen von Freileitungen, Erdkabeln sowie elektrischen Bahnen dar. Die wichtigsten Parameter zur Berechnung und Bewertung dieser drei Arten von elektrischen Anlagen werden im Detail untersucht und Methoden in Bezug auf eine schnelle und wirksame Worst-Case-Schätzung vorgestellt. Weiter wird mit Hilfe eines Optimierungsalgorithmus Leiteranordnung dahingehend verändert, sodass sie unter bestimmten Bedingungen zu den möglichst geringen elektrischen und/oder magnetischen Feldern führen. Für diese Aufgabe werden allgemeine Modelle entwickelt und die Auswirkungen verschiedener Nebenbedingungen und Zielfunktionen auf die resultierende Leiteranordnung untersucht.

Schlüsselwörter: elektromagnetische Felder, Berücksichtigung von Oberschwingungen, Freileitungen, Erdkabel, Bewertung von Exposition, Phasenverschiebungen und Unsymmetrien, Beeinflussung von Herzschrittmachern, Optimierung von Leiteranordnungen

Statutory Declaration

I declare that I have authored this thesis independently, that I have not used other than the declared sources / resources and that I have explicitly marked all material which has been quoted either literally or by content from the used sources.

date

signature

Contents

List of Symbols and Abbreviations	v
1 Introduction	1
1.1 Motivation	1
1.2 Objective	2
1.3 Scope of Research	2
1.4 Research Methods	2
1.5 Scientific Contribution	3
1.6 State of the Art	3
1.7 Research Questions	6
2 Methodology, Calculation and Standards	9
2.1 Analytical Calculation of Electric and Magnetic Field	9
2.1.1 Magnetic Field of a Line Conductor with Biot-Savart's Law	9
2.1.2 Approximate Formulas for Magnetic Flux Density	11
2.1.3 Calculation of the Electric Field with Charge Simulation Method	12
2.1.4 Time Dependent Field Values	14
2.2 Standards, Regulations and Other Limitations	19
2.2.1 Basic Restrictions According to ICNIRP	20
2.2.2 Reference Levels for Magnetic Flux Density and Electric Field Strength According to ICNIRP and IEEE	20
2.2.3 Exposure Ratio ER According to ICNIRP	23
2.2.4 Interference of Cardiac Pacemakers Due to EMF	25
2.3 Consideration of Harmonics and Harmonic Factor	31
2.3.1 Harmonic Factor	31
2.3.2 Phase Consideration	33
2.3.3 Exposure Ratios for Elliptic Fields	38
2.4 Impedances, Earth Return Impedances, Current Distribution	43
2.4.1 Calculation of Currents in Passive Conductors	43
2.4.2 Self and Mutual Impedances with Earth Return According to Carson	44

2.4.3	Self and Mutual Impedances with Earth Return According to Dubanton	46
2.4.4	Parameter-Study of Impedance Formulas	46
3	Parameters and EMF of Three-Phase Systems	51
3.1	Conductor Arrangements of OHL and UGL	51
3.1.1	OHL Conductor Arrangements	51
3.1.2	UGL Conductor Arrangements	54
3.2	Phase Allocation	55
3.2.1	Phase Allocation for a Single Circuit Line	55
3.2.2	Double Circuit Lines	57
3.2.3	Multiple Circuit Lines	61
3.3	Influence of the Earth Wire or Other Passive Conductors on the Electric and Magnetic Field	64
3.4	Influence of the Sag for OHL	67
3.5	Consideration of the Phase Shift and Unbalances Between Different Circuits of a Line	71
3.5.1	Double Circuit Lines	72
3.5.2	Multiple Circuit Lines	79
3.6	Non Symmetrical Conditions Within One Three-Phase Circuit	80
3.6.1	Single Circuit Lines in Compensated and Isolated Networks	81
3.6.2	Double Circuit Lines in Compensated Networks	85
3.6.3	Low Voltage Networks	88
3.7	Harmonic Factor Evaluation for Three-Phase Systems	91
3.8	Difference Between Peak and RMS-Values	99
3.9	Cardiac Pacemaker Interference Due To Three-Phase Systems	102
4	Parameters and EMF of Electric Railways Systems	107
4.1	General	107
4.2	Current Distribution	108
4.2.1	Inner Impedance of Rails	108
4.2.2	Current Distribution Between Rails, Earth and Return Conductors	112
4.2.3	Impact of the Current Distribution on the Magnetic Flux Density in the Vicinity of Railway Systems	116
4.3	Zigzag of the Contact Wire	119
4.4	Cardiac Pacemaker Interference Due to Electrical Railways	122

4.5	Difference Between Peak and RMS-Values	122
5	Optimisation	125
5.1	General	125
5.1.1	Objective Function	125
5.1.2	Variables	129
5.1.3	Congestions	129
5.2	Application of Conductor Arrangement Optimisation in Matlab	131
5.3	Models and Constraints for Three-Phase Systems	132
5.3.1	Model and Constraints for Single Circuit Lines	132
5.3.2	Model and Constraints for Double Circuit Overhead Lines	135
5.4	Conductor Arrangement Optimisation of Single Circuit Lines	137
5.4.1	Optimisation Results for Single Circuit OHLs Without Earth Wires	137
5.4.2	Optimisation Results for Single Circuit OHLs With One Earth Wires	140
5.4.3	Optimisation Results for Single Circuit OHLs With Two Earth Wires	140
5.4.4	Optimisation of the Height of a Single Circuit OHL	143
5.4.5	Optimisation Results for Single Circuit UGLs	144
5.5	Conductor Arrangement Optimisation of Double Circuit Overhead Lines	146
5.5.1	Reference Configuration	146
5.5.2	Variation of the Optimisation Model	148
5.5.3	Variation of the Geometric Congestion Parameters	149
5.5.4	Variation of the Objective Function	151
5.5.5	Variation of the Target Area	152
5.6	Optimisation of Electrical Railway Systems	154
5.6.1	Model and Constraints for Electrical Railway Systems	154
5.6.2	Conductor Arrangement Optimisation for Electrical Railway Sys- tems	156
6	Conclusion	161
	Bibliography	165

List of Symbols and Abbreviations

A	cross section
A_1	field value at fundamental frequency
A_ν	field value for ν^{th} harmonic
\underline{A}_ν	complex field value $\underline{A}_\nu = A_\nu e^{j\phi_\nu}$
A_i	value of the field at frequency i
B	absolut value of magnetic flux density
$B^{(0,1,2)}$	magnetic flux density resulting from zero, positive or negative sequence current
$B_1^{(0,1,2)}$	magnetic flux density at fundamental frequency for zero, positive or negative sequence system
B_x, B_y, B_z	components of the magnetic flux density in the orthogonal x -, y - and z -direction
$B_{L,i}$	magnetic flux density reference level at frequency i
$B_{L,\nu}$	magnetic flux density reference level for ν^{th} harmonic
B_ν	magnetic flux density for ν^{th} harmonic
$B_\nu^{(0,1,2)}$	magnetic flux density (RMS-value) for the ν^{th} harmonic for zero, positive or negative sequence system
B_i	magnetic flux density at frequency i
B_{peak}	peak-value of the vector $\vec{B}(t)$
B_{rms}	RMS-value of the vector $\vec{B}(t)$
\vec{B}	vector of the magnetic flux density
$\vec{B}(j\omega)$	vector of the magnetic flux density in the frequency domain
$\underline{B}_x(j\omega)$	components in x -direction of the magnetic flux density in the frequency domain
$\underline{B}_y(j\omega)$	components in y -direction of the magnetic flux density in the frequency domain
$\underline{B}_z(j\omega)$	components in z -direction of the magnetic flux density in the frequency domain
C	capacitance
\mathbf{C}	capacitance matrix

CNS	abbr. for central nervous stimulation
CPM	abbr. for cardiac pacemaker
CW	abbr. for contact wire of the electrical railway system
C_R, C_X	correction terms
EL_1	exposure limit (reference limit) at fundamental frequency
EL_ν	exposure limit (reference limit) for ν^{th} harmonic
EL_i	exposure limit (reference limit) at frequency i
EMF	abbr. for electromagnetic fields
ER	exposure ratio
ER_1	exposure ratio for the fundamental frequency
ER_B	exposure ratio for magnetic field
ER_E	exposure ratio for electric field
$ER_{B,1}^{(0,1,2)}$	exposure ratio of the zero, positive or negative sequence system at fundamental frequency
$ER_{B,1}^{(0,1,2)}$	exposure ratio of the zero, positive or negative sequence system at fundamental frequency
ER_{cpm}	exposure ratio for CPMs
$ER_{cpm}(f)$	exposure ratio at frequency f for CPMs
EW	abbr. for earth wire
E_x, E_y, E_z	components of the electric field strength in the orthogonal x -, y - and z -direction
$E_{L,i}$	reference level of electric field strength at frequency i
$E_{L,\nu}$	electric field strength reference level for ν^{th} harmonic
E_ν	electric field strength for ν^{th} harmonic
E_i	electric field strength at frequency i
\vec{E}	vector of the electrical field strength
FE	abbr. for feeder of the electrical railway system
GIL	abbr. for Gas Insulated Line
$\underline{G}(j\omega)$	complex filter function
$H_{L,i}$	reference level of magnetic field strength at frequency i
H_i	magnetic field strength at frequency i
$\underline{\mathbf{I}}$	column vector of the currents \underline{I}_i
$I(Q)\vec{e}_I$	incrementally current line segment at point Q with a current in direction \vec{e}_I
$\underline{I}^{(0)}, \underline{I}^{(1)}, \underline{I}^{(2)}$	zero, positive and negative sequence system of current I
$\underline{I}_\nu^{(0,1,2)}$	symmetrical component of ν^{th} harmonic
\hat{I}_1	amplitude of current at fundamental frequency

\hat{I}_1	complex amplitude of the current at fundamental frequency $\hat{I}_1 = \hat{I}_1 e^{j\varphi_1}$
ICNIRP	abbr. for International Commission on Non-Ionizing Radiation Protection
IEEE	abbr. for Institute of Electrical and Electronics Engineers
$\underline{I}_{L1}, \underline{I}_{L2}, \underline{I}_{L3}$	current of the phase L1, L2 or L3
$\underline{I}_{L1,\nu}$	ν^{th} harmonic of phase current L1
$\underline{I}_{cir1}^{(1)}$	current of the positive sequence system of circuit 1
$\underline{I}_{cir2}^{(1)}$	current of the positive sequence system of circuit 2
$\underline{I}_{max}^{(1)}$	maximum current of the positive sequence system of one circuit
$I_1^{(0)}$	RMS-value of the zero sequence current at fundamental frequency
$I_\nu^{(0)}$	RMS-value of the zero sequence current for the ν^{th} harmonic
\underline{I}_i	current of the conductor i
I_ν	RMS-value of the ν^{th} oscillation
\hat{I}_ν	amplitude of the ν^{th} oscillation
\underline{I}_ν	complex RMS-value of the ν^{th} oscillation $\underline{I}_\nu = I_\nu e^{j\varphi_\nu}$
$\hat{\underline{I}}_\nu$	complex amplitude of the ν^{th} oscillation $\hat{\underline{I}}_\nu = \hat{I}_\nu e^{j\varphi_\nu}$
L	length of the span
L'_i	internal inductance of the conductor i per unit length
ME	abbr. for messenger or track cable of the electrical railway system
OHL	abbr. for overhead line
P	perimeter of the rail
\mathbf{P}	potential coefficient matrix
PNS	abbr. for peripheral nervous stimulation
\mathbf{Q}	column vector of charges
R	resistance
R'_i	resistance of the conductor per unit length
RA	abbr. for rails of the electrical railway system
RC	abbr. for return conductor of the electrical railway system
RMS	abbr. for Root Mean Square
T	period of periodic signal
\mathbf{U}	column vector of the voltages \underline{U}_i
$\underline{U}^{(0)}, \underline{U}^{(1)}, \underline{U}^{(2)}$	zero, positive and negative sequence system of the voltage U
UGL	abbr. for underground line
$\underline{U}_{L1}, \underline{U}_{L2}, \underline{U}_{L3}$	voltage of the phase L1, L2 or L3
\underline{U}_i	voltage of the conductor i
$U_{i,max}$	maximum interference voltage due to electric and magnetic fields

$U_{i,thre}$	interference thresholds of a specific CPM
U_i	potential to earth of conductor i
$\underline{\mathbf{Z}}$	impedance matrix
$\underline{Z}'_{i,rail}$	inner impedance of the rail per unit length
$\underline{Z}'_{ii,CE}$	self impedance of conductor i with earth return per unit length according to Carson
$\underline{Z}'_{ii,DE}$	self impedance of conductor i with earth return per unit length according to Dubanton
$\underline{Z}'_{ik,CE}$	mutual impedance between conductor i and k with earth return per unit length according to Carson
$\underline{Z}'_{ik,DE}$	mutual impedance between conductor i and k with earth return per unit length according to Dubanton
\underline{Z}_{ii}	self impedance of the conductor i
\underline{Z}_{ik}	mutual impedance between the conductor i and k
δ	skin depth
δ_E	equivalent current depth
γ	Euler-Mascheroni constant $\gamma = 0.57721566\dots$
κ_E	specific conductivity of the earth
μ	permeability $\mu = \mu_r(I)\mu_0$
μ_0	permeability of empty space $\mu_0 = 4\pi 10^{-7} \text{Vs/Am}$
μ_r	relative permeability
ν	harmonic order
ω_1	fundamental angular frequency $\omega_1 = 2\pi f_1$
$\omega_c = 1/(RC)$	angular cut-off frequency
ϕ_ν	phase angle of the ν^{th} harmonic of the field value
ρ_E	specific resistivity of the earth
ρ_{rail}	electrical resistivity of the rail
$\vartheta_{EW,max}$	shielding angle of the earth wire
ε_0	permittivity of vacuum $\varepsilon_0 = 8.854 \cdot 10^{-12} \text{Vs/Am}$
φ_1	phase angle of the current at fundamental frequency
φ_ν	phase angle of the ν^{th} oscillation
\underline{a}	complex constant for phase shift of 120° , $\underline{a} = e^{j 2\pi/3}$
a_B	distance between sub-conductors
c	constant depending on sag and height of the conductors at the tower
d'_{ik}	distance between conductor i and mirrored conductor k'
$d_{ik,min}$	minimum distance between two conductors

d_{ik}	distance between conductor i and k
\vec{e}_B	unit vector in direction of the magnetic flux density
\vec{e}_r	unit vector in radial direction
$\vec{e}_x, \vec{e}_y, \vec{e}_z$	unit vector in x -, y - and z -direction
\vec{e}_φ	unit vector in peripheral direction
f_1	fundamental frequency
$h(y)$	height of the conductor at position y
h_0	height of the conductor in the middle of the span
h_P	height of field point P
h_i	height of conductor i
h_l	height of the lowest conductor of an OHL
h_u	height of the uppermost conductor of an UGL
$h_{l,max}$	maximum depth of the lowest conductor
$h_{l,min}$	minimum height of the lowest conductor at maximum sag
$h_{u,max}$	maximal height of the uppermost conductor
$h_{u,min}$	minimum depth of the uppermost conductor
$i(t)$	current in the time domain
k_H	harmonic factor
$k_{H,B}$	harmonic factor for magnetic field
$k_{H,B}^{(0,1,2)}$	harmonic factor for zero, positive or negative sequence system
$k_{H,E}$	harmonic factor for electric field
$k_{H,I}$	harmonic factor for magnetic field built from current signals
$k_{H,I}^{(0,1,2)}$	harmonic factor for zero, positive or negative sequence system
$k_{H,U}$	harmonic factor for electric field built from voltage signals
n	number of sub-conductors
\underline{p}	complex earth return depth
\underline{p}'	modified complex earth return depth
p_{ii}	self potential coefficient of conductor i
$p_{ik} = p_{ki}$	mutual potential coefficient between conductor i and k
pp	number of phase position
q_i	charge of conductor i per unit length
r_B	circumradius of the bundle
r_N	normal distance between field point and conductor
r_i	radius of conductor i
r_t	radius of a sub-conductor
$r_{PQ}\vec{e}_{PQ}$	vector between point P and Q
$r_{eq,A}$	cross section equivalent radius $r_{eq,A} = \sqrt{A/\pi}$

$r_{eq,P}$	perimeter equivalent radius $r_{eq,P} = P/2\pi$
r_{eq}	equivalent radius
s	sag
t	time
u_{iB}	specific interference voltage of the magnetic field
u_{iE}	specific interference voltage of the electric field
var.	variation
w_{max}	maximum width of a line
x_P	horizontal position of field point P
x_i	horizontal position of conductor i

1

Chapter 1

Introduction

1.1 Motivation

Electric power systems cause electric and magnetic fields in their vicinity. The lack of space, especially in towns, which comes from economic growth causes necessary infrastructure as railway tracks and electric power supplies getting closer to facilities which are more sometimes sensitive to the influence of electric and/or magnetic fields.

At environment-assessments for electrical power systems the subject of possible field exposure is a very widely and sometimes very unprofessional discussed part and as a consequence a very important part during the authorisation process. For that environment-assessments it is necessary to know the long term impact and the worst case impact due to the operation of the electrical power system. For example, for a high voltage overhead line, it is necessary to know the maximum electric and magnetic fields in the vicinity with respect to all possible operation conditions, including the highest possible voltage, maximum currents and so on. Further the consideration of harmonics have to be analysed.

The ongoing discussion about possible health effects of electric and magnetic field exposure on people as well as the electromagnetic compatibility of sensitive electronic devices forces erectors and operators of electric power systems to reduce the field emissions. The reduction should be fulfilled at reasonable low cost increase.

Very often the focus is only on magnetic field reduction, because people are typically more afraid of the long term effects due to the magnetic field exposure. That might be mainly, because long term effects of exposure to magnetic fields cannot be excluded, although many scientific publications fail to prove a significant evidence of an existent relation between very low values (e.g. $0.4 \mu\text{T}$) of extremely low frequency magnetic field (mainly power frequency magnetic fields) and, for example, childhood leukaemia.

Further, electric fields - in contrast to magnetic fields - can be shielded effectively with a conductive layer. Nonetheless, it has to be made sure that the electric field strength reference levels are not exceeded in all accessible areas for all possible operation conditions. In addition, for cardiac pacemakers, the summarising effect of electric and magnetic field has to be considered.

1.2 Objective

The thesis's main objective is first to evaluate electric and magnetic fields (EMF) of electric power systems. For overhead lines (OHL), underground power lines (UGL) and electric railways several parameters which influence the electric and magnetic field are analysed in detail. For example the effect of varying the positions of the phases, additional passive conductors, phase shifts and unbalances on the fields of three-phase systems are analysed. For electric railways for example the return current distribution was taken into account. The focus of the worst case analysis is on identifying the main parameters for worst case evaluation and finding appropriate ways to reduce the effort of field calculation considering these main parameters.

Further, a goal is to reduce electric and magnetic fields of electric power systems - especially of overhead lines (OHL), underground power lines (UGL) and electric railways. This is done by conductor arrangement optimisation. Therefore optimisation algorithms are applied on the conductor arrangement of real power systems. The result of the optimisation mainly depends on the chosen optimisation goal e.g. minimise magnetic or electric field in a certain target area, near or at a distant place from the field source. Therefore several possible optimisation goals are listed and analysed. Further a variety of congestions e.g. minimum distance between conductors or the height of a tower, and their effects on the optimisation goal is discussed in detail.

1.3 Scope of Research

This thesis focuses on identifying the main parameters for field calculation in vicinity of electrical power systems and finding appropriate methods to reduce calculation effort. Further the mitigation of electromagnetic fields by optimisation of the positions of the conductors is analysed. It will not focus on other reduction methods as there are e.g. mitigation with conductive or permeable shields. The exposure evaluation is done with reference levels given by standards and guidelines.

1.4 Research Methods

Computer models for calculation of electric and magnetic fields are developed and applied to an optimisation algorithm. Mainly the commercial software Matlab[®] was used as programming language for calculation of the fields and optimisation.

1.5 Scientific Contribution

The main contribution to science are

- Combined exposure ratio evaluating of OHLs concerning interference with cardiac pacemakers
- Development of a new method to consider harmonics for OHL using symmetrical components
- Consideration of rotating fields, especially with harmonics
- New illustration methodology of worst-case scenarios with envelop isolines
- Analysing the effect of unbalances and phase shifts for multi circuit three-phase lines on electric and magnetic fields
- Generalisation of the optimisation goals and constraints using optimisation algorithms in context of electrical power systems
- Applying the optimisation algorithm on special tasks as
 - Analysing the dependency of the resulting conductor arrangements for different optimisation goals (different objective functions)
 - Defining and analysing the effect of several congestions for OHLs and UGLs
 - Optimisation of return conductor and feeder of electric railways
 - Analysing the optimisation potentials of OHLs and UGLs
 - Optimisation of the conductor geometry

1.6 State of the Art

Many commercial computation programs as for example WinField EFC-400 on the base of calculation of Biot-Savart and equivalent charge simulation method are available. In order to make variations of parameters, analysis of harmonics, implementation of an optimisation,... it was necessary to create an appropriate calculation program in Matlab®. Kaune et al. developed in [37] simple formulas for analysing magnetic fields at far distances for different line configurations, including double circuit lines with different line phasing, but these formulas are not appropriate to analyse further parameters. The base for the analytical calculation EMF were taken from for example from Cigré [16] and from Bauhofer [10]. The base of the standards and guidelines for this thesis are

[31, 32, 33]. In [61] and in [3] general aspects about the interference of cardiac pacemakers as well as methods for evaluating them are given.

In [10] the phase cancellation due to allocation of the phases on given positions of a double circuit OHL (phasing) is discussed in detail for typical Austrian OHL. Furthermore in [63] the effect of two phasing possibilities (there called symmetrical and optimum conductor arrangement) on a Greek 400 kV transmission OHL are given. These publications have in common, that only the phasing is analysed on given conductor positions, but do not develop optimised conductor positions.

In [52], [53] and [9] the effect of a phase shift between two circuits of a double circuit overhead line were analysed. In the current thesis these considerations are analysed more in detail and also continued for multiple circuit lines.

In [28] measurement results of the magnetic flux density in vicinity of an Austrian electrical railway (15 kV/16.7 Hz) are compared with calculation results. Similarly is done in [43] for an Italian High Speed Railway Line (25 kV/50 Hz) while in [42] the magnetic field is analysed from a system equipped with an autotransformer. In [41] the influence of the current distribution for a selected railway system (single track system) is analysed. Further measured and calculated magnetic fields in form of isolines are presented.

Many analyses about the electrical parameters (e.g. the impedances) of railway systems are done in [47], [48] and [49].

In [40] and [45] the current distribution itself is calculated and analysed, in [40] for 16.7 Hz in [45] for a frequency range up to 500 Hz, while [68] and [67] are about current harmonics in electric railways.

While the mitigation of electric fields is possible with relatively little effort by screening with a (even less) conductive material, mitigation of low frequency magnetic field on the contrary is more complex. Nevertheless, for OHL also the reduction of the electric field strength is an important fact, as far the influence on e.g. cardiac pacemakers is of importance.

Great overviews of magnetic field mitigation methods are given in [30], [15] and there from derived publications as e.g [59]. Based on [15] mitigation methods can be classified in

- distance management
 - enlargement of the distance between target area and field source

- conductor arrangement
 - conductor geometry (in one line versus triangle)
 - phase cancellation: rearrangement of the phases for multi-circuit configurations
 - phase splitting: splitting of one or more phases into two or more conductors
- compensation
 - passive loops
 - active loops
 - compensation at the source
 - compensation at the interest area
- shielding by metallic materials
 - ferromagnetic material - attractive interaction
 - conductive material - repelling interaction
 - combination of ferromagnetic and conductive material

In sense of mitigation of electric and magnetic fields this work specified on the mitigation due to the conductor arrangement, especially a combination of optimisation the conductor geometry and phase cancellation. In [8] the mitigation technology "conductor arrangement" is applied with a particle swarm optimisation (PSO). In contrary to this thesis, no constraints, as e.g. a minimum distance between conductors were used. Therefore, the results of the optimisation are hardly applicable. The objective of the optimisation was to minimise both, electric and magnetic field, which was reached with a fitness function $FF = B \text{ [T]} + 8E-11 E \text{ [V/m]}$.

Cruz et al. made in [19] and [18] an extensive comparative analysis of the mitigation possibilities with passive loops near overhead line using a genetic algorithm (GA) within GAMS (General Algebraic Modeling System).

In [25] a combination of phase position analysis and tower geometry analysis is given, determining areas, where each combination would lead to the lowest magnetic flux density.

Based on [19] Del Pino et al. used in [20] a genetic algorithm (GA) to optimise compensated passive loops in cable trays. Their goal was to maximise the reduction factor, defined as the ratio of non-mitigated field to mitigated magnetic field in the target

area. Further they made a sensitivity analysis of parameters conductor location, resistance, and capacitance to ensure optimal mitigation even with not completely exact parameters.

Celozzi et al. describe in [14] an active shielding with a compensation wire with earth return. Currents and position of the compensation conductor are optimised in regard to minimise the magnetic field in a target area (a building nearby) by using a GA. As optimisation criteria the mean magnetic flux in the target area was chosen.

Canova et al. applied in [12] a multi-objective combinatorial optimisation (MOCO) based on a vector immune system (VIS) for optimising the magnetic field for the cable layout of multiple conductors between a power transformer and the main power board. A congestion for the magnetic field optimisation was the need of an as uniform as possible current distribution sharing between the conductors of one phase.

In [58] from Norway a compact 420 kV tower type (single circuit) for minimal magnetic field is applied, and a comparison of measurement results between the former configuration and the new one is given, which affirmed the improvement.

1.7 Research Questions

The following research questions are answered in chapter 3.

- How big is the effect of the earth wire in the sense of electromagnetic fields for OHLs?
- How can a worst case scenario be built without exactly knowing the allocation of the phases on given conductor positions?
- What is the effect of unbalances in currents and voltages on electromagnetic fields, and how can they be evaluated?
- How big is the error between a 2D field calculation and a 3D calculation in the sense of the sag of an OHL?
- How can a worst case scenario be built for phase shifts and unbalances between different circuits of a three-phase system?
- How can unbalances in harmonics be considered in sense of worst case exposure evaluation?
- How big are the differences between peak evaluation and RMS evaluation for rotary fields on actual OHL, UGL and electric railway configurations?

- How can the combined influence of magnetic and electric fields from OHLs and UGLs on persons with cardiac pacemaker be estimated?

The following research questions are answered in chapter 4.

- Which effects does the current distribution of the return current and the zigzag routing of the contact wire have on the magnetic flux density in the surrounding of electric railways?
- How can a realistic worst case scenario be built even without exact knowledge of the actual current distribution?
- How can the influence of electric railway systems on persons with cardiac pacemaker be evaluated?

The following research questions are answered in chapter 5.

- What does an optimal conductor arrangement in sense of electric and magnetic field look like?
- What optimisation goal for mitigation of electromagnetic fields can be formulated?
- How can optimisation goals and congestions for conductor arrangement optimisation be formulated in a general way?
- How sensitive are the resulting optimal conductor arrangements in sense of
 1. the optimisation goal ('What should be optimised?'),
 2. the target area ('Where should it be optimised?') and
 3. congestions ('What freedom of degree does a conductor configuration have?')?
- What optimisation potential does the conductor arrangement of feeder and return conductor have?

2 Chapter 2

Methodology, Calculation and Standards

2.1 Analytical Calculation of Electric and Magnetic Field

2.1.1 Magnetic Field of a Line Conductor with Biot-Savart's Law

Assuming a completely empty room and stationary or quasi-steady current distributions, the magnetic flux density at each point can be calculated by superposition. An empty space in this context is not a matter of space without any material, but a space in which no magnetisable body, such as iron parts, exist. It is therefore assumed that the linear relationship $\vec{B} = \mu_0 \vec{H}$ between magnetic flux density \vec{B} and magnetic field strength \vec{H} with the permeability of the empty space $\mu_0 = 4\pi 10^{-7}$ Vs/Am in the entire field area is valid.

The magnetic flux density \vec{B} in a point P caused by a current distribution along a curve C (see fig. 2.1) is obtained by eq. (2.1).

$$\vec{B} = \frac{\mu_0}{4\pi} \int_C \frac{I(Q)\vec{e}_I ds}{r_{PQ}^2} \times \vec{e}_{PQ} \quad (2.1)$$

\vec{B}	vector of the magnetic flux density
μ_0	permeability of empty space $\mu_0 = 4\pi 10^{-7}$ Vs/Am
$I(Q)\vec{e}_I$	incrementally current line segment at point Q with a current in direction \vec{e}_I
$r_{PQ}\vec{e}_{PQ}$	vector between point P and Q
C	curve of the conductor

Eq. (2.1) can now be applied on a straight line of length l with starting point A and endpoint E according to fig. 2.2. The flux density \vec{B} in a point P at a normal distance r_N to the conductor is obtained with eq. (2.2).

$$\vec{B} = \frac{\mu_0 I}{4\pi r_N} [\sin(\alpha_E) - \sin(\alpha_A)] \vec{e}_B = B \vec{e}_B \quad (2.2)$$

r_N	normal distance between field point and conductor
-------	---

α_A, α_E	angles according to fig. 2.2
B	absolut value of magnetic flux density
\vec{e}_B	unit vector in direction of the magnetic flux density

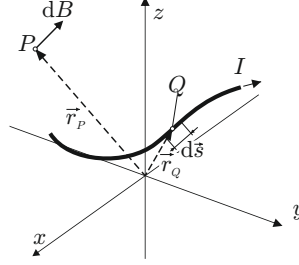


Figure 2.1: Model for calculating the magnetic flux density of any line conductor

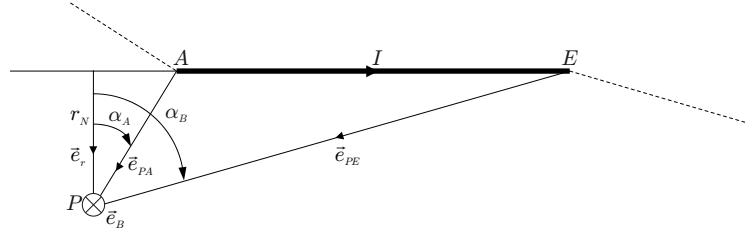


Figure 2.2: A line conductor segment with starting point A , endpoint E and current I in direction \vec{e}_I causes in point P a magnetic flux density B in the direction \vec{e}_B

It has proven advantageous to express the term $\sin(\alpha_A)$, $\sin(\alpha_E)$, the direction \vec{e}_B and the normal distance r_N vectorial as it is shown in [24]. The vectorial expressing allows fast calculations without coordinate transformation which would be necessary for the method described in [6], [10] or [16].

In the following an infinite long, straight conductor in z -direction is assumed (see fig. 2.3), resulting in a two dimensional problem. In that case eq. (2.2) simplifies to eq. (2.3):

$$\vec{B} = \frac{\mu_0 I}{2\pi r_N} \vec{e}_\varphi \quad (2.3)$$

r_N	normal distance between field point and conductor
\vec{e}_φ	unit vector in peripheral direction

The resulting magnetic flux density \vec{B} for that two dimensional problem (2D) can be expressed in 2D-Cartesian coordinates for a single conductor as shown in eq. (2.4).

$$\vec{B} = B_x \vec{e}_x + B_y \vec{e}_y = \frac{\mu_0 I}{2\pi} \cdot \frac{-(h_P - h_i) \vec{e}_x + (x_P - x_i) \vec{e}_y}{(x_P - x_i)^2 + (h_P - h_i)^2} \quad (2.4)$$

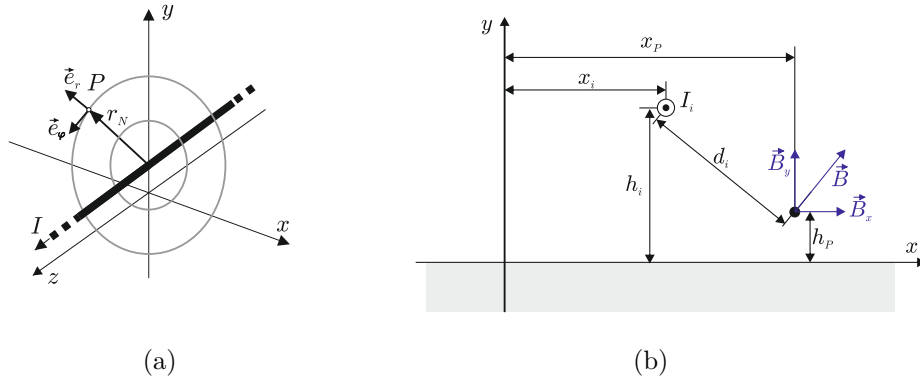


Figure 2.3: Model for calculating the magnetic field of infinite long straight line conductor

B_x, B_y	components of the magnetic flux density in the orthogonal x - and y -direction
\vec{e}_x, \vec{e}_y	unit vector in x - and y -direction
\vec{e}_φ	unit vector in peripheral direction
h_i	height of conductor i
h_P	height of field point P
x_i	horizontal position of conductor i
x_P	horizontal position of field point P

For worst-case analysis or for optimisation problems of overhead lines, cables and railways, typically an implementation of a 3D model not necessary, because the 3rd dimension (z -coordinate in fig. 2.3) doesn't bring additional information, because the conductors can be assumed to be straight by neglecting the sag of OHLs. Then, in case of overhead lines, for the calculation of the fields the height at the deepest point of a span of all conductor is taken into account. The error due to this assumption is discussed in sec. 3.4.

2.1.2 Approximate Formulas for Magnetic Flux Density

In literature simplifications for three-phase systems can be found. E.g. in [37] for a three phase system single circuit lines the following formulas result for conductors arranged in a line (horizontal or vertical) (2.5) or triangular (2.6) arrangements, while R is the distance to the center of the conductor arrangements, and s the distance between two conductors (see therefore fig. 2.4).

$$B_{rms} = \frac{\mu_0 \sqrt{3} s I^{(1)}}{2\pi R^2} \quad (2.5)$$

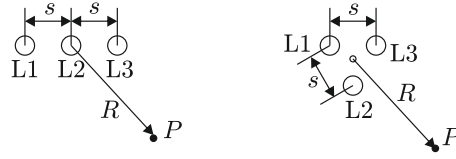


Figure 2.4: Sketch for the conductor arrangement to use for the approximate formulas

$$B_{rms} = \frac{\mu_0 \sqrt{6} s I^{(1)}}{4\pi R^2} \quad (2.6)$$

s	distance between two conductors
R	distance between field point and center of the conductor arrangement
$I^{(1)}$	positive sequence current of the three-phase system

Also for simple double circuit lines similar formulas are given in [37]. Because these formulas are only approximations, for this work, these formulas are not sufficient.

2.1.3 Calculation of the Electric Field with Charge Simulation Method

For the analytical calculation of the electric field strength the method of equivalent charges or charge simulation method is appropriate, especially for worst-case simulations and optimisation without disturbances through conductive objects in the vicinity. In the following the calculation of the electric field strength for a planar problem (2D) is described according to [16]. The influence of the conductive ground is considered using mirrored charges.

For the charge simulation method two relevant steps are necessary:

1. Determination of the equivalent charge of each conductor per unit length.
2. Calculation of the electric field strength caused by these charges.

The first step, the determination of the equivalent charges, is done using the capacitance matrix \mathbf{C} or its inverse, the potential coefficient matrix \mathbf{P} and the potential (voltage) matrix \mathbf{U} using (2.7).

$$\mathbf{Q} = \mathbf{C} \cdot \mathbf{U} = \mathbf{P}^{-1} \cdot \mathbf{U} \quad (2.7)$$

\mathbf{Q}	column vector of charges
\mathbf{C}	capacitance matrix
\mathbf{U}	column vector of line-to-earth voltages
\mathbf{P}	potential coefficient matrix

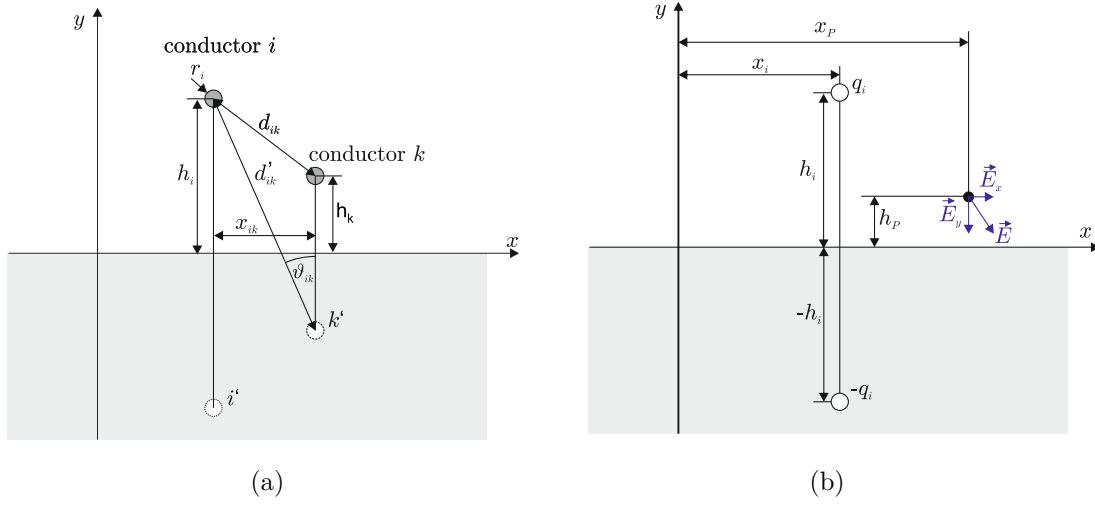


Figure 2.5: Model for the calculation of the potential coefficients (a) and the electric field strength (b)

The individual matrices are composed of the following components:

$$\begin{pmatrix} q_i \\ \vdots \\ q_k \end{pmatrix} = \begin{pmatrix} p_{ii} & \dots & p_{ik} \\ \vdots & \ddots & \vdots \\ p_{ki} & \dots & p_{kk} \end{pmatrix} \cdot \begin{pmatrix} U_i \\ \vdots \\ U_k \end{pmatrix} \quad (2.8)$$

q_i	charge of conductor i per unit length
$p_{ik} = p_{ki}$	mutual potential coefficient between conductor i and k
p_{ii}	self potential coefficient of conductor i
U_i	potential to earth of conductor i

The self and mutual potential coefficients can be calculated using (2.9).

$$p_{ii} = \frac{1}{2\pi\epsilon_0} \ln\left(\frac{h_i}{r_i}\right), \quad p_{ik} = \frac{1}{2\pi\epsilon_0} \ln\left(\frac{d'_{ik}}{d_{ik}}\right) \quad (2.9)$$

ϵ_0	permittivity of vacuum $\epsilon_0 = 8.854 \cdot 10^{-12} \text{Vs/Am}$
h_i	height of conductor i
r_i	radius of conductor i
d_{ik}	distance between conductor i and k
d'_{ik}	distance between conductor i and mirrored conductor k'

For conductors in bundles the radius r_i is replaced by the equivalent radius of the bundle r_{eq} , which is determined using (2.10) from [16].

$$r_{eq} = r_B \cdot \sqrt[n]{\frac{nr_T}{r_B}}, \quad r_B = \frac{a_B}{2 \sin(\pi/n)} \quad (2.10)$$

r_{eq}	equivalent radius of the bundle
r_B	circumradius of the bundle
r_t	radius of a sub-conductor
n	number of sub-conductors
a_B	distance between sub-conductors

The second step, the calculation of the electric field strength \vec{E} of the straight conductors, can be achieved using the theorem of Gauss:

$$\vec{E} = \frac{q_i}{2\pi\epsilon_0 r_{N,i}} \vec{e}_r \quad (2.11)$$

\vec{E}	vector of the electrical field strength
$r_{N,i}$	normal distance of a field point to conductor i
\vec{e}_r	unit vector in radial direction

The electric field strength $\vec{E} = E_x \vec{e}_x + E_y \vec{e}_y$ above ground results from the electric field strength of the conductor above ground and the fictive conductor below ground. The components E_x and E_y of the electric field strength in Cartesian coordinates can be determined using (2.12):

$$\begin{aligned} E_x &= \frac{q_i}{2\pi\epsilon_0} \left(\frac{x_P - x_i}{(x_P - x_i)^2 + (h_P - h_i)^2} - \frac{x_P - x_i}{(x_P - x_i)^2 + (h_P + h_i)^2} \right) \\ E_y &= \frac{q_i}{2\pi\epsilon_0} \left(\frac{h_P - h_i}{(x_P + x_i)^2 + (h_P - h_i)^2} - \frac{h_P + h_i}{(x_P - x_i)^2 + (h_P + h_i)^2} \right) \end{aligned} \quad (2.12)$$

E_x, E_y	components of the magnetic flux density in the orthogonal x - and y -direction
------------	--

These formulas are only valid for a smooth, planar conductive earth at $y=0$ m and field calculation point with $h_p \geq 0$ m.

2.1.4 Time Dependent Field Values

2.1.4.1 Nomenclature of Time Dependent Field Values in Time and Frequency Domain

The currents and voltages in electrical power systems typically are time dependent variables, ideally pure sinusoidal, practically a periodic variable with a fundamental frequency f_1 and with harmonics of order ν . Therefore also the electric and magnetic fields are time dependent. In the following the relationship between the time dependent current $i(t)$ and the magnetic flux density $\vec{B}(t)$ is described in detail. In an analogous manner the same can be done with the voltage $u(t)$ and the electric field strength $\vec{E}(t)$. The arbitrary periodic signal $i(t)$ can be expressed as a sum of sinusoidal signals by

applying a Fourier transform (or Fourier series) as it is shown in (2.13).

$$i(t) = \sum_{\nu=1}^{\nu_{max}} \hat{I}_{\nu} \cos(\nu\omega_1 t + \varphi_{\nu}) = \operatorname{Re} \left(\sum_{\nu=1}^{\nu_{max}} \hat{I}_{\nu} e^{j\nu\omega_1 t + \varphi_{\nu}} \right) = \operatorname{Re} \left(\sum_{\nu=1}^{\nu_{max}} \underline{\hat{I}}_{\nu} e^{j\nu\omega_1 t} \right) \quad (2.13)$$

$i(t)$	current in the time domain
t	time
ν	harmonic order
\hat{I}_{ν}	amplitude of the ν^{th} oscillation
$\underline{\hat{I}}_{\nu}$	complex amplitude of the ν^{th} oscillation $\underline{\hat{I}}_{\nu} = \hat{I}_{\nu} e^{j\varphi_{\nu}}$
\underline{I}_{ν}	complex RMS-value of the ν^{th} oscillation $\underline{I}_{\nu} = I_{\nu} e^{j\varphi_{\nu}}$
I_{ν}	RMS-value of the ν^{th} oscillation
ω_1	fundamental angular frequency $\omega_1 = 2\pi f_1$
f_1	fundamental frequency
φ_{ν}	phase angle of the ν^{th} oscillation

The set of currents $i(t)$ in the time domain becomes a set of complex variables $\underline{\hat{I}}_{\nu}$ in the frequency domain.

For a pure sinusoidal current the expression (2.13) becomes (2.14).

$$i(t) = \hat{I}_1 \cos(\omega_1 t + \varphi_1) = \operatorname{Re} \left(\underline{\hat{I}}_1 e^{j\omega_1 t} \right) \quad (2.14)$$

\hat{I}_1	amplitude of current at fundamental frequency
$\underline{\hat{I}}_1$	complex amplitude of the current at fundamental frequency $\underline{\hat{I}}_1 = \hat{I}_1 e^{j\varphi_1}$
φ_1	phase angle of the current at fundamental frequency

The calculation of the magnetic flux density can be done either way, in the time domain $i(t)$ or the frequency domain $\underline{I}(j\omega)$. The magnetic flux density resulting from a calculation in the frequency domain is then a vectorial, complex value which can be split in Cartesian coordinates as it is shown in equation (2.15).

$$\underline{\vec{B}}(j\omega) = \underline{B}_x(j\omega)\vec{e}_x + \underline{B}_y(j\omega)\vec{e}_y + \underline{B}_z(j\omega)\vec{e}_z \quad (2.15)$$

$\underline{\vec{B}}(j\omega)$	vector of the magnetic flux density in the frequency domain
$\underline{B}_x(j\omega)$	components in x -direction of the magnetic flux density in the frequency domain
$\underline{B}_y(j\omega)$	components in y -direction of the magnetic flux density in the frequency domain
$\underline{B}_z(j\omega)$	components in z -direction of the magnetic flux density in the frequency domain

In order to obtain the magnetic field in the time domain, the inverse transformation has to be done, for practical reason, split in Cartesian components, which can be seen in (2.16).

$$\begin{aligned} \vec{B}(t) &= \operatorname{Re} \left(\sum_{\nu=1}^{\nu_{max}} \left(\underline{\hat{B}}_{x,\nu} \vec{e}_x + \underline{\hat{B}}_{y,\nu} \vec{e}_y + \underline{\hat{B}}_{z,\nu} \vec{e}_z \right) e^{j\nu\omega_1 t} \right) \\ &= \operatorname{Re} \left(\sum_{\nu=1}^{\nu_{max}} \underline{\hat{B}}_{x,\nu} e^{j\nu\omega_1 t} \right) \vec{e}_x + \operatorname{Re} \left(\sum_{\nu=1}^{\nu_{max}} \underline{\hat{B}}_{y,\nu} e^{j\nu\omega_1 t} \right) \vec{e}_y + \operatorname{Re} \left(\sum_{\nu=1}^{\nu_{max}} \underline{\hat{B}}_{z,\nu} e^{j\nu\omega_1 t} \right) \vec{e}_z \\ &= B_x(t)\vec{e}_x + B_y(t)\vec{e}_y + B_z(t)\vec{e}_z \end{aligned} \quad (2.16)$$

The advantage of using the frequency domain in field calculation process comes with the better flexibility at superposition of fields from several conductors compared to the handling of cosine and sinus terms in the time domain. If the field is calculated for sampled current signals, there is no real advantage of calculating in the frequency domain (with a previous discrete Fourier Transform DFT), only the current distribution can be analysed analytical with frequency depending impedances (see sec. 2.4). More details about the consideration of harmonics in field values are described in sec. 2.2.3 and 2.3.

2.1.4.2 Graphical Illustration of Rotary Fields

In this thesis the term 'elliptical field' is used for field values where the trajectory curve of the phasor draws an ellipse (fig. 2.6, (a)), which is the most general case in vicinity of conductors carrying currents or voltages with pure sinusoidal pulse forms.

In this thesis the term 'rotating field' is used for all vectorial field values, for which not only the absolute value but also the direction of the field is dependent on time (fig. 2.6, (b)).

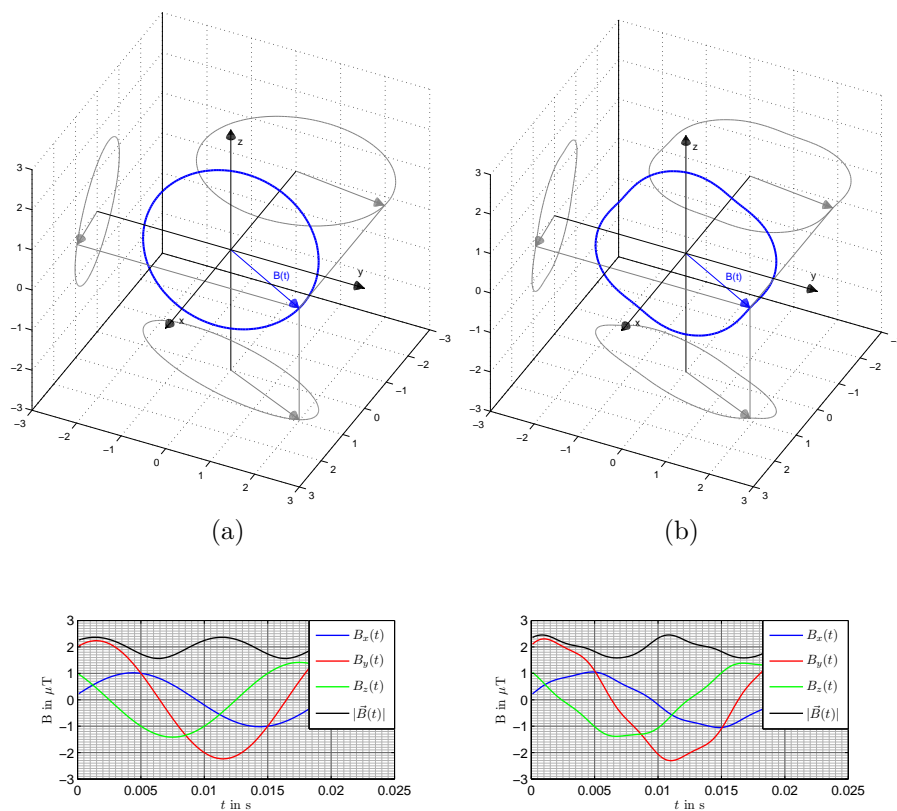


Figure 2.6: Rotary field without harmonics (elliptic field) (a) and with harmonics (b)

An extremity of the elliptic field is the 'alternating field' (fig. 2.7, (a)), where the direction of the field vector is not time-dependent. But, the alternating field must not necessarily have the shape of a pure sinusoidal pulse, e.g. if harmonics occur in the same direction (fig. 2.7, (b)), but the trajectory curve of the alternating field remains a straight line.

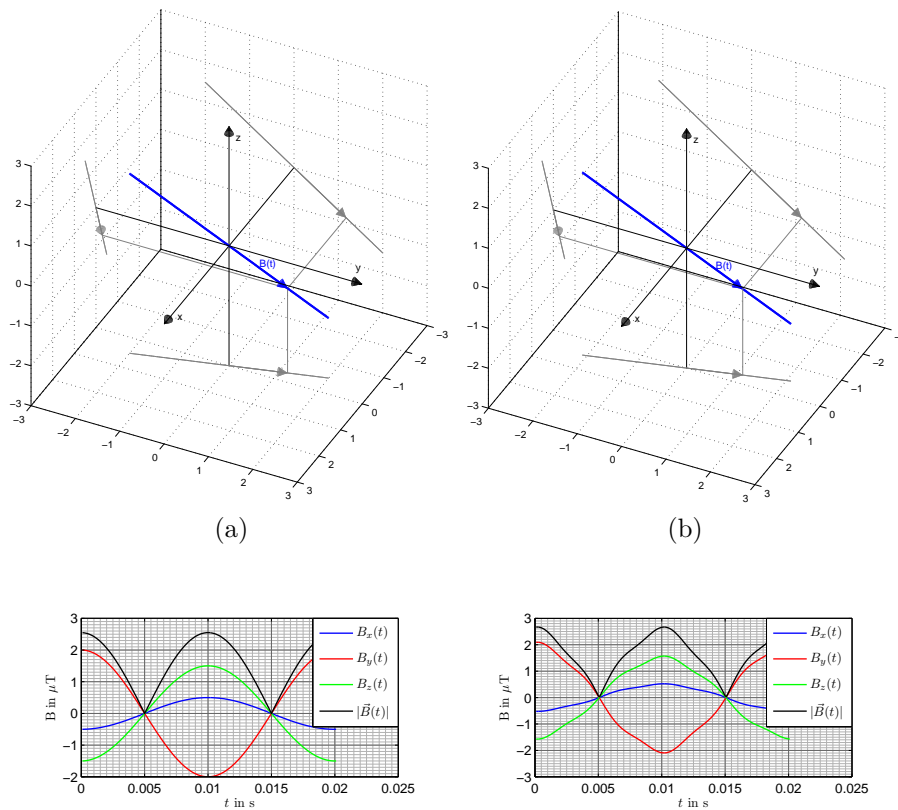


Figure 2.7: Alternating field without harmonics (a) and with harmonics (b)

2.1.4.3 Root Mean Square (RMS) and Peak Value of a Rotating Field

In order to compare the field values with limiting values given by standards or other regulations, the time dependent vector has to be transformed in representative scalar values, as there are in detail the RMS-value (route mean square) and the peak value. In the ICNIRP guidelines [31, 33] on one hand RMS-values as reference values are given. But the fact, that rotary fields might occur was not discussed. That means, that it is not completely clear, if the RMS-value or the peak-value divided by $\sqrt{2}$ has to be taken into account. The peak-value divided by $\sqrt{2}$ can also be found as the maximum displayed RMS-value of an uniaxial measurement instrument, which is turned in all possible directions. Most of the modern measuring instruments for power frequency

electric and/or magnetic field have three orthogonal arranged measurement axes. With these type of instruments, typically the peak and the RMS-values of a rotary field can be displayed easily. Computation programs should also be able to calculate both values. Nevertheless, some commercial programs do not offer an ordinary user the peak-value or the component in one direction.

The absolute value of a vector $\vec{B}(t)$ at any time step t can be calculated using (2.17).

$$|\vec{B}(t)| = \sqrt{B_x^2(t) + B_y^2(t) + B_z^2(t)} \quad (2.17)$$

$|\vec{B}(t)|$ absolute value of the vector $\vec{B}(t)$ at time step t

The RMS-value of the field for the time period T can then be calculated using the fundamental formula for the quadratic mean eq.(2.18):

$$B_{rms} = \sqrt{\frac{1}{T} \int_0^T |\vec{B}(t)|^2 dt} \quad (2.18)$$

B_{rms} RMS-value of the vector $\vec{B}(t)$
 T period of periodic signal

If the rms values of each component in x -, y - and z -direction are known, the RMS-value of the overall field becomes (2.19).

$$B_{rms} = \sqrt{B_{x,rms}^2 + B_{y,rms}^2 + B_{z,rms}^2} \quad (2.19)$$

The peak value B_{peak} , on the other hand, can be evaluated searching for the maximum value during one period T with (2.20).

$$B_{peak} = \max_{t=0\dots T} (|\vec{B}(t)|) \quad (2.20)$$

B_{peak} peak-value of the vector $\vec{B}(t)$

For an elliptical field without harmonics, the peak value of the field can be calculated analytically by searching the extrema of the absolute value by differentiating the equation of the ellipse (2.21) as shown in detail in the Cigre brochure No. 21 [16].

$$|\vec{B}(t)|^2 = |\vec{B}_x(t)|^2 + |\vec{B}_y(t)|^2 \quad (2.21)$$

The result of these mathematical operations, is shown in the following equations (2.22)

which is according to [21].

$$B_{x,Re} = \text{Re}(\underline{B}_x), B_{x,Im} = \text{Im}(\underline{B}_x), B_{y,Re} = \text{Re}(\underline{B}_y), B_{y,Im} = \text{Im}(\underline{B}_y) \quad (2.22)$$

$$B_a^2 = B_{x,Re}^2 + B_{x,Im}^2 + B_{y,Re}^2 + B_{y,Im}^2$$

$$B_{peak} = \sqrt{\frac{B_a^2}{2} \left(1 + \sqrt{1 - 4 \left(\frac{B_{x,Im}B_{y,Re} - B_{x,Re}B_{y,Im}}{B_a^2} \right)^2} \right)}$$

B_a auxiliary variable

For field values with 3D components, with result in an inclined orientation of the ellipse in space, the ellipse has to be first rotated by a coordinate transformation in a plain coordinate system. One applicable way to find an appropriate coordinate system is to split the vector \vec{B} in real and imaginary part and build the vectorial product $\text{Re}(\vec{B}) \times \text{Im}(\vec{B})$. The resulting vector is normal to the ellipse. After this affine transformation in a plain coordinate system eq. (2.22) can be applied.

The practical occurrence of rotary fields and alternating fields is discussed in sec. 3.8 for three-phase systems and in sec. 4.5 for railway systems.

2.2 Standards, Regulations and Other Limitations

Standards and regulation or other limits are necessary for both, a worst-case-analysis and for an optimisation. For a worst-case-analysis these limits must be known, in order to know the levels to comply with. For the optimisation these limits, or ratios of the actual value and the limit (=exposure ratio ER), are main input parameters.

In 1998 the International Commission on Non-Ionizing Radiation Protection (ICNIRP) published the 'Guidelines for limiting exposure to time-varying electric, magnetic and electromagnetic fields (up to 300 GHz)' [31]. Based on that document the EU recommended with the 'council recommendation' of 12th of July 1999 the limitation of exposure of the general public to electromagnetic fields (0 Hz to 300 GHz)' [17]. These recommendations were followed by most European countries, and the ICNIRP guidelines were taken over in their national standards. The standard 'Vornorm ÖVE/ÖNORM E 8850' [4] is the valid standard in Austria, with mainly the same limits as given in [31]. In December 2010 ICNIRP renewed their guidelines published with [33], but these guidelines are not taken over into the Austrian standardisation by now.

The American Institute of Electrical Engineers (IEEE) also published a standard according to safety levels with respect to human exposure to electromagnetic fields in 2002 [35] with quite dissenting reference levels comparing to ICNIRP.

These listed regulations explicitly do not cover the influence of the fields on electronic implants which can be handled using e.g. DIN VDE 0848-3-1 [3], the values from Fachinfo ÖVE [62] or values given by Prof. Silny [61].

Additionally, levels for the immunity requirements of equipment as given e.g. in IEC 61000-4-8 [34] have to be obeyed for 50 Hz and 60 Hz, in case they are lower than levels from other regulations. In hospitals or other buildings with very sensitive equipment to magnetic fields (e.g. in rooms with EEGs, ECGs, EMGs) it has to be guaranteed that levels according to ÖVE/ÖNORM E 8007 [5] or equivalent international standards for hospitals are not exceeded, otherwise more resilient equipment has to be used, which would usually cause additional costs.

2.2.1 Basic Restrictions According to ICNIRP

Basic restrictions are restrictions, which are based on established and scientifically approved health effects. For electromagnetic fields according to ICNIRP 1998 [31] they are defined as current densities J in the human nervous system for a frequency range up to 10 MHz. Because of the possibility of more accurate and steadier numerical calculations in the new publication ICNIRP 2010 [33] the basic restrictions are based on the internal (induced, influenced) electric field strengths E_i , taking the basic physical and physiological effects into account. The values of the basic restrictions given in ICNIRP 1998 and 2010 are compared in fig. 2.8. In [31] the basis restrictions aims to the exposure in the CNS (central nervous stimulation) only. Further ICNIRP 2010 [33] offers additionally basic restriction for the PNS (peripheral nervous stimulation), and the exposure evaluation of the extremities is possible now (with a higher limit).

2.2.2 Reference Levels for Magnetic Flux Density and Electric Field Strength According to ICNIRP and IEEE

Both, the internal electric field strength and the current densities are difficult to assess. Therefore, for practical exposure assessments in the guidelines so called reference values are provided. These reference values are derived from the basic restrictions, in such a way, that a compliance with the reference levels will ensure compliance with the relevant basic restriction.

In the following figures 2.9 and 2.10 reference levels of different standards, guidelines or recommendations are compared (ICNIRP1998 [31], ICNIRP 2010 [33], IEEE C95.6 [35] and for pace maker, Fachinfo ÖVE [62]).

As can be seen in fig. 2.9, the reference levels of the magnetic flux density of the new

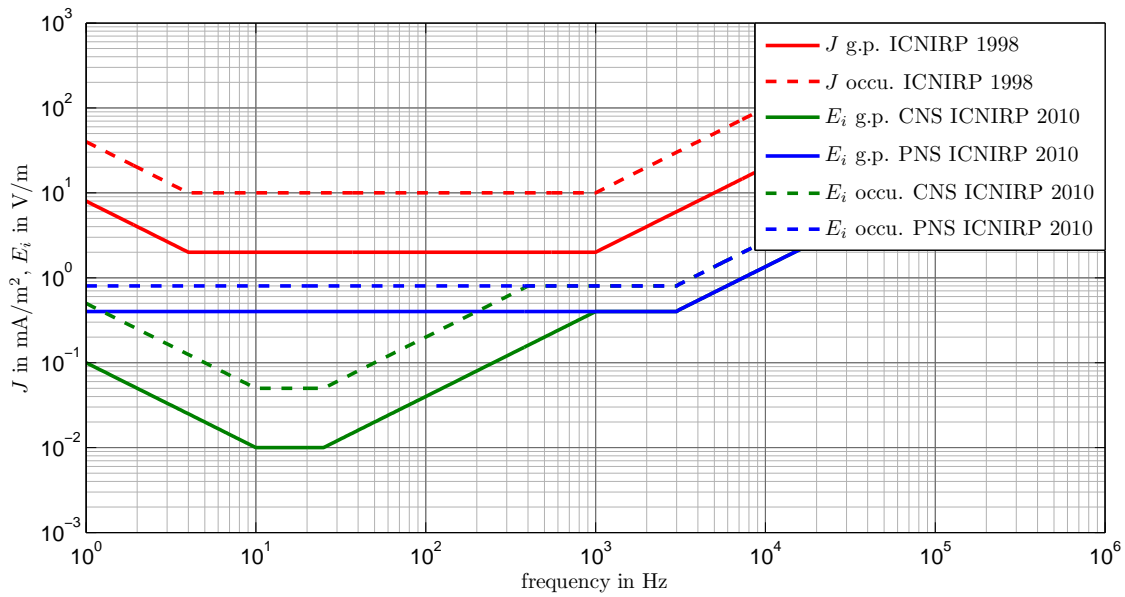


Figure 2.8: Basic restrictions (RMS-values): current density J (ICNIRP 1998 [31]) and internal electric field strength E_i (ICNIRP 2010 [33]) for general public (g.p), occupational exposure (occu.)

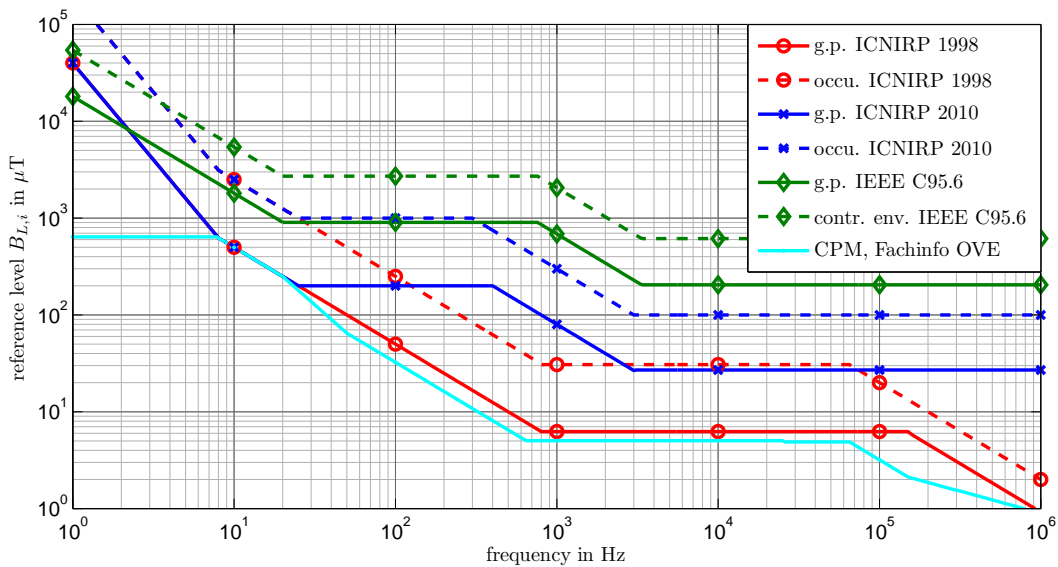


Figure 2.9: Reference levels of the magnetic flux density $B_{L,i}$ (RMS-values) for general public (g.p.) and occupational exposure (occu.) or in a controlled environment (contr. env.) of different standards or guidelines

guidelines are higher than the previous, but they are still more conservative than the actual IEEE standard. According to ICNIRP the reference levels only changed because of

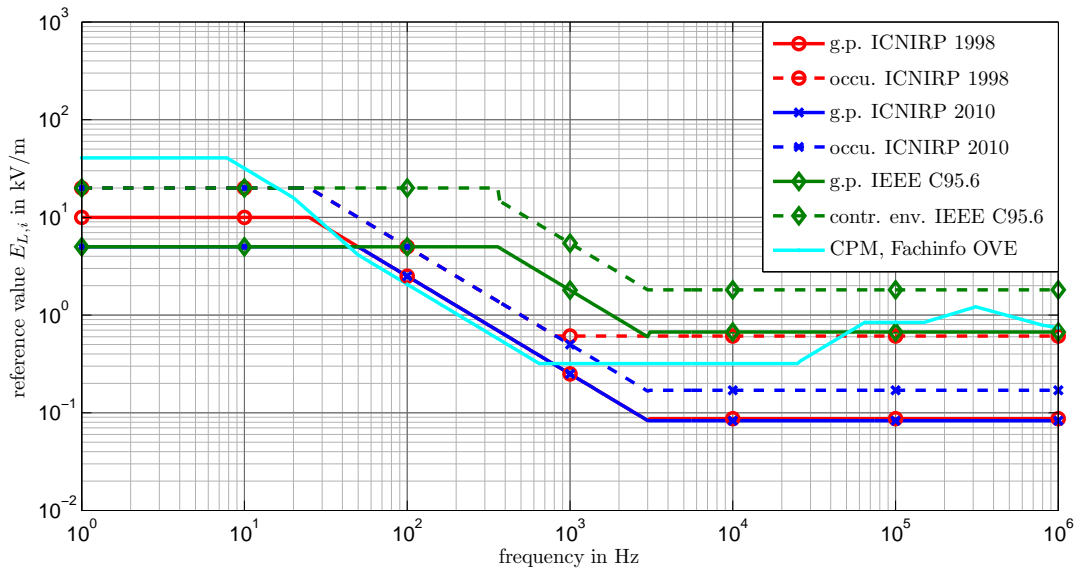


Figure 2.10: Reference levels of the electric field strength $E_{L,i}$ (RMS-values) for general public (g.p.) and occupational exposure (occu.) or in a controlled environment (contr. env.) of different standards or guidelines

more accurate numerical estimation. While the reference levels of the previous ICNIRP guidelines are similar to the restrictions for cardiac pacemakers (CPM), the reference levels of the new guidelines are much higher. Therefore it can be concluded, that an assessment for cardiac pacemakers has to be done additionally in future, because the new reference levels do not cover the risk of interference of active implants.

For the electrical field strength of fig. 2.10 between ICNIRP 1998 [31] and ICNIRP 2010 [33] fewer differences can be observed. Only in the low frequency range (<50 Hz) the reference levels for general public (g.p.) and for a higher frequency range (>1 kHz) the reference levels for occupational exposure (occu.) were decreased. The limits for cardiac pacemakers (for electrical field only) are more or less covered with the levels for general public of both [31] and [33]. In the frequency range lower than 50 Hz the reference levels of the new guidelines are now adapted toward the IEEE standard [35]. For a frequency range higher than 150 Hz for occupational exposure and higher than 800 Hz for general public the ICNIRP guidelines are more conservative than the IEEE standard [35].

For European electrical power systems the reference levels for frequencies of 50 Hz and 16.7 Hz (fundamental frequencies) are the most important. Therefore, tab. 2.1 provides a summary of these levels.

For the magnetic flux density the new reference level are 200 μT for general public (g.p.) and 1000 μT for occupational exposure (occu.). This doubling of the reference level is

Table 2.1: Selected reference levels (RMS-values) from various standards/guidelines

	f in Hz	$B_{L,i}$ in μT			
		ICNIRP 1998	ICNIRP 2010	IEEE C95.6	cpm Fachinfo
general	16.7	300	300	1086	298.92
public	50	100	200	904	64.84
occupational	16.7	1500	1500	3258	-
exposure	50	500	1000	2710	-

	f in Hz	$E_{L,i}$ in kV/m			
		ICNIRP 1998	ICNIRP 2010	IEEE C95.6	cpm Fachinfo
general	16.7	10	5	5	19.03
public	50	5	5	5	4.13
occupational	16.7	20	20	20	-
exposure	50	10	10	20	-

contradictory to the ongoing discussions of many medical scientists, which typically claim a decrease of the limits to values i.e. 0.2, 0.4, 1, 3 or 10 μT for long time exposure for places with high requirements (e.g. kindergartens, schools, playgrounds, bedrooms). For engineering tasks of electric power systems the decrease eases requirements, because minimum distances to field sources e.g. cables with high currents etc. can be reduced, if these reference levels are taken over in national standardisation.

For 16.7 Hz the reference level of the electric field strength for the new ICNIRP guidelines is decreased from 10 kV/m to 5 kV/m for general public. For railway systems only this does not have a big effect in the exposure assessment, because maximum electric field strengths in areas, accessible to general public, usually do not exceed 3 kV/m . In the vicinity of a crossing of the railway system with a high voltage overhead lines (OHL) the effect of both electric and magnetic field sources (16.7 Hz and 50 Hz) have to be observed, which is described in detail in [27].

2.2.3 Exposure Ratio ER According to ICNIRP

According to ICNIRP guidelines 1998 [31], 2003 [32] and 2010 [33] simultaneous exposure to electric and magnetic fields with multiple frequencies are additive in their effects. This effect for the electrical stimulation is expressed in ICNIRP 1998 [31] in formulas (2.23)

and in the newer guidelines ICNIRP 2010 [33] in formulas (2.24).

$$\sum_{i=1\text{Hz}}^{65\text{kHz}} \frac{H_i}{H_{L,i}} + \sum_{i>65\text{kHz}}^{10\text{MHz}} \frac{H_i}{a} \leq 1, \quad \sum_{i=1\text{Hz}}^{1\text{MHz}} \frac{E_i}{E_{L,i}} + \sum_{i>1\text{MHz}}^{10\text{MHz}} \frac{E_i}{b} \leq 1 \quad (2.23)$$

$$\sum_{i=1\text{Hz}}^{10\text{MHz}} \frac{H_i}{H_{L,i}} \leq 1, \quad \sum_{i=1\text{Hz}}^{10\text{MHz}} \frac{E_i}{E_{L,i}} \leq 1 \quad (2.24)$$

E_i	electric field strength at frequency i
H_i	magnetic field strength at frequency i
$E_{L,i}$	reference level of electric field strength at frequency i
$H_{L,i}$	reference level of magnetic field strength at frequency i
a	610 Vm^{-1} for occupational exposure and 87 Vm^{-1} for general public
b	524.4 Am^{-1} ($30.7 \text{ }\mu\text{T}$) for occupational exposure and 5 Am^{-1} ($6.25 \text{ }\mu\text{T}$) for general public

The reference levels used in (2.23) and (2.24) can be read from fig. 2.9 and fig. 2.10. For easier handling in the following these sums of the ratios of the actual field values and the reference levels at the certain frequencies are named exposure ratios ER in the style of [61]. These equations (2.23) to (2.24) can be generalised to:

$$ER = \sum_{i=1\text{Hz}}^{10\text{MHz}} \frac{A_i}{EL_i} \leq 1 \quad (2.25)$$

ER	exposure ratio
A_i	value of the field at frequency i
EL_i	exposure limit (reference limit) at frequency i

The reference limits in ICNIRP-guidelines are always given as unperturbed RMS-values (see therefore table 4 in [33]).

The exposure ratio can also be used with peak values (for 1D-fields=amplitude). Then the reference limits have to adapted by multiplying them with $\sqrt{2}$. The indices B and E are added to distinguish between an exposure ratio of the magnetic (B) and the electric (E) field. With the valid equation $B = \mu_0 H$ in non-permeable space and with that indices B and E equation e.g. (2.24) becomes (2.26).

$$ER_B = \sum_{i=1\text{Hz}}^{10\text{MHz}} \frac{H_i}{H_{L,i}} = \sum_{i=1\text{Hz}}^{10\text{MHz}} \frac{B_i}{B_{L,i}} \leq 1, \quad ER_E = \sum_{i=1\text{Hz}}^{10\text{MHz}} \frac{E_i}{E_{L,i}} \leq 1 \quad (2.26)$$

ER_B	exposure ratio for magnetic field
ER_E	exposure ratio for electric field
B_i	magnetic flux density at frequency i
$B_{L,i}$	magnetic flux density reference level at frequency i

Especially when it comes to the evaluation of non sinusoidal electric and magnetic fields or to an evaluation in vicinity of field sources with differing frequencies (e.g. 50 Hz-system and 16.7 Hz electric railways), the exposure ratio is the adequate choice. Detailed investigations on harmonics are further described in section 2.3.

2.2.4 Interference of Cardiac Pacemakers Due to EMF

For cardiac pacemakers (CPMs) only few guidelines concerning low-frequency electric and magnetic fields exist. Nevertheless a limit based on the interference voltage can be induced from the draft of DIN VDE 0848-3-1 [3]. Additionally Prof. Silny made an extensive analysis about CPMs amongst others in [61].

In analogy to the exposure ratio for electrical field strength ER_E and magnetic flux density ER_B , an exposure ratio for CPMs ER_{cpm} can be defined as the ratio between the maximum induced interference voltage $U_{i,max}$ within the conductor loop of the CPM and the interference threshold $U_{i,thre}$ of a specific CPM.

$$ER_{cpm}(f) = \frac{U_{i,max}(f)}{U_{i,thre}(f)} \quad (2.27)$$

$ER_{cpm}(f)$	exposure ratio at frequency f for CPMs
$U_{i,max}$	maximum interference voltage due to electric and magnetic fields
$U_{i,thre}$	interference thresholds of a specific CPM

An exposure ratio ER_{cpm} lower than 1 means, that for that specific interference voltage a risk concerning CPMs and electric and magnetic fields can be excluded according to different research results.

2.2.4.1 Interference Voltage of Cardiac Pacemakers According to Draft DIN VDE 0848-3-1

The draft DIN VDE 0848-3-1 [3] distinguishes between three categories of CPMs according to their immunity to interference:

- category 0 - appropriate immune to interference,
- category 1 - limited immune to interference and
- category 2 - susceptible to interference.

While for CPMs of category 0 and 1 the interference thresholds are given, CPMs of category 2 have to be studied one by one because their treatment is not further specified in the standard.

For a frequency range of up to 10 MHz the interference thresholds for CPMs of category 0 and 1 according to [3] are shown in fig. 2.11. From that figure, for CPMs of category 0,

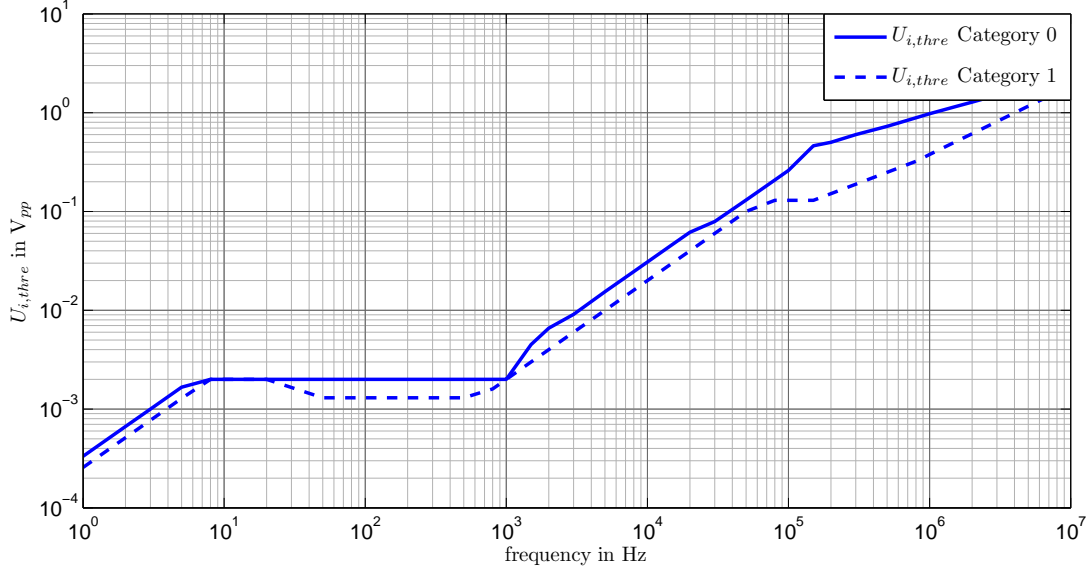


Figure 2.11: Interference thresholds $U_{i,thre}$ for CPMs of category 0 and category 1 according to [3]

the threshold interference voltage $U_{i,thre}$ can be read out with 2000 μV_{pp} (peak to peak) within a frequency range between 6 Hz and 1000 Hz. For CPMs of category 1, $U_{i,thre}$ between 7.8 Hz and 20 Hz is 2000 μV_{pp} , and between 50 Hz and 650 Hz it is 1300 μV_{pp} . For the evaluation of the maximum open-loop interference voltage $U_{i,max}$ due electric and magnetic field exposure of persons with CPMs of category 0 and 1 further evaluation formulas are given in [3] sectioned into several frequency ranges. For example equation (2.28) represents the formula for a frequency range of $0 \text{ Hz} < f < 25 \text{ kHz}$, which covers the typical power frequency range.

$$\frac{U_{i,max}}{V_{pp}} = 0.0089 \cdot \max \left(\frac{|H(t)|}{1 \text{ Am}^{-1}} + \frac{|E(t)|}{80 \text{ Vm}^{-1}} \right) \cdot \frac{f}{25 \text{ kHz}} < \frac{U_{i,thre}}{V_{pp}} \quad (2.28)$$

$U_{i,max}$	maximum interference voltage, here in V_{pp} (peak-to-peak)
$ H(t) $	absolute value of the magnetic field strength at a time t
$ E(t) $	absolute value of the electric field strength at a time t
$U_{i,thre}$	interference thresholds of the CPM in V_{pp}

With (2.28) and the corresponding formulas for other frequency ranges the flux densities and electric field strengths which would cause the threshold voltages $U_{i,thre}$ can be evaluated. Therefore, the maximum magnetic flux density (RMS-value) without any occurrence of electric field ($E = 0$) depending on frequency is shown in fig. 2.9 and

the maximum electric field strength (RMS-value) without occurrence of magnetic field ($B = 0$) is given in fig. 2.10. These are the same values as published in [62] (there the peak values were offered, which can easily be converted by dividing them by $\sqrt{2}$).

For fields with multiple frequencies it is recommended in DIN VDE 0848-3-1 [3] that for each frequency the ratio $U_{i,max}(f)/U_{i,thre}(f)$ has to be evaluated and summed up geometrically (square the values, add them and extract the square root). Expressed in terms of exposure ratios ER_{cpm} this can be transformed as shown in (2.29), whereas similar to the exposure ration ER before, the sum has to be lower than 1 in order to achieve the standard. It should be mentioned, that in contrast to the formula given by ICNIRP for example (2.25), here the summing up is geometrically.

$$ER_{cpm} = \sqrt{\sum_f ER_{cpm}^2(f)} = \sqrt{\sum_f \left(\frac{U_{i,max}(f)}{U_{i,thre}(f)} \right)^2} < 1 \quad (2.29)$$

ER_{cpm} exposure ratio for CPMs

2.2.4.2 Interference Voltage for Cardiac Pacemakers According to Silny

Other expansive investigations were carried out by Prof. Silny in [61]. There, the interference voltage depending on the type and the location of the CPM as well as the circumference of the exposed body for nominated electric field strengths and magnetic flux densities are shown. From that publication the following general equation (2.30) in analogy to (2.28) can be generated.

$$U_{i,max} = u_{iB} \cdot B_{rms} + u_{iE} \cdot E_{rms} < U_{i,thre} \quad (2.30)$$

$U_{i,max}$	maximum interference voltage
u_{iB}	specific interference voltage of the magnetic field
B_{rms}	RMS-value of the influencing magnetic flux density
u_{iE}	specific interference voltage of the electric field
E_{rms}	RMS-value of the influencing electric field strength
$U_{i,thre}$	interference thresholds of the CPM

The specific interference voltages u_{iB} and u_{iE} are summarised for different types and locations of CPMs in tab. 2.2.

body circum- ference	sensing	sensor location		$U_{i,thre}$	50 Hz		16,7 Hz	
					u_{iB}	u_{iE}	u_{iB}	u_{iE}
cm	-	-	-	μV_{pp}	$\mu V_{pp}/\mu T$	$\mu V_{pp}/kVm^{-1}$	$\mu V_{pp}/\mu T$	$\mu V_{pp}/kVm^{-1}$
75	unipolar	atrium	left pectoral	> 1000	11.85	664.4	3.95	221.5
			right pectoral	> 1000	7.40	664.4	2.47	221.5
		ventricle	left pectoral	5000	13.38	1191.9	4.46	397.3
			right pectoral	5000	7.65	1191.9	2.55	397.3
	bipolar	atrium	-	500	0.26	112.5	0.09	37.5
		vetricle	-	4000	0.26	94.7	0.09	31.6
135	unipolar	atrium	left pectoral	> 1000	21.32	205.9	7.11	68.6
			right pectoral	> 1000	13.33	205.9	4.44	68.6
		ventricle	left pectoral	5000	24.08	380.6	8.03	126.9
			right pectoral	5000	13.77	380.6	4.59	126.9
	bipolar	atrium	-	500	0.26	34.5	0.09	11.5
		vetricle	-	4000	0.26	34.2	0.09	11.4

Table 2.2: Interference voltages due to electric and magnetic field with a frequency of 50 Hz and 16.7 Hz for CPMs according to Silny

It has to be mentioned, that the specific interference voltages are based on sinusoidal alternating fields (see sec. 2.1.4) taking the RMS-value of the field into account. That means, that for rotary fields this evaluation would lead to an overestimation of up to $(\sqrt{2} - 1) \cdot 100\% = 41.4\%$ if the RMS-values for the rotary fields are used in (2.30). Because this is more important for three-phase systems the impact of the elliptic field on the evaluation of exposure ratios for CPMs is discussed more in detail in sec. 3.9.

2.2.4.3 Summarising the Interference of Cardiac Pacemakers

The thresholds according to DIN VDE 0848-3-1 [3] and Silny [61] for 50 Hz and 16.7 Hz are now summarised in this section. In tab. 2.3 the maximum allowed magnetic flux densities without occurrence of an electric field ($B_{max}(E = 0)$) and the maximum allowed electric field strengths without occurrence of a magnetic field ($E_{max}(B = 0)$) are shown.

In fig. 2.12 and fig. 2.13, the points are connected, where the simultaneous exposure of the electric field strength E_{rms} and magnetic flux density B_{rms} would lead to an interference voltage which is higher than the interference threshold of a specific CPM. In other words, these curves are isolines for the function $ER_{cpm} = f(E, B) = 1$. Below these curves, CPMs should not be influenced, which means, that these values of the fields are allowed simultaneously. For the threshold according to [3] it is assumed for a worst case investigation, that E and H are alternating fields and $\max(E(t))$ is reached at the same time as $\max(H(t))$. The curves for category 0 and category 1 would overlap in fig. 2.13, and therefore combined, because for 16.7 Hz the interference thresholds of CPMs of category 0 and 1 are the same.

Table 2.3: Maximum allowed magnetic flux densities and electric field strength (RMS-values), without occurrence of the other field value

evaluation according to	type of cardiac pacemaker	$B_{max}(E = 0)$ in μT		$E_{max}(B = 0)$ in kV/m	
		16.7 Hz	50 Hz	16.7 Hz	50 Hz
Silny	75 cm unipolar atrium left	253.3	84.4	4.52	1.51
	75 cm unipolar atrium right	405.2	135.1	4.52	1.51
	75 cm unipolar ventricle left	1121.4	373.8	12.58	4.19
	75 cm unipolar ventricle right	1960.7	653.6	12.58	4.19
	75 cm bipolar atrium	5868.5	1956.2	13.34	4.45
	75 cm bipolar vetricle	46948.4	15649.5	126.70	42.23
	135 cm unipolar atrium left	140.7	46.9	14.57	4.86
	135 cm unipolar atrium right	225.1	75.0	14.57	4.86
	135 cm unipolar ventricle left	623.0	207.7	39.41	13.14
	135 cm unipolar ventricle right	1089.3	363.1	39.41	13.14
	135 cm bipolar atrium	5882.4	1960.8	43.45	14.48
	135 cm bipolar vetricle	47058.8	15686.3	350.66	116.89
	VDE 0848-3-1	category 0	299.5	99.8	19.07
category 1		299.5	64.9	19.07	4.13

The curve for the bipolar CPM with sensing at ventricle according to Silny [61] would be out of range in fig. 2.12 and 2.13 and therefore is not shown. For further information, additionally the reference levels according to ICNIRP 1998 and ICNIRP 2010 are presented in fig. 2.12 and fig. 2.13.

The most sensitive CPMs according to Silny are those with an unipolar sensing and a sensor location at the atrium left. While for slim people with a body circumference of 75 cm the electric field strength has more interference influence, for bigger people with a body circumference of 135 cm the magnetic flux density has more influence. Bipolar CPMs are the most insensitive ones, and the reference values according to ICNIRP are lower than these maximum allowed values, with one exception - 75 cm bipolar atrium at 50 Hz. That means, that by achieving the reference values according to ICNIRP almost all bipolar CPMs should not be influenced. The same is valid for an evaluation of CPMs of category 0 according to [3], as long as no simultaneous exposure to electric and magnetic field occurs. Further that is only valid for ICNIRP 1998 because for ICNIRP 2010 the reference level of the magnetic flux density are higher. But it can be seen clearly, that when complying with ICNIRP guidelines, it is not sure, that there is no risk of interfering unipolar CPMs, especially, when electric and magnetic field occur simultaneously (which is usually the case for OHLs and electric railways).

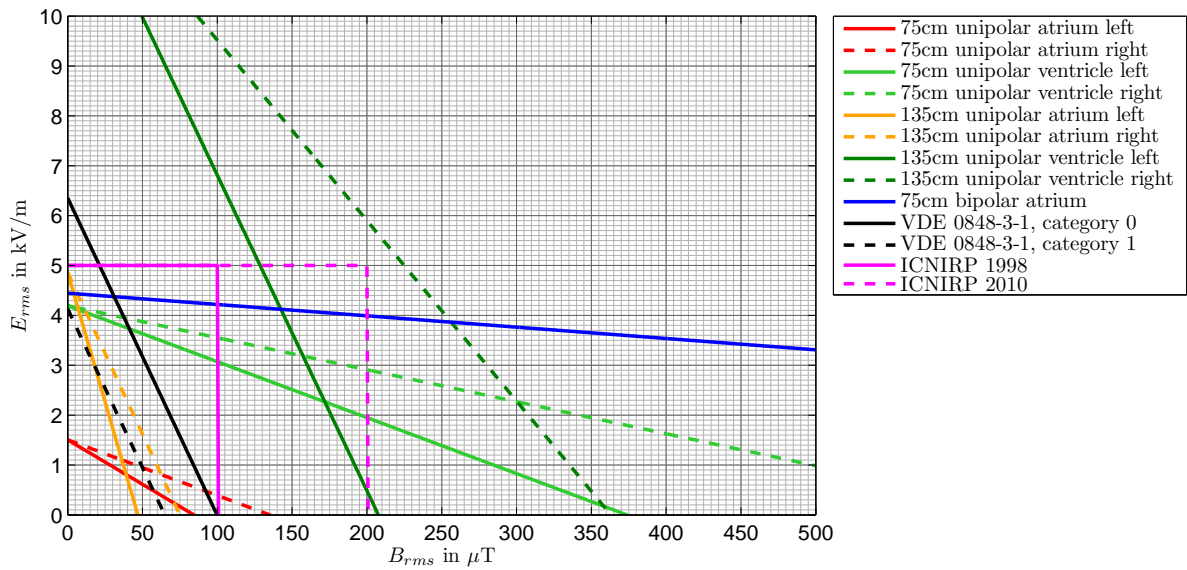


Figure 2.12: Thresholds for simultaneous exposure to electric and magnetic field of **50 Hz** for CPMs according to Silny [61] and DIN VDE 0848-3-1 [3] and reference values according to ICNIRP [31, 33]

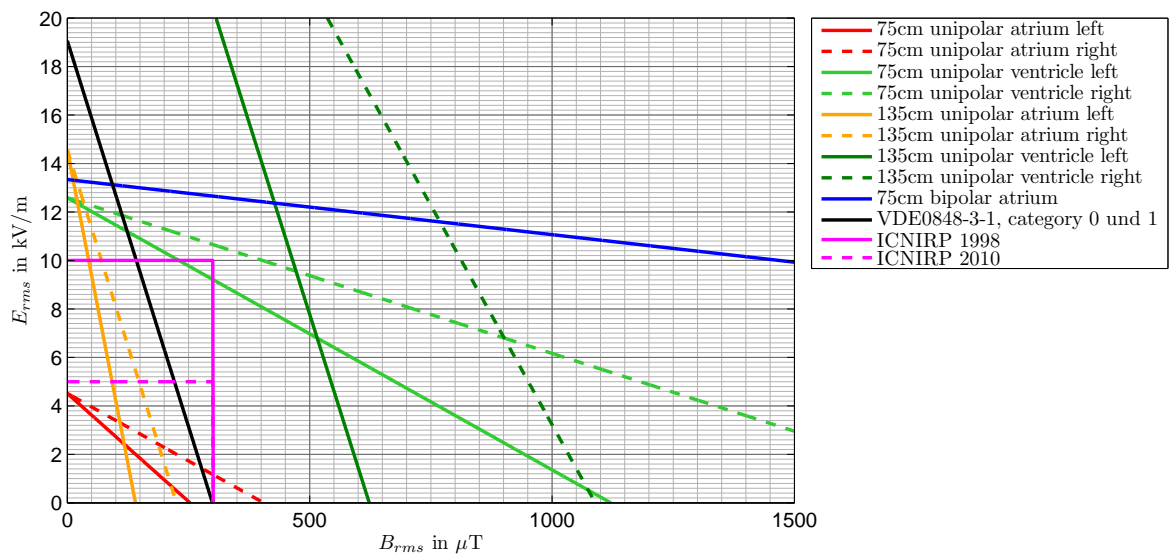


Figure 2.13: Thresholds for simultaneous exposure to electric and magnetic field of **16.7 Hz** for CPMs according to Silny [61] and DIN VDE 0848-3-1 [3] and reference values according to ICNIRP [31, 33]

In section 3.9 the actual exposure ratios for CPMs (ER_{cpm}) in vicinity of OHLs are analysed. For electric railways the same analysis is done in sec. 4.4.

2.3 Consideration of Harmonics and Harmonic Factor

Harmonics in currents and voltages also cause harmonics in electric and magnetic fields. The reference values of ICNIRP guidelines [31] or [33] for higher frequencies differ from the reference values of the fundamental frequencies (see therefore e.g. fig. 2.9. Therefore the consideration of the harmonics has to be done not linearly but with the correct reference values. A method for considering harmonics in a convenient way is the implementation of a harmonic factor [61, 60, 7, 26], which is described in the following.

2.3.1 Harmonic Factor

The aim of implementing a harmonic factor is to reduce evaluation effort when dealing with electric and magnetic field exposure with harmonics. Therefore the general multi frequency rule (2.25) is reformed to (2.31) in order to get a measure of the influence of the harmonics compared to the influence of the field of the fundamental frequency. The index i from (2.25) which stands for the frequency in Hz is transformed in an index ν , the order of the harmonics.

$$ER = \sum_{\nu=1}^{\nu_{max}} \frac{A_{\nu}}{EL_{\nu}} = \frac{A_1}{EL_1} \sum_{\nu=1}^{\nu_{max}} \frac{A_{\nu}}{A_1} \frac{EL_1}{EL_{\nu}} = \frac{A_1}{EL_1} k_H = ER_1 \cdot k_H \quad (2.31)$$

ν	order of the harmonic
ν_{max}	maximum practically existing order of harmonic
A_{ν}	field value for ν^{th} harmonic
EL_{ν}	exposure limit (reference limit) for ν^{th} harmonic
A_1	field value at fundamental frequency
EL_1	exposure limit (reference limit) at fundamental frequency
k_H	harmonic factor
ER_1	exposure ratio for the fundamental frequency

Resultant, the harmonic factor k_H as a value for the weight of the harmonics in sense of exposure ratio, is defined with (2.32).

$$k_H = \sum_{\nu=1}^{\nu_{max}} \frac{A_{\nu}}{A_1} \frac{EL_1}{EL_{\nu}} = \frac{ER}{ER_1} \quad (2.32)$$

At this stage, the harmonic factor might make no sense, because either the total exposure ratio ER or all spectral components of the field value A_{ν} have to be known, and the simplification for the calculation is not immediately apparent. But, if the ratio A_{ν}/A_1 is constant over the entire field space, in other words, if the field will have the same shape of signal - independent from the amplitude of the fundamental frequency - than the harmonic factor need to be evaluated for one field point only. The calculation of

the exposure ratio of the entire field space results then in a field calculation for the fundamental frequency A_1 only.

The harmonic factor of magnetic flux density $k_{H,B}$ and for electric field strength $k_{H,E}$ become (2.33) and (2.34).

$$k_{H,B} = \sum_{\nu=1}^{\nu_{max}} \frac{B_{\nu}}{B_1} \frac{B_{L,1}}{B_{L,\nu}} \quad (2.33)$$

$$k_{H,E} = \sum_{\nu=1}^{\nu_{max}} \frac{E_{\nu}}{E_1} \frac{E_{L,1}}{E_{L,\nu}} \quad (2.34)$$

$k_{H,B}$	harmonic factor for magnetic field
B_{ν}	magnetic flux density for ν^{th} harmonic
$B_{L,\nu}$	magnetic flux density reference level for ν^{th} harmonic
$k_{H,E}$	harmonic factor for electric field
E_{ν}	electric field strength for ν^{th} harmonic
$E_{L,\nu}$	electric field strength reference level for ν^{th} harmonic

This harmonic factors $k_{H,B}$ and $k_{H,E}$ can be calculated directly from the harmonics of the current I or of the voltage U as long as the following relation between the harmonics and the value of the fundamental frequency is valid (2.35):

$$\frac{I_{\nu}}{I_1} = \frac{B_{\nu}}{B_1} \text{ or } \frac{U_{\nu}}{U_1} = \frac{E_{\nu}}{E_1} \quad (2.35)$$

In order to highlight that the harmonic factor is calculated directly from the harmonics in voltage or harmonics in current, U respectively I replace the indices E or B of k_H .

$$k_{H,U} = \sum_{\nu=1}^{\nu_{max}} \frac{U_{\nu}}{U_1} \frac{E_1}{E_{L,\nu}} \quad (2.36)$$

$$k_{H,I} = \sum_{\nu=1}^{\nu_{max}} \frac{I_{\nu}}{I_1} \frac{B_1}{B_{L,\nu}} \quad (2.37)$$

As it can be seen, the harmonic factors are the relative harmonics weighted with the inverse ratio of the reference levels. In tab. 2.4 an example for the calculation of a $k_{H,U}$ is given. Because the harmonic factor is strongly dependent on the reference values, it is evaluated for ICNIRP 1998 and ICNIRP 2010.

It must be mentioned that this approach with a single harmonic factor is - strictly spoken - valid for single phase systems only and therefore can be used for e.g. railway systems, as long the current distribution between the participating conductors is more

Table 2.4: Example for the calculation of the harmonic factor $k_{H,U}$ for electric field strength from a voltage signal with fundamental frequency of 16.7 Hz on the base of ICNIRP 1998 and ICNIRP 2010 for general public exposure

ν	f	$\frac{U_\nu}{U_1}$	ICNIRP 1998		ICNIRP 2010	
			$\frac{E_{L,1}}{E_{L,\nu}}$	$\frac{U_\nu}{U_1} \cdot \frac{E_{L,\nu}}{E_{L,1}}$	$\frac{E_{L,1}}{E_{L,\nu}}$	$\frac{U_\nu}{U_1} \cdot \frac{E_{L,\nu}}{E_{L,1}}$
-	Hz	%	%	-	%	-
1	16.7	100.00	100.0	1.000	100.0	1.000
3	50.0	6.64	200.0	0.133	100.0	0.066
5	83.3	4.82	333.3	0.161	166.7	0.080
7	116.7	2.97	466.7	0.139	233.3	0.069
9	150.0	2.12	600.0	0.127	300.0	0.064
11	183.3	1.53	733.3	0.112	366.7	0.056
13	216.7	1.43	866.7	0.124	433.3	0.062
15	250.0	2.52	1000.0	0.252	500.0	0.126
17	283.3	1.66	1133.3	0.188	566.7	0.094
			$k_{H,U} =$	2.236	$k_{H,U} =$	1.618

or less frequency independent. Nevertheless, the harmonic factor evaluation enables to analyse the effect of the harmonics for a wide spectrum of harmonics easily, and reduces the calculation effort of the fields, because the field calculation has not to be done for each harmonic separately.

Because especially for three-phase systems it might happen, that not all harmonics will lead to the same field configuration, an expansion of this method for three-phase systems with symmetrical components is carried out in sec. 3.7.

2.3.2 Phase Consideration

The multi frequency rule (2.25) is known to be very conservative for an application on signals with harmonics, because the phase angle information of the signal is neglected and all spectral components of the signal are considered to be in phase [32]. This conservative analysis is advantageous in order to analyse a worst case scenario, especially if the phase angles are not known or are changing in a wide range. Nevertheless, the consequential overestimation of the physiological effects of the harmonics is very unfavourable when the resulting exposure ration is very close to 1. Then, it is preferable to evaluate the exposure ratios with less safety margin.

For that reason in ICNIRP 2003 [32] and ICNIRP 2010 [33] other restrictions - which do consider the phase angle information of the signals - are additionally given. There,

the conservative multi frequency rule (2.38)

$$ER = \sum_{\nu=1}^{\nu_{max}} \frac{A_{\nu}}{EL_{\nu}} = \sum_{\nu=1}^{\nu_{max}} \frac{\hat{A}_{\nu}}{\hat{EL}_{\nu}} \leq 1 \quad (2.38)$$

is modified to a formula (2.39), considering both, the phase angles of the harmonics and the angle of a filter function which is related to the basic restriction or reference level according to [32] and [33].

$$ER(t) = \left| \sum_{\nu=1}^{\nu_{max}} \frac{A_{\nu}}{EL_{\nu}} \cos(\nu\omega_1 t + \phi_{\nu} + \varphi_{\nu}) \right| \leq 1 \quad (2.39)$$

This evaluation recommended by ICNIRP is based on the analyses and publications of Kari Jokela [36].

ν	order of the harmonic
A_{ν}	field value of the ν^{th} harmonic of the field value e.g. E_{ν}, B_{ν}
EL_{ν}	exposure level of ν^{th} harmonic e.g. $EL_{L,\nu}, BL_{L,\nu}$
ω_1	fundamental angular frequency $\omega_1 = 2\pi f_1$
ϕ_{ν}	phase angle of the ν^{th} harmonic of the field value
φ_{ν}	correction phase angle of the ν^{th} harmonic

In analogy to (2.38) in (2.39) the exposure value is not exceeded as long as all $ER(t)$ are lower than 1, which means, that the maximum value of $ER(t)$ has to be lower than 1. As it can be seen in (2.38) it is irrelevant, if the amplitudes \hat{A}_{ν} or the RMS-values A_{ν} of the signal are taken into account, only the reference levels have to be chosen accordingly (peak or RMS-value). Because in the ICNIRP guidelines the reference values are given as RMS-values in the following the methodology is given for RMS-values only.

The exposure evaluation with phase consideration can be done in two ways:

1. Piecewise linear with formula (2.39)
2. RC-filter functions

For the piecewise linear method with (2.39) the correction angle φ_{ν} is required. According to ICNIRP 2003 [32], this correction angle φ_{ν} for frequencies lower than cut-off frequency $f_{\nu} < f_c$ is equal to $\varphi_{\nu} = \pi/2$, for higher frequencies $f_{\nu} > f_c$ the angle becomes $\varphi_{\nu} = 0^{\circ}$. This equals to an approximation of a first order high pass filter with a cut-off frequency f_c . The cut-off frequencies f_c for E and B -field for general public and occupational exposure are summarised in tab. 2.5. These frequencies coincide with the bends of the reference curves for ICNIRP 1998 (see fig. 2.9 and 2.10).

In ICNIRP 2010 [33] this correction angle φ_{ν} is depending on the gradient of the basic restriction level curve or the reference level curve as it is shown in tab. 2.6.

Table 2.5: cut-off frequencies f_c according to ICNIRP 2003 [32]

	f_c for E in Hz	f_c for B in Hz
general public	3000	800
occupational exposure	820	820

 Table 2.6: filter angles φ depending on the reference-value curve

variation of the level proportional to	f^{-2}	f^{-1}	f^0	f^1
φ in rad	π	$\pi/2$	0	$-\pi/2$

For the second method - the use of RC-filter functions - it is more convenient to rewrite (2.39) into (2.40).

$$ER = \left| \sum_{\nu=1}^{\nu_{max}} \operatorname{Re} \left\{ \frac{1}{EL_{\nu}} \cdot e^{j\varphi_{\nu}} \cdot \underline{A}_{\nu} \cdot e^{j\nu\omega_1 t} \right\} \right| \leq 1 \quad (2.40)$$

\underline{A}_{ν} complex field value $\underline{A}_{\nu} = A_{\nu} e^{j\varphi_{\nu}}$

The first two terms, the inverse of the exposure level and the correction angle φ_{ν} , can be merged to an complex frequency response function $\underline{G}(j\omega)$, further called 'filter function'. To make it more general, the order of harmonics is replaced by the angular frequency ω . EL_{ω} represents the reference value at angular frequency ω and φ_{ω} stands for the correction angle at that angular frequency.

$$\underline{G}(j\omega) = \frac{1}{EL_{\omega}} \cdot e^{j\varphi_{\omega}} \quad (2.41)$$

$\underline{G}(j\omega)$ complex filter function

The filter function $G(j\omega)$ of the high pass RC-filter can be expressed as (2.42).

$$\underline{G}(j\omega) = \frac{\underline{U}_a(j\omega)}{\underline{U}_c(j\omega)} = \frac{R}{R + \frac{1}{j\omega C}} = \frac{j\omega RC}{j\omega RC + 1} = \frac{j\omega/\omega_c}{j\omega/\omega_c + 1} \quad (2.42)$$

The frequency response of the corresponding low pass filter (2.43) then comes to (2.43).

$$\underline{G}(j\omega) = \frac{\underline{U}_a(j\omega)}{\underline{U}_c(j\omega)} = \frac{\frac{1}{j\omega C}}{R + \frac{1}{j\omega C}} = \frac{1}{j\omega RC + 1} = \frac{1}{j\omega/\omega_c + 1} \quad (2.43)$$

R resistance

C capacitance
 $\omega_c = 1/(RC)$ angular cut-off frequency

In the following the Bode diagram of the frequency response for simple low and high pass RC-circuits and their approximation are presented.

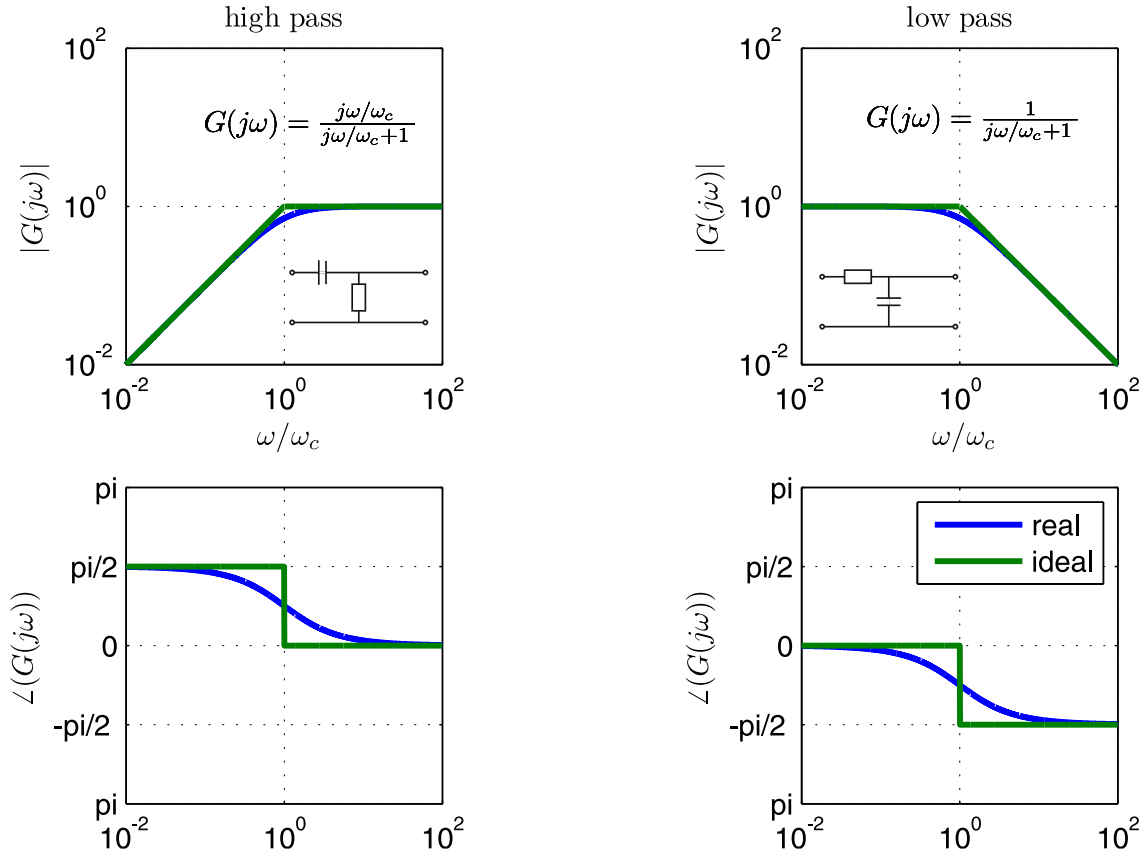


Figure 2.14: Frequency response of a high pass filter(left) and a low pass filter (right) of a RC circuit with cut-off angular frequency $\omega_c = (RC)^{-1}$

While for the evaluation according to ICNIRP 2003 only one high pass filter is necessary for the frequency range 8 Hz to 100 kHz for general public and 8 Hz to 65 kHz for occupational exposure (see [32], p. 386), for compliance with ICNIRP 2010 a combination of high and low pass-filter is necessary.

The design of the filter function $\underline{G}(j\omega)$ built out of a RC-filter for the magnetic flux density signal (in μT) for general public exposure for a frequency range 1 Hz to 100 kHz according to ICNIRP 2010 is shown in (2.44).

$$\underline{G} = \frac{1}{200\mu\text{T}} \cdot \frac{j f/8\text{Hz}}{j f/8\text{Hz} + 1} \cdot \frac{j f/25\text{Hz}}{j f/25\text{Hz} + 1} \cdot (j f/400\text{Hz} + 1) \cdot \frac{1}{j f/3000\text{Hz} + 1} \quad (2.44)$$

The Bode diagram of this filter function as well as of all single terms of it is presented in fig. 2.15, comparing the piecewise linear function given from the reference value and the resulting RC-filter functions.

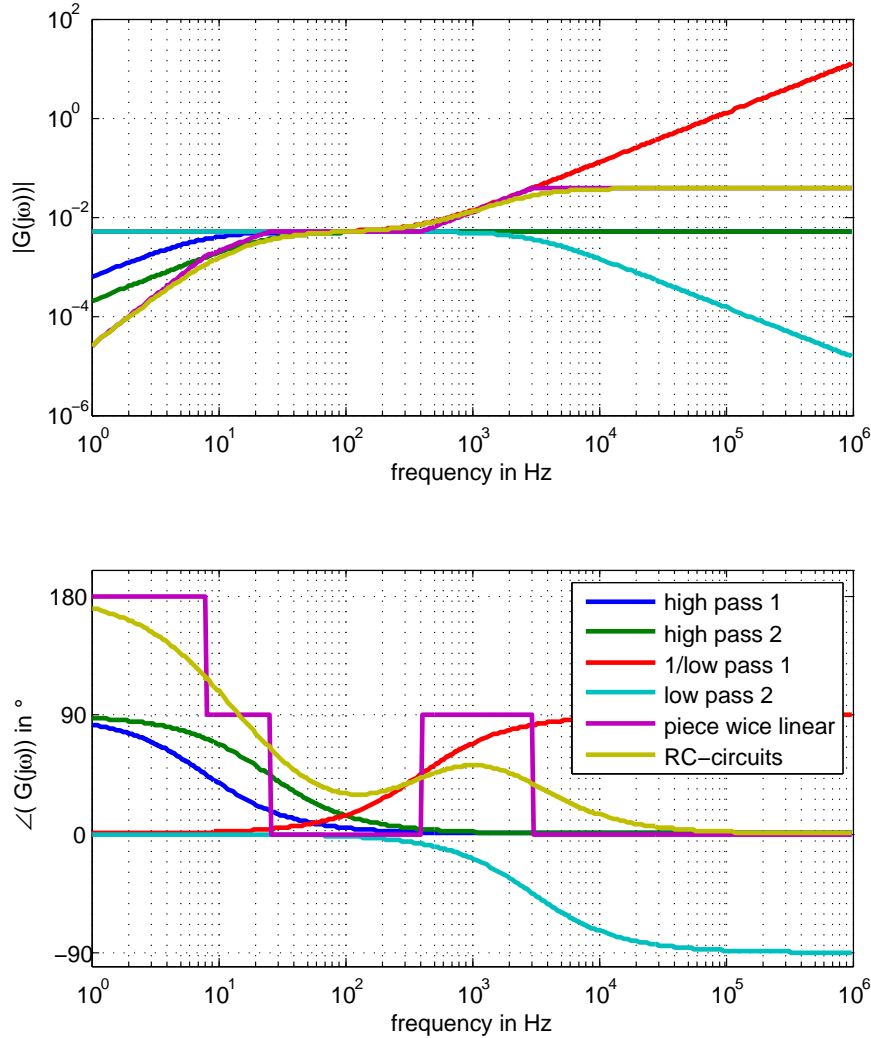


Figure 2.15: Bode diagram of the filter function for exposure evaluation of magnetic flux density (the input signal has to be in μT)

It can be seen that the absolute value and the correction angle of the RC-filterfunction deviates especially at the cut-off-frequencies from the values of the piecewise linear function, which of course causes different results for the exposure ratio.

For a synthetic, but typical signal $B(t)$ the effect of the different methods with consideration of the phase (piecewise linear, RC filter) as well as the consideration without phase (multi-frequency rule) are shown in time domain for [31, 32] in fig. 2.16 and for [33] in fig. 2.17. The synthetic signal has a RMS-value for the 50 Hz-component of exactly $100 \mu\text{T}$ and some harmonics, which are typical for the (400 V) power supply

of households at low load. In tab. 2.7 the RMS-values for the first 10 harmonics of odd order are shown. Harmonics of even order also exist in the signal, but are very low compared to the odd harmonics.

Table 2.7: RMS-values and phase angles of the odd synthetic signal frequency components

ν	1	3	5	7	9	11	13	15	17	19
f_j in Hz	50	150	250	350	450	550	650	750	850	950
B_j in μT	100	2.11	0.79	0.53	0.39	0.32	0.13	0,03	0.05	0.03
ϕ_j in $^\circ$	0	28	-62	141	48	119	166	117	18	-35

It can be seen, that the effect of the harmonics is much lower in fig. 2.17 than in fig. 2.16, because of the much higher reference levels for the harmonics. Additionally the reference level of the magnetic flux density is doubled in fig. 2.16 (200 μT instead of 100 μT), and the maximum of the resulting exposure ratio $\max(ER_B(t))$ is much lower than in fig. 2.16 for all 3 methods.

The harmonic factors k_H for that signal build with (2.45) are shown in tab. 2.8 for different Methods and ICNIRP guidelines.

$$k_{H,B} = \frac{\max(ER_B(t))}{ER_{B,1}} = \max(ER_B(t)) \frac{B_{L,1}}{B_1} \quad (2.45)$$

Table 2.8: Harmonic factor $k_{H,B}$ for signal $B(t)$ shown in fig. 2.16 and 2.17 evaluated with different weighting functions/filter

	all harmonics in phase	piecewise linear	RC-filter
ICNIRP 1998/2003	2.47	1.22	1.16
ICNIRP 2010	1.29	1.06	1.10

2.3.3 Exposure Ratios for Elliptic Fields

In this section 2.3 so far, the exposure ratio was defined only for an one dimensional signal of the electric field strength or magnetic flux density, which is the same as an alternating field in one defined direction. But, the time varying field components exist generally in all 3 space (spatial) dimensions. Therefore for each spatial component of the field A_x , A_y and A_z the exposure ratio has to be evaluated. No procedure concerning rotary fields is described in ICNIRP guidelines therefore an own approach for that is given in the following.

If no phase consideration is necessary (e.g. the harmonics are rather low and there is enough distance to exposure ratio limit) the worst case evaluation can be done with the

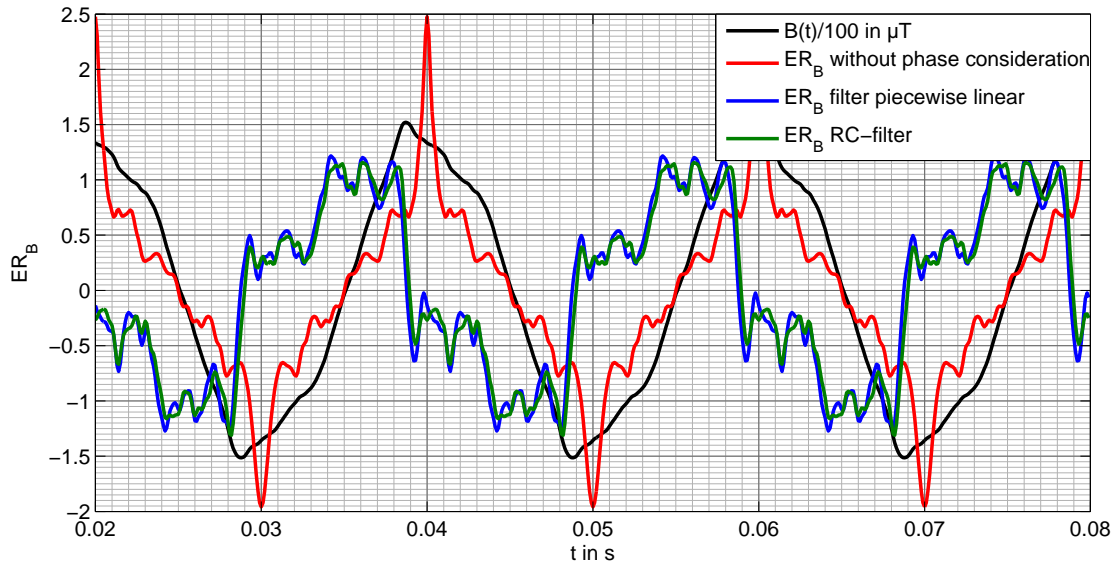


Figure 2.16: Magnetic flux density and resulting exposure ratio for ICNIRP 1998/2003 [31, 32] evaluated with different weighting functions in time domain

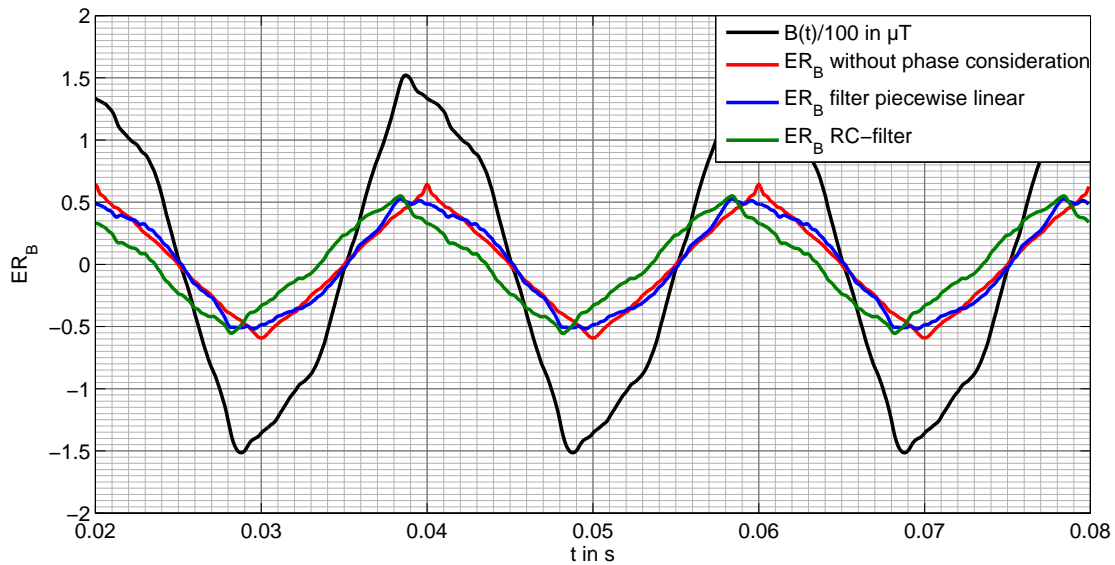


Figure 2.17: Magnetic flux density and resulting exposure ratio for ICNIRP 2010 [33] evaluated with different weighting functions in time domain

conservative multi frequency rule by determining the RMS-value of each harmonic component ν . The total RMS-value A_ν can be build from the RMS-values of the components

in each direction $A_x(\nu)$, $A_y(\nu)$ and $A_z(\nu)$, using (2.46).

$$A_\nu = \sqrt{A_x(\nu)^2 + A_y(\nu)^2 + A_z(\nu)^2} \quad (2.46)$$

For the signal in frequency domain A_ν there is no phase information left and a phase consideration is no more possible. With these RMS-values A_ν for each harmonic component the exposure evaluation can then be done using the conservative evaluation formula (2.38).

If a phase consideration is wanted or necessary, first, for each direction the exposure ratios ER_x , ER_y , ER_z in time domain have to be build. This can be done as described before either with the filter function or with the piecewise linear method according to sec. 2.3.2. In a second step, the absolute value of the function $ER(t) = ER_x(t)\vec{e}_x + ER_y(t)\vec{e}_y + ER_z(t)\vec{e}_z$ has to be evaluated for each time step using (2.47):

$$|ER(t)| = \sqrt{ER_x(t)^2 + ER_y(t)^2 + ER_z(t)^2} \quad (2.47)$$

As before, the exposure limit is exceeded if the maximum of $|ER(t)|$ exceeds the value 1.

For example a measured signal in time domain of the magnetic flux density in three orthogonal axes in vicinity of a railway station is shown in fig. 2.18 (top). From that components of the signal (top), the exposure ratios $ER_{B,x}$, $ER_{B,y}$ and $ER_{B,z}$ are built for ICNIRP 2003 (middle) and ICNIRP 2010 (bottom) using digital filters. Additionally, the absolute values of the resulting magnetic flux density, and of resulting exposure ratios are given.

The trajectory of the head of the space phasor during a time period of the same signal are shown in fig. 2.19.

In principle, this evaluation can also be done for calculated field values with measured currents. The problem only is, that for the evaluation the signals in time domain or frequency domain (with phase information) of all conductors have to be known. The results from typical power quality measurement campaigns are therefore only of limited use, because usually, the signals are averaged over some period of time, and no phase information is given. These measurement results can only be used for worst-case analysis of the harmonic factors. An evaluation of a harmonic factor from voltage and current signals, considering the phase can only be done for single phase systems, because the resulting harmonics of a three-phase system will always be a mixture of the currents/voltages of all corresponding phases. In this case the equality (2.35) is no longer

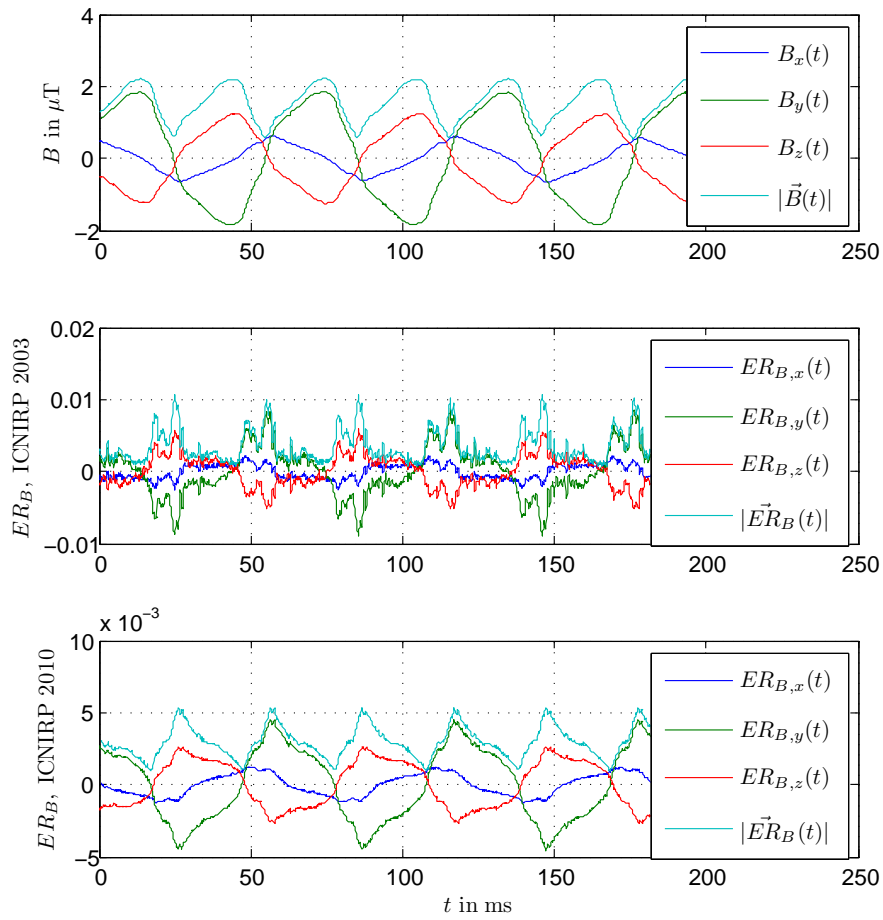


Figure 2.18: Components of a measured rotating field in time domain for 3 axes (top) and the resulting exposure ratios in each direction for ICNIRP 2003 (middle) and ICNIRP 2010 (bottom)

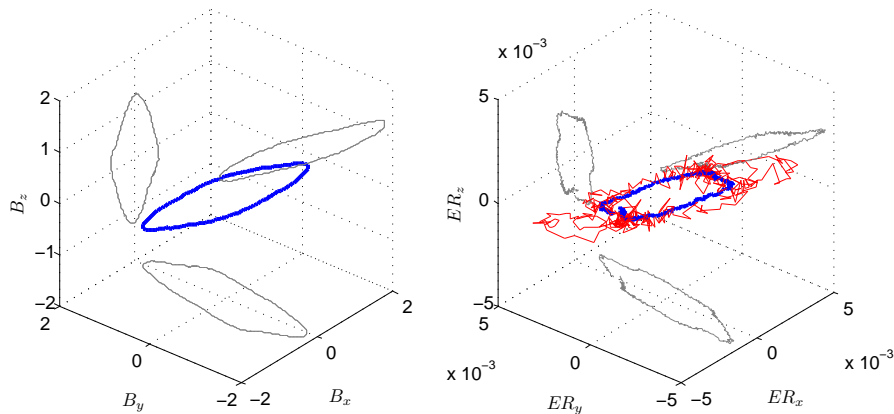


Figure 2.19: Reconstruction of the rotating field (left) measured with 3 axes in time domain and of the exposure ratio (right) results from filtering with reference levels according to ICNIRP 2003 (red) and ICNIRP 2010 (blue)

valid. As a consequence, the evaluation of a harmonic factor with phase consideration can only be done with the resulting signal components for each field point and is valid for that single field point only. When neglecting the phase information of the signal, the evaluation should be followed as described later on in sec. 3.7.

2.4 Impedances, Earth Return Impedances, Current Distribution

2.4.1 Calculation of Currents in Passive Conductors

For the calculation of the magnetic field all currents in all conductors have to be known. This includes the induced currents in passive conductors (conductors which are connected on both sides with earth) or other passive loops. Passive conductors are for example earth wires, reduction conductors, return conductors, cable screens, rails or other conductors in earth, which are influenced by the currents of the active conductors. The active conductors are the phase conductors or in other words, the conductors connected to an external voltage or current source.

In general for a system with k conductors the following relation can be described:

$$\underline{\mathbf{U}} = \underline{\mathbf{Z}} \cdot \underline{\mathbf{I}} \quad (2.48)$$

$\underline{\mathbf{U}}$ column vector of the voltages \underline{U}_i
 $\underline{\mathbf{Z}}$ impedance matrix
 $\underline{\mathbf{I}}$ column vector of the currents \underline{I}_i

$$\begin{pmatrix} \underline{U}_1 \\ \vdots \\ \underline{U}_i \\ \vdots \\ \underline{U}_k \end{pmatrix} = \begin{pmatrix} \underline{Z}_{11} & \cdots & \underline{Z}_{1i} & \cdots & \underline{Z}_{1k} \\ \vdots & \ddots & \vdots & & \vdots \\ \underline{Z}_{i1} & \cdots & \underline{Z}_{ii} & \cdots & \underline{Z}_{ik} \\ \vdots & & \vdots & \ddots & \vdots \\ \underline{Z}_{k1} & \cdots & \underline{Z}_{ki} & \cdots & \underline{Z}_{kk} \end{pmatrix} \cdot \begin{pmatrix} \underline{I}_1 \\ \vdots \\ \underline{I}_i \\ \vdots \\ \underline{I}_k \end{pmatrix} \quad (2.49)$$

\underline{Z}_{ii} self impedance of the conductor i
 \underline{Z}_{ik} mutual impedance between the conductor i and k
 \underline{I}_i current of the conductor i
 \underline{U}_i voltage of the conductor i

To evaluate the current in the passive conductors, these matrices are split into groups of active (index a) and passive (index p) conductors.

$$\begin{pmatrix} \underline{\mathbf{U}}_a \\ \underline{\mathbf{U}}_p \end{pmatrix} = \begin{pmatrix} \underline{\mathbf{Z}}_{aa} & \underline{\mathbf{Z}}_{ap} \\ \underline{\mathbf{Z}}_{pa} & \underline{\mathbf{Z}}_{pp} \end{pmatrix} \cdot \begin{pmatrix} \underline{\mathbf{I}}_a \\ \underline{\mathbf{I}}_p \end{pmatrix} \quad (2.50)$$

If the passive conductors are perfectly grounded on both sides (or the ends of a passive loop are connected to each other), thus the voltages $\underline{\mathbf{U}}_p$ are equal to zero. Then the currents, induced in these passive conductors $\underline{\mathbf{I}}_p$ can be calculated using (2.51).

$$\underline{\mathbf{I}}_p = -\underline{\mathbf{Z}}_{pp}^{-1} \cdot \underline{\mathbf{Z}}_{pa} \cdot \underline{\mathbf{I}}_a \quad (2.51)$$

Because of the connections to earth, the elements of the \mathbf{Z} -Matrix have to be calculated using formulas with terms, which consider the earth return. In this thesis, the given formulas for impedances with earth return of Carson and Pollaczek are compared to the formulas given by Dubanton. The general conductor arrangement for two conductors for calculating the self and mutual impedances with earth return is given in fig. 2.20.

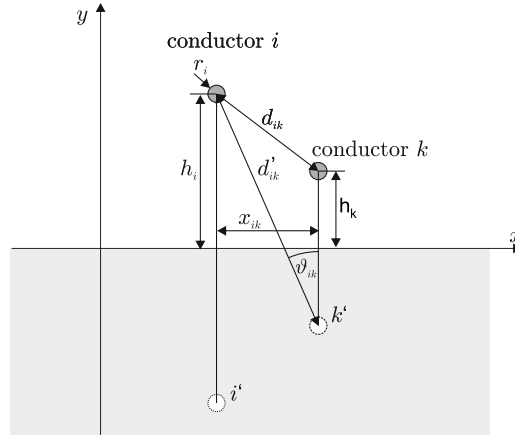


Figure 2.20: Model for calculation of the self and mutual impedances

2.4.2 Self and Mutual Impedances with Earth Return According to Carson

According to the publications of Carson [13] and Pollaczek [57] the self impedance of conductor i ($Z_{ii,E}$) and the mutual impedance between conductor i and k ($Z_{ik,E}$) with earth return can be calculated with equation (2.52) and (2.53). The correction terms C_R and C_X are infinite series and consider the change of the impedances due to the earth return. Well prepared formulas for the calculation of these infinite series can be found e.g. in [29] p.241 and [55] p.274.

$$\underline{Z}'_{ii,CE} = R'_i + \frac{\omega\mu_0}{2\pi}C_R + j\omega L'_i + j\frac{\omega\mu_0}{2\pi}\left(\ln\frac{2h_i}{r_i} + C_X\right) \quad (2.52)$$

$$\underline{Z}'_{ik,CE} = \frac{\omega\mu_0}{2\pi}C_R + j\frac{\omega\mu_0}{2\pi}\left(\ln\frac{d'_{ik}}{d_{ik}} + C_X\right) \quad (2.53)$$

$\underline{Z}'_{ii,CE}$ self impedance of conductor i with earth return per unit length according to Carson
 $\underline{Z}'_{ik,CE}$ mutual impedance between conductor i and k with earth return per unit length according to Carson

R'_i	resistance of the conductor per unit length
L'_i	internal inductance of the conductor i per unit length
μ_0	permeability of the vacuum $\mu_0 = 4\pi 10^{-7}$ Vs/Am
r_i	radius of the conductor
h_i	height of the conductor above earth
d_{ik}	distance between conductor i and k
d'_{ik}	distance between conductor i and mirrored conductor k
C_R, C_X	correction terms

As long as the height of the conductor above earth (h_i) and the distance between the conductors (d_{ik}) are much smaller than the equivalent earth current depth (2.56), only little divergences occur, when only the first term of the infinite series C_R and C_X are considered. Equations (2.52) and (2.53) then become to (2.54) and (2.55).

$$\underline{Z}'_{ii,CE} = R'_i + \frac{\omega\mu_0}{8} + j\omega L'_i + j\frac{\omega\mu_0}{2\pi} \ln\left(\frac{\delta_E}{r_i}\right) \quad (2.54)$$

$$\underline{Z}'_{ik,CE} = \frac{\omega\mu_0}{8} + j\frac{\omega\mu_0}{2\pi} \ln\left(\frac{\delta_E}{d_{ik}}\right) \quad (2.55)$$

The equivalent earth current depth δ_E has to be calculated with (2.56).

$$\delta_E = \frac{2e^{\frac{1}{2}-\gamma}}{\sqrt{\omega\mu_0\kappa_E}} \cong \frac{1.85137}{\sqrt{\omega\mu_0\kappa_E}} = 1.85137 \sqrt{\frac{\rho_E}{\omega\mu_0}} \quad (2.56)$$

δ_E	equivalent current depth
γ	Euler-Mascheroni constant $\gamma = 0.57721566\dots$
$\omega = 2\pi f$	angular frequency
κ_E	specific conductivity of the earth
ρ_E	specific resistivity of the earth

According to [13] this simplification is appropriate with little deviations for $h_i < 0.3 \cdot \delta_E$ and $d_{ik} < 0.3 \cdot \delta_E$.

The equivalent earth current depth δ_E for a specific earth resistance of 100 Ωm at 50 Hz equals to 931 m, at 16.7 Hz it equals to 1614 m. That means, that up to a distance and height above ground of about 300 m at 50 Hz and of about 500 m at 16.7 Hz the simplified formulas can be used.

2.4.3 Self and Mutual Impedances with Earth Return According to Dubanton

An alternative form for the impedances with earth return to the infinite series of Carson and Pollaczek are the formulas given by Dubanton. According to [55] therefore the impedances with earth return can be calculated with (2.57) and (2.58) using a complex earth return \underline{p} .

$$\underline{Z}'_{ii,DE} = R'_i + j\omega \frac{\mu_0}{2\pi} \left(\frac{1}{4} + \ln \frac{2(h_i + \underline{p})}{r_i} \right) \quad (2.57)$$

$$\underline{Z}'_{ik,DE} = j\omega \frac{\mu_0}{2\pi} \ln \frac{\sqrt{(h_i + h_k + 2\underline{p})^2 + x_{ik}^2}}{d_{ik}} \quad (2.58)$$

$\underline{Z}'_{ii,DE}$	self impedance of conductor i with earth return per unit length according to Dubanton
$\underline{Z}'_{ik,DE}$	mutual impedance between conductor i and k with earth return per unit length according to Dubanton
\underline{p}	complex earth return depth

The complex earth return depth \underline{p} therefore is defined with (2.59).

$$\underline{p} = \sqrt{\frac{\rho_E}{j\omega\mu_0}} \quad (2.59)$$

In order to get less deviation to the Carson-formula at low frequencies (up to 1 kHz) it is useful to use a modified complex earth return depth \underline{p}' (2.60). Then the absolute value of \underline{p}' equals to $2\delta_E$.

$$\underline{p}' = e^{\frac{1}{2}-\gamma} \cdot \sqrt{\frac{\rho_E}{j\omega\mu_0}} \cong 0.9257 \cdot \sqrt{\frac{\rho_E}{j\omega\mu_0}} \quad (2.60)$$

\underline{p}'	modified complex earth return depth
------------------	-------------------------------------

2.4.4 Parameter-Study of Impedance Formulas

In this section the influence of the impedance calculation methods as described before is shortly discussed in order to explain the chosen formulas for calculating the currents in passive conductors.

First the attention is drawn to the frequency dependency of the different impedance evaluations. In fig. 2.21 the Carson formulas with correction term up to the order of 20 ($\underline{Z}'_{ii,CE,n=19}$, $\underline{Z}'_{ik,CE,n=19}$) are taken as reference values and the relative deviation of

other impedance evaluations to these values are shown. The discussed evaluations are self and mutual impedances with earth return.

- $\underline{Z}'_{ii,CE,n=0}$, $\underline{Z}'_{ik,CE,n=0}$ with the simplified Carson formulas (2.54),(2.55)
- $\underline{Z}'_{ii,CE,n=1}$, $\underline{Z}'_{ik,CE,n=1}$ with the Carson formula with a termination after the 2nd term of C_R and C_X (2.52), (2.53)
- $\underline{Z}'_{ii,DE}$, $\underline{Z}'_{ik,DE}$ formulas of Dubanton with original complex earth return depth \underline{p} (2.57), (2.58), (2.59)
- $\underline{Z}'_{ii,DE,mod}$, $\underline{Z}'_{ik,DE,mod}$ formulas of Dubanton with modified complex earth return depth \underline{p}' (2.57), (2.58), (2.60)

The relative deviations are shown for the absolute value (solid), as well as the real (dashed) and imaginary part (dotted). The values of h_i , h_k and d_{ik} are chosen according to [55] in order to be comparable.

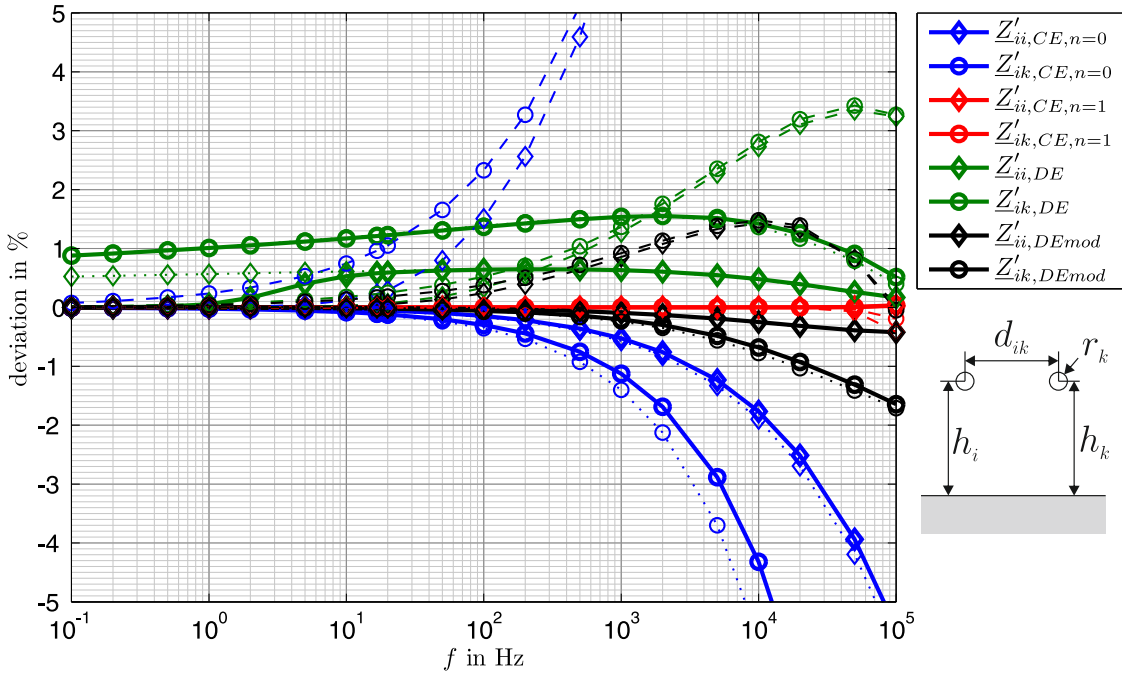


Figure 2.21: Deviation in % of the absolute value (solid) as well as the real (dashed) and the imaginary (dotted) part of the self and mutual impedances with earth return with different formulas, constant parameters (conductor AL/St 635/117) $R'_i = 0.052 \Omega/\text{km}$, $L'_i = \mu_0/(8\pi)$, $r_i = r_k = 15 \text{ mm}$, $h_i = h_k = 10 \text{ m}$, $d_{ik} = 5 \text{ m}$, $\rho_E = 100 \Omega\text{m}$ and varying frequency f

Typically for the impedance evaluation of railways and three-phase power supply systems the frequency range of up to 2 kHz is interesting, especially when harmonics have

to be taken into account. It can be seen, that the original and modified Dubanton formulas ($Z'_{ii,DE}$, $Z'_{ik,DE}$, $Z'_{ii,DE,mod}$, $Z'_{ik,DE,mod}$) have smaller deviations especially for $f > 100$ Hz compared to the simplified Carson formulas (2.54), (2.55). If correction terms up to the order of 2 for Carson formulas are considered ($Z'_{ii,CE,n=1}$, $Z'_{ik,CE,n=1}$), the deviation in the chosen diagram is always smaller than with other formulas. A significant difference between consideration of correction terms until the order of 20 or order of 2 starts at 200 kHz.

The corresponding reference values of the impedances are shown in fig. 2.22.

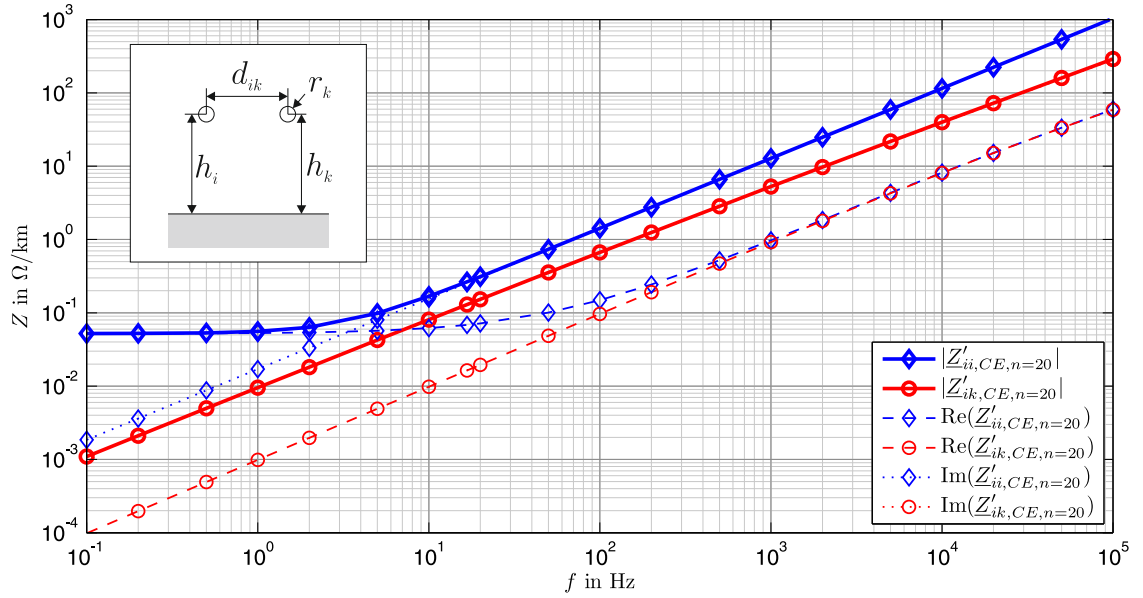


Figure 2.22: Absolute value (solid), real (dashed) and imaginary part (dotted) of the self and mutual impedances with earth return determined with Carson formula considering terms up to the order of 20, constant parameters (conductor AL/St 635/117) $R'_i = 0.052 \Omega/\text{km}$, $L'_i = \mu_0/(8\pi)$, $r_i = r_k = 15$ mm, $h_i = h_k = 10$ m, $d_{ik} = 5$ m, $\rho_E = 100 \Omega\text{m}$ and varying frequency f

In fig. 2.21 and 2.22 the conductors are arranged horizontal. For a vertical configuration of the conductors (e.g. $h_i=10\text{m}$, $h_k=15\text{m}$, no horizontal distance) the deviation to fig. 2.21 and 2.22 are very small, and therefore these figures are not shown here.

Fig. 2.21 and 2.22 were made for a rather small distance d_{ik} of 5 m between the conductors and heights $h_i = h_k$ of 10 m above ground. For the evaluation of screening effects through passive conductors in bigger distance to the field source, it is necessary to know the dependency of the mutual impedances $Z_{ik,E}$ for different distances and earth resistivity. Therefore in fig. 2.23 the absolute value, as well as real and imaginary part of the mutual impedance for three different frequencies is provided. In compliance with [29] here the heights of the conductors are chosen with $h_i = h_k = 0$ m.

It can be seen that at a certain distance d_{ik} , depending on the frequency, the impedances calculated with smaller orders of considered terms (e.g. $n=2, 3, 4, \dots$), are drifting away, while the formula of Dubanton has smaller deviation for $d_{ik} > \delta_E$ than the simplified formulas. That is the reason why, in [29] and [55] it is considered to use other simplified formulas for mutual impedances for $d_{ik} > \delta_E$. Because for field calculations such distances are much higher than interesting distances to a field source, these formulas are not part of these thesis. Further as a consequence of this analysis, in the further course, the modified formula of Dubanton is used for impedance calculations in this dissertation. This is mainly because of the simplicity compared to Carson terms of higher order and little deviations compared to the simplified Carson formula. For further completeness

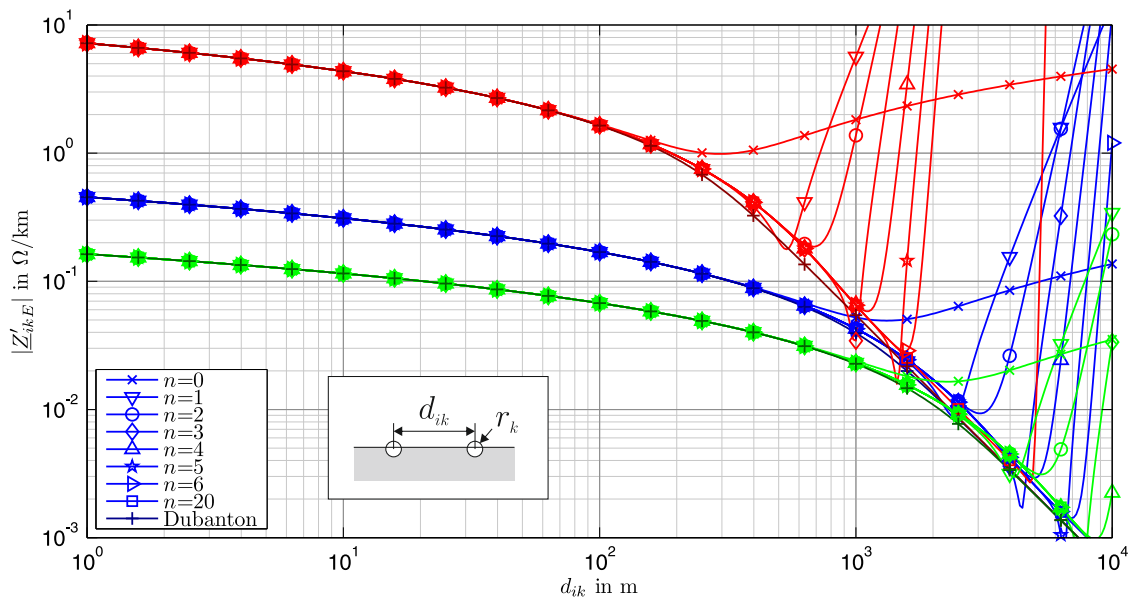


Figure 2.23: Absolute value of the mutual impedance with earth return determined with Carson formula ($Z_{ik,CE}$) considering correction terms C_R and C_X up to different orders ($n = 1, 2, 3, 4, 5, 6, 20$) and with the formula from Dubanton (original), constant parameters are $h_i = h_k = 0$ m, $\rho_E = 200$ Ω m for 2 different frequencies $f = 50$ Hz (blue), $f = 16.7$ Hz (green) and $f = 1000$ Hz (red) and varying d_{ik}

in fig. 2.24 the dependency of the mutual impedance on the specific earth resistivity ρ_E is given. As can be seen, the specific earth resistivity ρ_E has little effects on the absolute value of the real part of the mutual impedance, especially for small distances $d_{ik} < 100$ m.

Nevertheless, the real effect on the actual magnetic field in the vicinity of the field source, cannot be read from that graphs. Therefore in section 3.3 the effect of an earth wire on the magnetic field with variations of these parameters among others is shown. The effect of the current distribution on railway systems is given in sec. 4.2.2.

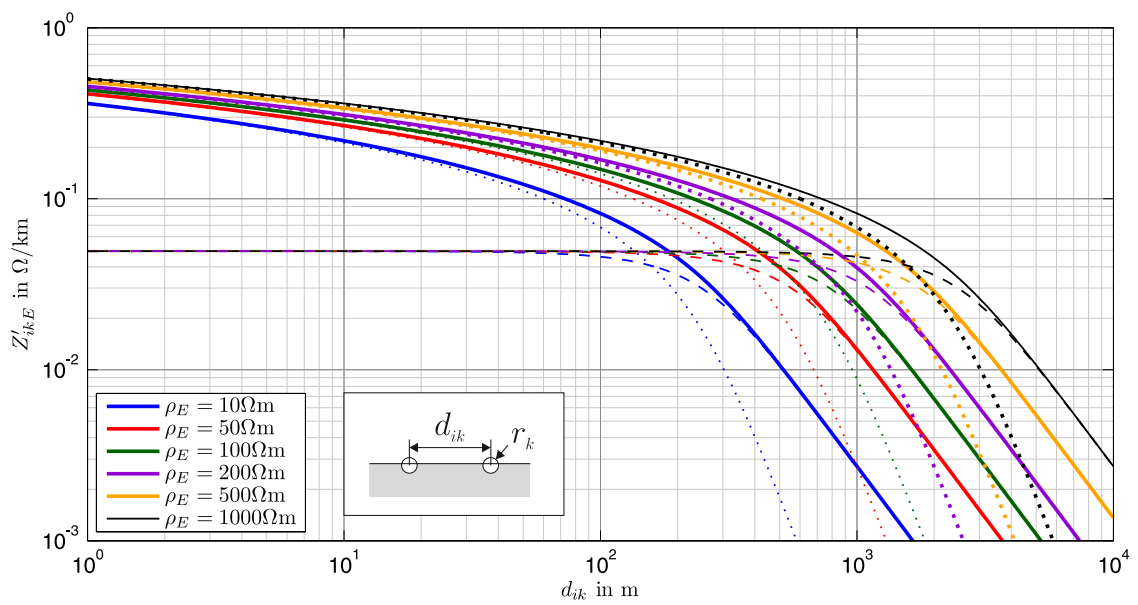


Figure 2.24: Absolute value (solid), real (dashed) and imaginary part (dotted) of the mutual impedance with earth return determined with Dubanton formula, constant parameters are $h_i = h_k = 0$ m, $x_i = 0$ m, $f = 50$ Hz for different specific earth resistances ρ_E and varying d_{ik}

3 Chapter 3

Parameters and EMF of Three-Phase Systems

3.1 Conductor Arrangements of OHL and UGL

In order to describe the influences of different parameters on electric and magnetic fields some OHL tower types and cable conductor configuration are chosen as reference values.

The reference currents for the investigations are chosen with 1000 A, because then, the resulting magnetic flux density can easily be converted to other currents. Only if the rated current of a system is far from that 1000 A, e.g. for low voltage cables, this current is adapted. The line voltages are always chosen as the maximum operation voltage depending on the voltage level according to [1]. The most important values of the maximum phase-to-phase voltages are 420 kV for a voltage level of 380 kV/400 kV, 245 kV for a 220 kV network and 123 kV for a 110 kV network. If not given separately, all three-phase circuits are symmetrical. If there is more than one three-phase circuits, all circuits are equally loaded.

3.1.1 OHL Conductor Arrangements

The heights of the conductors along the line axis are not constant for OHLs because of the sag s , varying heights of towers and non-planar ground. In order to compare line conductor configurations independently from the actual height of the towers and the ground level, the conductor configurations are unified by using for all configurations the same height of the lowest conductor h_l . All other heights of the conductors are determined according to this value and the tower configuration. In fig. 3.1 one possible height of the lowest conductor within a span and the corresponding conductor positions are shown. The chosen value of $h_l = 10$ m is a compromise between typical minimum heights at maximum sag of about 8 m for 110 kV line and of about 12 m for 380 kV lines .

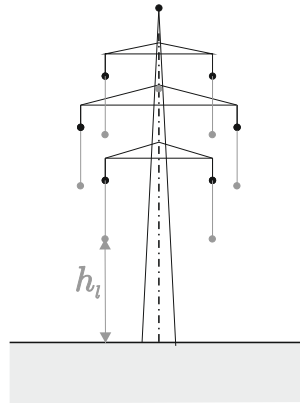


Figure 3.1: Sketch for the definition of h_l , the height of the lowest conductor to ground, which can vary along the line axis

In fig. 3.2 some possible configurations for single circuit overhead lines with one or two earth wires are given. For the voltage level of 110 kV the typical positions of the conductors can be taken from tab. 3.1.

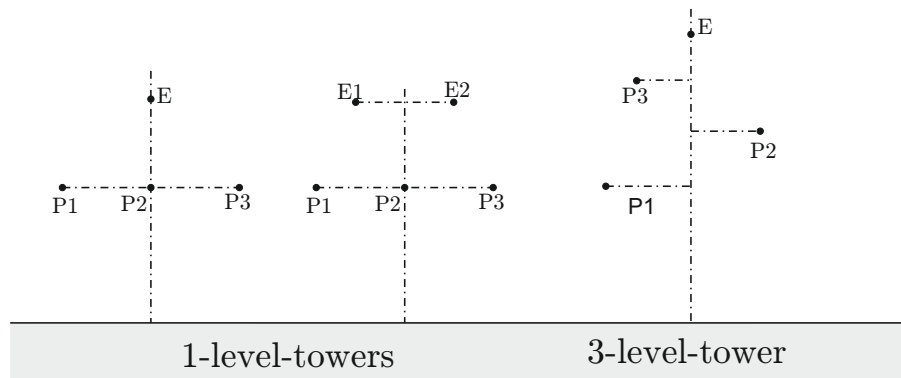


Figure 3.2: Some tower types for a single circuit OHL

A categorisation of typical double circuit OHLs is shown in fig. 3.3. A common term for the 3-level-tower is 'ton'. The 2-level-tower is further called 'Danube', if the lowest arm is shorter than the second and 'tan' if the lowest arm is longer than the second. In this thesis several existing cross sections of Austrian high voltage OHLs were analysed. The results of minimum and maximum values of the parameters from fig. 3.3, separated according to voltage level and tower type are given in tab. 3.2.

Exemplary for typical Austrian double circuits lines the conductor positions according to [61] which are used in the following, are given in tab. 3.3, separated for voltage levels 110 kV, 220 kV and 380 kV.

Table 3.1: Positions of conductors for single circuit 110 kV towers according to fig. 3.2, EW...earth wire

Position	1-level, 1 EW		1-level, 2 EW		3-level, 1 EW	
	x	h	x	h	x	h
P1	-5.0	10.0	-5.0	10.0	-4.7	10.0
P2	0.0	10.0	0.0	10.0	4.1	15.0
P3	5.0	10.0	5.0	10.0	-3.5	20.0
E (E1)	0.0	14.0	-3.0	14.0	0.0	25.0
E2	-	-	3.0	14.0	-	-

Table 3.2: Maximum and minimum dimensions according to fig. 3.3 from existing Austrian double circuits OHLs

voltage level	tower type	110 kV			220 kV		380 kV	
		3-level	2-level	1-level	3-level	2-level	3-level	2-level
a	min	6.4	5.2	5.7	11.0	10.0	13.8	14.0
	max	8.4	6.8	6.4	12.0	14.8	19.0	15.2
b	min	6.4	12.4	12.9	14.0	20.4	18.8	25.4
	max	11.2	14.4	14.6	16.0	25.4	24.0	27.2
c	min	4.4	8.8	20.0	10.0	15.4	12.8	14.0
	max	6.6	10.4	23.0	11.0	20.1	15.0	19.8
d	min	3.2	0.0	0.0	6.1	0.0	7.2	0.0
	max	6.5	0.0	0.0	7.0	0.0	9.5	0.0
e	min	3.2	4.0	0.0	6.7	6.5	8.5	9.0
	max	6.5	4.3	0.0	7.0	9.5	9.6	11.5
f	min	3.1	4.7	5.0	5.5	6.5	6.5	8.6
	max	5.6	6.9	8.4	9.3	13.7	12.3	13.5

Table 3.3: Reference dimension according to fig. 3.3 for the following analysis of different towers

	110 kV		220 kV		380 kV	
	3-level	2-level	3-level	2-level	3-level	2-level
a	7.5	5.5	11.0	10.0	17.0	15.0
b	9.0	12.7	14.0	22.0	23.0	26.0
c	6.0	9.1	10.0	16.0	15.0	20.0
d	4.5	0.0	6.0	0.0	8.0	0.0
e	5.0	4.3	7.0	6.5	9.5	9.0
f	5.5	7.0	8.5	8.0	11.5	13.5

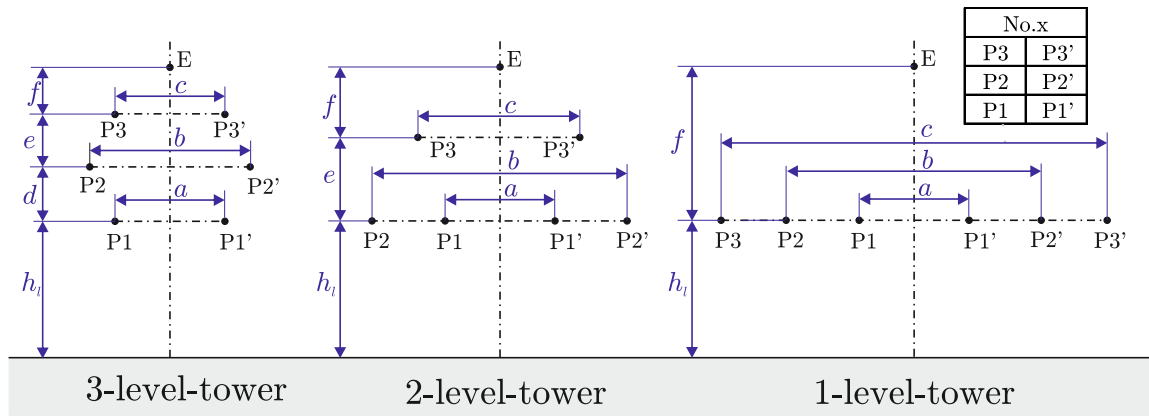


Figure 3.3: Three principal conductor arrangements (tower types) for three-phase double circuit OHLs

3.1.2 UGL Conductor Arrangements

In fig. 3.4 some typical double circuit cable configurations are sketched. The vertical configuration is typical for a cable tunnel. The horizontal configuration is the most common configuration for laying in earth. The triangle configuration is often presented as an alternative for the horizontal configuration, with its advantage of lower magnetic fields. Due to the screening of the earth and of the cable shields, the electric field above ground can be neglected and is not analysed further.

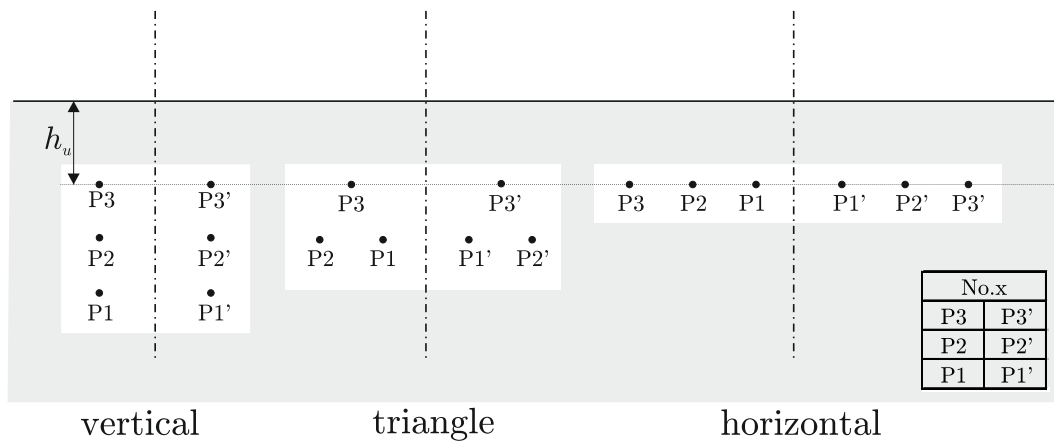


Figure 3.4: Three principal conductor arrangements for three-phase double circuit UGLs, h_u ...height of the uppermost conductor

The distance between the phases and the installation depth are limited by the thermal rated current of the cables. The greater the current and the deeper the installation depth, the greater the distance between the two phases has to be, in order to ensure the

dissipation of thermal losses and to avoid overheating. On the other hand, with increasing distance between the phases, also the magnetic flux density increases. According to [56] for a typical 380 kV cable configuration with a rated operation current of 2279 A for a single circuit and 1671 A per circuit for a double circuit line, the distance between conductors is between 0.5 m for laying in earth, 0.8 m for an installation in pipes and about 1.1 m for a gas insulated line (GIL). The installation depth is typically at 1.5 m. For double circuit installations, the distance between 2 circuits is between 1.5 m and 2 m.

3.2 Phase Allocation

Phasing is - strictly speaking - the allocation of the electrical phases (L1, L2, L3) to the conductor positions (P1, P2, P3) of three-phase lines. Typically these phase allocations are defined during transposition. To avoid asymmetries of the operating parameters (capacitances, impedances) all high voltage overhead lines of significant length are divided into three more or less equal sections where each circuit is cyclically exchanged. Therefore typically the field relevant phasing remains constant along the whole line. The allocation of the phases on fixed conductor positions has a significant effect on the electric and the magnetic field in the vicinity of a line if there are more than one three-phase circuit.

For power cables it is not necessary to transpose the phases because the asymmetries of the operation parameters are negligible. Only for cables with shields, cross bonding is necessary, but this has no effect on the allocation of the phases. Anyhow, the actual position of the phases for multiple three-phase circuits within a cable trench has an effect on the magnetic flux density in vicinity of these cables.

3.2.1 Phase Allocation for a Single Circuit Line

Theoretical there are six possibilities for allocating the three phases L1, L2 and L3 on three conductor positions P1, P2 and P3 as shown in tab. 3.4. Variation (var.) 2 and variation 3 can be achieved from variation 1 by cyclically exchanging the phases (L1 with L2, L2 with L3 and L3 with L1). Variation 4 is achieved from variation 1 by exchanging L2 and L3, which is equal to changing the rotation of the circuit. Variation 5 and variation 6 again are cyclically exchanges from variation 4. Hence, the variation can be grouped according to their rotation, in a category positive rotation and a category negative rotation.

For a start, the fields of the 1-level tower single circuit line according to fig. 3.2 without

any earth wire is discussed. In fig. 3.5 the vector curves (field ellipses) of the magnetic flux density $B(t)$ of this OHL with its 6 variations of the phase allocation are shown. It can be seen, that all ellipses have the same shape, therefore the same RMS- and peak-values. But, the starting points (circles $\omega t = 0$) and end points (dots $\omega t = 2\pi \cdot 0.98$) differ. The factor 0.98 for the endpoint is chosen in order to distinguish between starting and endpoint in the figure. Additionally, the field ellipses of variation 1 to variation 3 are traversed in the opposite direction than variation 4 to variation 6.

Table 3.4: All phasing possibilities for a single circuit line

		positive rotation			negative rotation		
		var. 1	var. 2	var. 3	var. 4	var. 5	var. 6
P3		L3	L1	L2	L2	L1	L3
P2		L2	L3	L1	L3	L2	L1
P1		L1	L2	L3	L1	L3	L2

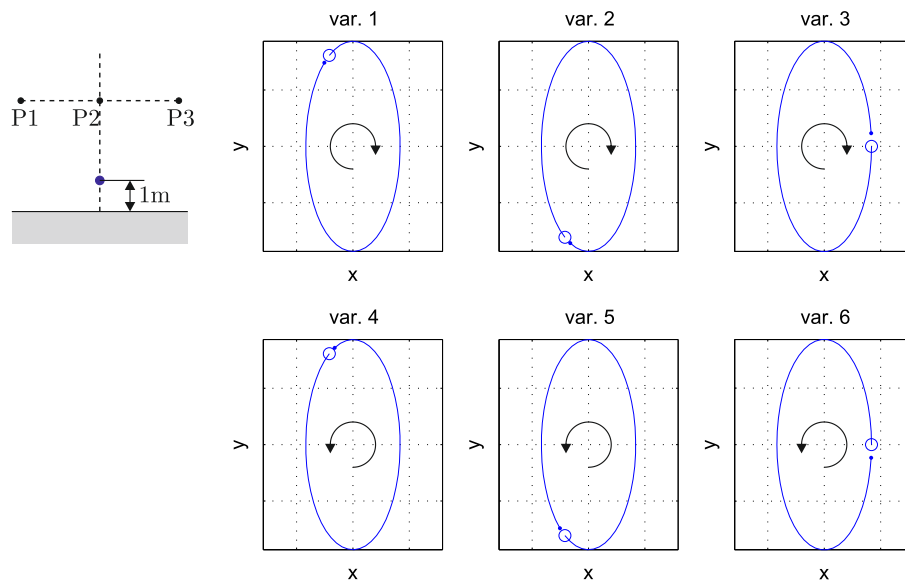


Figure 3.5: Vector curves of the magnetic flux density for a 1-level-tower at point $x=0$ m and $y=1$ m with different variations of the phases L1 to L3 according to tab. 3.4, start of the ellipses at $\omega t = 0$ ($\underline{I}_{L1} = 1200 \text{ A} \angle 0^\circ$, $\underline{I}_{L2} = 1200 \text{ A} \angle -120^\circ$, $\underline{I}_{L3} = 1200 \text{ A} \angle 120^\circ$) are marked with circles, the point $\omega t = 2\pi \cdot 0.98$ with dots

The equality of the form of the ellipses is only given as long no passive conductor as e.g. earth wires exist in vicinity of the line. The induced currents in the passive conductor-earth-loops effect the original magnetic flux density, for a positive rotating circuit in a different way than for a negative rotating circuit while cyclically exchanging has no effect. This impact is described in detail in the sec. 3.3.

3.2.2 Double Circuit Lines

As presented in [22], for a double circuit line there are 36 (6 times 6) different possibilities of allocation the phases on 6 given positions, considering, that the phases of one circuit do not change position with the phases of the other circuit (across the line axis).

Cyclically exchanging of the phases (L1 to L2, L2 to L3, L3 to L1) does not change the results of the electric field strength and the magnetic flux density in point of view of RMS-values or peak values as discussed above for a single circuit line. Without occurrence of a passive conductor, similarly to single circuit lines, also the exchanging of 2 phases, which results in a rotation in the opposite direction, does not influence the RMS- and peak values of the tower.

All possible allocations of the phases for double circuit three-phase lines are shown in tab. 3.5. The interpretation for a vertical conductor arrangement as for example for a 3-level tower is obvious. The six conductor positions P1, P2, P3, P1', P2', P3' according to fig. 3.3 are arranged as given in fig. 3.3 and fig. 3.4.

No.x	
P3	P3'
P2	P2'
P1	P1'

Figure 3.6: Arrangement of the six positions P1, P2, P3, P1', P2', P3' according to fig. 3.3 and fig. 3.4 for tab. 3.5

It can be seen, that the order of the conductor positions on the tower are numbered first from the center of the line outward and then bottom up, each circuit separately.

Bauhofer describes the effect of phasing in [10] too, while the author used Greek symbols in order to distinguish them. This corresponding labelling of the phasing is additionally given in the top of tab. 3.5.

It must be pointed out, that in this section it is assumed, that both circuits are equally loaded without any phase shifts, unbalances and harmonics, as it will be discussed later on. Also the effect of the earth wires is neglected here, but will be discussed in sec. 3.3. Only the phase positions in the first row of tab. 3.5 are analysed, because the other variations (variation 2 to variation 6) would lead to exactly the same field profile as variation 1 in sense of RMS-values.

OHL

For a 380 kV 2-level-tower the magnetic and electric fields were calculated for different phase positions No. 1 to No. 6. The isolines of each phase position are shown in fig. 3.7

Table 3.5: All phasing possibilities for a double circuit line

		γ No.1	ϑ No.2	η No.3	ζ No.4	β No.5	δ No.6
positive rotation	var. 1	L3 L3' L2 L2' L1 L1'	L2 L3' L3 L2' L1 L1'	L1 L3' L2 L2' L3 L1'	L3 L3' L1 L2' L2 L1'	L1 L3' L3 L2' L2 L1'	L2 L3' L1 L2' L3 L1'
	var. 2	L1 L1' L3 L3' L2 L2'	L3 L1' L1 L3' L2 L2'	L2 L1' L3 L3' L1 L2'	L1 L1' L2 L3' L3 L2'	L3 L2' L2 L1' L1 L3'	L1 L2' L3 L1' L2 L3'
	var. 3	L2 L2' L1 L1' L3 L3'	L1 L2' L2 L1' L3 L3'	L3 L2' L1 L1' L2 L3'	L2 L2' L3 L1' L1 L3'	L2 L1' L1 L3' L3 L2'	L3 L1' L2 L3' L1 L2'
negative rotation	var. 4	L2 L2' L3 L3' L1 L1'	L3 L2' L2 L3' L1 L1'	L1 L2' L3 L3' L2 L1'	L2 L2' L1 L3' L3 L1'	L1 L2' L2 L3' L3 L1'	L3 L2' L1 L3' L2 L1'
	var. 5	L1 L1' L2 L2' L3 L3'	L2 L1' L1 L2' L3 L3'	L3 L1' L2 L2' L1 L3'	L1 L1' L3 L2' L2 L3'	L3 L1' L1 L2' L2 L3'	L1 L3' L2 L1' L3 L2'
	var. 6	L3 L3' L1 L1' L2 L2'	L1 L3' L3 L1' L2 L2'	L2 L3' L1 L1' L3 L2'	L3 L3' L2 L1' L1 L2'	L2 L3' L3 L1' L1 L2'	L2 L1' L3 L2' L1 L3'

for the magnetic flux density and in fig. 3.9 for the electric field strength. The graph at the bottom of these figures represents the envelop curves of the highest values in each point for all phase positions. This graph is especially useful for a worst case evaluation of an OHL, where the actual phase arrangement is not known or might change.

In order to find the phase configuration, with the lowest magnetic flux density fig. 3.8 might offer assistance, or for electric field strength fig. 3.10.

There in subfigures (a) the magnetic flux density or the electric field strength 1 m above ground are shown.

In subfigure (b) the colours show, where a specific phase position would lead to the lowest magnetic field (fig. 3.8) or lowest electric field (fig. 3.10) compared to all other phase positions. For this type of tower, phase position No. 4 would lead to the lowest magnetic flux density in an area directly below the OHL, in a more distant area, but near ground No. 3 will lead to the lowest magnetic flux density. For the electric field strength the best configurations changes very often. Therefore other decision criteria are necessary, e.g. lowest maximum RMS-value of the electric field strength in an area 1 m above ground. It can be seen, that for that tower configuration and a height of the

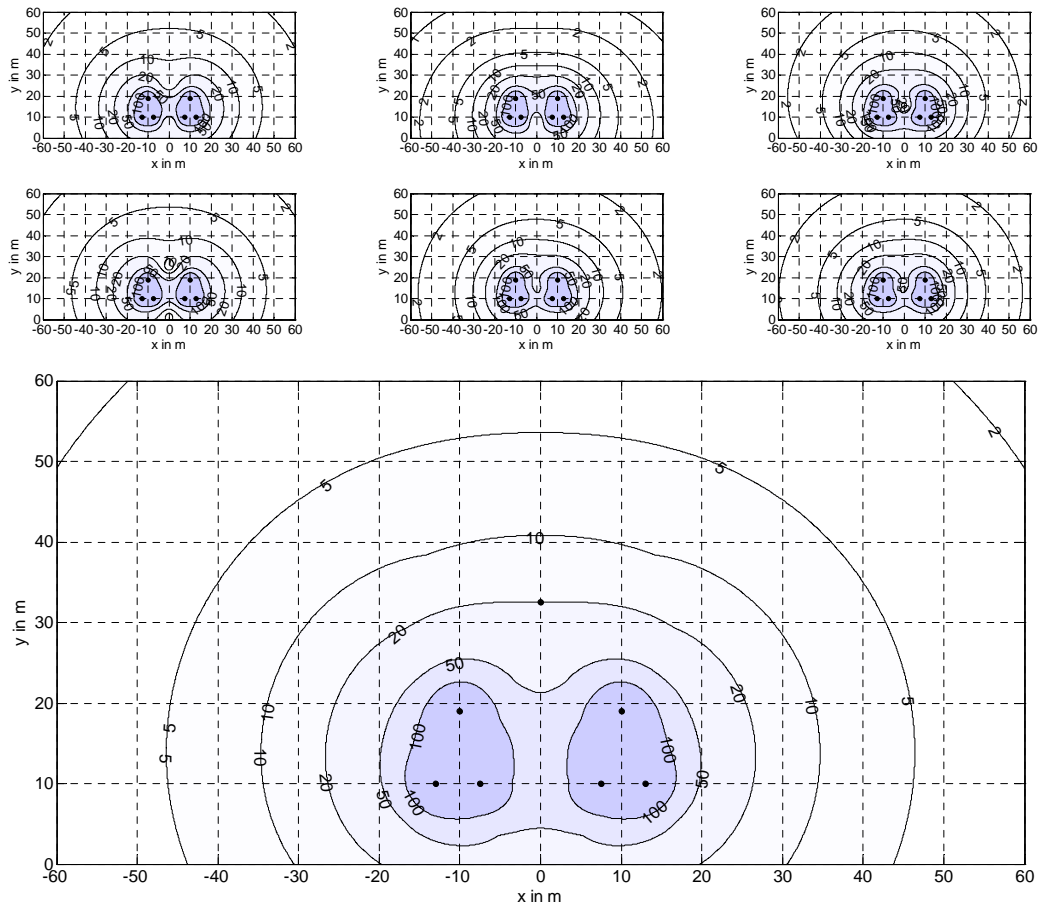


Figure 3.7: Isolines of the magnetic flux density (RMS-value) for different phase positions (from left to right and top to bottom No. 1 to No. 6) and the isolines of the worst case at the bottom, B_{rms} in μT

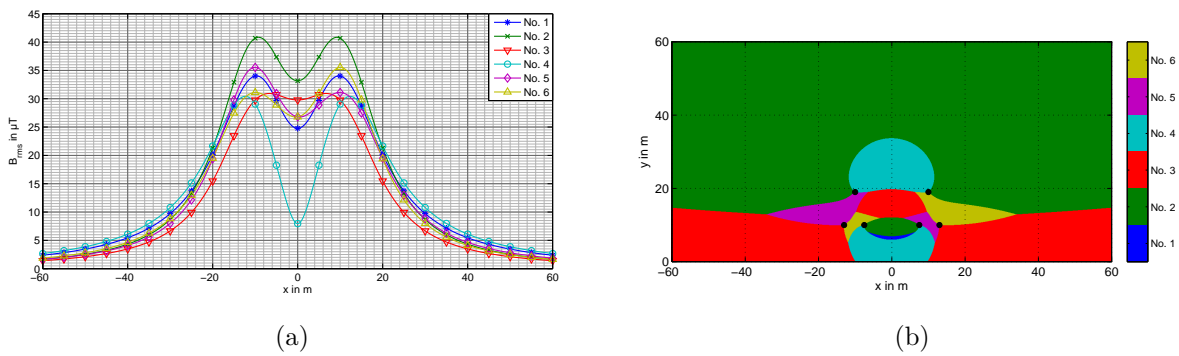


Figure 3.8: (a) Magnetic flux density, 1 m above ground area for different phase positions, (b) Areas, where the different phase allocation cases No. 1 to No. 6 cause the lowest values of magnetic flux density

lowest conductor $h_l = 10$ m phase configuration No. 3 will lead to the lowest maximum of 4.37 kV/m (without earth wire).

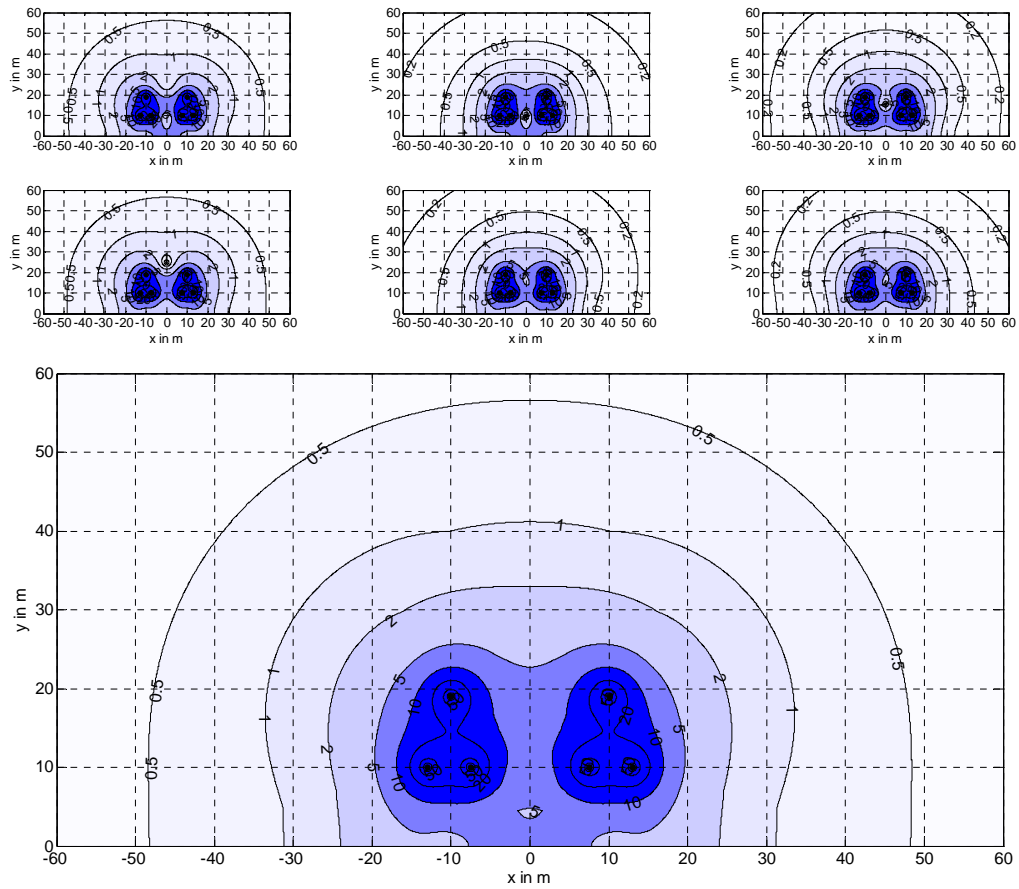


Figure 3.9: Isolines of the electric field strength (RMS-value) for different phase positions and the isolines of the worst case at the bottom, E_{rms} in kV/m

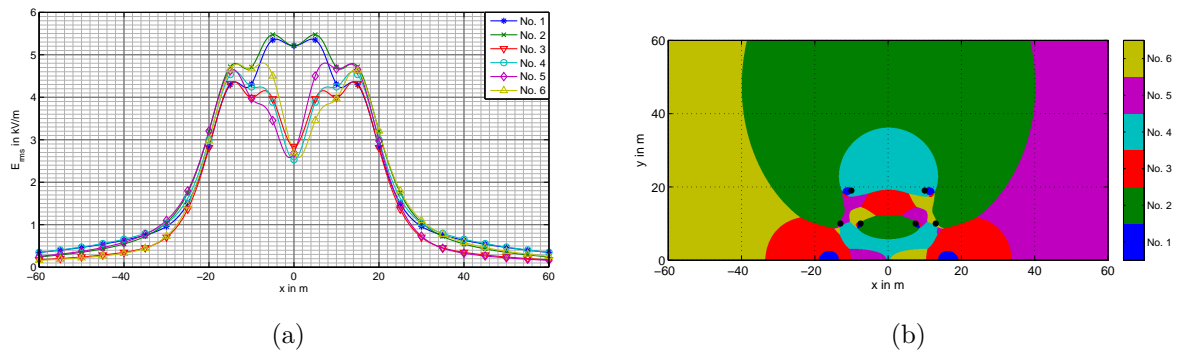


Figure 3.10: (a) Electric field strength, 1 m above ground area for different phase positions, (b) Areas, where the different phase allocation cases No. 1 to No. 6 cause the lowest values of electric field strength

The conclusion for this conductor arrangement is, that phase position No. 3 would be the best choice, considering the magnetic flux density in a distant point, and the maximum electric field strength 1 m above ground. However, with No. 3 higher magnetic

flux densities near the line axis would occur compared to the best configuration for that area (No. 4). Other criteria and conductor arrangements might lead to other choices. This circumstance is discussed more in detail in chapter 5.5 and in [25].

UGL

The matter of positioning the phases can also be discussed with double circuit cable configurations, only the study of the electric field strength becomes no longer necessary. In the following a double circuit underground cable system in horizontal configuration, with a distance between each conductor $d_{ik}=1$ m, installation depth $h_u=1.5$ m is analysed.

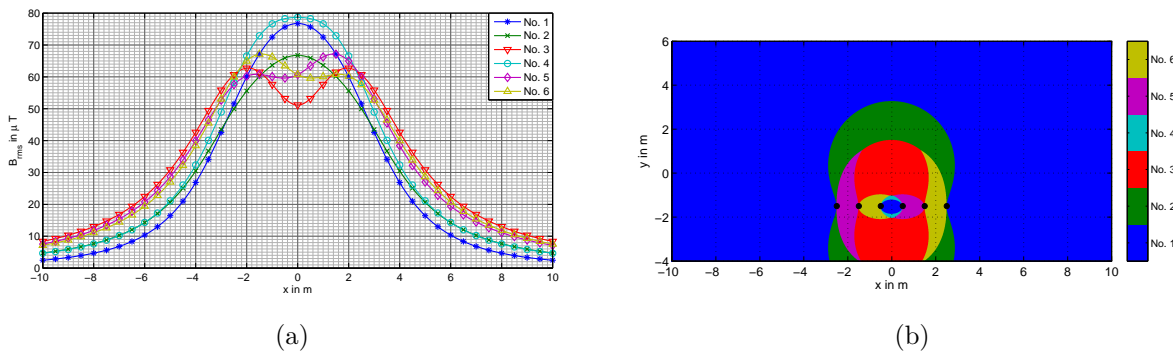


Figure 3.11: (a) Magnetic flux density, 1 m above ground area for different phase positions, (b) Areas where the different phase allocation cases No. 1 to No. 6 cause the lowest values of magnetic flux density of a double circuit underground line, horizontal configuration, distance between the conductors $d_{ik}=1$ m, installation depth $h_u=1.5$ m

Again, most interesting is the area above ground, where people and electronic equipment might be located. According to fig. 3.11 in a distant area (for distances of about >3 m from any conductor) phase position No. 1 will lead to the lowest magnetic flux densities. In an area near the conductors, or if the maximum magnetic flux density for phase position No. 1 above ground is close to the reference value, other configurations than for example No. 2 or No. 3 should be considered, because this configuration would lead to lower maximum magnetic flux densities.

3.2.3 Multiple Circuit Lines

When continuing the considerations of phase allocations for more than two circuits more and more possibilities arise. For n circuits, there are 6^n possibilities of allocating the phases on $3 \cdot n$ conductor positions, while only 6^{n-1} possibilities would lead to different field characteristics.

Nevertheless, this analysis makes only sense, if the circuits can be considered to be equally loaded, or in other terms, the symmetrical components of currents and voltages of each circuit are equal. This condition is very unlikely for OHL but for UGL e.g. three or more parallel circuits are more common. Because cables get more and more unwieldy when dimensioning them for higher transport capability and because of reliability, often they are split into several circuits. In the following for example all possible phase positions for three parallel UGL three-phase circuits are analysed.

In fig. 3.12 the conductor positions for the analysed cable configuration are shown, in tab. 3.6 the corresponding possible phase allocations are given, except the ones which would result from cyclically exchanging of all phases. The distances between the conductors within a circuit are 1 m, the distance between the center of the circuits is 3 m and the installation depth is 1.5 m below ground.

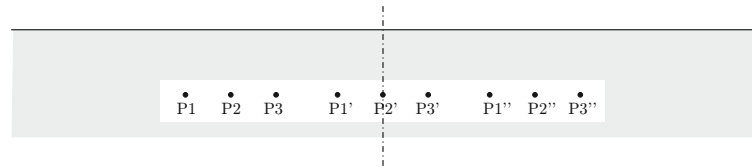


Figure 3.12: Conductor positions for an UGL with three circuits

Table 3.6: All phasing possibilities for a triple circuit line

<table border="1"> <tr><td>P3</td><td>P3'</td><td>P3''</td></tr> <tr><td>P2</td><td>P2'</td><td>P2''</td></tr> <tr><td>P1</td><td>P1'</td><td>P1''</td></tr> </table>	P3	P3'	P3''	P2	P2'	P2''	P1	P1'	P1''		<table border="1"> <tr><td>L3</td><td>L1</td><td>L3''</td></tr> <tr><td>L2</td><td>L2</td><td>L2''</td></tr> <tr><td>L1</td><td>L1'</td><td>L1''</td></tr> </table>	L3	L1	L3''	L2	L2	L2''	L1	L1'	L1''		<table border="1"> <tr><td>L2</td><td>L3</td><td>L3''</td></tr> <tr><td>L3</td><td>L2</td><td>L2''</td></tr> <tr><td>L1</td><td>L1'</td><td>L1''</td></tr> </table>	L2	L3	L3''	L3	L2	L2''	L1	L1'	L1''		<table border="1"> <tr><td>L1</td><td>L3</td><td>L3''</td></tr> <tr><td>L2</td><td>L2</td><td>L2''</td></tr> <tr><td>L3</td><td>L1'</td><td>L1''</td></tr> </table>	L1	L3	L3''	L2	L2	L2''	L3	L1'	L1''		<table border="1"> <tr><td>L3</td><td>L1</td><td>L3''</td></tr> <tr><td>L1</td><td>L2</td><td>L2''</td></tr> <tr><td>L2</td><td>L1'</td><td>L1''</td></tr> </table>	L3	L1	L3''	L1	L2	L2''	L2	L1'	L1''		<table border="1"> <tr><td>L1</td><td>L3</td><td>L3''</td></tr> <tr><td>L3</td><td>L2</td><td>L2''</td></tr> <tr><td>L2</td><td>L1'</td><td>L1''</td></tr> </table>	L1	L3	L3''	L3	L2	L2''	L2	L1'	L1''		<table border="1"> <tr><td>L2</td><td>L1</td><td>L3''</td></tr> <tr><td>L1</td><td>L2</td><td>L2''</td></tr> <tr><td>L3</td><td>L1'</td><td>L1''</td></tr> </table>	L2	L1	L3''	L1	L2	L2''	L3	L1'	L1''
P3	P3'	P3''																																																																									
P2	P2'	P2''																																																																									
P1	P1'	P1''																																																																									
L3	L1	L3''																																																																									
L2	L2	L2''																																																																									
L1	L1'	L1''																																																																									
L2	L3	L3''																																																																									
L3	L2	L2''																																																																									
L1	L1'	L1''																																																																									
L1	L3	L3''																																																																									
L2	L2	L2''																																																																									
L3	L1'	L1''																																																																									
L3	L1	L3''																																																																									
L1	L2	L2''																																																																									
L2	L1'	L1''																																																																									
L1	L3	L3''																																																																									
L3	L2	L2''																																																																									
L2	L1'	L1''																																																																									
L2	L1	L3''																																																																									
L1	L2	L2''																																																																									
L3	L1'	L1''																																																																									
<table border="1"> <tr><td>o</td><td>o</td><td>o</td></tr> </table>	o	o	o		<table border="1"> <tr><td>L3</td><td>L2</td><td>L3''</td></tr> <tr><td>L2</td><td>L1</td><td>L2''</td></tr> <tr><td>L1</td><td>L1'</td><td>L1''</td></tr> </table>	L3	L2	L3''	L2	L1	L2''	L1	L1'	L1''		<table border="1"> <tr><td>L1</td><td>L3</td><td>L3''</td></tr> <tr><td>L2</td><td>L2</td><td>L2''</td></tr> <tr><td>L3</td><td>L1'</td><td>L1''</td></tr> </table>	L1	L3	L3''	L2	L2	L2''	L3	L1'	L1''		<table border="1"> <tr><td>L3</td><td>L1</td><td>L3''</td></tr> <tr><td>L1</td><td>L2</td><td>L2''</td></tr> <tr><td>L2</td><td>L1'</td><td>L1''</td></tr> </table>	L3	L1	L3''	L1	L2	L2''	L2	L1'	L1''		<table border="1"> <tr><td>L1</td><td>L3</td><td>L3''</td></tr> <tr><td>L3</td><td>L2</td><td>L2''</td></tr> <tr><td>L2</td><td>L1'</td><td>L1''</td></tr> </table>	L1	L3	L3''	L3	L2	L2''	L2	L1'	L1''		<table border="1"> <tr><td>L2</td><td>L1</td><td>L3''</td></tr> <tr><td>L1</td><td>L2</td><td>L2''</td></tr> <tr><td>L3</td><td>L1'</td><td>L1''</td></tr> </table>	L2	L1	L3''	L1	L2	L2''	L3	L1'	L1''		<table border="1"> <tr><td>L2</td><td>L3</td><td>L3''</td></tr> <tr><td>L1</td><td>L2</td><td>L2''</td></tr> <tr><td>L3</td><td>L1'</td><td>L1''</td></tr> </table>	L2	L3	L3''	L1	L2	L2''	L3	L1'	L1''						
o	o	o																																																																									
L3	L2	L3''																																																																									
L2	L1	L2''																																																																									
L1	L1'	L1''																																																																									
L1	L3	L3''																																																																									
L2	L2	L2''																																																																									
L3	L1'	L1''																																																																									
L3	L1	L3''																																																																									
L1	L2	L2''																																																																									
L2	L1'	L1''																																																																									
L1	L3	L3''																																																																									
L3	L2	L2''																																																																									
L2	L1'	L1''																																																																									
L2	L1	L3''																																																																									
L1	L2	L2''																																																																									
L3	L1'	L1''																																																																									
L2	L3	L3''																																																																									
L1	L2	L2''																																																																									
L3	L1'	L1''																																																																									
<table border="1"> <tr><td>o</td><td>o</td><td>o</td></tr> </table>	o	o	o		<table border="1"> <tr><td>L3</td><td>L2</td><td>L1''</td></tr> <tr><td>L2</td><td>L1</td><td>L2''</td></tr> <tr><td>L1</td><td>L3'</td><td>L3''</td></tr> </table>	L3	L2	L1''	L2	L1	L2''	L1	L3'	L3''		<table border="1"> <tr><td>L2</td><td>L3</td><td>L1''</td></tr> <tr><td>L3</td><td>L2</td><td>L2''</td></tr> <tr><td>L1</td><td>L1'</td><td>L3''</td></tr> </table>	L2	L3	L1''	L3	L2	L2''	L1	L1'	L3''		<table border="1"> <tr><td>L1</td><td>L3</td><td>L1''</td></tr> <tr><td>L2</td><td>L2</td><td>L2''</td></tr> <tr><td>L3</td><td>L3'</td><td>L3''</td></tr> </table>	L1	L3	L1''	L2	L2	L2''	L3	L3'	L3''		<table border="1"> <tr><td>L3</td><td>L1</td><td>L1''</td></tr> <tr><td>L1</td><td>L2</td><td>L2''</td></tr> <tr><td>L2</td><td>L3'</td><td>L3''</td></tr> </table>	L3	L1	L1''	L1	L2	L2''	L2	L3'	L3''		<table border="1"> <tr><td>L1</td><td>L3</td><td>L1''</td></tr> <tr><td>L3</td><td>L2</td><td>L2''</td></tr> <tr><td>L2</td><td>L1'</td><td>L3''</td></tr> </table>	L1	L3	L1''	L3	L2	L2''	L2	L1'	L3''		<table border="1"> <tr><td>L2</td><td>L3</td><td>L1''</td></tr> <tr><td>L1</td><td>L2</td><td>L2''</td></tr> <tr><td>L3</td><td>L3'</td><td>L3''</td></tr> </table>	L2	L3	L1''	L1	L2	L2''	L3	L3'	L3''						
o	o	o																																																																									
L3	L2	L1''																																																																									
L2	L1	L2''																																																																									
L1	L3'	L3''																																																																									
L2	L3	L1''																																																																									
L3	L2	L2''																																																																									
L1	L1'	L3''																																																																									
L1	L3	L1''																																																																									
L2	L2	L2''																																																																									
L3	L3'	L3''																																																																									
L3	L1	L1''																																																																									
L1	L2	L2''																																																																									
L2	L3'	L3''																																																																									
L1	L3	L1''																																																																									
L3	L2	L2''																																																																									
L2	L1'	L3''																																																																									
L2	L3	L1''																																																																									
L1	L2	L2''																																																																									
L3	L3'	L3''																																																																									
<table border="1"> <tr><td>o</td><td>o</td><td>o</td></tr> </table>	o	o	o		<table border="1"> <tr><td>L3</td><td>L2</td><td>L3''</td></tr> <tr><td>L2</td><td>L1</td><td>L1''</td></tr> <tr><td>L1</td><td>L3'</td><td>L3''</td></tr> </table>	L3	L2	L3''	L2	L1	L1''	L1	L3'	L3''		<table border="1"> <tr><td>L2</td><td>L3</td><td>L3''</td></tr> <tr><td>L3</td><td>L2</td><td>L2''</td></tr> <tr><td>L1</td><td>L1'</td><td>L1''</td></tr> </table>	L2	L3	L3''	L3	L2	L2''	L1	L1'	L1''		<table border="1"> <tr><td>L1</td><td>L3</td><td>L3''</td></tr> <tr><td>L1</td><td>L2</td><td>L1''</td></tr> <tr><td>L3</td><td>L1'</td><td>L2''</td></tr> </table>	L1	L3	L3''	L1	L2	L1''	L3	L1'	L2''		<table border="1"> <tr><td>L3</td><td>L1</td><td>L3''</td></tr> <tr><td>L3</td><td>L2</td><td>L1''</td></tr> <tr><td>L2</td><td>L3'</td><td>L2''</td></tr> </table>	L3	L1	L3''	L3	L2	L1''	L2	L3'	L2''		<table border="1"> <tr><td>L1</td><td>L3</td><td>L3''</td></tr> <tr><td>L3</td><td>L2</td><td>L2''</td></tr> <tr><td>L2</td><td>L1'</td><td>L1''</td></tr> </table>	L1	L3	L3''	L3	L2	L2''	L2	L1'	L1''		<table border="1"> <tr><td>L2</td><td>L3</td><td>L3''</td></tr> <tr><td>L1</td><td>L2</td><td>L2''</td></tr> <tr><td>L3</td><td>L1'</td><td>L1''</td></tr> </table>	L2	L3	L3''	L1	L2	L2''	L3	L1'	L1''						
o	o	o																																																																									
L3	L2	L3''																																																																									
L2	L1	L1''																																																																									
L1	L3'	L3''																																																																									
L2	L3	L3''																																																																									
L3	L2	L2''																																																																									
L1	L1'	L1''																																																																									
L1	L3	L3''																																																																									
L1	L2	L1''																																																																									
L3	L1'	L2''																																																																									
L3	L1	L3''																																																																									
L3	L2	L1''																																																																									
L2	L3'	L2''																																																																									
L1	L3	L3''																																																																									
L3	L2	L2''																																																																									
L2	L1'	L1''																																																																									
L2	L3	L3''																																																																									
L1	L2	L2''																																																																									
L3	L1'	L1''																																																																									
<table border="1"> <tr><td>o</td><td>o</td><td>o</td></tr> </table>	o	o	o		<table border="1"> <tr><td>L3</td><td>L1</td><td>L1''</td></tr> <tr><td>L2</td><td>L3</td><td>L3''</td></tr> <tr><td>L1</td><td>L1'</td><td>L2''</td></tr> </table>	L3	L1	L1''	L2	L3	L3''	L1	L1'	L2''		<table border="1"> <tr><td>L2</td><td>L3</td><td>L1''</td></tr> <tr><td>L3</td><td>L2</td><td>L3''</td></tr> <tr><td>L1</td><td>L1'</td><td>L2''</td></tr> </table>	L2	L3	L1''	L3	L2	L3''	L1	L1'	L2''		<table border="1"> <tr><td>L1</td><td>L3</td><td>L1''</td></tr> <tr><td>L2</td><td>L2</td><td>L3''</td></tr> <tr><td>L3</td><td>L1'</td><td>L2''</td></tr> </table>	L1	L3	L1''	L2	L2	L3''	L3	L1'	L2''		<table border="1"> <tr><td>L3</td><td>L1</td><td>L1''</td></tr> <tr><td>L1</td><td>L2</td><td>L3''</td></tr> <tr><td>L2</td><td>L1'</td><td>L2''</td></tr> </table>	L3	L1	L1''	L1	L2	L3''	L2	L1'	L2''		<table border="1"> <tr><td>L1</td><td>L3</td><td>L1''</td></tr> <tr><td>L3</td><td>L2</td><td>L3''</td></tr> <tr><td>L2</td><td>L1'</td><td>L2''</td></tr> </table>	L1	L3	L1''	L3	L2	L3''	L2	L1'	L2''		<table border="1"> <tr><td>L2</td><td>L3</td><td>L1''</td></tr> <tr><td>L1</td><td>L2</td><td>L3''</td></tr> <tr><td>L3</td><td>L1'</td><td>L2''</td></tr> </table>	L2	L3	L1''	L1	L2	L3''	L3	L1'	L2''						
o	o	o																																																																									
L3	L1	L1''																																																																									
L2	L3	L3''																																																																									
L1	L1'	L2''																																																																									
L2	L3	L1''																																																																									
L3	L2	L3''																																																																									
L1	L1'	L2''																																																																									
L1	L3	L1''																																																																									
L2	L2	L3''																																																																									
L3	L1'	L2''																																																																									
L3	L1	L1''																																																																									
L1	L2	L3''																																																																									
L2	L1'	L2''																																																																									
L1	L3	L1''																																																																									
L3	L2	L3''																																																																									
L2	L1'	L2''																																																																									
L2	L3	L1''																																																																									
L1	L2	L3''																																																																									
L3	L1'	L2''																																																																									
<table border="1"> <tr><td>o</td><td>o</td><td>o</td></tr> </table>	o	o	o		<table border="1"> <tr><td>L3</td><td>L3</td><td>L2''</td></tr> <tr><td>L2</td><td>L1</td><td>L1''</td></tr> <tr><td>L1</td><td>L1'</td><td>L3''</td></tr> </table>	L3	L3	L2''	L2	L1	L1''	L1	L1'	L3''		<table border="1"> <tr><td>L2</td><td>L3</td><td>L2''</td></tr> <tr><td>L3</td><td>L2</td><td>L1''</td></tr> <tr><td>L1</td><td>L1'</td><td>L3''</td></tr> </table>	L2	L3	L2''	L3	L2	L1''	L1	L1'	L3''		<table border="1"> <tr><td>L1</td><td>L3</td><td>L2''</td></tr> <tr><td>L2</td><td>L2</td><td>L1''</td></tr> <tr><td>L3</td><td>L3'</td><td>L3''</td></tr> </table>	L1	L3	L2''	L2	L2	L1''	L3	L3'	L3''		<table border="1"> <tr><td>L3</td><td>L1</td><td>L3''</td></tr> <tr><td>L1</td><td>L2</td><td>L1''</td></tr> <tr><td>L2</td><td>L1'</td><td>L2''</td></tr> </table>	L3	L1	L3''	L1	L2	L1''	L2	L1'	L2''		<table border="1"> <tr><td>L1</td><td>L3</td><td>L2''</td></tr> <tr><td>L3</td><td>L2</td><td>L3''</td></tr> <tr><td>L2</td><td>L1'</td><td>L1''</td></tr> </table>	L1	L3	L2''	L3	L2	L3''	L2	L1'	L1''		<table border="1"> <tr><td>L2</td><td>L3</td><td>L2''</td></tr> <tr><td>L1</td><td>L2</td><td>L1''</td></tr> <tr><td>L3</td><td>L1'</td><td>L3''</td></tr> </table>	L2	L3	L2''	L1	L2	L1''	L3	L1'	L3''						
o	o	o																																																																									
L3	L3	L2''																																																																									
L2	L1	L1''																																																																									
L1	L1'	L3''																																																																									
L2	L3	L2''																																																																									
L3	L2	L1''																																																																									
L1	L1'	L3''																																																																									
L1	L3	L2''																																																																									
L2	L2	L1''																																																																									
L3	L3'	L3''																																																																									
L3	L1	L3''																																																																									
L1	L2	L1''																																																																									
L2	L1'	L2''																																																																									
L1	L3	L2''																																																																									
L3	L2	L3''																																																																									
L2	L1'	L1''																																																																									
L2	L3	L2''																																																																									
L1	L2	L1''																																																																									
L3	L1'	L3''																																																																									

In analogy to fig. 3.11 the magnetic flux density 1 m above ground and the areas where the phase corresponding phase allocation (numbered as shown in tab. 3.6) is given in fig. 3.13. It can be seen, that the lowest maximum of the magnetic flux density at 1 m

height can be reached with phase position No. 1. Unfavourably, in a distant area, exactly this configuration would lead to the highest magnetic flux density. For distant areas on the left side, phase position No. 3 and for distant areas on the right side phase position No. 13 would lead to the lowest magnetic flux densities. This can also be figured out with help of fig. 3.14.

If a worst case investigation is necessary, the variation of all these 36 phase allocations can be rather extensive. For that case, it is faster, to evaluate in a first step the RMS-values of each circuit (dashed lines in fig. 3.13) separately and build the sum of them (solid black line in fig. 3.13). As it is shown later on for other conditions (e.g. sec. 3.6), this non-vectorial summation will always lead to the worst case and no phase allocation has to be considered.

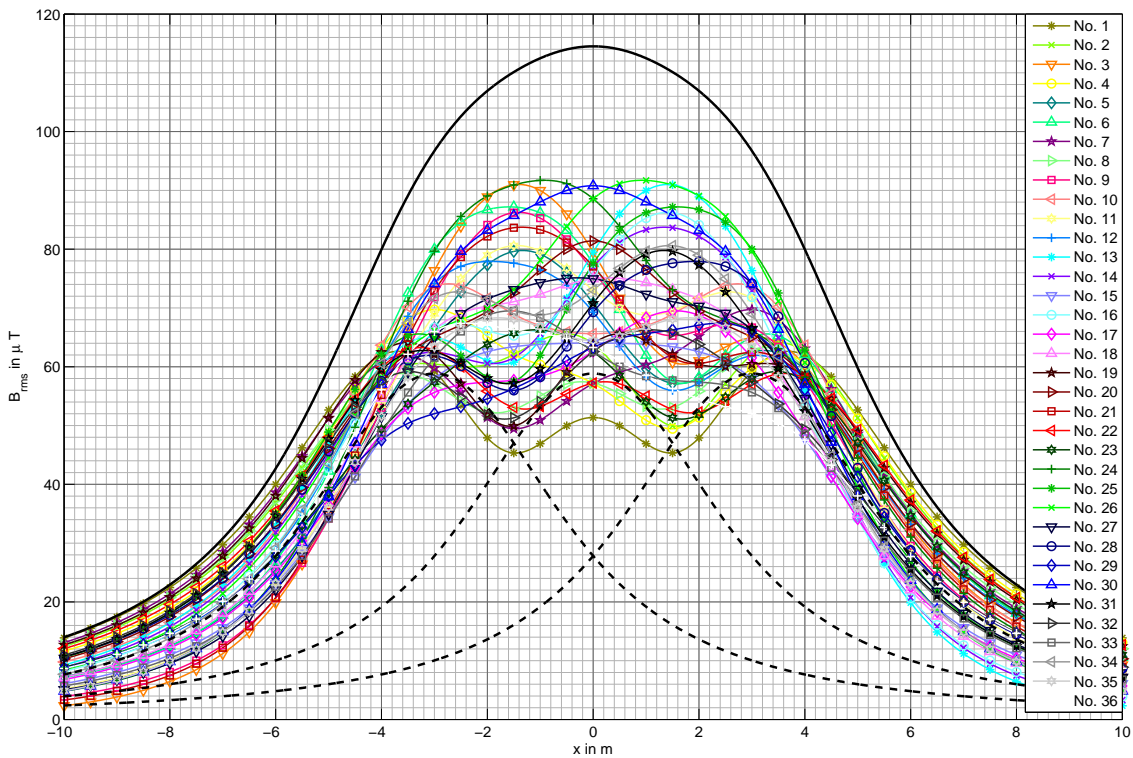


Figure 3.13: Magnetic flux density 1 m above ground above an UGL with three circuits for different phase allocations according to tab. 3.6

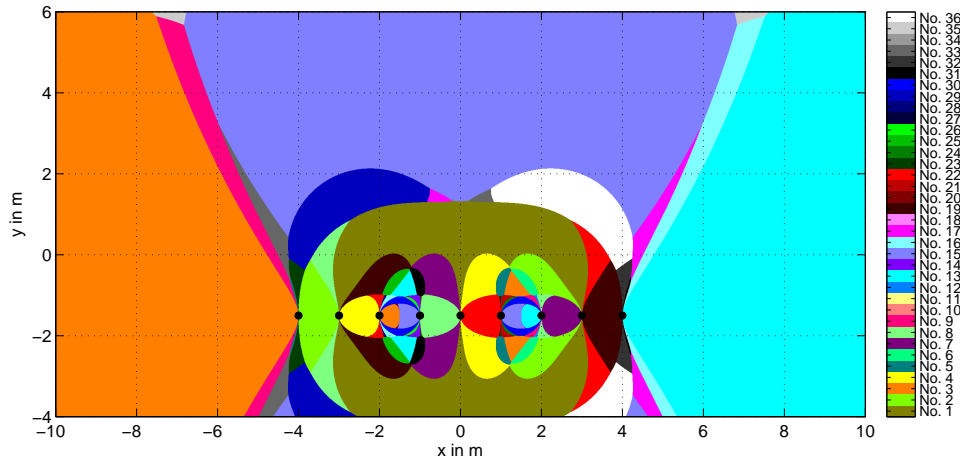


Figure 3.14: Areas where the different phase allocation cases No. 1 to No. 36 cause the lowest values of magnetic flux density of an UGL with three circuits according to tab. 3.6

3.3 Influence of the Earth Wire or Other Passive Conductors on the Electric and Magnetic Field

The existences of passive conductors influences the electric and magnetic field in the vicinity of lines. As described in sec. 2.4 in a low impedance conductor loop current is induced due to alternating magnetic fields in vicinity. This induced current counteracts the original magnetic field. The resulting magnetic flux density is slightly deformed compared to the original field. In some areas the effective magnetic flux density increases, in other areas it decreases, depending on the geometrical configuration of the conductors.

The current in the earth wire, and therefore the effect on the magnetic field, is dependent on the resistance of the earth wire, the position of the earth wire, the specific resistivity of the earth and the geometry of the tower. Additionally also the earthing resistance of the towers changes the results, but then the earth wire has to be modelled as a lattice network. For analysing the influence on the magnetic field this can be neglected for a first step.

To see the effect of a single earth wire on the magnetic flux density, the deviation *dev* according to (3.1) is calculated for a single circuit OHL, variation 1 while changing different parameters (resistivity and height of the earth wire, resistivity of the earth). The deviations for the 1-level-tower from fig. 3.2 are shown in fig. 3.15.

$$dev = B_{rms}(\text{with EW}) - B_{rms}(\text{without EW}) \quad (3.1)$$

It can be seen, that this absolute deviation dev decreases with the distance to the earth wire, and cannot be given as a constant factor. For the negative rotating system (var. 4 to var. 6 in tab. 3.4) the deviation would be mirrored to the y -axis at $x=0$ m. The absolute value of the current in the earth wire for the given configuration ranges between 2 A to 40 A per 1000 A phase current. Further, the influence of the specific earth resistance is only minimal compared to the influence of the resistance of the earth wire itself. The lower the resistance of the earth wire/earth - loop, the higher the influence directly below the line.

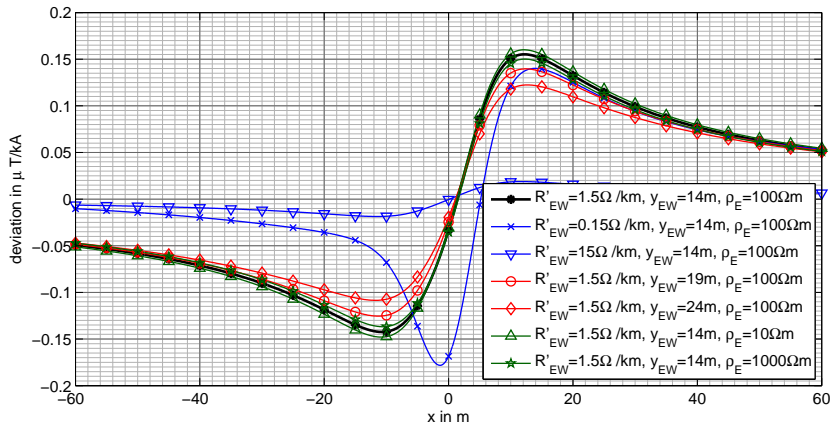


Figure 3.15: Deviation $dev = B_{rms}(\text{with EW}) - B_{rms}(\text{without EW})$ of the magnetic flux density at 1 m above ground with an earth wire (different parameters) to the magnetic flux density without any earth wire, R'_{EW} ...resistivity of the earth wire per unit length, y_{EW} ...height above ground of the earth wire, ρ_E ...specific earth resistivity

In fig. 3.16 the influence of positive and negative rotating system are compared for one parameter set of earth and earth wire. In the green areas, the earth wire reduces the magnetic flux density without any earth wire, in blue areas, the field with earth wire is higher than without any earth wire. Unsurprisingly, the effect is the same with two earth wires, which is shown in fig. 3.17.

In fig. 3.18 and fig. 3.19 the effect on the magnetic flux density and electric field strength for a double circuit line 380 kV OHL type Danube, at 1 m above ground can be seen. Depending on phase position (No. 1 to No. 6) and rotation (pos, neg) the magnetic flux density changes up to about $\pm 0.4 \mu\text{T}$ per kA.

The rotation does not effect the influence of the earth wire on the electric field strength. Nevertheless, the influence of an earth wire on the electric field strength is up to about $\pm 100 \text{ V/m}$ for this 380 kV line.

For worst case estimations it is important to know, that the earth wire does not only reduce the magnetic and electric field in all areas. Therefore an assumption that the

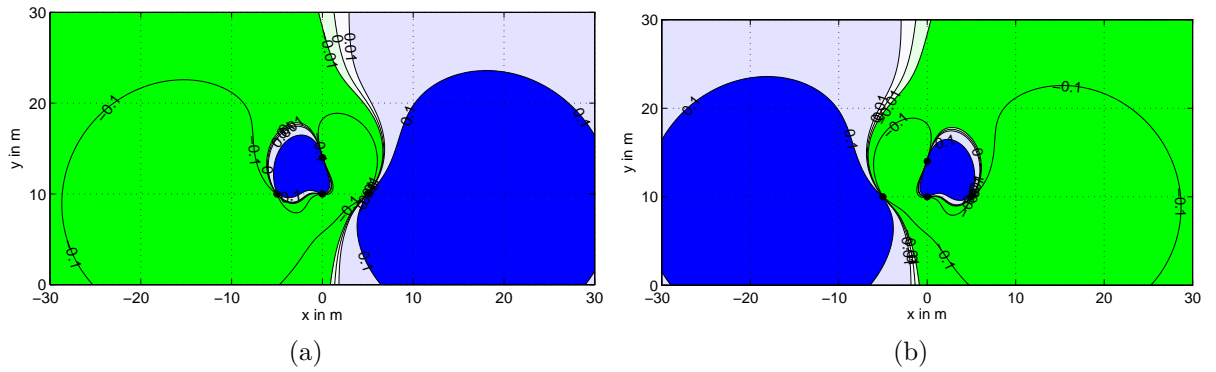


Figure 3.16: Deviation $dev = B_{rms}(\text{with EW}) - B_{rms}(\text{without EW})$ of the magnetic flux density for parameters $R'_{EW}=1.5\Omega /\text{km}$, $y_{EW}=14\text{m}$, $\rho_E=100\Omega\text{m}$, (a) positive rotating system - var. 1 to var. 3, (b) negative rotating system - var. 4 to var. 6

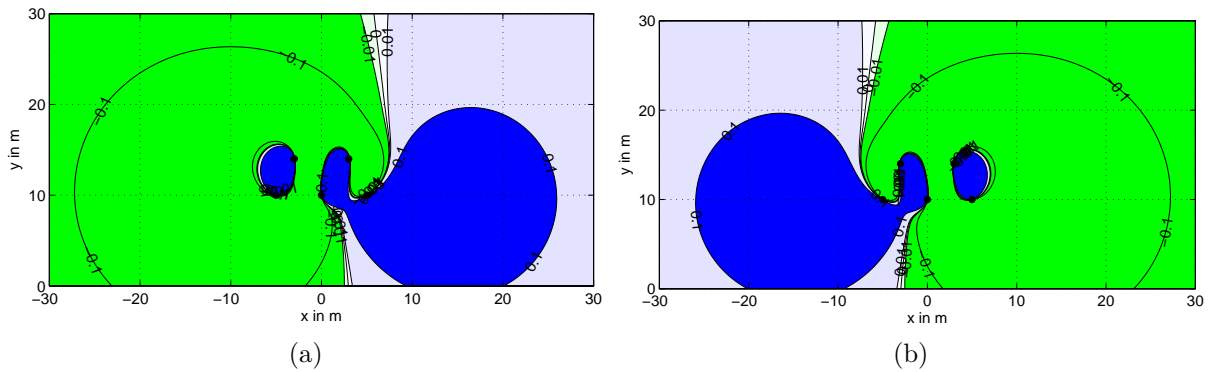


Figure 3.17: Deviation $dev = B_{rms}(\text{with EWs}) - B_{rms}(\text{without EWs})$ of the magnetic flux density for tow earthwires with parameters $R'_{EW}=1.5\Omega /\text{km}$, $y_{EW}=14\text{m}$, $\rho_E=100\Omega\text{m}$, (a) positive rotating system - var. 1 to var. 3, (b) negative rotating system - var. 4 to var. 6,

earth wire only reduces the magnetic flux density is wrong, and neglecting the earth wire is not allowed.

The same is valid for the electric field. Neglecting the earth wire might lead to an underestimation of up to 100 V/m in the middle of the line.

For UGLs passive conductors are the screens of the cables or parallel grounding straps. For that passive conductors similar calculations concerning the magnetic flux density can be done.

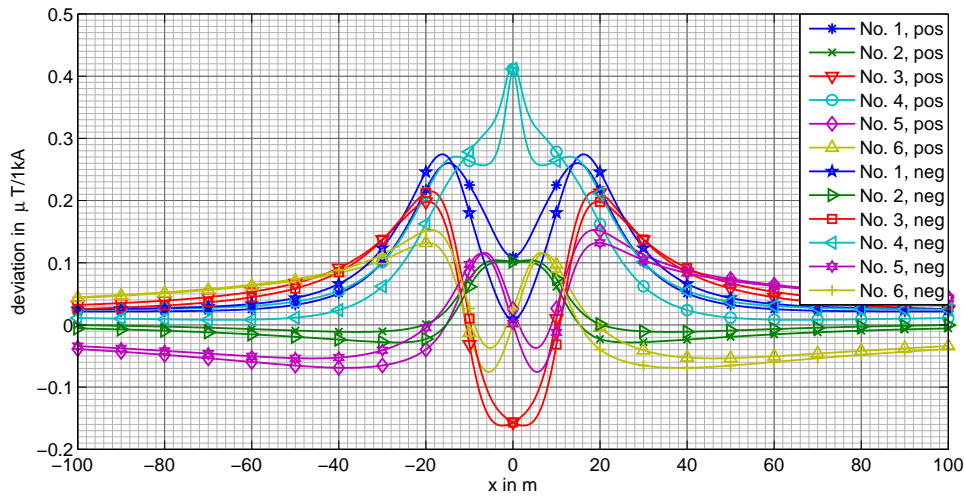


Figure 3.18: Absolute deviation dev in $\mu\text{T}/\text{A}$ of the magnetic flux density at 1 m above ground with a single earth wire compared to the magnetic flux density without any earth wire for phase positions according to tab 3.5 for a 380 kV OHL type Danube

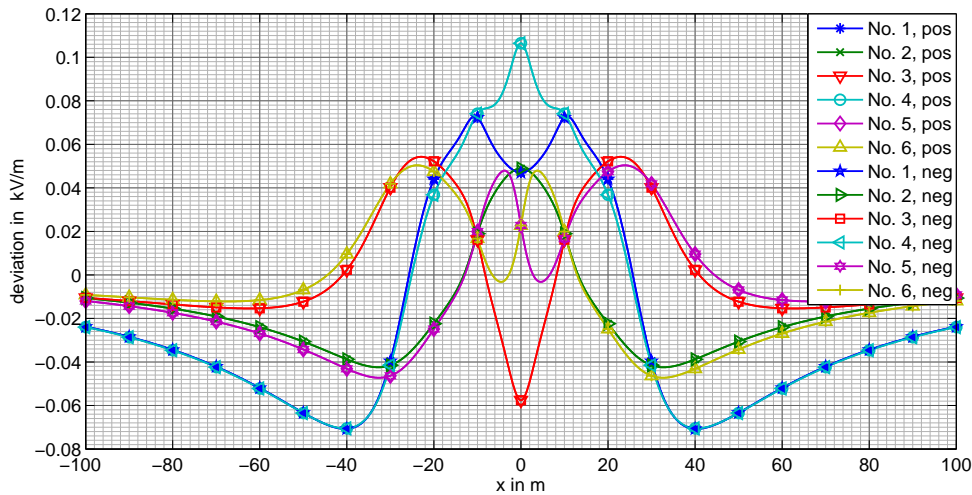


Figure 3.19: Absolute deviation dev in kV/m of the electric field strength at 1 m above ground with an earth wire compared to the electric field strength without any earth wire for phase positions according to tab 3.5 for a double circuit 380 kV OHL type Danube

3.4 Influence of the Sag for OHL

Until now, all conductors are assumed to be infinite and straight in order to perform a 2D calculation. The different heights along a span are only considered with the height of the lowest conductor as shown in fig. 3.1. In this section the difference between this

assumption and the reality is analysed.

It is well known, that the shape of conductors, spanned between two fixed points form a so called catenary curve, which can be described with the following function from e.g. [44].

$$h(y) = \frac{1}{c} (\cosh cy - 1) + h_0 \tag{3.2}$$

The factor c can be evaluated for a line with sag s , height of the conductor in the middle of the span h_0 and span length L by solving (3.2) at the point of suspension ($y = L/2$ see fig. 3.20):

$$h_0 + s = \frac{1}{c} \cosh(cL/2) + h_0 \tag{3.3}$$

y	position along the line axis, $y=0$ is at maximum sag
$h(y)$	height of the conductor at position y
h_0	height of the conductor in the middle of the span
s	sag
c	constant depending on sag and height of the conductors at the tower
L	length of the span

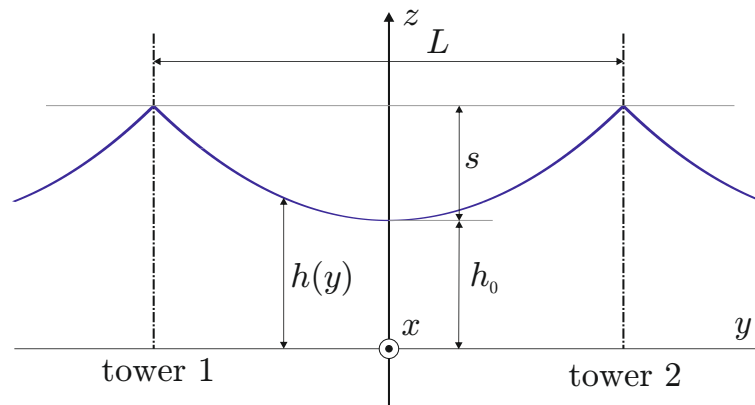


Figure 3.20: Catenary curve of an overhead wire along a span of length L

A sufficiently accurate approximation for typical span lengths of $L=100\dots500$ m and sags $s=5\dots15$ m for HV-OHL is the parabolic function (3.4).

$$h(y) = s \left(\frac{2}{L} y \right)^2 + h_0 \tag{3.4}$$

As it is shown in the following fig. 3.21 the difference of the catenary curve (3.2) and the parabolic function (3.4) is for practical lengths of span and sags for OHLs very

small (only some millimetre) compared to i.e. the accuracy of the measurement of the conductor position at the tower and variation of the sag due to temperature shifts. Therefore the parabolic approximation function is used for the catenary curve in the following.

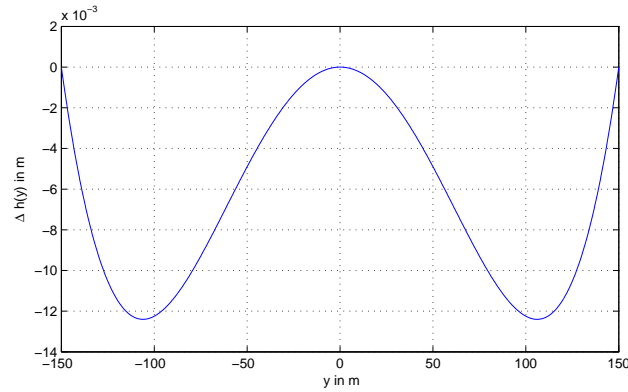


Figure 3.21: Difference $\Delta h(y) = h(y)_{catenary} - h(y)_{parabolic}$ between catenary curve and parabolic approximation in m for a conductor with a span of $L=300$ m and a sag s of 15 m

Now the difference in the magnetic field for a conductor with a catenary curve, compared to the magnetic field of straight conductors is analysed. Therefore the catenary curve is segmented in small pieces of straight lines (as can be seen in fig. 3.22). The height of the straight conductors is depending on the position y along the line axis and is equal to the height of the catenary curve at y .

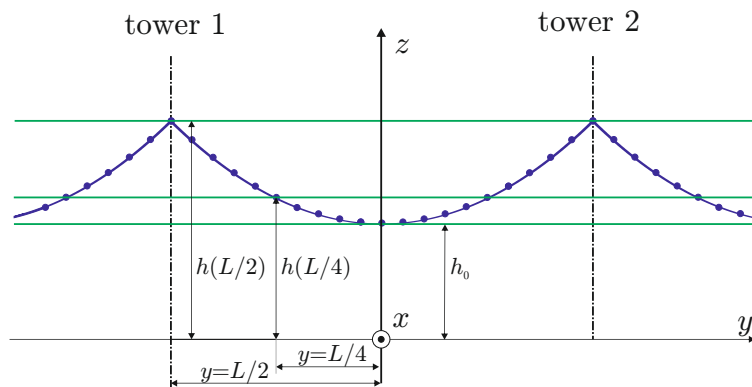


Figure 3.22: Approximation of the catenary curve with straight line segments (blue) or with straight conductors at actual height $h(y)$ (green)

For a 380 kV OHL, type ton, with a span of length $L=300$ m and a sag of $s=10$ m, the difference between the model with catenary curved conductors and straight conductors is analysed for different phasing and different positions along the line axis y .

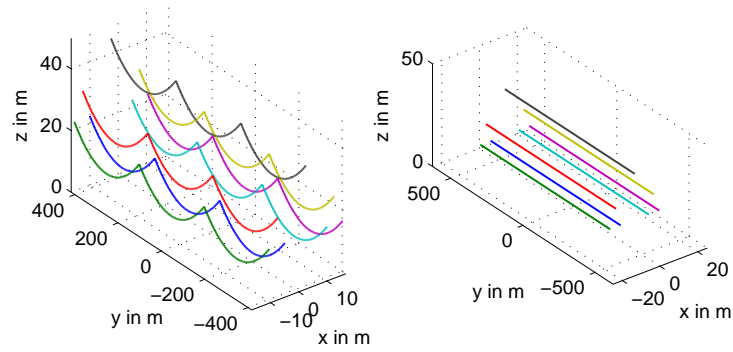


Figure 3.23: 3D-models of the conductor of an OHL with 3 spans, left: modelling with catenary curved conductors, right: modelling with straight conductors

As can be seen in fig. 3.24 and tab. 3.7 for calculations in the middle of the span ($y = 0$ m) and at a position at the quarter of the length of the span ($y = 75$ m) the results for straight conductors are mostly higher than with catenary curved conductors. Additionally, the deviation between the two calculation methods is quite small compared to other parameters. The calculation at the point of suspension ($y = L/2 = 150$ m) with straight conductors would lead to an underestimation of the magnetic field of up to $0.86 \mu\text{T}/\text{kA}$ for a maximum magnetic flux density of $4.8 \mu\text{T}/\text{kA}$. In order to reduce the deviation, the height of the conductors for the straight conductors has to be set on a lower level than the actual value.

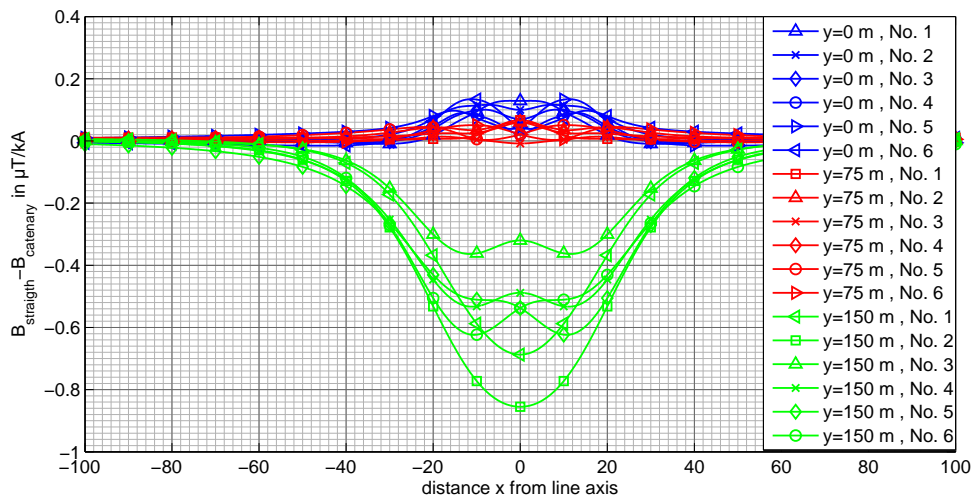


Figure 3.24: Difference between the magnetic flux density with straight conductors B_{straight} and the magnetic flux density of catenary curved conductors B_{catenary} in μT per kA for a 380 kV OHL, type ton, height of the lowest conductor at maximum sag $h_0=10$ m

Table 3.7: Maximum and minimum values of the difference between the magnetic flux density of straight conductors B_{straight} to the magnetic flux density of catenary curved conductors B_{catenary}

		Phase Position					
		No. 1	No. 2	No. 3	No. 4	No. 5	No. 6
		deviation $B_{\text{straight}} - B_{\text{catenary}}$ in $\mu\text{T}/\text{kA}$					
$y=0$ m	max	0.13	0.12	0.10	0.09	0.13	0.13
	min	-0.01	0.00	0.00	0.00	-0.02	-0.02
$y=75$ m	max	0.07	0.06	0.01	0.06	0.05	0.05
	min	0.00	0.00	-0.01	0.01	0.00	0.00
$y=150$ m	max	0.01	0.00	0.00	0.00	0.00	0.00
	min	-0.69	-0.86	-0.36	-0.53	-0.62	-0.62

To summarise, for calculation of the worst case scenario of the magnetic flux density in vicinity of a high voltage OHL, it is adequate to consider the conductors to be indefinite long, while the height of the conductor should be the height in the middle of the span.

3.5 Consideration of the Phase Shift and Unbalances Between Different Circuits of a Line

For OHLs and UGLs with more than one circuit, possible differences concerning the current between these circuits in terms of phase angle and absolute value might occur, which would effect the magnetic flux density. In the previous sections, it was assumed, that all circuits are operated in parallel. That means, that there is no phase shift between the circuits and the absolute value of the currents are equal. For example for a double circuit line this can be expressed mathematically with positive sequence currents of circuit 1 and 2 as $\underline{I}_{\text{cir1}}^{(1)} = \underline{I}_{\text{cir2}}^{(1)}$.

Even if all circuits are operated in parallel most of the time, due to for example maintenance procedures one circuit might be out of operation. Furthermore, restructuring of a network with additional single loop substations or non-standard switching of the network might cause phase shifts between the circuits and non linear load distributions. But also multiple circuit lines exist, where the circuits connect completely different points in a network. This might happen for example, when because of lack of place two different lines are placed on one tower for a part of the length of the line.

The voltage phasors of the circuits of one line typically will not vary much, even if the circuits feed different points in a network. Therefore, the electric field strength is not analysed in this section. With one exception, if one circuit is switched of and earthed on

both ends, the voltage of this circuit will be zero and therefore the electric field strength of the multi-circuit OHL will change.

In [52], [53] and [9] the effect of phase shifts were analysed for a double circuit overhead line. In this thesis these considerations are analysed more in detail and are further continued for multiple circuits lines.

3.5.1 Double Circuit Lines

In order to find the worst case in sense of magnetic flux density for a double circuit OHL or UGL with two independent currents, the following two relations between the currents of circuit 1 (*cir1*) and circuit 2 (*cir2*) are defined.

$$\underline{I}_{cir1}^{(1)} = k_{cir1} \cdot \underline{I}_{max}^{(1)} \tag{3.5}$$

$$\underline{I}_{cir2}^{(1)} = k_{cir2} \cdot \underline{I}_{max}^{(1)} \cdot e^{j\varphi} \tag{3.6}$$

$\underline{I}_{max}^{(1)}$	maximum current of the positive sequence system of one circuit
$\underline{I}_{cir1}^{(1)}$	current of the positive sequence system of circuit 1
$\underline{I}_{cir2}^{(1)}$	current of the positive sequence system of circuit 2
k_{cir1}, k_{cir2}	proportional factor for load flow for circuit 1 or 2, $k_{cir1,2} = 0...1$
φ	phase shift between circuit 1 and 2, $\varphi = -180^\circ...+180^\circ$

The proportional factors k_{cir1} , k_{cir2} give the relationship between the amplitudes of the positive sequence currents to the maximum current $\underline{I}_{max}^{(1)}$ and the angle φ the phase shift between these currents. The goal is, to find that combination of k_{cir1} , k_{cir2} and φ in each field point, which will lead to the maximum magnetic flux density there. One option is, to variate these three variables in their possible ranges, which would lead to huge calculation effort. A much more effective option is, to implement an optimisation algorithm which finds the combination k_{cir1} , k_{cir2} and φ for maximum flux density in each point. In this thesis the 'GlobalSearch' algorithm from Matlab was used to solve this optimisation problem. For details according to optimisation algorithm see chapter 5. The result is, that for independent OHLs (when φ can vary between -180° and 180°) there is no combination with $k_{cir1} < 1$ or $k_{cir2} < 1$ which would lead to a higher magnetic flux density than a combination with $k_{cir1} = k_{cir2} = 1$ and varying $\varphi = \pm 180^\circ$. That's why in fig. 3.25 only the phase angles φ which would lead to the maximum magnetic flux density in this field point are demonstrated in form of contour plots for 2 different phase positions (No. 1 and No. 3).

In fig. 3.26 the magnetic flux density at 1 m above ground for the same configuration is shown. The black line represents the magnetic flux density for the case where no phase shift between both circuits ($\varphi = 0^\circ$) exist. The light gray lines demonstrate the magnetic

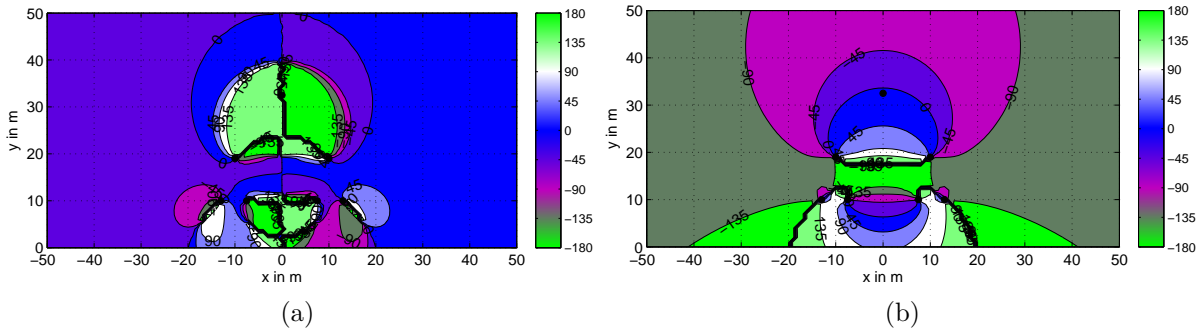
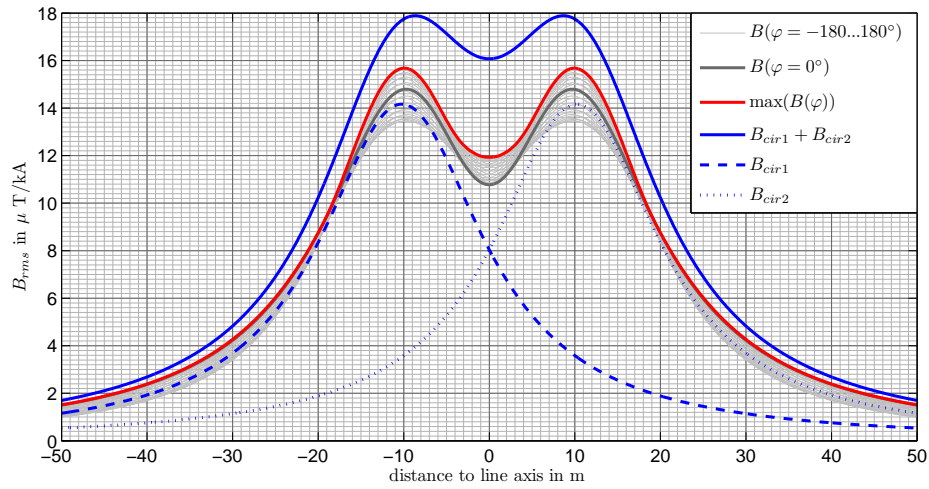


Figure 3.25: Phase shift φ between the currents of the two circuits for each field point, which would lead there to the maximum magnetic flux density of a 380 kV OHL type Danube for phase position No. 1 (a) and No. 3 (b)

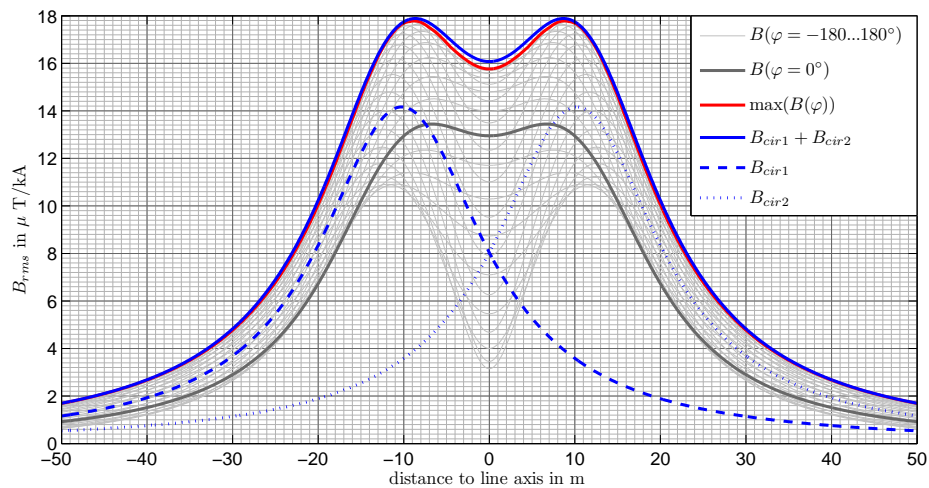
flux density for different values of φ between $\pm 180^\circ$. The red line is the maximum of all these lines. The blue dashed and dotted lines are the magnetic flux densities with only one circuit in operation. It can be seen that the solid blue line, which represents the sum of the RMS-values of the magnetic flux densities, calculated separately for each circuit ($B_{cir1} + B_{cir2}$), will always lead to higher values than the maximum RMS-value of the magnetic flux density for various φ . That means that this method of calculation would always lead to the worst case. In case of phase position No. 3 it would mean only little overestimation, while for phase position No. 1 significant overestimation would be the result.

It has to be mentioned, that phase position No. 5 and No. 6 will lead to the same maximum B as No. 1 and phase positions No. 2 and No. 4 to the same as No. 3, when the lines are independent. An explanation for that phenomenon is, that through cyclically exchanging of the phases of only one circuit, which is the same as a phase shift φ of either $+120^\circ$ or -120° , No. 3 turns to No. 4 and No. 2 or No. 1 turns to No. 5 and No. 6 (see fig. 3.27). Additionally, it is remarkable, that although the magnetic flux density with a phase shift $\varphi = 0^\circ$ of phase position No. 3 is lower than that for No. 1 (compare black lines in fig. 3.26), this advantage of the phase position No. 3 gets lost when the lines are independent and the phase shifts can variate in the hole range (red line of No. 3 is higher than that No. 1).

Of course, it is possible, that the phase shift may not vary in the hole range between -180° and $+180^\circ$, because for example one of the parallel lines feeds an additional substation. Therefore, for e.g. the maximum magnetic flux density for smaller ranges of φ is analysed, in fact, values between $\varphi = -45^\circ \dots +45^\circ$. The results therefore are presented in fig. 3.28. With this smaller range of phase shifts, it occurs, that the magnetic flux density for only one circuit in operation (B_{cir1}, B_{cir2}) might be higher than the maximum



(a)



(b)

Figure 3.26: Magnetic flux density of a double circuit 380 kV OHL type Danube with phase position No. 1 (a) and No. 3 (b), with $k_{cir1} = k_{cir2} = 1$ and different phase shifts $\varphi = -180... + 180^\circ$ at 1 m height

magnetic flux density for both circuits with phase shift $\varphi = -45... 45^\circ$ ($\max(B(\varphi))$). In fig. 3.28 this occurs for phase position No. 3 (b) in an area $x = -30...-15$ m and $x = 15...30$ m.

In the following it is analysed, what are the maximum magnetic flux densities for a different range of phase shifts φ in order to find the threshold of phase shift range, where it might be preferable in sense of magnetic flux density, to choose phase position No. 1 instead of No. 3. Therefore, for different ranges of phase shift angles, the maximum

3.5 Consideration of the Phase Shift and Unbalances Between Different Circuits of a Line

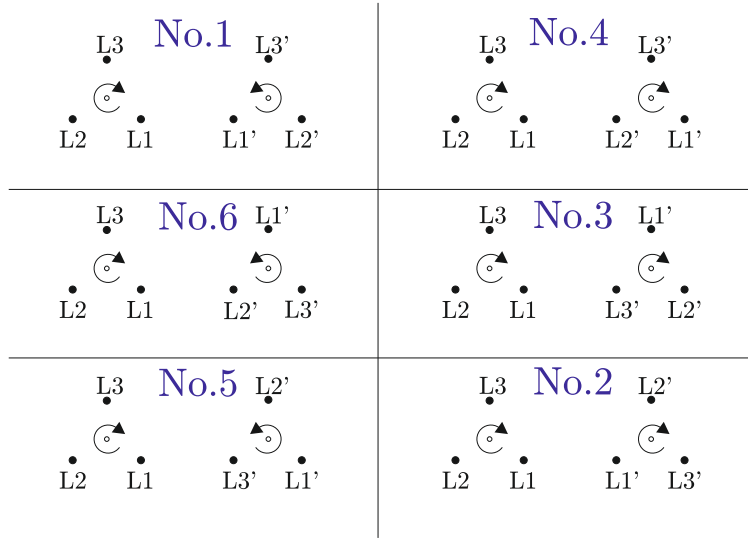


Figure 3.27: Changing between phase positions due to cyclically exchanging the phase of only one circuit

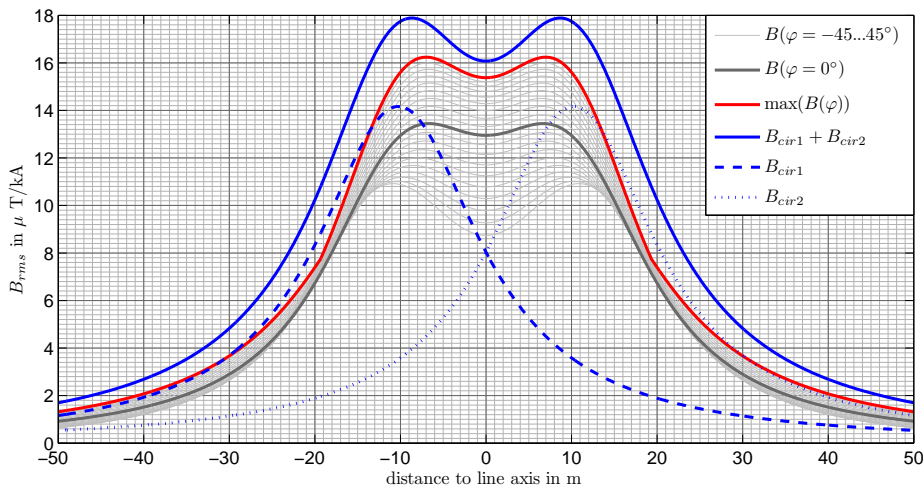


Figure 3.28: Magnetic flux density of a double circuit 380 kV OHL type Danube with phase position and No. 3 with $k_{cir1} = k_{cir2} = 1$ and different phase shift $\varphi = -45...45^\circ$ at 1 m height

magnetic flux density is summarised in fig. 3.29 for phase position No. 1 (red) and No. 3 (blue). The threshold for this configuration can be found with $\varphi = \pm 90^\circ$ for the far field ($|x| > 30$ m) and with $\varphi = \pm 45^\circ$ in sense of maximum B transverse to the line axis.

But it must not be forgotten, that the voltages, and therefore the electric field strength might not vary in the same range as the currents. So even, if it might be better to choose phase position No. 1 because of possible phase shifts, still, in sense of maximum

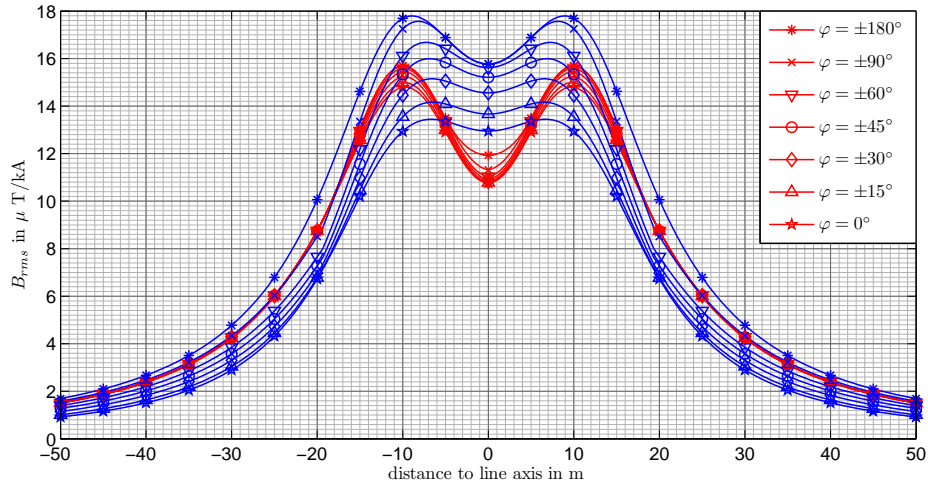


Figure 3.29: Maximum magnetic flux density for different ranges of phase shift angles φ for phase consideration No. 1 (red) and No. 3 (blue)

electric field strength No. 3 might be the better selection (see therefore fig. 3.10).

If two equal circuits are parallel over the entire length (connected on both ends to the same network points), the phase shift between the current of these circuits is zero. As mentioned before, it can be seen in fig. 3.26 (b) or 3.28 (b), that the magnetic flux density of the only one circuit in operation (blue dashed and dotted lines B_{cir1} , B_{cir2}) might be higher than the magnetic flux density of both circuits in operation with zero phase shift (black line B , $\varphi = 0^\circ$) in certain areas. To find the worst case for a parallel line, the maximum field value (electric and magnetic field) of the following 3 operation modes have to be evaluated:

- both circuits in operation ($k_{cir1} = 1$, $k_{cir2} = 1$)
- circuit 1 in operation only ($k_{cir1} = 1$, $k_{cir2} = 0$)
- circuit 2 in operation only ($k_{cir1} = 0$, $k_{cir2} = 1$)

The result for the OHL discussed above, when both circuits are parallel, is shown in fig. 3.30. It can be seen, that for the chosen phase position No. 3 the operation mode with only one circuit will lead to significant higher fields than operating both circuits in parallel. This fact is very important to know for a worst-case estimation.

It can be assumed that the effect of the phase shifts decreases with decreasing ratio of the distance between the phases of one circuit to the distance between two independent circuits. To demonstrate this, two three-phase cable circuits with varying distance of the phases a and between these circuits b according to fig. 3.31 are analysed.

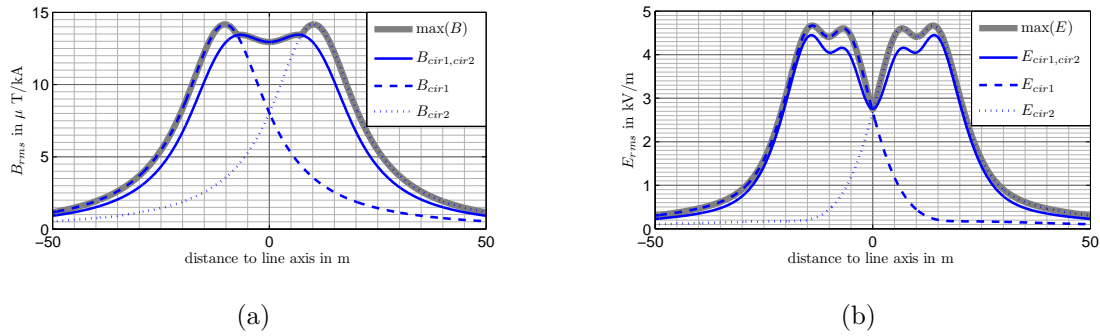


Figure 3.30: Evaluation of the maximum magnetic flux density (a) and electric field strength (b) of a double circuit 380 kV OHL type Danube operated parallel with phase position No. 3 at 1 m height

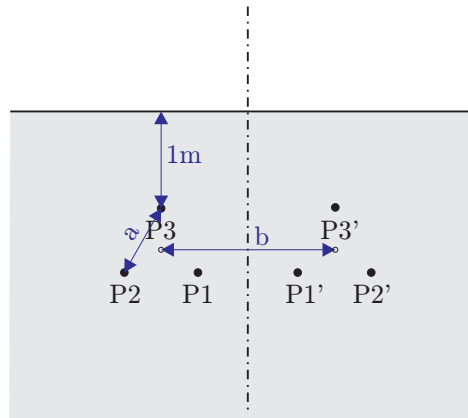


Figure 3.31: Model for analysing the effect of phase shift dependent on distance between the phases a and distance between the circuits b , phase positions according to tab. 3.5

For a distance a between the phases of 0.2 m the maximum magnetic flux density $\max(B(\varphi))$ and the minimum magnetic flux density $\min(B(\varphi))$ at ground level (1 m above the uppermost conductor) are given for a distance between the circuits b of 1 m in fig. 3.32. There, phase position No. 2, No. 3 and No. 4 are considered.

In fig. 3.33 only the differences between $\max(B(\varphi))$ and $\min(B(\varphi))$ for varying b and additionally the phase positions No. 1, No. 5 and No. 6 are shown.

It can be seen that the difference between lowest and highest magnetic flux density dependent on φ is in fact smaller for bigger distances between the circuits. This makes sense, because with increasing distance between the two circuits the effect of field cancellation gets smaller. The difference between the worst case and the best case for the distance $b=1$ m ($b/a=5$) can be up to about 55 μT per 1000 A, compared to a maximum

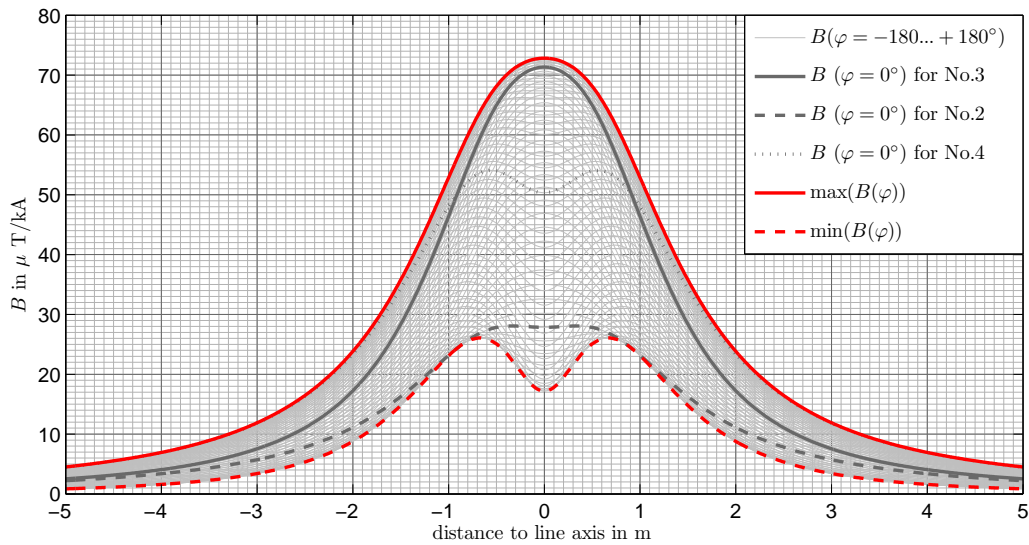


Figure 3.32: Maximum $\max(B(\varphi))$ and minimum magnetic flux $\min(B(\varphi))$ due to variation of the phase shift angle φ for a double circuit cable in triangle shape, with a distance between the phases a of 0.2 m, and a distance between the circuits b of 1 m ($b/a=5$)

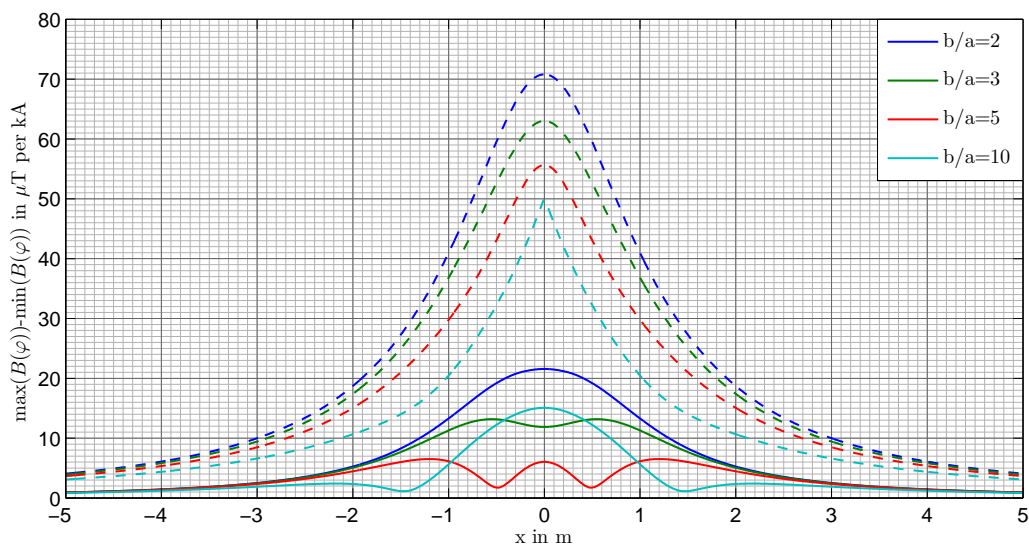


Figure 3.33: Difference between $\max(B(\varphi))$ and $\min(B(\varphi))$ for a double circuit cable in triangle shape, with a distance between the phases a of 0.2 m, solid line...phase position No. 1, 5, 6, dashed line...phase position No. 2, 3, 4

magnetic flux density of 72 μT per 1000 A for that configuration. This implies, that by unthoughtful selection of a phase shift for calculation, the result of the field analysis might be only the half of the value which might be caused by these circuits at the most disadvantageous operation condition (phase shift between the current of the circuits which would lead to the maximum magnetic flux density).

3.5.2 Multiple Circuit Lines

Similar analysis of the phase shift effect can be done for more than two circuits. Exemplary for a cable tray with 11 independent cable systems the magnetic flux density along the cross section is analysed in the following. In fig. 3.34 the effect of three different evaluation methods on the magnetic flux density are shown.

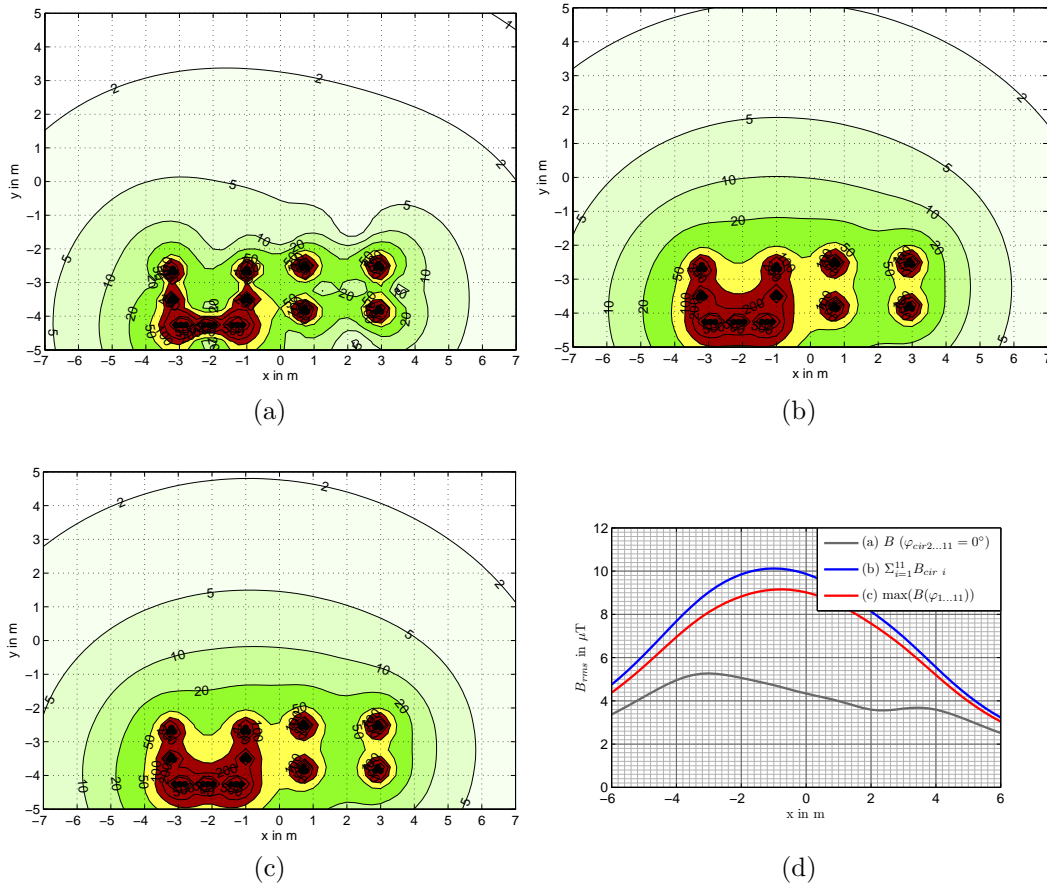


Figure 3.34: Magnetic flux density of a cable tray with 11 circuits (a) no phase shift between the circuits $\varphi_{cir2...11} = 0$ (b) sum of $B_{cir i}$ for each circuit separately, (c) maximum flux density for different phase shifts, (d) comparison of the magnetic flux density of these three methods at ground level ($y=0$ m)

In subfigure (a) these 11 circuits with different absolute values of maximum currents, are first analysed in the conventional way without any consideration of phase shifts between the circuits ($\varphi_{cir2...11}=0^\circ$). For the second analysis (b) the RMS-values of B are calculated for each circuit separately, and afterwards these values are summed up. For the third analysis in subfigure (c) the phase shift angles $\varphi_{cir2...11}$ which would lead to the maximum magnetic flux density for each field point are determined using an optimisation algorithm.

Again it can be seen, that the magnetic flux density for phase shifts ($\varphi_{cir2\dots11}=0^\circ$) is much smaller than the worst case of phase shifts. In contrast, the method where only the RMS-values of each circuit are summed up, would lead to a significant over estimation.

To summarise, if more than one three-phase circuit exist within an area it is necessary first to analyse, if these circuits are independent or dependent in sense of possible phase shifts between these circuits. If the phase shift between these circuits can vary, the easiest way to find the worst case of the magnetic flux density is to evaluate the RMS-value of the magnetic flux density of each circuit separately and sum them up afterwards. Nevertheless, this might lead to a significant overestimation. The effect of phase cancelling is reduced with the increasing distance between the circuits, therefore the difference between the maximum and minimum magnetic flux density for different phase shifts gets smaller. For double circuit lines with varying phase shifts, it might be an advantage to use a different phase arrangement than for parallel operated lines.

3.6 Non Symmetrical Conditions Within One Three-Phase Circuit

In the previous sections it was assumed, that all circuits carry a symmetrical three-phase current and voltage systems. Nevertheless, an asymmetry in the currents and voltages effects the electric and magnetic field configurations. In electrical power theory asymmetries typically are described in form of symmetrical components. The hypothesis of this section is, that an analysis of the symmetrical components of the currents and voltages brings also advantages in the field calculation in terms of worst case analysis and harmonics. The analysis in this section is done for the fundamental frequency only, it is expanded later on in sec. 3.7. For clarity, in this section the index 1 for the fundamental frequency is omitted.

The transformation of phase currents to their symmetrical components is done with the following equation (3.7). The reverse operation is shown in (3.8).

$$\begin{pmatrix} \underline{I}^{(0)} \\ \underline{I}^{(1)} \\ \underline{I}^{(2)} \end{pmatrix} = \frac{1}{3} \begin{pmatrix} 1 & 1 & 1 \\ 1 & \underline{a} & \underline{a}^2 \\ 1 & \underline{a}^2 & \underline{a} \end{pmatrix} \cdot \begin{pmatrix} \underline{I}_{L1} \\ \underline{I}_{L2} \\ \underline{I}_{L3} \end{pmatrix} \quad (3.7)$$

$$\begin{pmatrix} \underline{I}_{L1} \\ \underline{I}_{L2} \\ \underline{I}_{L3} \end{pmatrix} = \begin{pmatrix} 1 & 1 & 1 \\ 1 & \underline{a}^2 & \underline{a} \\ 1 & \underline{a} & \underline{a}^2 \end{pmatrix} \cdot \begin{pmatrix} \underline{I}^{(0)} \\ \underline{I}^{(1)} \\ \underline{I}^{(2)} \end{pmatrix} \quad (3.8)$$

$\underline{I}^{(0)}, \underline{I}^{(1)}, \underline{I}^{(2)}$ zero, positive and negative sequence system of current I
 $\underline{I}_{L1}, \underline{I}_{L2}, \underline{I}_{L3}$ current of the phase L1, L2 or L3
 \underline{a} complex constant for phase shift of 120° , $\underline{a} = e^{j2\pi/3}$

In analogy the same transformation can be done for the phase voltages $\underline{U}_{L1}, \underline{U}_{L2}, \underline{U}_{L3}$ and their corresponding symmetrical components $\underline{U}^{(0)}, \underline{U}^{(1)}, \underline{U}^{(2)}$.

3.6.1 Single Circuit Lines in Compensated and Isolated Networks

At normal operation conditions high voltage and medium voltage networks are typically very well balanced, in other words, the zero sequence system and the negative sequence system should be zero or very small compared to the positive sequence system. The zero sequence current, especially in networks with isolated neutral point, is at normal operating conditions is very small and can practically be neglected. Only low values of negative sequence current exist next to the positive sequence current. Fault conditions which would last only some fractions of a second are normally neglected when analysing the magnetic and electric field in vicinity of an electrical network. Only for asymmetric fault situations (single phase fault, double phase fault), relatively high zero and negative sequence currents might occur. One exception are earth faults in compensated and isolated networks, because these type of networks can be operated even during a single phase earth fault. For this reason, the fault conditions, and therefore the zero sequence current, can last up to hours, until the earth fault location is detected and the fault is cleared. Double phase faults are not considered in the following, because they have to be switched off shortly. Although ongoing discussions about the actual maximum value of self-extinguishing current limits in compensated and isolated networks, in the following the maximum zero sequence current is set with $3\underline{I}^{(0)}=132$ A for a 110 kV network according to [2]. For a 110 kV line with a rated current of e.g. 1000 A, the zero sequence current at maximum load amounts to about 4% ($132 \text{ A}/3/1000 \text{ A}$) of the positive sequence current.

In fig. 3.35 the effect of unbalances in currents of a hypothetical three-phase 110 kV OHL, 1-level-tower without earth wire according to fig. 3.2 is shown. Therefore an unbalance of 4% of $I^{(1)}$ for the zero sequence system as an example for a single phase earth fault condition was taken into account. The angle of the zero sequence current $\varphi^{(0)}$ is varied

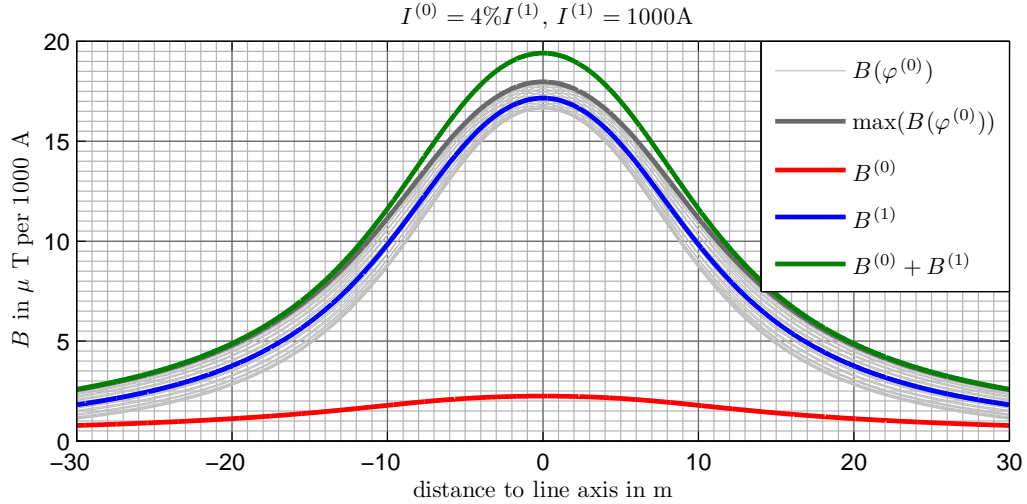


Figure 3.35: Magnetic flux density of a 110 kV OHL, 1-level-tower without earth wire according to fig. 3.2 for a mixture of zero sequence system and positive sequence system at 1 m above ground

between -180° and 180° in 15° steps, as it was done in the previous section with the phase shift between two circuits. The resulting magnetic flux density of the OHL with these currents with varying $\varphi^{(0)}$ are shown as light gray lines. The maximum off all these lines is marked as a black line. Additionally, the RMS-value of the magnetic flux density $B^{(0)}$ for the zero sequence current $I^{(0)}$ only, and RMS-value of the magnetic flux density $B^{(1)}$ of the positive sequence current $I^{(1)}$ are calculated separately. The sum of $B^{(0)}$ and $B^{(1)}$ is presented in form of the green line ($B^{(0)} + B^{(1)}$). It can be seen, that the sum of these RMS-values $B^{(1)}$ and $B^{(0)}$ is higher than the value of the maximum of the variation of the phase angle of $I^{(0)}$, and will give the worst case with an overestimation especially in the middle of the line.

Mathematically, this can be expressed, consistently expanded with the component for a negative sequence system, with (3.9):

$$B(\underline{L}_{L1,L2,L3}) \leq B^{(0)}(\underline{I}^{(0)}) + B^{(1)}(\underline{I}^{(1)}) + B^{(2)}(\underline{I}^{(2)}) \quad (3.9)$$

B	magnetic flux density of a line configuration with specific phase currents
$B^{(0,1,2)}$	magnetic flux density resulting from zero, positive or negative sequence current, RMS-value

It should be mentioned, that, of course, if the summation of the resulting fields of zero and positive and negative sequence system symmetrical components is done complex and vectorial, no difference exists between the analysis with symmetrical components

and phase currents, this can be expressed with (3.10).

$$\vec{B}(I_{L1,L2,L3}) = \vec{B}^{(0)}(I^{(0)}) + \vec{B}^{(1)}(I^{(1)}) + \vec{B}^{(2)}(I^{(2)}) \quad (3.10)$$

The advantage of calculation with the RMS-values for each symmetrical component is, that the actual angle of the zero sequence $\varphi^{(0)}$ or negative sequence system $\varphi^{(2)}$ need not be known, and the worst case for all angles can be estimated in one step.

Exactly the same analysis can also be done with unbalances in voltages and the resulting electrical field strength. High voltage networks with a solidly grounded neutral point and network with insulated star points do not have a zero sequence component in voltage at normal operation conditions. Again the compensated networks occupy a special position. There, even without any fault, a zero sequence system exists because of the neutral displacement voltage due to capacitive unbalances. According to [54] a typical allowed maximum neutral displacement voltage reaches about 10% of the normal operation phase voltage. In fig. 3.36 the effect of a displacement voltage of $U^{(0)} = 4\%U^{(1)}$ is shown.

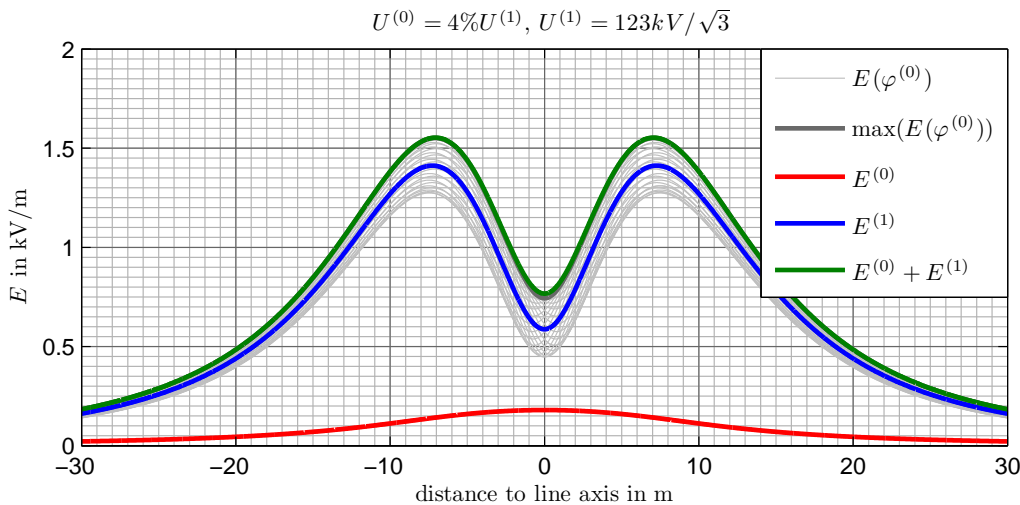


Figure 3.36: Electric field strength of a 110 kV line (1-level-tower) for a mixture of zero sequence system (4%) and positive sequence system

It is remarkable, that for this analysed configuration the displacement voltage of only 4% of $U^{(1)}$ would lead to an increase of the maximum electrical field strength up to 18% compared without zero sequence component (compare green and blue line in fig. 3.36).

Additionally, for isolated and compensated networks the effect of a single phase earth fault on the electrical field strength has to be analysed. In theory, if phase L1 is con-

nected to earth, the zero sequence voltage $\underline{U}^{(0)}$ is equal to $-\underline{U}_{L1}$ at normal operation conditions. Therefore for a single circuit OHL in sense of electrical field strength, 4 cases have to be analysed.

1. normal operation condition with maximum allowed displacement voltage $\underline{U}^{(0)} = x\%U^{(1)}$ with various $\varphi^{(0)}$
2. fault at phase L1 with $\underline{U}^{(0)} = -\underline{U}_{L1} = -\underline{U}^{(1)}$
3. fault at phase L2 with $\underline{U}^{(0)} = -\underline{U}_{L2} = -a^2\underline{U}^{(1)}$
4. fault at phase L3 with $\underline{U}^{(0)} = -\underline{U}_{L3} = -a\underline{U}^{(1)}$

In fig. 3.37 this worst case evaluation was done for the same single circuit OHL as analysed before.

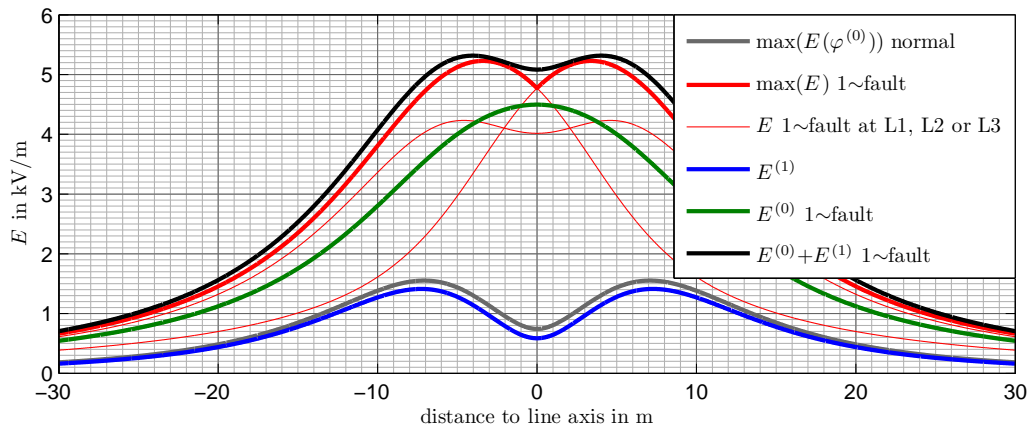


Figure 3.37: Worst Case evaluation of the electric field strength 1 m above ground of a single circuit 110 kV line (1-level-tower) in a compensated network considering single phase fault conditions

Additionally for the 3-level-tower the results are shown in fig. 3.38.

Here, the illustrated electric field strength for the zero sequence system ($E^{(0)}$ 1 fault) was calculated for fault condition, that means the absolute value of the zero sequence system is equal to the absolute value of the positive sequence system $U^{(0)} = U^{(1)}$. Again, the sum $E^{(0)} + E^{(1)}$ for single phase fault condition provides only little higher electric field strengths than the maximum electric field strength ($\max(E)1\sim\text{fault}$) resulting from single phase faults at various phases L1, L2 and L3. It can also be seen, that the electric field strength at normal operation conditions ($\max(E)\text{normal}$) is much smaller than for single phase earth fault conditions ($\max(E)1\sim\text{fault}$).

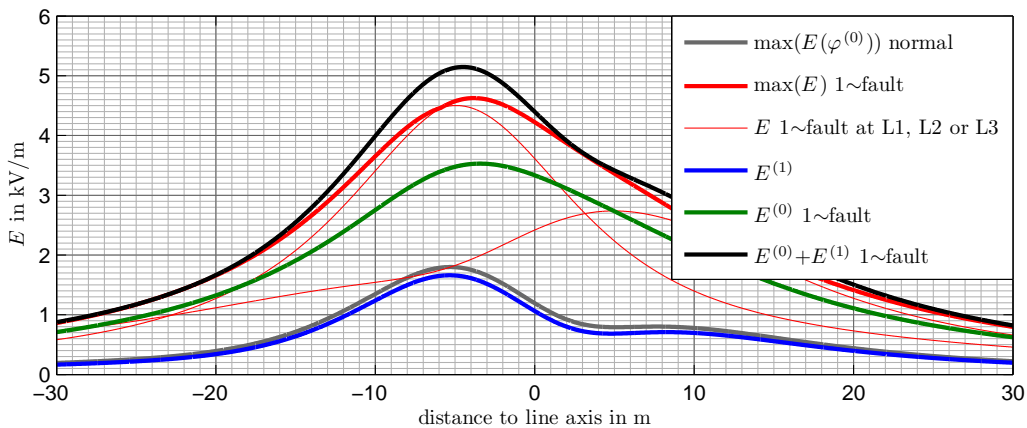


Figure 3.38: Worst Case evaluation of the electric field strength 1 m above ground of a single circuit 110 kV line (3-level-tower) in a compensated network considering single phase fault conditions

For better imagination in fig. 3.39 the isolines of the electric field strength (a) for a single phase fault at the most left conductor of the 1-level-tower compared to (b) the electric field strength at normal operation condition is given.

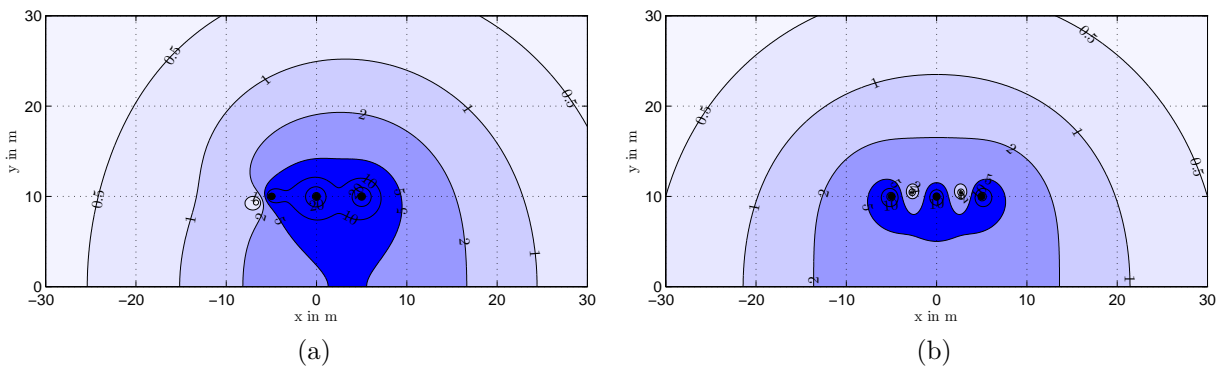


Figure 3.39: Electric field strength in kV/m of a single circuit 110 kV 1-level-line in a compensated network (a) for single phase earth fault at the left conductor (b) at normal operation conditions (without any displacement voltage)

3.6.2 Double Circuit Lines in Compensated Networks

The analysis of the electric field strength at fault and normal conditions is here extended for the double circuit lines. Again for an operation at normal conditions, a displacement voltage of 4% is considered. In the fig. 3.40 the resulting electric field strength for the more common 110 kV double circuit line (2-level-tower, phase allocation No. 3) is shown. If both circuits are part of the same network, then the unbalances in voltage at normal operation and fault conditions are the same for both circuits.

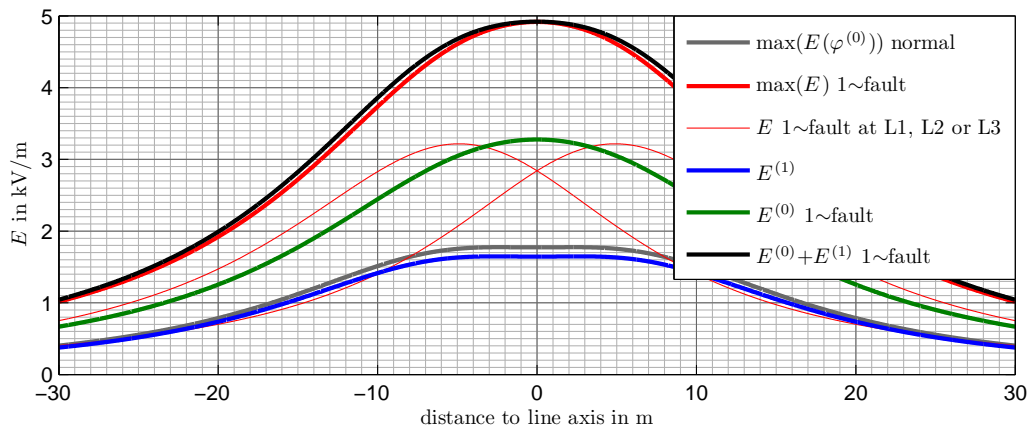


Figure 3.40: Electric field strength 1 m above ground of a double circuit 110 kV OHL (2-level-tower, phase position No. 3, $h_l = 10m$) in a compensated network considering single phase fault (1~fault) conditions

Further it was analysed which influence the phase position as well as the tower type has on this worst case analysis. In fig. 3.41 and fig. 3.42 therefore the maximum electric field strengths transverse to the line axis at 1 m height are compared.

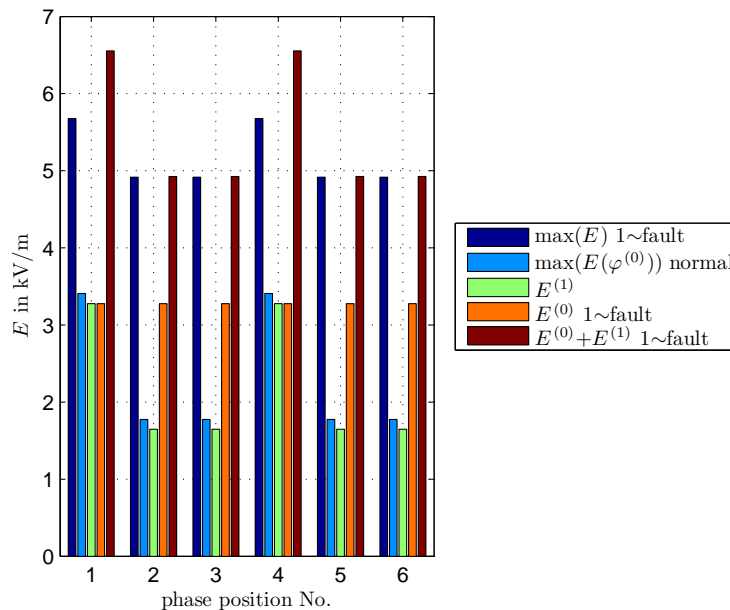


Figure 3.41: Maximum electric field strength 1 m above ground of a double circuit 110 kV OHL (2-level-tower, $h_l = 10 m$) for different phase positions in a compensated network considering single phase fault (1~fault) conditions

Significant is, that for an OHL where at normal operation conditions the electric field strengths are far away from the reference limits (5 kV/m for 50 Hz), in case of a single phase fault these limits might be exceeded.

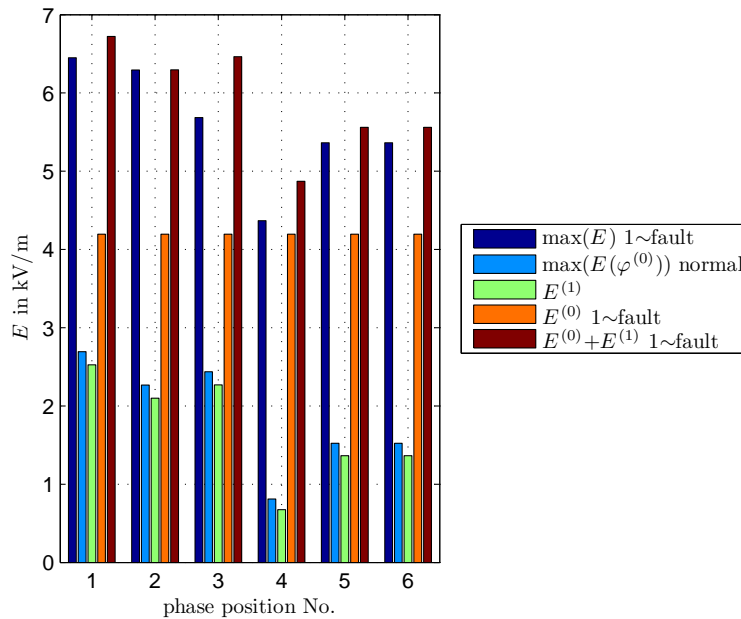


Figure 3.42: Maximum electric field strength 1 m above ground of a double circuit 110 kV OHL (3-level-tower, $h_l = 10$ m) for different phase positions in a compensated network considering single phase fault (1~fault) conditions

The consequence from that analysis is, that for OHLs in compensated networks the single phase fault is the worst case operation mode (it is not switched off shortly) and should be considered for electric field calculations. This might be critical, because the reference values of the electric field strength might be exceeded, although at normal operation the resulting electric field strength is far from the reference limit.

In order to estimate the necessary height of the lowest conductors h_l above ground in order to comply with the standards and guidelines [31, 33] for a single phase fault operation condition in compensated and isolated networks the following fig. 3.43 and fig. 3.43.

Depending on the tower type and phase arrangement from these figures it follows, that the minimum height of the conductor should be between 8 and 15 m. This analysis with single phase faults is not necessary of course for OHLs of high voltage networks with low resistance earthed star points. There the corresponding areas with the fault have to be switched off immediately due to the fact, that a single phase earth fault acts as a short circuit, which would lead to currents, much higher than at normal operation.

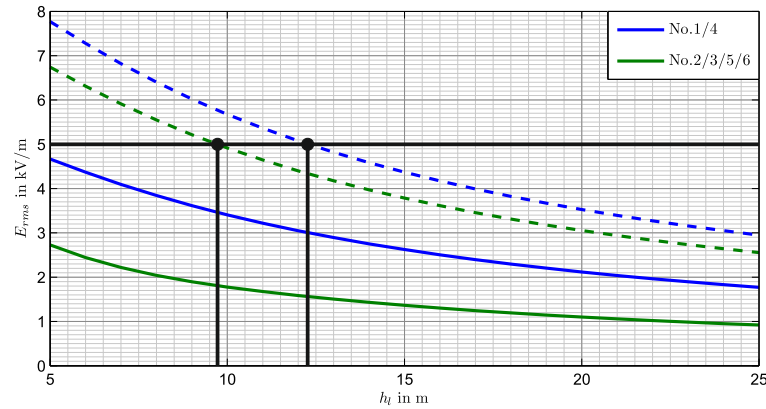


Figure 3.43: Maximum electric field strength 1 m above ground of a double circuit 110 kV OHL (2-level-tower) for different phase positions in a compensated network considering displacement voltage of 4% at normal operation ($\max(E(\varphi^{(0)}))$ normal, solid lines) and at single phase fault conditions ($\max(E)$ 1~fault, dashed lines), depending on the height of the lowest conductor h_l

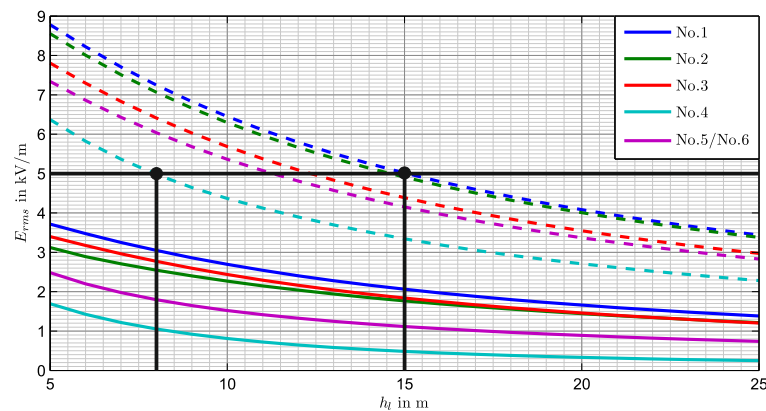


Figure 3.44: Maximum electric field strength 1 m above ground of a double circuit 110 kV OHL (3-level-tower) for different phase positions in a compensated network considering displacement voltage of 4% at normal operation ($\max(E(\varphi^{(0)}))$ normal, solid lines) and at single phase fault conditions ($\max(E)$ 1~fault, dashed lines), depending on the height of the lowest conductor h_l

3.6.3 Low Voltage Networks

Another instance are unbalanced loads in low voltage networks, where zero sequence currents occur also at normal operation conditions.

In the following a low voltage sheathed cable with 4 conductors (L1, L2, L3 and N) with a cross section of 120 mm^2 is analysed. Depending on the type of installation (in earth, air,...) the maximum current per conductor is according to [64] about 300 A. To find the maximum magnetic flux density, zero, positive and negative sequence of the currents have to be varied with the following congestions to be fulfilled:

- the RMS-value of the current in each conductor has to be smaller or equal the maximum allowed current of 300 A: $I_{L1} \leq 300$ A, $I_{L2} \leq 300$ A, $I_{L3} \leq 300$ A, $I_N \leq 300$ A
- the sum of all currents is zero: $\underline{I}_{L1} + \underline{I}_{L2} + \underline{I}_{L3} + \underline{I}_N = 0$

Once again, the easiest way to find the combination with the maximum flux density at a distance d is to leave it to an optimisation algorithm finding these currents, which simultaneously respect the congestions. The result is, that the maximum magnetic flux density in a distance d is always caused by phase (+neutral) currents which have all the same absolute value ($I_{L1} = I_{L2} = I_{L3} = I_N = 300$ A), but different phase angles in such a way, that the sum off all currents is equal to zero. In fig. 3.45 (b) two possible sets of currents (blue and green) are demonstrated, which fulfil that conditions. For this configuration the currents which lead to the maximum field are equal to the blue currents shown in fig. 3.45 (b). The green phasors are arbitrary. The red phasors are the corresponding symmetrical components to blue set of phase currents.

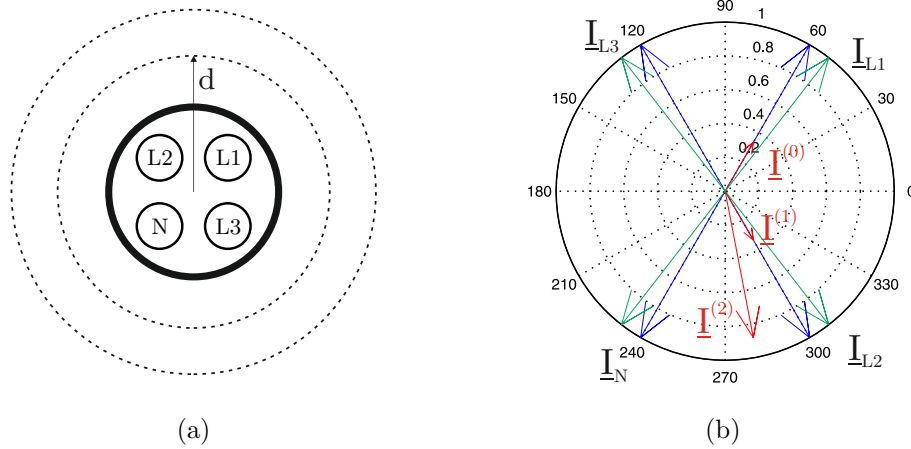


Figure 3.45: (a) Model for evaluation the maximum magnetic flux density in the vicinity of a cable, depending on distance d and the currents \underline{I}_{L1} , \underline{I}_{L2} , \underline{I}_{L3} and \underline{I}_N , (b) two possible sets of currents (blue and green) and the symmetrical components of the blue set of currents (red)

In fig. 3.45 the maximum magnetic flux densities along a circle in a distance d for different sets of currents are shown:

- $\max B(\underline{I}^{(0,1,2)})$ is obtained by the currents $\underline{I}_{L1} = 300$ A $\angle 60^\circ$, $\underline{I}_{L2} = 300$ A $\angle -60^\circ$, $\underline{I}_{L3} = 300$ A $\angle 120^\circ$ and $\underline{I}_N = 300$ A $\angle -120^\circ$ (blue phasors in fig. 3.45 (b)) which fulfil the congestions and will lead to the maximum magnetic flux density.

- $\max B(\underline{I}^{(0)})$ represents a (physically - in terms of grid operation -rather unrealistic) system with a zero sequence current of $\underline{I}^{(0)} = 100 \text{ A } \angle 0^\circ$ and positive and negative sequence currents are zero. The currents in the phases are therefore $\underline{I}_{L1} = 100 \text{ A } \angle 0^\circ$, $\underline{I}_{L2} = 100 \text{ A } \angle 0^\circ$, $\underline{I}_{L3} = 100 \text{ A } \angle 0^\circ$ and $\underline{I}_N = 300 \text{ A } \angle 180^\circ$.
- $\max B(\underline{I}^{(1)})$ stands for a positive sequence current of $\underline{I}^{(1)} = 300 \text{ A } \angle 0^\circ$, while zero and negative sequence currents are zero. The currents in the phases are therefore $\underline{I}_{L1} = 300 \text{ A } \angle 0^\circ$, $\underline{I}_{L2} = 300 \text{ A } \angle -120^\circ$, $\underline{I}_{L3} = 300 \text{ A } \angle 120^\circ$ and $\underline{I}_N = 0 \text{ A}$.
- $\max B(\underline{I}^{(0)}) + \max B(\underline{I}^{(1)})$ is the sum of the magnetic flux density, which are described above.

It can be seen, that if only a symmetrical system $\max(B(\underline{I}^{(1)}))$ is considered, an underestimation of about 40% compared to the maximum flux density $\max(B(\underline{I}^{(0,1,2)}))$ might be the consequence. On the other hand, if again the maximum magnetic flux density for zero sequence system and positive sequence system $\max(B(\underline{I}^{(0)})) + \max(B(\underline{I}^{(1)}))$ are evaluated, the sum of these RMS-values would be higher than the actual maximum flux density. Evaluations with this method would therefore be worst case evaluations with an overestimation of about 30%.

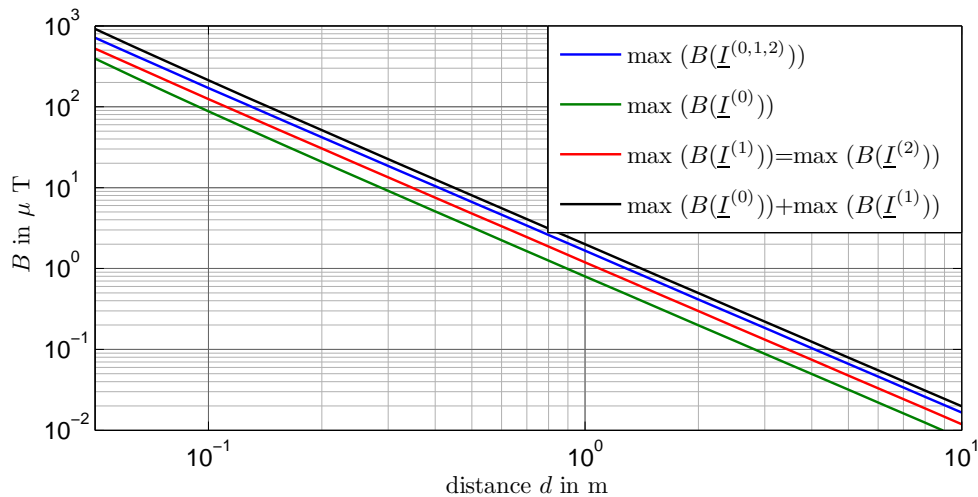


Figure 3.46: Maximum magnetic flux density in a distance d of a 3 phase cable with neutral conductor for different currents, maximum current of each conductor is 300 A

3.7 Harmonic Factor Evaluation for Three-Phase Systems

In this section it is proposed to apply the concept of symmetrical components to calculate the resulting field exposure for three-phase systems in analogy to sec. 2.3. For harmonics the transformation in symmetrical components can be expressed, as it is shown in (3.11).

$$\begin{pmatrix} \underline{I}_\nu^{(0)} \\ \underline{I}_\nu^{(1)} \\ \underline{I}_\nu^{(2)} \end{pmatrix} = \frac{1}{3} \begin{pmatrix} 1 & 1 & 1 \\ 1 & \underline{a} & \underline{a}^2 \\ 1 & \underline{a}^2 & \underline{a} \end{pmatrix} \cdot \begin{pmatrix} \underline{I}_{L1,\nu} \\ \underline{I}_{L2,\nu} \\ \underline{I}_{L3,\nu} \end{pmatrix} \quad (3.11)$$

$\underline{I}_{L1,\nu}$ ν^{th} harmonic of phase current L1
 $\underline{I}_\nu^{(0,1,2)}$ symmetrical component of ν^{th} harmonic

As seen in the previous sec. 3.6, the zero, positive and negative sequence system result in different field profiles. But, the harmonic factor evaluation in sec. 2.3 implies that the field profiles for each harmonic are the same. In other words, the assumptions (2.35) as given in sec. 2.3 is no more valid, when a mixture of symmetrical components occurs. In analogy to the inequality (3.9) given in sec. 3.6 for a single frequency, the following inequality (3.12) can be given for the harmonics of the magnetic flux density.

$$B_\nu(\underline{I}_{L1,\nu}, \underline{I}_{L2,\nu}, \underline{I}_{L3,\nu}) \leq B_\nu^{(0)}(\underline{I}_\nu^{(0)}) + B_\nu^{(1)}(\underline{I}_\nu^{(1)}) + B_\nu^{(2)}(\underline{I}_\nu^{(2)}) \quad (3.12)$$

That means, that a splitting of the magnetic flux density of the ν^{th} harmonic into symmetrical components would lead to the same or a higher value than the calculation of the magnetic flux density directly from the ν^{th} harmonic of the phase currents. Due to the splitting into the symmetrical components and summing up them in sense of RMS-values, the phases of the spectral components are getting lost. That implies, that with this methodology of consideration the harmonics, a phase consideration as described in sec. 2.3.2 is no more possible, and only the conservative multi frequency rule according to (2.38) can be taken into account.

In the following transformation (3.13)ff, the sum of the symmetrical components $B_\nu^{(0)} + B_\nu^{(1)} + B_\nu^{(2)}$ is inserted instead of B_ν in the multi frequency rule (2.38).

$$ER_B = \sum_{\nu=1}^{\nu_{max}} \frac{B_\nu}{B_{L,\nu}} \leq \sum_{\nu=1}^{\nu_{max}} \frac{B_\nu^{(0)} + B_\nu^{(1)} + B_\nu^{(2)}}{B_{L,\nu}} \quad (3.13)$$

$$= \sum_{\nu=1}^{\nu_{max}} \frac{B_\nu^{(0)}}{B_{L,\nu}} + \sum_{\nu=1}^{\nu_{max}} \frac{B_\nu^{(1)}}{B_{L,\nu}} + \sum_{\nu=1}^{\nu_{max}} \frac{B_\nu^{(2)}}{B_{L,\nu}} \quad (3.14)$$

$$= \frac{B_1^{(0)}}{B_{L,1}} \sum_{\nu=1}^{\nu_{max}} \frac{B_\nu^{(0)}}{B_1^{(0)}} \frac{B_{L,1}}{B_{L,\nu}} + \frac{B_1^{(1)}}{B_{L,1}} \sum_{\nu=1}^{\nu_{max}} \frac{B_\nu^{(1)}}{B_1^{(1)}} \frac{B_{L,1}}{B_{L,\nu}} + \frac{B_1^{(2)}}{B_{L,1}} \sum_{\nu=1}^{\nu_{max}} \frac{B_\nu^{(2)}}{B_1^{(2)}} \frac{B_{L,1}}{B_{L,\nu}} \quad (3.15)$$

$$= ER_{B,1}^{(0)} \cdot k_{H,B}^{(0)} + ER_{B,1}^{(1)} \cdot k_{H,B}^{(1)} + ER_{B,1}^{(2)} \cdot k_{H,B}^{(2)} \quad (3.16)$$

ER_B	total exposure ratio of magnetic flux density
$B_\nu^{(0,1,2)}$	magnetic flux density (RMS-value) for the ν^{th} harmonic for zero, positive or negative sequence system
$B_1^{(0,1,2)}$	magnetic flux density at fundamental frequency for zero, positive or negative sequence system
$B_{L,\nu}$	reference value for the ν^{th} harmonic of the magnetic flux density
$B_{L,1}$	reference value at fundamental frequency of the magnetic flux density
$k_{H,B}^{(0,1,2)}$	harmonic factor for zero, positive or negative sequence system
$ER_{B,1}^{(0,1,2)}$	exposure ratio of the zero, positive or negative sequence system at fundamental frequency

As can be seen, for example for the zero sequence harmonic factor $k_{H,B}^{(0)}$ the following equation is valid:

$$k_{H,B}^{(0)} = \sum_{\nu=1}^{\nu_{max}} \frac{B_\nu^{(0)}}{B_1^{(0)}} \frac{B_{L,1}}{B_{L,\nu}} \quad (3.17)$$

Instead of the proportionality (2.35) between current and magnetic flux density, for the zero sequence system the following proportionality (3.18) is valid for three-phase systems. This proportionality can be inserted in (3.17).

$$\frac{I_\nu^{(0)}}{I_1^{(0)}} = \frac{B_\nu^{(0)}}{B_1^{(0)}} \quad (3.18)$$

$I_1^{(0)}$	RMS-value of the zero sequence current at fundamental frequency
$I_\nu^{(0)}$	RMS-value of the zero sequence current for the ν^{th} harmonic

The zero sequence current of the fundamental frequency $I_1^{(0)}$ might be zero (e.g. in networks with insulated star point). As a consequence the magnetic flux density evaluated for this zero sequence current, $B_1^{(0)}$ might be zero, too, which would lead to a division by zero.

To avoid this, the $B_1^{(0)}$ can be evaluated with a reference current which is greater than 0. For practical reasons, the reference current is chosen with the absolute value of the positive sequence current $I_1^{(1)}$. The magnetic flux density $B_1^{(0)}$ is therefore evaluated with the same absolute value as the positive sequence current ($I_1^{(0)} = I_1^{(1)}$). The resulting $B_1^{(0)}$

is a hypothetical value, and might be much higher than the resulting magnetic field. For the positive and negative sequence currents the same reference currents are chosen. The corresponding phase currents for calculating $B_1^{(0)}$, $B_1^{(1)}$ and $B_1^{(2)}$ can be found in tab. 3.8.

Table 3.8: Phase currents for evaluation of the magnetic flux densities for zero, positive and negative sequence

	\underline{I}_{L1}	\underline{I}_{L2}	\underline{I}_{L3}
$B_1^{(0)}$	$I_1^{(1)}$	$I_1^{(1)}$	$I_1^{(1)}$
$B_1^{(1)}$	$I_1^{(1)}$	$\underline{a}^2 \cdot I_1^{(1)}$	$\underline{a} \cdot I_1^{(1)}$
$B_1^{(2)}$	$I_1^{(1)}$	$\underline{a} \cdot I_1^{(1)}$	$\underline{a}^2 \cdot I_1^{(1)}$

The harmonic factors, calculated from the current harmonics $k_{H,I}^{(0,1,2)}$ are evaluated similar to the formula (2.36) and (2.37), taking the symmetrical components according to (3.18) into account:

$$k_{H,I}^{(0)} = \sum_{\nu=1}^{\nu_{max}} \frac{I_{\nu}^{(0)}}{I_1^{(1)}} \cdot \frac{B_{L,1}}{B_{L,\nu}} \quad (3.19)$$

$$k_{H,I}^{(1)} = \sum_{\nu=1}^{\nu_{max}} \frac{I_{\nu}^{(1)}}{I_1^{(1)}} \cdot \frac{B_{L,1}}{B_{L,\nu}} \quad (3.20)$$

$$k_{H,I}^{(2)} = \sum_{\nu=1}^{\nu_{max}} \frac{I_{\nu}^{(2)}}{I_1^{(1)}} \cdot \frac{B_{L,1}}{B_{L,\nu}} \quad (3.21)$$

The total exposure ratio can then be evaluated using (3.22)ff.

$$ER_B \leq \frac{B_1^{(0)}}{B_{L,1}} \cdot k_{H,I}^{(0)} + \frac{B_1^{(1)}}{B_{L,1}} \cdot k_{H,I}^{(1)} + \frac{B_1^{(2)}}{B_{L,1}} \cdot k_{H,I}^{(2)} \quad (3.22)$$

$$= ER_{B,1}^{(0)} \cdot k_{H,I}^{(0)} + ER_{B,1}^{(1)} \cdot k_{H,I}^{(1)} + ER_{B,1}^{(2)} \cdot k_{H,I}^{(2)} \quad (3.23)$$

ER_B	total exposure ratio of magnetic flux density
$B_1^{(0,1,2)}$	magnetic flux density at fundamental frequency for zero, positive or negative sequence system
$B_{\nu}^{(0,1,2)}$	magnetic flux density (RMS-value) for the ν^{th} harmonic for zero, positive or negative sequence system
$B_{L,1}$	reference value at fundamental frequency of the magnetic flux density
$k_{H,I}^{(0,1,2)}$	harmonic factor for zero, positive or negative sequence system
$ER_{B,1}^{(0,1,2)}$	exposure ratio of the zero, positive or negative sequence system at fundamental frequency

Because the negative sequence system has the same field profile as the positive sequence system, (3.22) can be simplified into (3.24).

$$ER_B \leq ER_{B,1}^{(0)} \cdot k_{H,I}^{(0)} + ER_{B,1}^{(1)} \cdot (k_{H,I}^{(1)} + k_{H,I}^{(2)}) = ER_{B,1}^{(0)} \cdot k_{H,I}^{(0)} + ER_{B,1}^{(1)} \cdot k_{H,I}^{(1+2)} \quad (3.24)$$

In theory, if all phase current signals ($I_{L1}(t)$, $I_{L2}(t)$, $I_{L3}(t)$) have the same shape, harmonics of order $\nu = 3n$ ($n \in \mathbb{N}$) form a zero sequence system, harmonics of order

$(\nu = 3n+1)$ form a positive sequence system and harmonics of order $(\nu = 3n - 1)$ form a negative sequence system. Then for the zero sequence harmonic factor $k_{H,I}^{(0)}$ only harmonics of order $\nu = 3n$ have to be considered and for the factor $k_{H,I}^{(1+2)}$ the rest of harmonics. Practically in real power systems, the shape of the signals are not equal, and a mixture of the symmetrical components of each harmonic exist.

In fig. 3.47 two different three-phase signals, a theoretical and a practical signal, in time domain are shown. Signal 1 (blue) is a measured (real) three-phase signal of one circuit in a low voltage network at high load. The amplitudes of the phase signals are normalised to the RMS-value of phase L1 (I_{L1}). It can be seen, that not only the amplitudes vary, but also the form of the signals. Signal 2 (red) is a constructed 'ideal' signal, where the phase signals L2 and L3 have exactly the same form and amplitudes as phase L1, only with an offset in time of $\pm 120^\circ$ ($20/3$ ms).

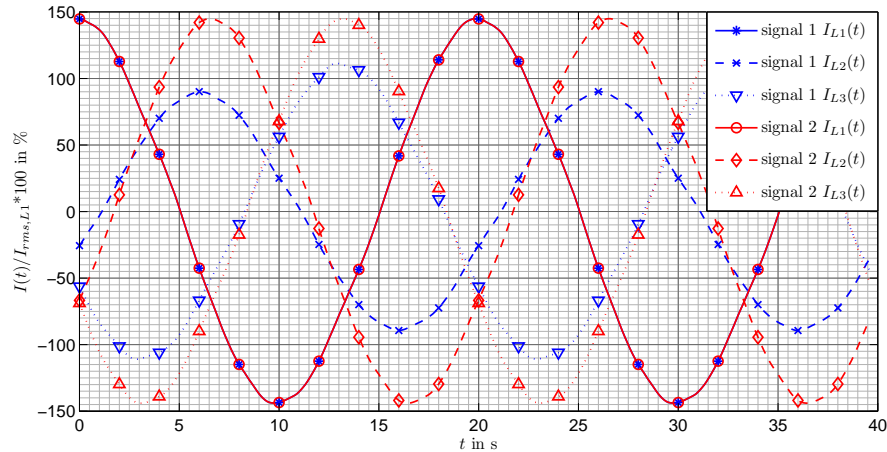


Figure 3.47: Two three-phase signals of a low voltage network in time domain, signal 1 real, signal 2 is ideal but with harmonics

The spectra of these signals are shown in fig. 3.48, split in their symmetrical components. For signal 1, for each harmonic a mixture of symmetrical components exist, while the dominant spectral component shows the consistent with the theory. For signal 2, clearly only the theoretical symmetrical components exist.

In fig. 3.49 typical examples of real voltage and current spectra in a 110 kV network with resonant grounded star point, split in their symmetrical components are given.

Compared to the real spectra of the low voltage network, it attracts attention, that the zero sequence currents almost do not exist. This is mainly because of the non existing neutral conductor.

The harmonic content of the currents in real systems depends strongly on the load situation. The relative current distortion (THDi) decreases for higher loads and so does the harmonic factors $k_{H,I}$. Because of that, the current spectra, given in fig. 3.48 and

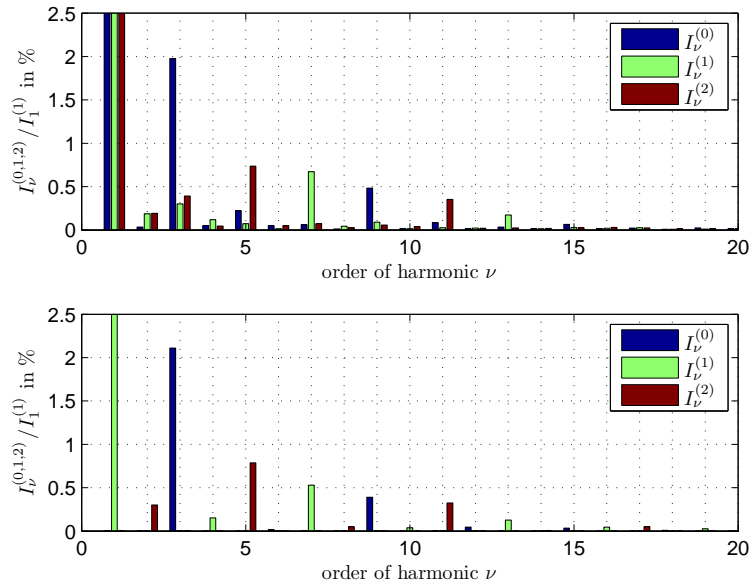


Figure 3.48: Current spectra of two three-phase signals of a low voltage network, split in symmetrical components and normalised to the positive sequence current of the fundamental frequency $I_1^{(1)} = 100\%$, top: signal 1 real (cut off $>2.5\%$: $I_1^{(1)} = 100\%$, $I_1^{(0)} = 17\%$, $I_1^{(2)} = 13\%$), bottom: signal 2 theoretical (cut off $>2.5\%$: $I_1^{(1)} = 100\%$)

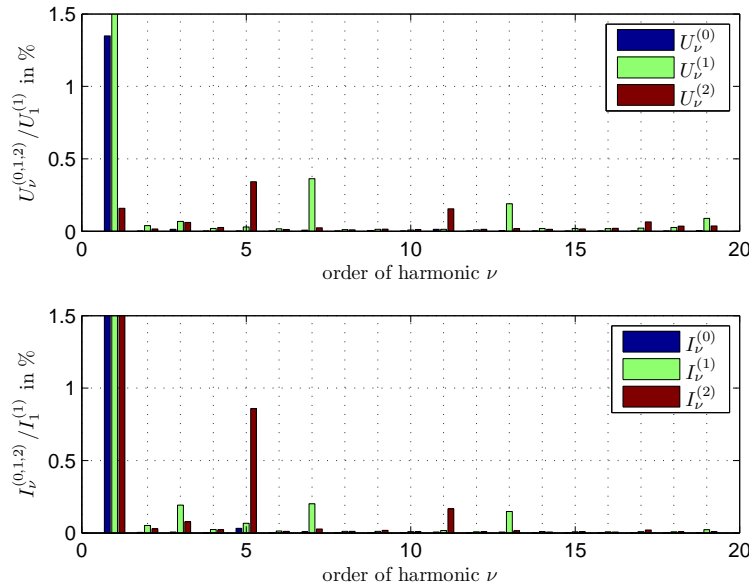


Figure 3.49: Voltage and current harmonics in % of a 110 kV network split in symmetrical components, (cut off $>1.5\%$: $U_1^{(1)} = 100\%$, $I_1^{(1)} = 100\%$, $I_1^{(0)} = 3\%$, $I_1^{(2)} = 2\%$)

3.49 are evaluated for a high load conditions only.

Considering the reference values of ICNIRP 1998 and ICNIRP 2010 for public exposure with harmonics up to the order of $\nu=20$ the results for harmonic factors are presented in tab. 3.9. Additionally the mean and maximum values of the harmonic factors, calculated

for each phase current or voltage separately are given as follows:

$$k_{H,Umean} = (k_{H,U,L1} + k_{H,U,L2} + k_{H,U,L3}) / 3 \quad (3.25)$$

$$k_{H,Umax} = \max(k_{H,U,L1}, k_{H,U,L2}, k_{H,U,L3}) \quad (3.26)$$

$$k_{H,Imean} = (k_{H,I,L1} + k_{H,I,L2} + k_{H,I,L3}) / 3 \quad (3.27)$$

$$k_{H,Imax} = \max(k_{H,I,L1}, k_{H,I,L2}, k_{H,I,L3}) \quad (3.28)$$

Table 3.9: Exemplary harmonic factors for a 110 kV network

	$k_{H,U}^{(0)}$	$k_{H,U}^{(1+2)}$	$k_{H,Umean}$	$k_{H,Umax}$
ICNIRP 1998/2010	0.024	1.170	1.134	1.140
	$k_{H,I}^{(0)}$	$k_{H,I}^{(1+2)}$	$k_{H,Imean}$	$k_{H,Imax}$
ICNIRP 2010	0.036	1.102	1.028	1.031
ICNIRP 1998	0.044	1.288	1.178	1.196

The results for the exposure ratio ER_E of a 1-level-tower (110 kV) 1 m above ground for a calculation with these $k_{H,U}$ s is compared in the fig. 3.50 (top) with the direct calculation for each harmonic with phase values. Additionally the more simple approaches with $k_{H,Umean}$ and $k_{H,Umax}$ are shown. On one hand it can be seen, that at each distance the ER_E resulting from calculations with harmonic factors with symmetrical components (green) is higher than the $ER_E(U_{\nu,L1}, U_{\nu,L2}, U_{\nu,L3})$ obtained by a set of field calculation using the spectrum of the phase voltages (dark blue). On the other hand the simple approach with a mean $k_{H,Umean}$ or maximum $k_{H,Umax}$ of the phases (red and turquoise) would both lead to an underestimation in some areas. It can be seen, that the difference between an evaluation with $k_{H,Umean}$ and $k_{H,Umax}$ is insignificant.

The consideration of a zero or negative sequence system of the fundamental frequency is included in these harmonic factors $k_{H,U}^{(0,1,2)}$ and $k_{H,I}^{(0,1,2)}$, and an additional evaluation as shown in the previous sec. 3.6 has to be done only for compensated networks at fault condition. The overestimations (green > blue) solely develops due to the mixture of the symmetrical systems. If the form of the signals would be equal, as for the signal 2 in fig. 3.47 and fig. 3.49 the green would coincide with the blue line.

In [26] typical values of k_H for low-, medium-, and high voltage networks at a high load condition are given, which are based on a measurement campaign organised by OesterreichsEnergie (formerly Association of the Austrian Electricity Companies -VEÖ), which are summarised in the following tab. 3.10.

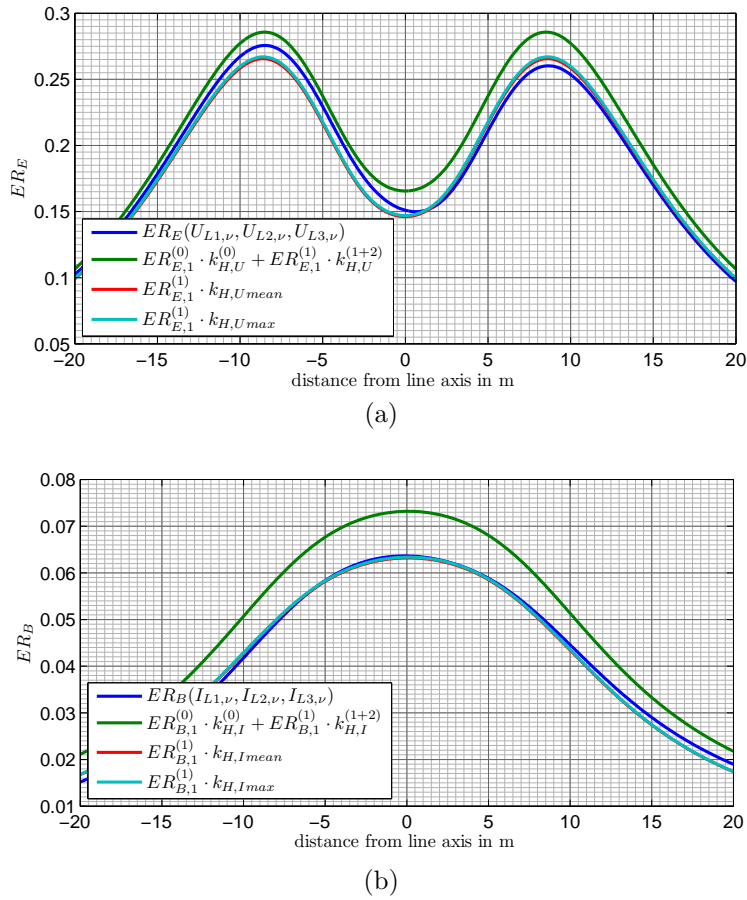


Figure 3.50: Exposure ratios ER_E (a) and ER_B (b) calculated with 4 different approaches for a 1-level-tower, $U_1^{(1)} = 66$ kV, $I_1^{(1)} = 123$ A

Table 3.10: Typical harmonic factors for low voltage (LV), medium voltage (MV) and high voltage (HV) networks

	ICNIRP 1998/2010		ICNIRP 2010		ICNIRP 1998	
	$k_{H,U}^{(0)}$	$k_{H,U}^{(1+2)}$	$k_{H,I}^{(0)}$	$k_{H,I}^{(1+2)}$	$k_{H,I}^{(0)}$	$k_{H,I}^{(1+2)}$
LV	0.03	1.3	0.2	1.2	0.5	1.5
MV	0.02	1.2	0.1	1.15	0.15	1.3
HV	0.03	1.25	0.03	1.1	0.05	1.2

The only problem with that different values of k_H evaluated in [26] is, that the base of data did not allow to consider the mixture of symmetrical components, because only RMS-values of each harmonic and phase were measured (without phase information). Therefore, the analysis of the content in symmetrical components was not possible and the harmonics were considered to be ideal similar to fig. 3.49 (bottom), which could be seen is not that far from reality. Nevertheless, the effect of a zero sequence system at fundamental frequency has to be evaluated separately when dealing with this harmonic factors. For example, if a 110 kV network has a voltage displacement due to the resonant grounded star point of 5%, a value of 0.05 has to be added to the harmonic factor $k_{H,U}^{(0)}$ in order to consider this displacement in the exposure evaluation.

3.8 Difference Between Peak and RMS-Values

Due to phase difference in currents and voltages, rotary fields as mentioned in sec. 2.1.4.3 might occur. In the following the rotating fields of three-phase systems are analysed. Therefore the RMS- and the peak-values of a 220 kV OHL ($h_l=10$ m) are analysed for several phase positions. When comparing peak- and RMS-values of a rotary field, it makes sense to divide the peak-values by $\sqrt{2}$ in order to represent the RMS-value in the major axis of the field ellipse.

In fig. 3.51 the RMS-value of the magnetic flux density B_{rms} and the peak value representative $B_{peak}/\sqrt{2}$ below a 220 kV OHL are shown. If in a point the field is an alternating field, then the RMS-value B_{rms} and the peak-value B_{peak} divided by $\sqrt{2}$ should be equal. It can be seen, that for this example for phase position No. 1 in 1 m above ground almost a pure alternating field exists (the blue solid and dashed line overlap each other). For a better illustration in fig. 3.52 the ratio $B_{rms}/(B_{peak}/\sqrt{2})$ is

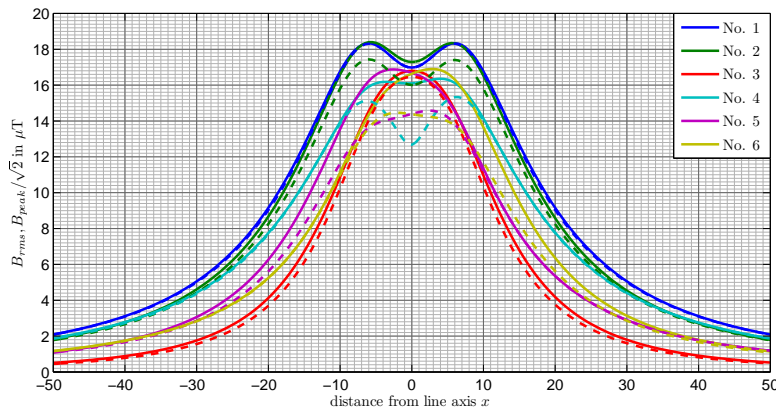


Figure 3.51: RMS-value of the magnetic flux densities B_{rms} (solid) and the peak-value B_{peak} divided by $\sqrt{2}$ (dashed) at 1 m height below a 220 kV OHL type ton ($h_l=10$ m), for several phase positions No. 1 to No. 6

shown. Here, the value 1 means that the field is an alternating field. In contrast, the value $\sqrt{2} = 1.4142$ indicates a field point, where the field ellipse becomes a circle, which is the other extreme of the field ellipse. E.g. for phase position No. 6 the field ellipse at $x=3$ m is mutated almost to a circle.

In fig. 3.53 the same for the electric field strength is shown. It can be noticed, that the electric field strength in 1 m above ground is almost everywhere an alternating field. This could also be observed for other tower types and heights of the lowest conductors (h_l) and has an effect on the evaluation for cardiac pacemakers, as will be seen in sec. 3.9. In fig. 3.54 and 3.55 further isolines of the factors $B_{rms}/(B_{peak}/\sqrt{2})$ and $E_{rms}/(E_{peak}/\sqrt{2})$

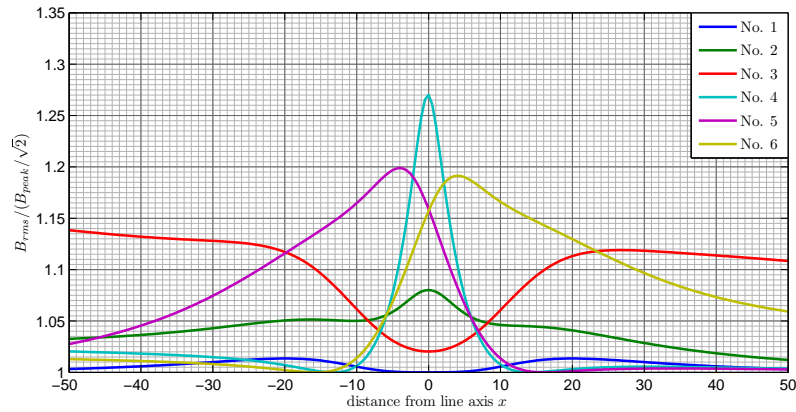


Figure 3.52: Ratio $B_{rms}/(B_{peak}/\sqrt{2})$, at 1 m height below a 220 kV OHL type ton ($h_l=10$ m), for several phase positions No. 1 to No. 6

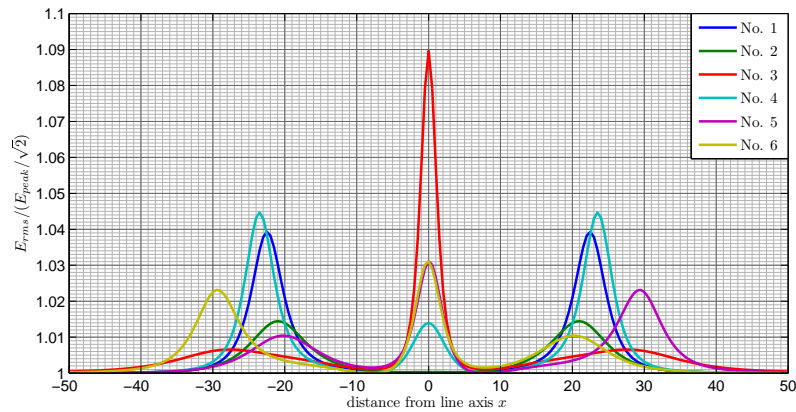


Figure 3.53: Ratio $E_{rms}/(E_{peak}/\sqrt{2})$, at 1 m height below a 220 kV OHL type ton ($h_l=10$ m), for several phase positions No. 1 to No. 6

are shown in order to get a feeling, where around an OHL the magnetic flux density or electric field strength would be an alternating (white areas) and where the field ellipse would become a circle (blue areas). The conductors of the discussed OHLs are indicated with red circles.

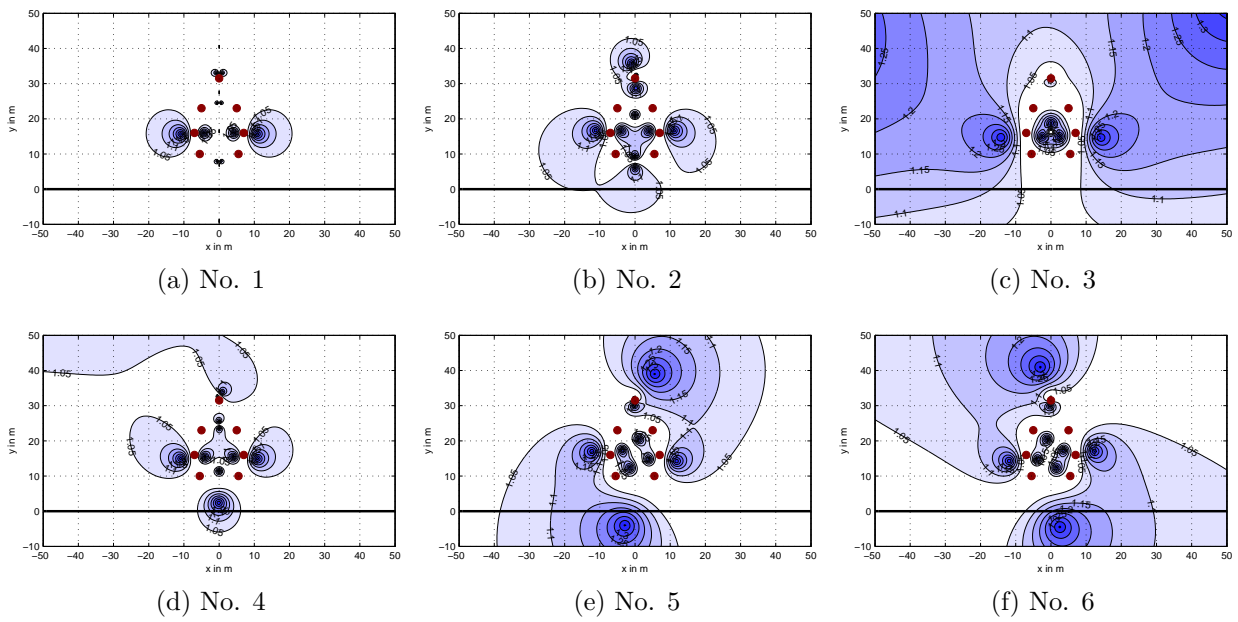


Figure 3.54: $B_{rms}/(B_{peak}/\sqrt{2})$ for several phase position cases (No. 1 to No. 6) of a 220 kV OHL type ton

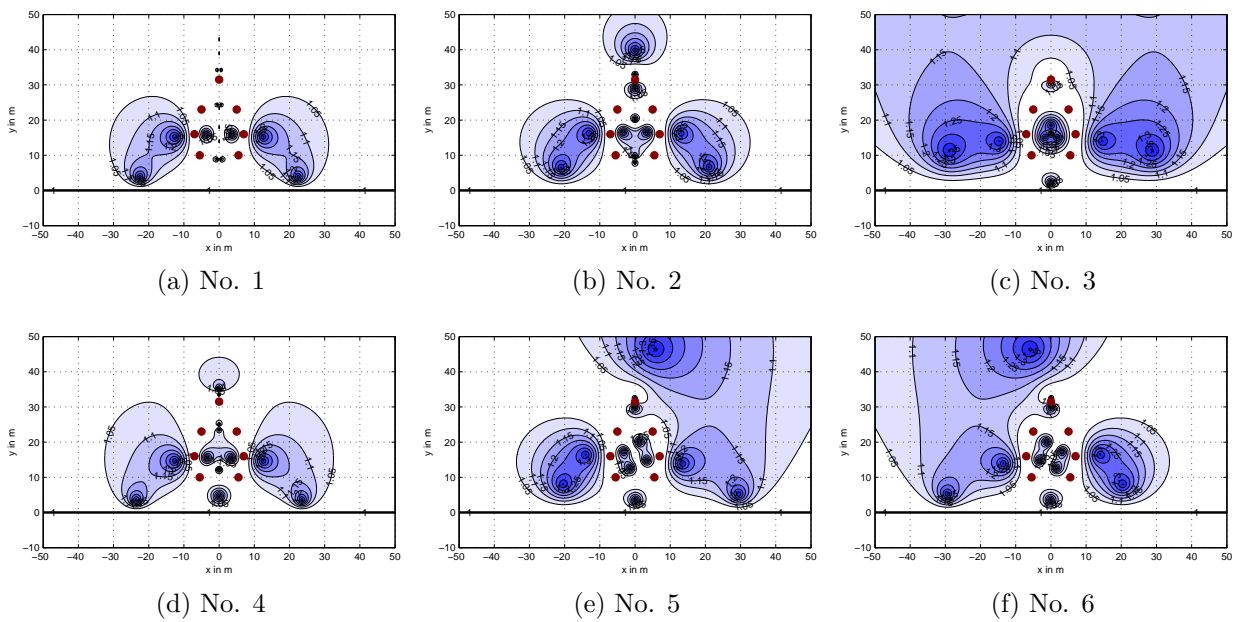


Figure 3.55: $E_{rms}/(E_{peak}/\sqrt{2})$ for several phase position cases (No. 1 to No. 6) of a 220 kV OHL type ton

In fig. 3.56 a single circuit cable system is analysed. The conductor configurations are horizontal and triangle form, respectively. It can be seen, that in the vicinity of a three phase horizontal configuration the alternating field is dominant. In contrast, for the

three-phase configuration in triangle form the field is elliptic, the bigger the distance the more circular the field becomes.

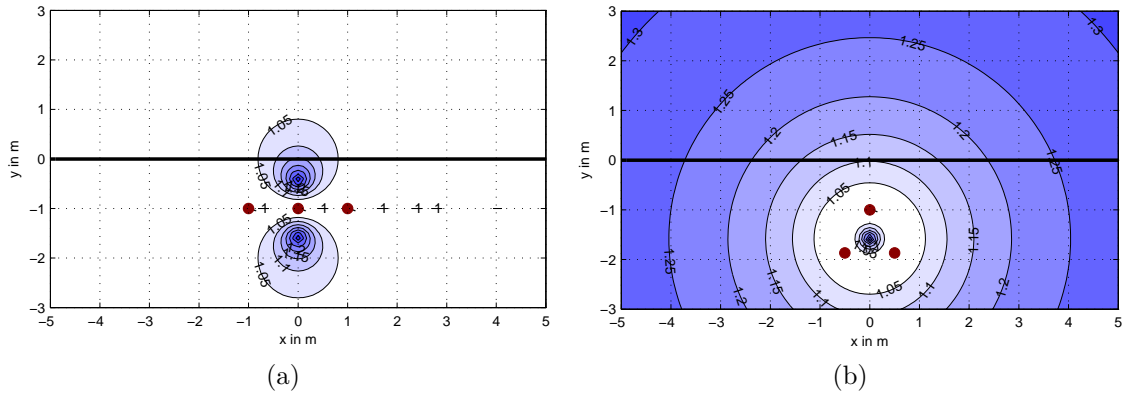


Figure 3.56: $B_{rms}/(B_{peak}/\sqrt{2})$ for a horizontal (a) and a triangle (b) cable configuration

3.9 Cardiac Pacemaker Interference Due To Three-Phase Systems

In this section the combined influence of the electric and magnetic field, caused by three-phase OHLs on cardiac pacemakers is examined more closely. Therefore the exposure ratios ER_{cpm} , as described in section 2.2.4 (p. 25 ff) exemplary of a typical 220 kV OHL are analysed in fig. 3.57 and fig. 3.58.

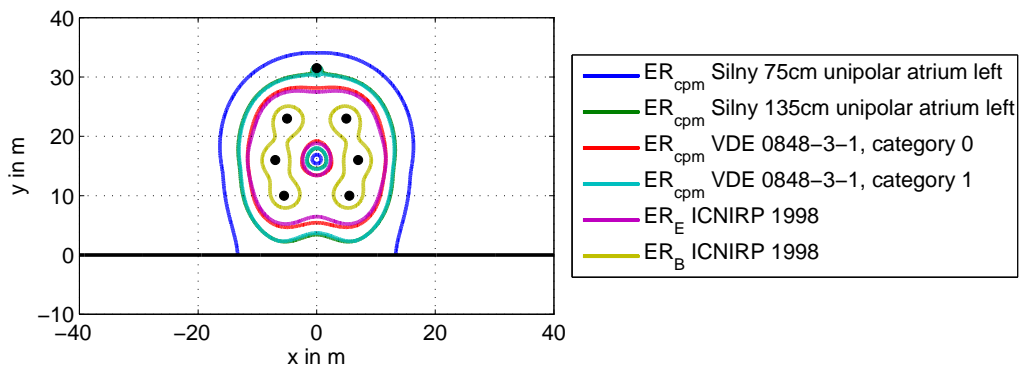


Figure 3.57: Isolines of exposure ratios for different CPMs $ER_{cpm}=1$ as well for reference values according to ICNIRP 1998 ($ER_E=1$, $ER_B=1$) for a 220 kV OHL type ton, $h_l=10$ m, phase position No. 3, $U^{(1)} = 245/\sqrt{3}$ kV, $I^{(1)} = 1000$ A

As it can be seen in fig. 3.58, the exposure ratio for CPM for the worst case cardiac pacemaker according to Silny (Silny 75 cm, unipolar atrium left) would exceed the value 1 within a distance of ± 17 m around the line axis. No other exposure ratio exceeds the

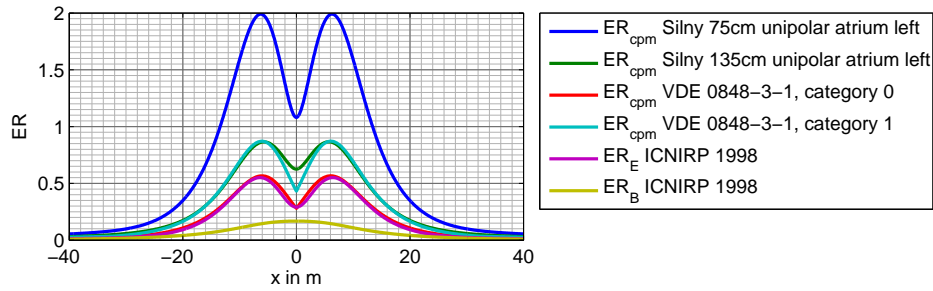


Figure 3.58: Exposure ratios for different CPMs ER_{cpm} as well for reference values according to ICNIRP 1998 (ER_E , ER_B) in 1 m above ground, for a 220 kV OHL type ton, $h_l=10$ m, phase position No. 3, $U^{(1)} = 245/\sqrt{3}$ kV, $I^{(1)} = 1000$ A

value 1 at 1 m above ground. Because the value ER_{cpm} is dependent on both, the electric and the magnetic field and therefore the actual current and voltage, this exposure ratios can not be transformed proportional for different currents.

In order to see the impact of the magnetic flux density on the exposure ratio of CPMs, in the following fig. 3.59 the maximum exposure ratios at 1 m above ground for three different currents (0 A...solid, 1000 A...dashed, 3000 A...dotted) are given. The height of the lowest conductor h_l is varied in a range of 5 to 30 m. According to the previous example of fig. 3.58 for example the maximum ER_{cpm} of 'Silny 75 cm unipolar atrium left' with a current of 1000 A per circuit and a $h_l=10$ m of the lowest conductor is again $ER_{cpm}=2$ (dashed blue line). With help of such a fig. 3.59 the minimum height of the lowest conductor h_l can be evaluated in order to avoid interference of CPMs. For example in order to comply with the maximum interference according to Silny 75 cm unipolar, a minimum h_l of 14.1 m has to be kept, considering a current of 1000 A per circuit. Further it can be seen, that the magnetic flux density contributes less than the electric field strength to the exposure ratio ER_{cpm} , because the solid dashed and dotted lines are rather close together although the range of current is between 0 and 3000 A.

In order to see the influence of the phase position, in fig. 3.60 the ER_{cpm} for various phase positions at 1 m above ground are demonstrated. In compliance with sec. 3.2 this is done for a 380 kV OHL of type danube. Comparing this figure with fig. 3.10, it is obvious, that again the electric field strength plays the major part for the influence of CPMs, because the characteristics of the curves are very similar. Further for that low h_l of only 10 m, the maximum ER_{cpm} would be higher than 1 for all phase positions, and an interference of the CPM of category 1 is possible.

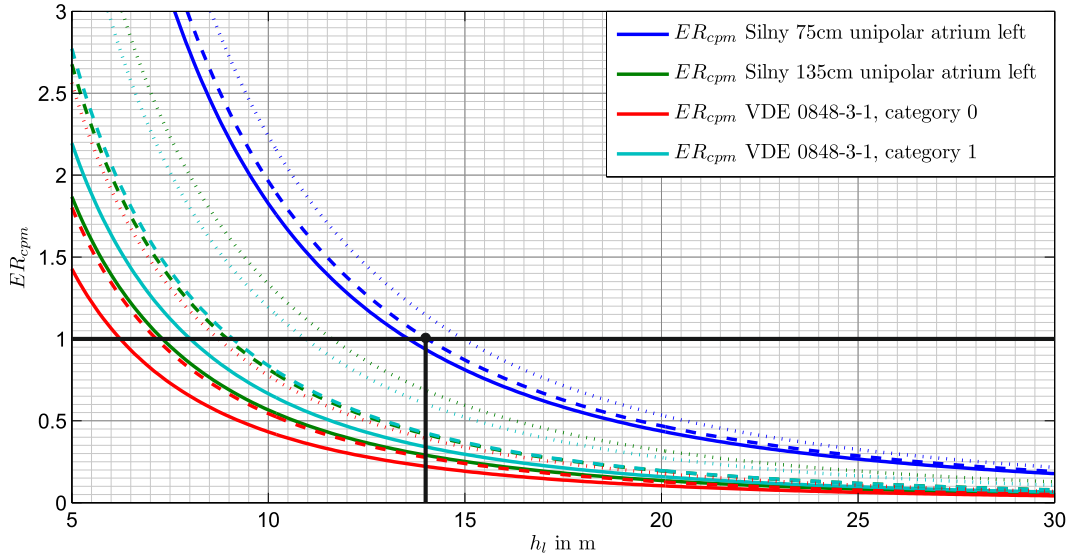


Figure 3.59: Maximum exposure ratios for different CPMs ER_{cpm} in 1 m above ground, for a 220 kV OHL, type ton, dependent on height of the lowest conductor h_l , for currents 0 A (solid), 1000 A (dashed) and 3000 A (dotted) per circuit, phase position No. 3, $U^{(1)} = 245/\sqrt{3}$ kV

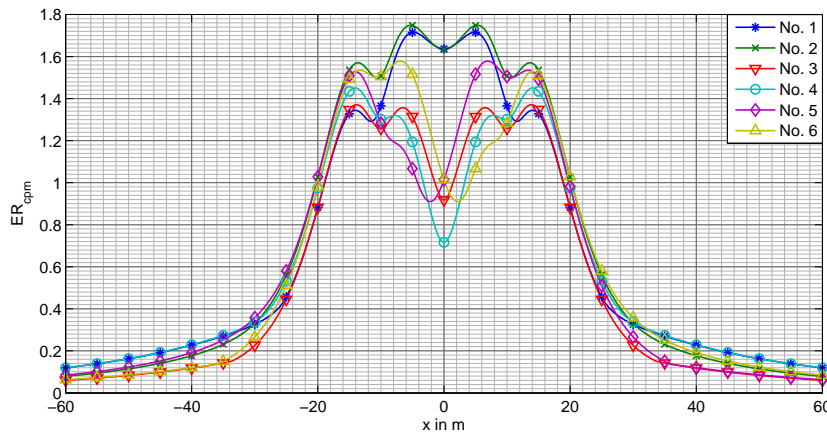


Figure 3.60: Exposure Ratio of CMP (VDE, category 1) in 1 m above ground below a 380-kV OHL, 2-level tower

In analogy to fig. 3.8 and fig. 3.10, in the following fig. 3.61 the areas, where a phase position No. 1 to No. 6 will lead to the lowest ER_{cpm} are given. The phase position with the lowest interference of CPMs (VDE 0848-3-1, category 1) is phase position No. 3, therefore this phase position would be for that specific configuration the best choice.

As it is described in section 2.2.4.2, the specific interference voltages u_{iB} and u_{iE} are calculated for RMS-values of sinusoidal alternating fields and because of rotary fields an

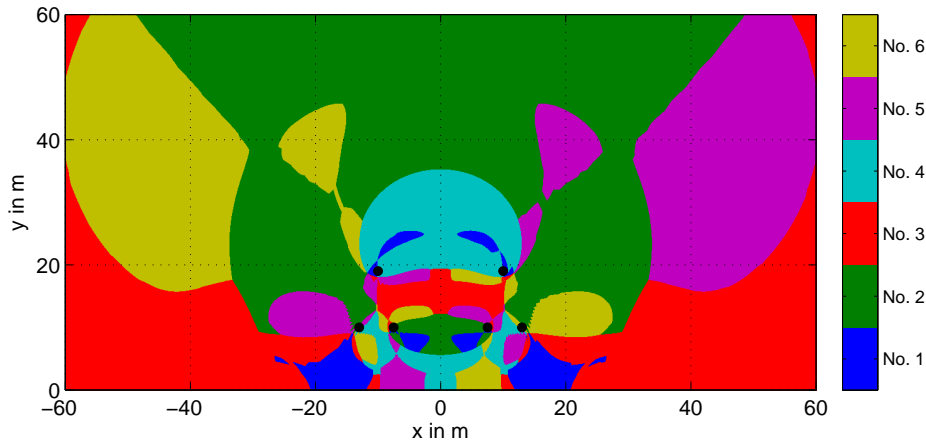


Figure 3.61: Areas, where the different phase allocation cases No. 1 to No. 6 cause the lowest values of ER_{cpm} for VDE 0848-3-1, category 1

overestimation for CPMs might occur. Therefore in the following the exposure ratios for CPMs according to Silny are analysed on one hand with RMS-values (rms) and on the other hand with the RMS-values of the major axis of the field ellipse (peak value divided by $\sqrt{2}$). As it can be seen in fig. 3.62, the differences between these two evaluation methods (rms, peak) has only little effects on the exposure ratios of CPMs, as the curves are overlapping each other. The effect is only minor, because the electric field strength contributes major to ER_{cpm} and the electric field strength at 1 m above ground - as it could be seen in section 3.8 - occurs to be mainly an alternating field. For the most common double circuit tower types according to tab. 3.3 the minimum height of the lowest conductor to achieve $ER_{cpm} < 1$ for the best and worst phase position and a current of 1000 A is evaluated, and presented in the following tab. 3.11. For all tower types phase position No. 3 is the one with the lowest maximum ER_{cpm} and phase position No. 1 is the one with the highest maximum ER_{cpm} . Especially eye-catching in this table is further, that the tower height for the most sensitive CPM according to Silny would be unrealistic high, even for the best phase position.

At the end of this section it should be mentioned, that for UGL no electric fields occur. Therefore the evaluation of the ER_{cpm} is the same as the evaluation of the magnetic flux density and no additional analysis is necessary.

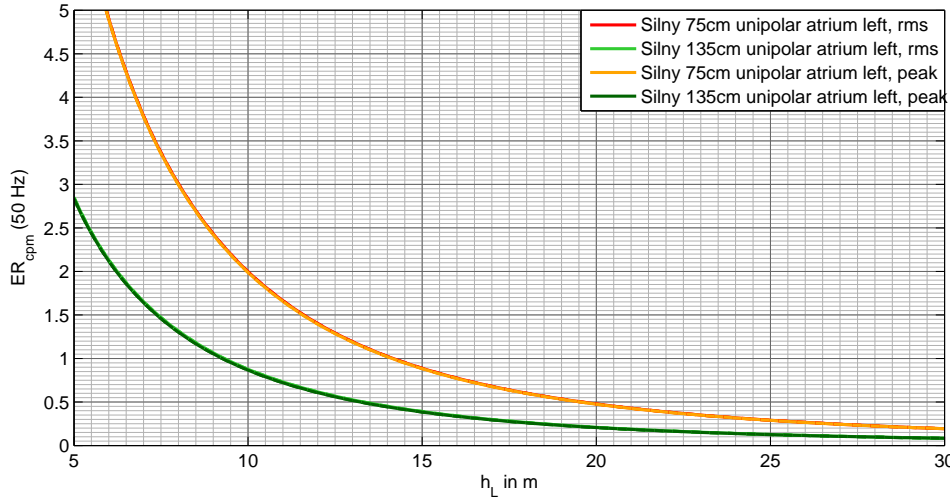


Figure 3.62: Maximum exposure ratios ER_{cpm} for selective CPMs validated with the Silny-formulas for a 220 kV OHL (type ton) in 1 m above ground dependent on the height of the lowest conductor h_l for phase positions No. 3 comparing evaluation with RMS-value and peak-value/ $\sqrt{2}$

Table 3.11: Minimum height of the lowest conductor h_l to achieve $ER_{cpm} = 1$ for $I=1000$ A per circuit and maximum voltage for best phase position and worst phase position

voltage- level	type of ER_{cpm} evaluation	h_l for $ER_{cpm}=1$			
		2-level-tower		3-level-tower	
		best	worst	best	worst
110kV	Silny 75 cm unipolar atrium left	8.0	11.5	9.1	15.0
	Silny, 135 cm unipolar atrium left	5.6	7.6	6.5	8.3
	Silny, 75 cm bipolar atrium	4.4	5.5	4.9	5.5
	VDE 0848-3-1, category 0	4.5	5.5	5.0	5.5
	VDE 0848-3-1, category 1	5.5	7.5	6.3	8.2
220kV	Silny 75 cm unipolar atrium left	13.2	19.0	14.1	24.0
	Silny, 135 cm unipolar atrium left	8.2	11.0	9.0	12.0
	Silny, 75 cm bipolar atrium	7.3	9.2	7.8	9.6
	VDE 0848-3-1, category 0	6.7	8.0	7.2	8.2
	VDE 0848-3-1, category 1	8.4	11.3	9.1	12.6
380kV	Silny 75 cm unipolar atrium left	18.0	26.4	21.1	36.0
	Silny, 135 cm unipolar atrium left	10.6	13.2	12.7	16.1
	Silny, 75 cm bipolar atrium	10.0	12.0	11.8	14.5
	VDE 0848-3-1, category 0	8.8	10.0	10.4	11.6
	VDE 0848-3-1, category 1	11.1	14.2	13.3	17.7

4 Chapter 4

Parameters and EMF of Electric Railways Systems

4.1 General

As for the OHL and UGL, the conductor positions of the electric railway system are significant when it comes to a field evaluation in the surrounding of an electrical railway. Therefore, in fig. 4.1 the main elements of a typical Austrian double track railway system are illustrated. The nominal operation voltage of the system is 15 kV, the maximum voltage amounts to 18 kV. The operation frequency is given with 16.7 Hz.

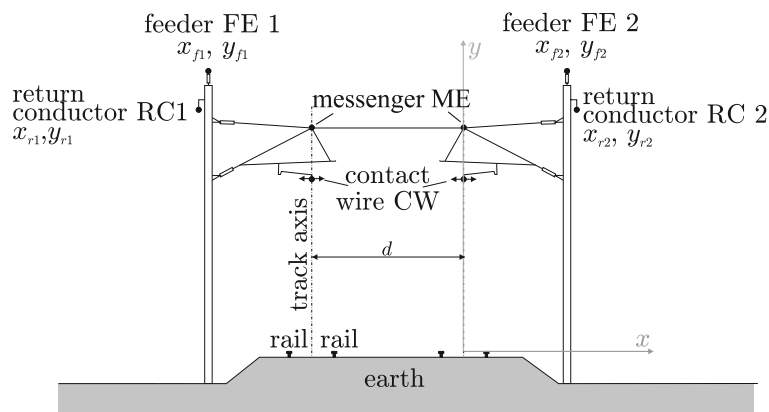


Figure 4.1: Cross section of a typical Austrian double track railway system, distance between 2 track systems $d=4.7\text{m}$,

The abbreviations and positions of the conductor are:

- contact or catenary wire CW $\Delta x = 0$ m from track axis, $\Delta y = 5.5$ m
- messenger or track cable ME $\Delta x = 0$ m from track axis, $\Delta y = 7.1$ m
- rails RA, track gauge 1.4 m
- feeder FE $\Delta x = \pm 3.2$ m from track axis, $\Delta y = 8.7$ m
- return conductor RC $\Delta x = \pm 3.5$ m from track axis, $\Delta y = 7.6$ m

These positions are either used as the reference configuration for the following analysis or as the starting configuration for the optimisation of feeder and return conductor, which is carried out in sec. 5.6.2.

In the following sections a selection of important parameters on electrical railway systems are discussed in detail.

4.2 Current Distribution

The current distribution of the traction current between messenger, contact wire and feeder on the one side and rails, return conductor and earth on the other side has a big influence on the characteristic of the magnetic field. This current distribution is dependent on the position of the locomotive on the track, the type of energy supply (from one side, from both sides, coupled,...), the earthing, positions of the connection between rails or between feeder and messenger and the impedances of the conductors. A model of a railway track with the power supply from one side is shown in fig. 4.2. Here the coupling of the impedances is only sketched for one position, although it exists all way long. The circumstance, that the impedances of the rails are even dependent on the current, complicates the calculation of the current distribution in a way, that the currents have to be calculated recursively. Therefore, the calculation of the impedances of the rails and their dependency on the current are given in the following subsection 4.2.1. With that base, further in subsection 4.2.2 the return current distribution is analysed. After all in subsection 4.2.3 the influence of the current distribution on the magnetic flux density in vicinity of the railway system is analysed.

4.2.1 Inner Impedance of Rails

Due to the higher relative permeability μ_r of the material used for rails (steel, $\mu_r = 10...5000$) compared to overhead wire (copper, aluminium, $\mu_r = 1$) the skin effect has to be considered even for low (power) frequencies. Because the relative permeability of steel depends on the magnetic field strength H it also depends on the current flow through the conductor, and as a consequence, the inner impedance $\underline{Z}_{i,rail}$ of a specific rail becomes dependent on frequency and permeability. The publications [39] and [11] provide empiric formulas for inner impedance of the rails, which are original extracted from [50]. These numerical value equations from [39] are rendered in (4.1).

$$\frac{\underline{Z}'_{i,rail}}{\Omega/\text{km}} = 0.446 \left(\frac{r_{eq,P}}{\text{mm}} \right)^{-1} \sqrt{\mu_r \frac{\rho_{rail}}{\Omega\text{mm}^2/\text{m}} \frac{f}{\text{Hz}}} + j 2.7 \cdot 10^{-3} \sqrt[4]{\left(\frac{f}{\text{Hz}} \right)^3 (\mu_r - 6)} \quad (4.1)$$

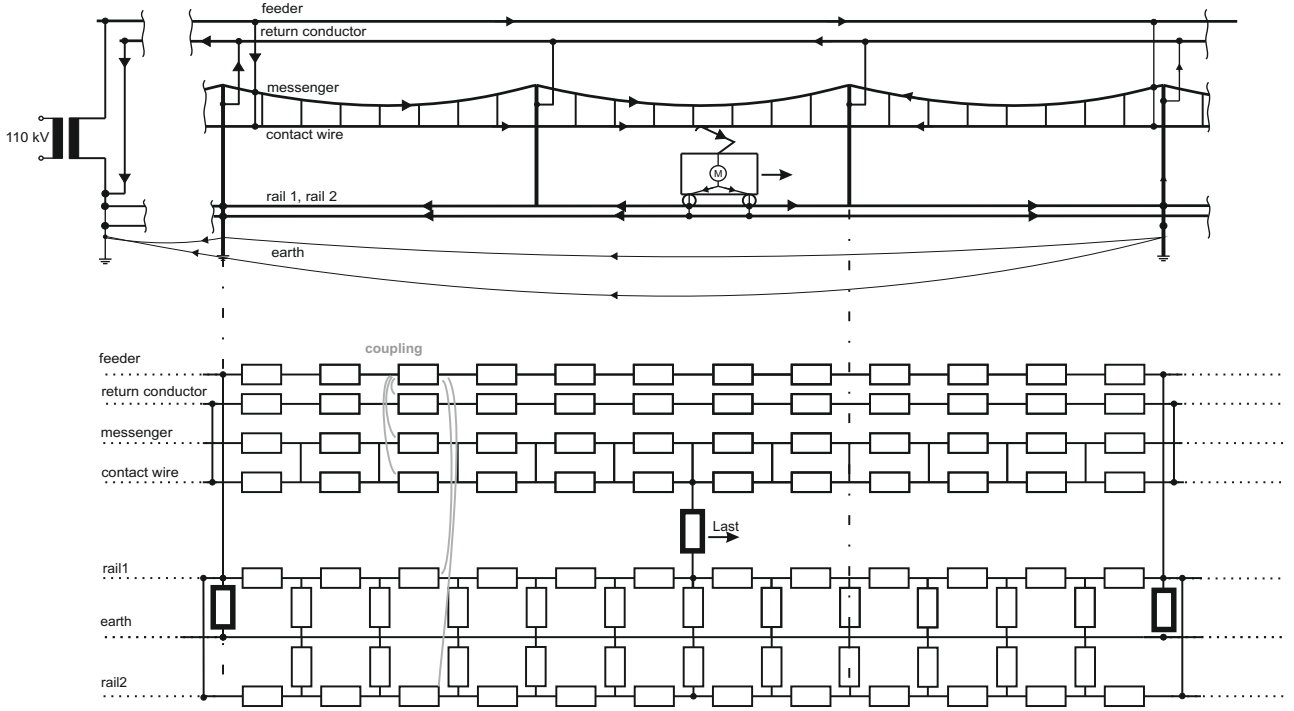


Figure 4.2: Model for calculation of the current distribution along a railway track

$Z'_{i,rail}$	inner impedance of the rail per unit length
$r_{eq,P}$	perimeter equivalent radius $r_{eq,P} = P/2\pi$
P	perimeter of the rail
μ_r	relative permeability
ρ_{rail}	electrical resistivity of the rail
f	frequency

As an alternative, in [48] the following simplified formulas for cylindrical conductors (4.2) and (4.3), with a skin depth of $\delta = (\pi f \mu / \rho_{rail})^{-1/2}$ are given. There, a distinction is made between a 'low frequency' range, where the current distribution is mainly unified along the cross section (defined with $r_{eq} < 2\delta$) and between a 'high frequency' range, where the current distribution is almost only along the perimeter ($r_{eq} > 2\delta$).

$$r_{eq} < 2\delta: \quad Z'_{i,rail} = \frac{\rho_{rail}}{\pi r_{eq}^2} + j\omega \frac{\mu}{8\pi} \quad (4.2)$$

$$r_{eq} > 2\delta: \quad Z'_{i,rail} = \frac{1}{2r_{eq}} \sqrt{\frac{\mu f \rho_{rail}}{\pi}} + j \frac{f}{2r_{eq}} \sqrt{\frac{\mu \rho_{rail}}{f\pi}} \quad (4.3)$$

δ	skin depth
r_{eq}	equivalent radius
μ	permeability $\mu = \mu_r(I)\mu_0$

The equivalent radius r_{eq} for the rails in the 'low frequency' range with an almost unified current distribution can be computed from the cross section $r_{eq,A} = \sqrt{A/\pi}$. For 'higher frequency', where the current flows mainly along the perimeter the equivalent radius is derived from the perimeter P to $r_{eq,P} = P/2\pi$.

The necessary parameters for impedance evaluation of common rails are listed in tab. 4.1. The typical cross section of a rail type UIC 60 is presented in fig. 4.3.

Table 4.1: Rail parameters collected from [11] and [46], A ...cross section, P ...perimeter

railtype	A mm ²	P mm	$r_{eq,P}$ mm	$r_{eq,A}$ mm
S 49	6297	600	95.49	44.77
R 50	6450	620	98.68	45.31
S 54	6948	630	100.27	47.03
UIC 54	6934	630	100.27	46.98
S 60	7650	680	108.23	49.35
UNI 60	7678	656	104.41	49.44
UIC 60	7686	680	108.23	49.46
R 65	8288	700	111.41	51.36

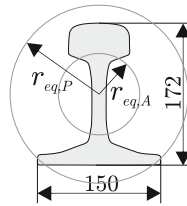


Figure 4.3: Profile of a rail type UIC 60 with the equivalent radii derived from the cross section $r_{eq,A}$ and from the perimeter $r_{eq,P}$

Additionally, for the calculation of the inner impedance it is necessary to know the relative permeability μ_r . The relative permeability of ferromagnetic material is dependent on the magnetic field strength H . According to [39] the correlation between the magnetic field strength and the current in a rail can be described with the following equation.

$$\frac{H}{\text{A cm}^{-1}} = 4\pi \frac{I_{rail}}{\text{A}} \left(\frac{P}{\text{mm}} \right)^{-1} \quad (4.4)$$

For a given relative permeability depending on the magnetic field strength, the dependency of the relative permeability depending on the rail current can be evaluated. In fig. 4.4 the relative permeability μ_r for different types of rails are summarised, collected

from [11] and [39]. Because the parameter μ_r of the very often used rail of type UIC 60 was not listed in either source, a mean value (curve c) of the μ_r for UIC 50, R 65, S 49/R 50 and R 65 was built, because the weight and the cross section of UIC 60 lays between these types of rails. It has to be mentioned, that the Parameter μ_r in dependency of the current I_{rail} was evaluated by measurement of the impedance of the rail

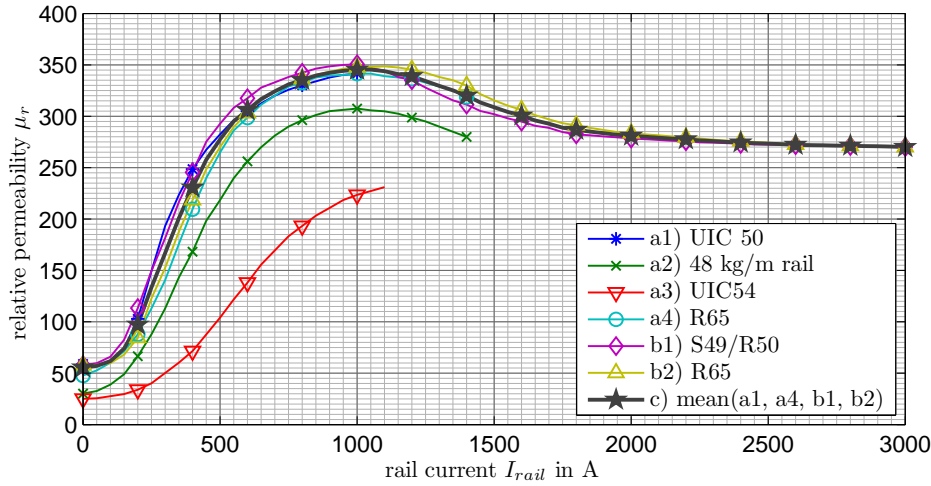


Figure 4.4: Permeability of several rails depending on the rail current values a) from [11], b) from [39], c) is the mean value of a1, a4, b1 and b2

In fig. 4.5 the skin depth δ of a conducting material with parameters like a common rail for a frequency of 16.7 Hz is given. It can be seen that for equivalent radii given in tab. 4.1 and the range of relative permeability μ_r given with fig. 4.4, the equivalent radius for $\mu_r > 25$ at 16.7 Hz is always bigger than 2δ . Therefore, in sense of the skin effect in a permeable conductor, the frequency of 16.7 Hz belongs to the 'high frequency range', and equations (4.3) have to be used with the perimeter equivalent radius $r_{eq,P}$ for the radius of the conductor .

In fig. 4.6 the absolute value as well as the real and imaginary part of inner impedance $Z'_{i,rail}$, the impedance of a rail-earth-loop $Z'_{rail,E}$ and of an earth return loop with 2 rails $Z'_{2rail,E}$ depending on the current through each rail I_{rail} for rails of type UIC 60 are given. For the relative permeability μ_r curve c) of fig. 4.4 was taken into account. For the calculation of the impedance of the rail impedance with earth return, the modified Dubanton earth return impedances eq. (2.57-2.59) were used. The specific resistance of the rails is chosen with $\rho_{rail} = 2.4 \cdot 10^{-7} \Omega\text{m}$ according to [39]. These impedances in sub-figure (a) were calculated using (4.1) for the inner impedance, the ones in sub-figure (b) according to [48] with (4.3).

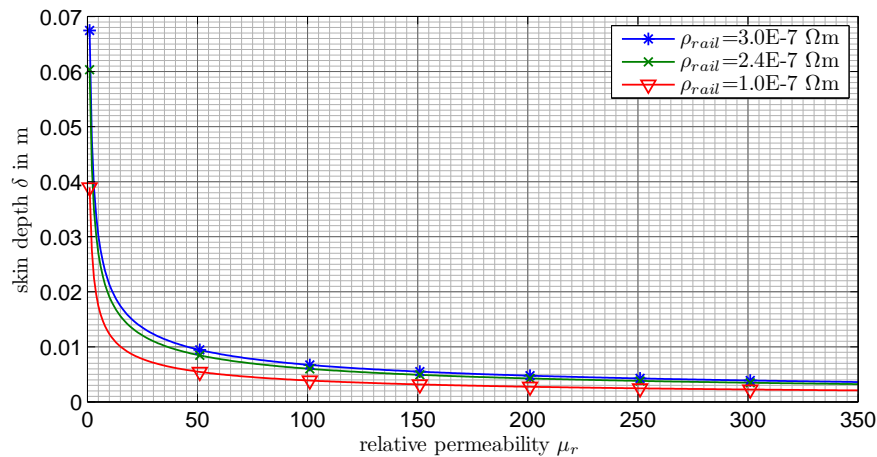


Figure 4.5: Skin depth δ of a conducting material with various specific resistance ρ_{rail} dependent on the relative permeability of the material μ_r at 16.7 Hz

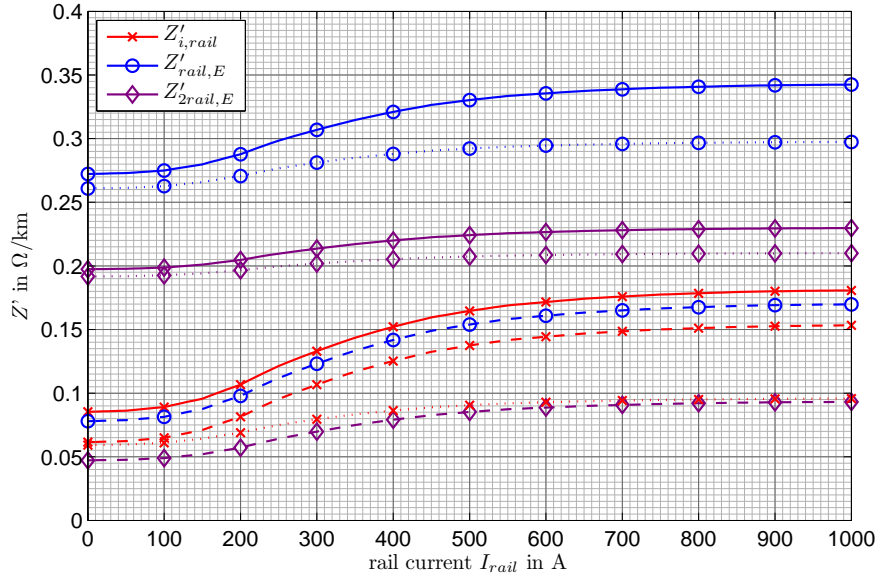
Comparing (a) and (b) of fig. 4.6, it can be seen, that the differences between these formulas is not very big, especially when analysing the impedance of the loop with two rails and earth return ($Z'_{2rail,E}$). Therefore, the currents in the rails and as a consequence the magnetic field in the surrounding will not be effected strongly through the choice of the impedance formula for the inner impedance of the rail. Because measurements in [48] further show compliance with the calculated impedances, in the following, the inner impedances are mainly calculated using (4.3).

Nevertheless, as shown in [65] for a third rail (contact bar) the inner impedance of a rail can be also calculated by dividing the rail into small coupled subconductors. The Z-Matrix of these subconductors can easily be computed. In [46] it is described, that this possibility is rather numerical than analytical with the advantage of better results, but higher effort in modelling and calculation.

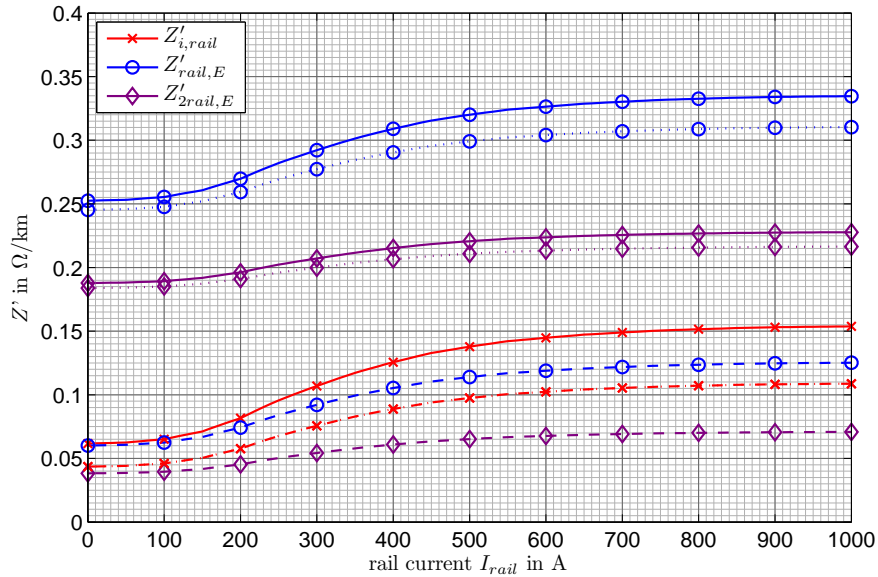
Further a time-harmonic eddy-current problem with a finite element method (FEM) could have been implemented, but for the analytical way of calculating the magnetic field in the surrounding of the electric railway, this would be an inefficient way, because for each current a FEM-analysis have to be done.

4.2.2 Current Distribution Between Rails, Earth and Return Conductors

In the following the dependency of the return current distribution on the system configuration (e.g. number of tracks, number of return conductors) are analysed using a typical single track and double track example. Further the results are compared with measured values from similar railway tracks.



(a) calculation with (4.1)



(b) calculation with (4.3)

Figure 4.6: Absolute value (solid), real part (dashed) and imaginary part (dotted) of the impedances per unit length depending on the current through the rail, inner impedance $Z'_{i,rail}$, rail-earth-loop-impedance $Z'_{rail,E}$, impedance of earth return loop with 2 rails $Z'_{2rail,E}$

This results of the double track system are very similar to measurement results of the current distribution given in [66]. In [40] the current distribution for a single railway track with FE and RC is given with RC 30.1%, rails 40.7% and earth 29.2% which concurs well for a railway track with a low traction current.

Fig. 4.7 further testifies, that the current distribution is quite steady in a range of

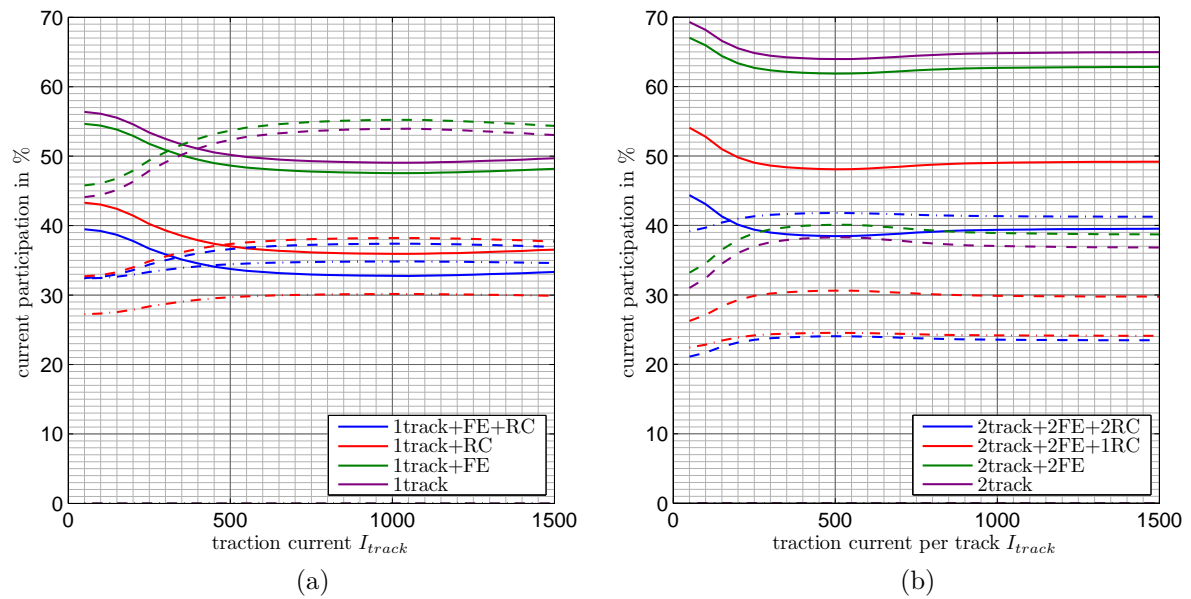


Figure 4.7: Current distribution of the return current between rails (solid), earth (dashed) and return conductor (dot-dashed) for a single track (a) and double track (b) with or without feeder(s) (FE) or return conductor(s) (RC)

500 A to 1500 A per track, so for worst-case estimations with high traction currents it is possible to linearise the current distribution and as a conclusion also the magnetic field of simple configurations. Further it can be seen, that also the feeder influences the current participation of the earth. That is due to a better coupling with rails and with the return conductors (if installed).

In fig. 4.8 additional to fig. 4.7 (b) the dependency of the earth resistivity can be seen clearly. The current participation of rail and return conductor (if present) rises, because the earth has a higher resistivity.

For worst case evaluation and optimisation of the positions of return conductor and feeders it is important to know further, that the positions of these conductors does not only change the magnetic and electric field in the surrounding, but also the current distribution within the system. Therefore, for the single track system the positions of the return conductor is varied in fig. 4.9. It can be seen, that the coupling of the return conductor with the contact wire and feeder is best, when the return conductor is mounted at the inner side of the tower. Then the current participation of the return conductor is the highest. But, it can not necessarily be concluded, that this position of the return conductor has also the minimum electric and magnetic field. The effect of the current distribution on the magnetic field is discussed further in the next section.

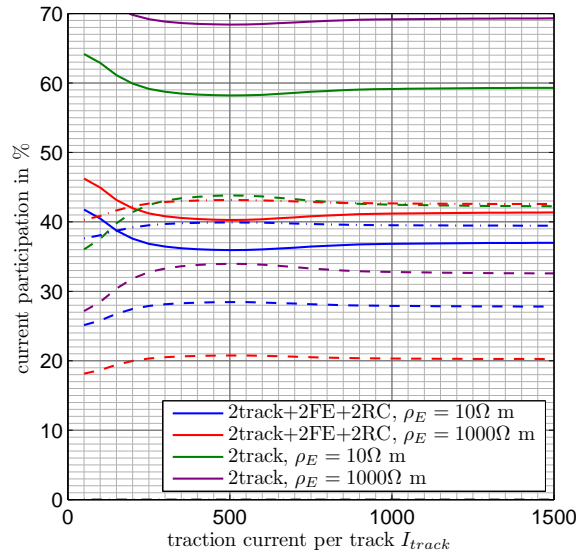
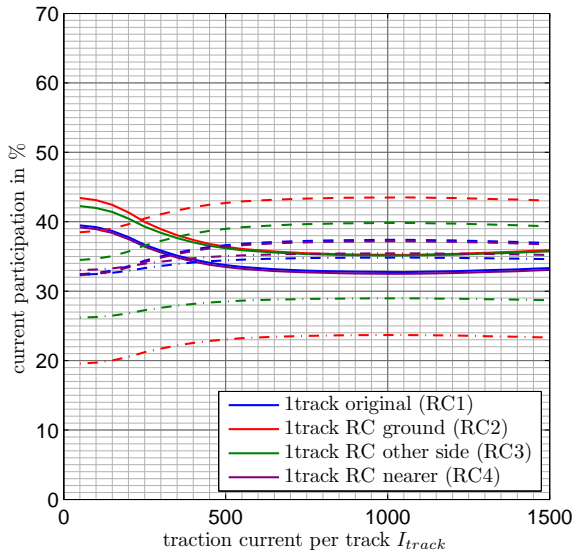
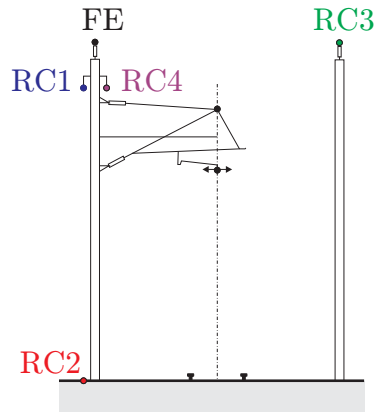


Figure 4.8: Current distribution of the return current between rails (solid), earth (dashed) and return conductor (dot-dashed) for a double track with or without feeders (FE) or return conductors (RC) with variant earth resistivity



(a)



(b)

Figure 4.9: Current distribution of the return current between rails (solid), earth (dashed) and return conductor (dot-dashed) for a single track with feeder at fixed position ($x=-3.2$ m $y=8.7$ m) and varying return conductor position (RC); original ($x=-3.5$ m, $y=7.6$ m), on ground level ($x=-3.5$ m, $y=0$ m), on a tower on the other side of the track axis ($x=3.2$ m, $y=8.7$ m), on the inner side of the feeder tower ($x=-3$ m, $y=7.6$ m)

4.2.3 Impact of the Current Distribution on the Magnetic Flux Density in the Vicinity of Railway Systems

In the following, the effect of the return current participation of rails, return conductor(s) and earth on the magnetic flux density is discussed in detail for the conductor arrangement given in fig. 4.1. In [23] and [61] the effect of the current distribution is discussed theoretically on the base of some fictive cases of current distributions, which are reported in the following table.

Table 4.2: Various fictive cases of current distributions within an electric railway systems [61]

case No.	participation of the return conductors (RC)	participation of the rails (RA)	participation of the earth (E)
1	0%	10%	90%
2	0%	50%	50%
3	0%	100%	0%
4	40%	40%	20%
5	80%	10%	10%

Case 1 is a representative for a current distribution with a majority of the current through the earth. This case only might happen if the rails are insulated to earth and if only near the traction low resistant connections between rails and earth exist. Only then, the earth is more attractive for the return current. The current distribution of case 2 can be compared to the typical current distribution of a railway system without any return conductor (see therefore fig. 4.7 (a)). Case 3, with only the rails participating in the return current would only occur when no connection between earth and rails exists, or if a booster transformer forces the current into the rails. All under the premise, that no return conductor is installed. Case 4 represents the typical current distribution of a double track system with two return conductors. An installation with a booster transformer, which forces the return current to go mainly through the return conductors, might lead to the current distribution of case 5.

The resulting magnetic flux density of a double track system according to fig. 4.1 with 1000 A current per track for that five current distribution cases is given in fig. 4.10 at 1 m above ground, and in fig. 4.11 in form of isolines. Additionally in fig. 4.11 the worst case of all cases - the envelop-curve - is presented (bottom right). It can be seen, that for an area 1 m above ground, the case 5, where the return conductor mainly carries the return current, would lead to the smallest magnetic flux densities, in both, a near position and a distant position. Case 3 with the main current transport in the rails on

the other hand effects the highest magnetic flux densities near the rail axes. In a distant point, case 1 with the earth as the main conductor of the return current, would be the most disadvantageous case. The results of case 2 and case 4 lay in between the other analysed cases.

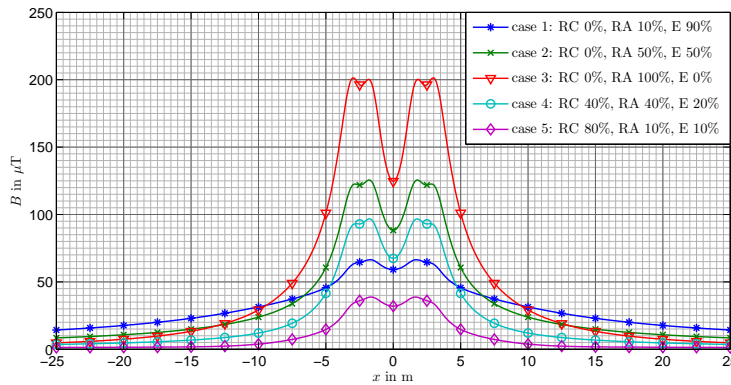


Figure 4.10: Magnetic flux density 1 m above ground for different cases of return current distribution between return conductors (RC), rails (RA) and earth (E), $I_{track}=1000$ A per track

This conclusion can also be confirmed with fig. 4.12 where the areas are indicated with the colour of the return current distribution case which would lead to the maximum (a) or to the minimum magnetic flux density (b) in that point. Case 2 and 4 are absent in (a), because compared to the other cases these cases would not lead to a maximum magnetic field. Case 5 would only lead in an area between the contact wire, feeder and return conductor to higher magnetic flux densities than the others. But in the most accessible area - as can be seen in (b) - this case 5 would lead to the lowest magnetic flux densities and would therefore be preferable.

In the following the magnetic flux densities for calculated current distribution as seen in sec. 4.2.2 are evaluated for a double track system with or without return conductors and feeders.

In fig. 4.13 the effect of existing feeders and return conductors can be seen for a double track system with 1000 A per track. If feeders as well as return conductors exist (2 RC and 2 FE), the magnetic flux density at 1 m above ground would be minimised compared to other cases. Only in a distant area, the configuration without feeders but with return conductors would be a bit more advantageous.

On the contrary, the configuration without RC and FE would lead to the highest maximum magnetic field, the configuration with only feeders to the highest field values in a distant point. Additionally in that figure, the effect of different inner impedance calculation according to sec. 4.2.1 can be made out. For each configuration there are always two lines, which almost completely overlap each other. Hence, the evaluation of the

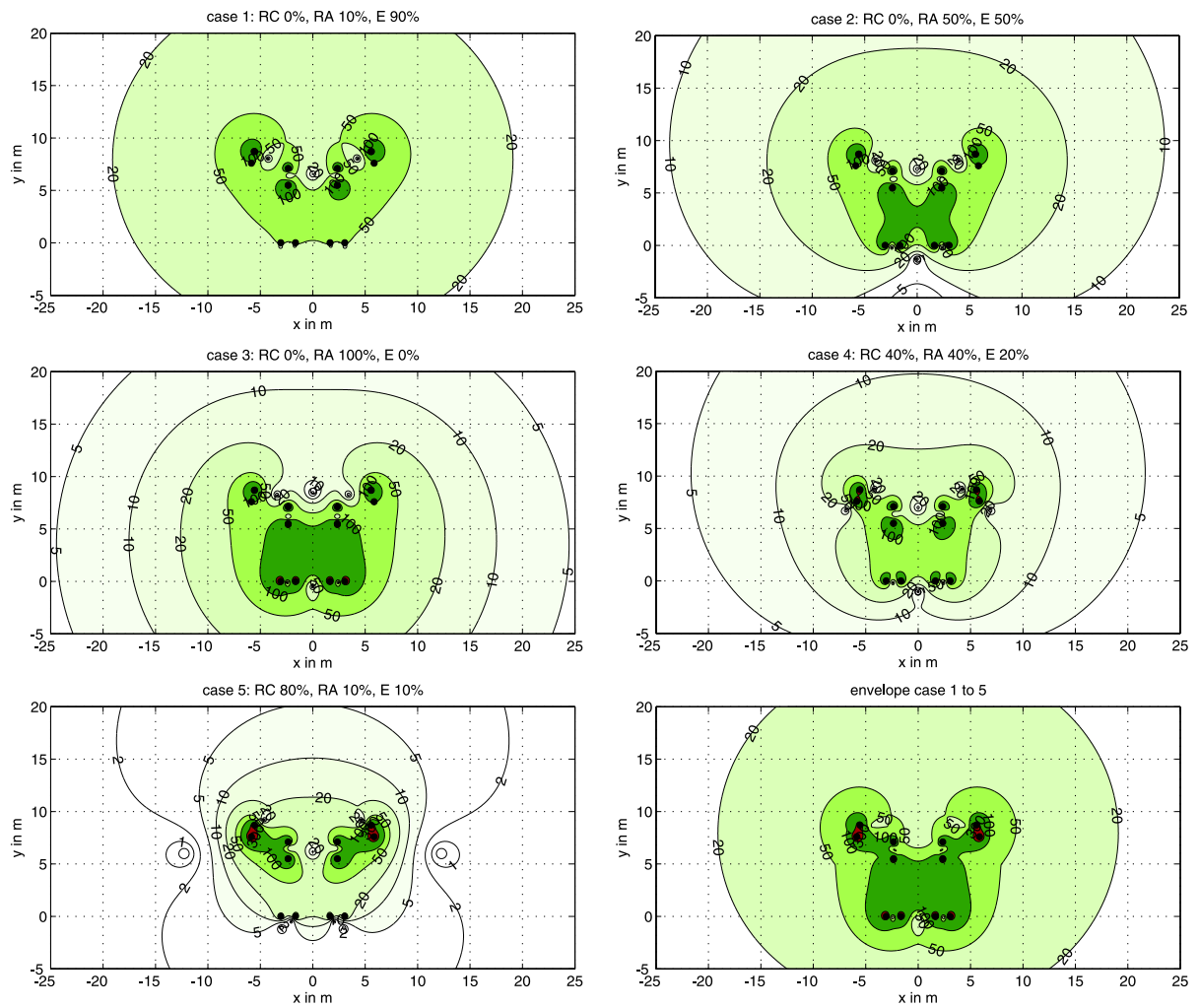


Figure 4.11: Isolines of the magnetic flux density for different cases of return current distribution between return conductors (RC), rails (RA) and earth (E), $I_{track}=1000$ A per track

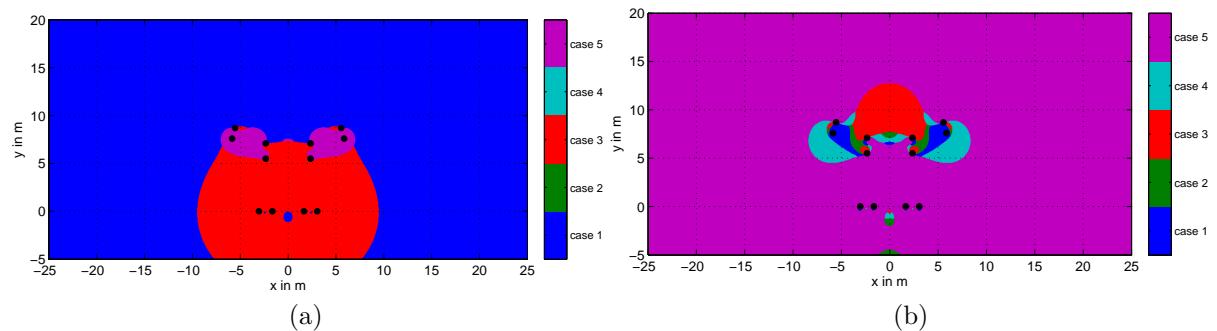


Figure 4.12: Areas, where the specific return current distribution cases would lead to the maximum magnetic field (a) or to the lowest magnetic fields (b), $I_{track}=1000$ A per track

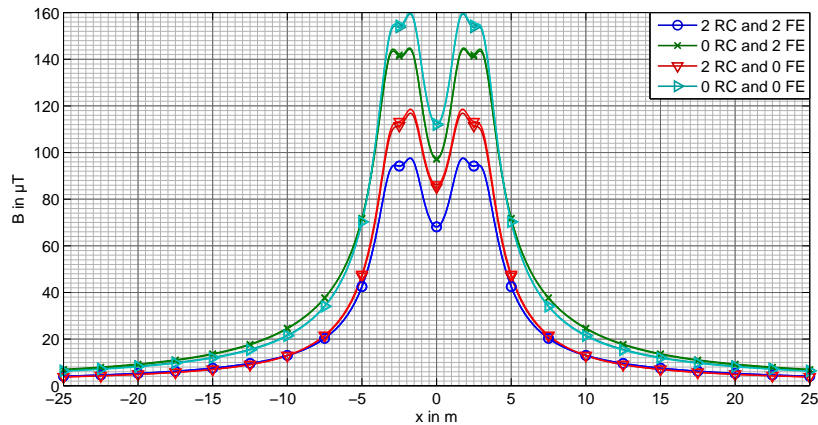


Figure 4.13: Isolines of the magnetic flux density for a double track system with or without return conductors (RC) or feeders (FE)

inner impedances of the rails in sense of magnetic field calculation can be done with either formula (4.1) or (4.3), because the effect on the magnetic flux density is only minor.

4.3 Zigzag of the Contact Wire

In order to prevent unnecessary abrasion of the pantographs, the contact wire is typically mounted with a zigzag deflection from the track axis. For the typical Austrian railway system this horizontal deflection is ± 0.4 m from the track axis. This deflection does not have an influence on the current distribution because the position is on average in the middle of the track axis. Even so, this deflection has an influence on the magnetic and the electric field.

In fig. 4.1 the deflection of the contact wire is denoted with two arrows. For a single track system the deviation in the magnetic flux density due to the deflection is given in fig. 4.14.

As anticipated, the effect is not very big. For the maximum deflection and a track current of 1000 A the deviation of the maximum flux density to a position of the contact wire in the center of the track amounts to only 1.6 μT for a maximum flux density of about 70 μT (evaluated from the base data from fig. 4.14).

For the double track system only the most extreme deflections for both contact wires are analysed. The resulting deviations in the magnetic flux density are given in fig. 4.15 for a $I_{track}=1000$ A per track.

The major deviation for a double track system therefore is, when both contact wires

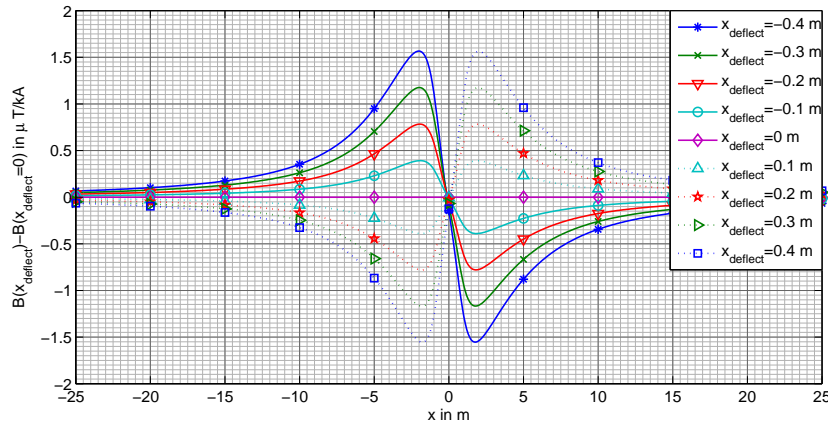


Figure 4.14: Deviation of the magnetic flux density of a single track system due to the zigzag of the contact wire compared to a centred contact wire, $I_{track}=1000$ A

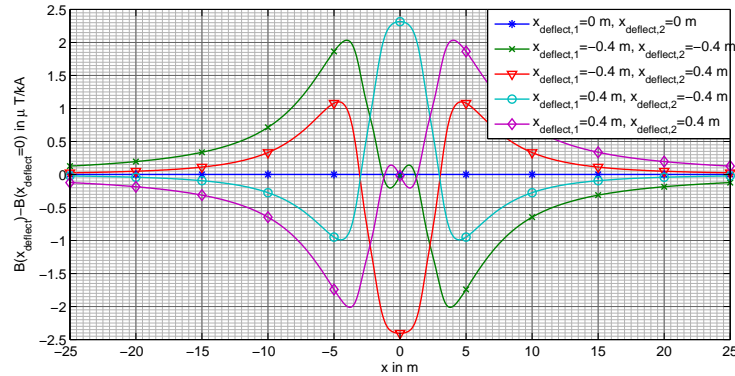
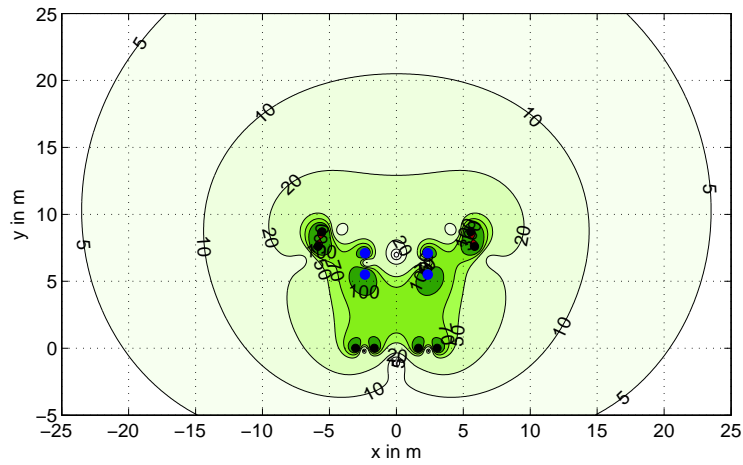
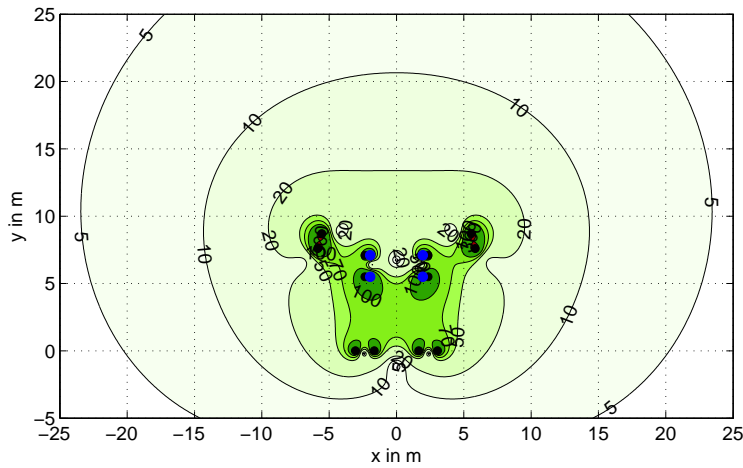


Figure 4.15: Deviation of the magnetic flux density due to the zigzag of the contact wire of a single track system compared to centred contact wires, $I_{track}=1000$ A per track

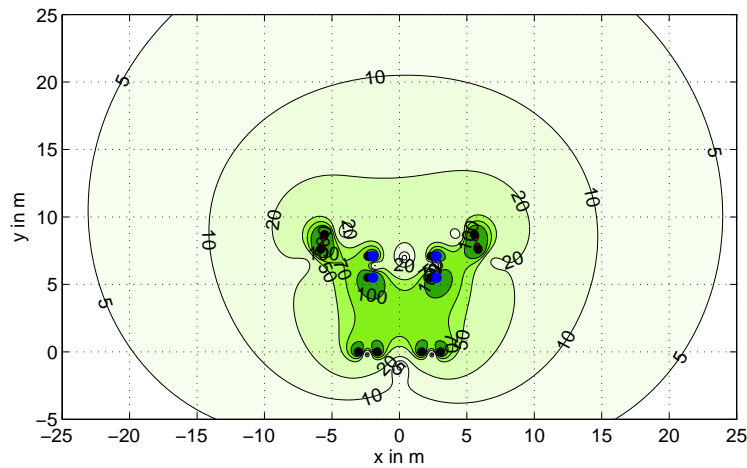
are either on the leftmost side ($x_{deflect,1} = -0.4$ m and $x_{deflect,2} = -0.4$ m), both on the most centred position ($x_{deflect,1} = 0.4$ m and $x_{deflect,2} = -0.4$ m) or at the rightmost side ($x_{deflect,1} = 0.4$ m and $x_{deflect,2} = 0.4$ m) and are up to $2.3 \mu\text{T}$ for 1000 A track current for each track. For a worst case evaluation therefore these three cases have to be analysed. Nevertheless, the effect is minor compared to the effect of the current distribution, which is much more difficult to assess. This analysis can be expanded for the hole area around the conductors. Therefore, in fig. 4.17 once again, the positions, which would result in the worst case magnetic field are indicated by their colour. For better illustration of the deflection in fig. 4.16 for three cases of 4.15 the isolines of the magnetic flux density and the positions of the conductors are given.



(a) $x_{deflect,1} = 0$ m and $x_{deflect,2} = 0$ m



(b) $x_{deflect,1} = 0.4$ m and $x_{deflect,2} = -0.4$ m



(c) $x_{deflect,1} = 0.4$ m and $x_{deflect,2} = 0.4$ m

Figure 4.16: Isolines of the magnetic flux density for different deflections of the contact wire, black circles...original position of the conductors, blue...actual position of the conductors

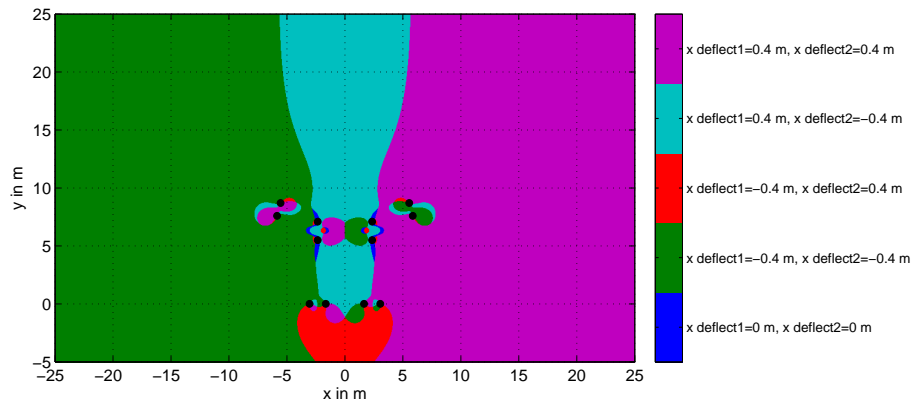


Figure 4.17: Areas, where a specific deflection of the contact wires will lead to the maximum magnetic flux density

4.4 Cardiac Pacemaker Interference Due to Electrical Railways

According to sec. 3.9 also for electrical railways the interference of cardiac pacemakers can be analysed by evaluation of the exposure ratios ER_{cpm} . Therefore, in fig. 4.18 the isolines of various exposure ratios (ER_{cpm}) for several cardiac pacemakers are given. An exceeding of the allowed values (when $ER_{cpm} > 1$) occurs only for the most sensitive configuration to the magnetic field (Silny 135 cm unipolar atrium left) at the track axes, and that area is typically not accessible. Because for railway tracks with feeder and return conductors up to 1500A per track might be possible fig. 4.18 is evaluated with a traction current I_{track} of 1500 A per track in order to define a worst case scenario. In vicinity of railways, in contrast to the evaluations for OHLs in sec. 3.9 (p. 102ff), the pacemaker for people with bigger chest (135 cm) are interfered most. The reason is, that the magnetic flux density is higher in vicinity of railways, while for OHLs the electric field strength has more effect (see therefore fig. 2.12 and 2.13 (p. 30ff)).

An evaluation of the influence of cardiac pacemakers in vicinity of electric railways is only necessary, if there are higher currents, more tracks or crossings of OHLs, which would additionally influence the cardiac pacemakers.

4.5 Difference Between Peak and RMS-Values

Electric Railways (16.7 Hz) cause normally only alternating fields. Only because of the small phase differences of the currents (due to the current distribution) and because of

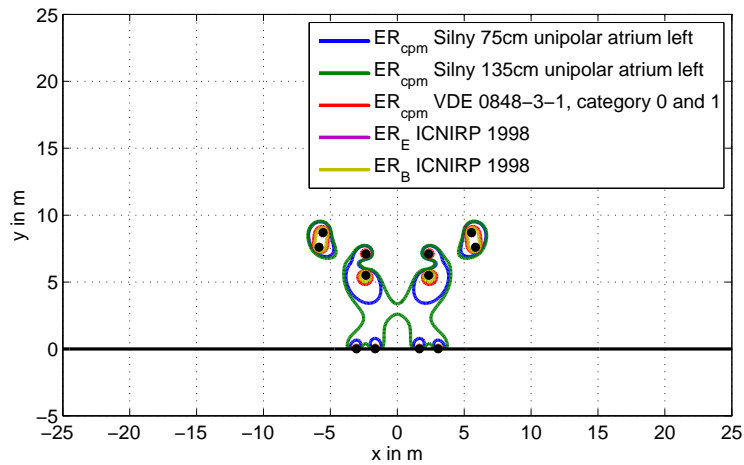


Figure 4.18: Isolines of exposure ratios for different cardiac pacemakers $ER_{cpm}=1$ as well for reference values according to ICNIRP 1998 ($ER_E=1$, $ER_B=1$) for a double track railway system (with 2 RC and 2 FE, 1500 A for each track, $U=18$ kV)

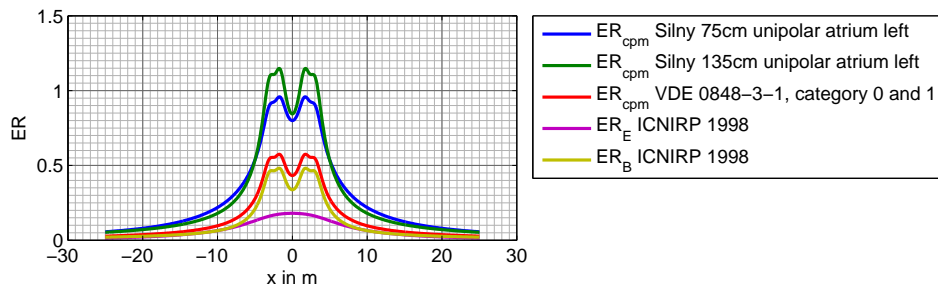


Figure 4.19: Exposure ratios for different cardiac pacemakers ER_{cpm} as well for reference values according to ICNIRP 1998 (ER_E , ER_B) at 1 m above ground for a double track railway system (with 2 RC and 2 FE, 1500 A for each track, $U=18$ kV)

a superposition with other field sources, also in the vicinity of electric railways elliptic fields exists. In fig. 4.20 the ratios RMS-values to the peak values divided by $\sqrt{2}$ for a double track railway system are shown. Elliptic fields exist only very close to the conductors and in a distant area the alternating field is dominant. Therefore for a distant point - a point with a distance of more than about 3 m from any conductor - an alternating flux density can be considered. For the use of harmonic factors with phase consideration as described in sec. 2.3 this is an important fact. Further the electric field

strength too, results in an alternating field.

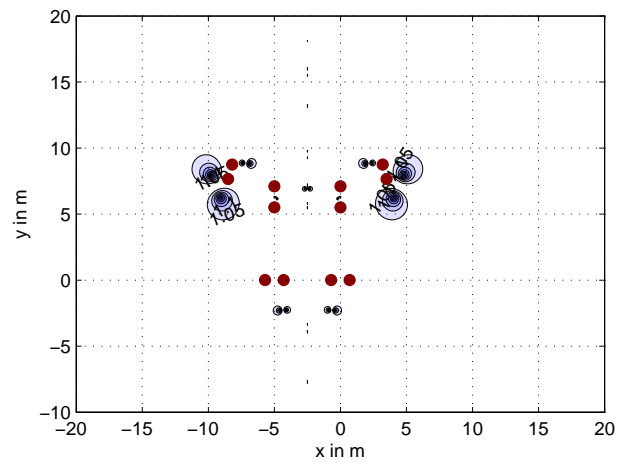


Figure 4.20: Isolines of the ratio $B_{\text{rms}}\sqrt{2}/B_{\text{peak}}$ of a double track railway system

5 Chapter 5

Optimisation

5.1 General

The goal of this section is, to manipulate a conductor arrangement of an electrical power system (OHL, UGL, electric railway system) in such a way, that the electromagnetic influence of this system will be minimised in a specified target area, whereat simultaneously all congestions, as e.g. the minimum distance between two conductors have to be fulfilled. Because the positions of the conductors are characterised by more than one variable, this would lead to a multi variable objective optimisation problem.

The characterisation of such a multi variable objective optimisation problem mainly exists of three input parameters:

- objective function $f(x)$
- parameters or variables $x = [x_1, x_2, \dots, x_i]$ to vary
- congestions to be considered $c(x) \leq 0$

Mathematically this can be expressed with (5.1).

$$\min_x f(x), \quad c(x) \leq 0, \quad x \in \mathbb{R}^n, \quad f(x) \in \mathbb{R}^n, \quad c(x) \in \mathbb{R}^m \quad (5.1)$$

If the objective function $f(x)$ or the congestion functions $c(x)$ are non-linear, this is called a multi-variable non-linear congestion problem, which is a very well known optimisation problem with lots of existing algorithms. In Matlab for example this problem can be solved using the function *fmincon* of the 'Optimization Toolbox' or *ga* of the 'Genetic Algorithm and Direct Search Toolbox' (for details see 5.2).

5.1.1 Objective Function

A general question before starting applying any optimisation algorithm is about the main goal to optimise. In case of electromagnetic fields of electrical power systems this can be structured into the following parts:

5.1.1.1 Minimisation of Costs

Typically in general optimisation problem it is a factor of cost which should be minimised. The problem is, that the occurrence of electric or magnetic field is very hard to express in terms of cost. One possibility might be compensation payments for areas, where fields are higher than a specific value. But here again, the problem with the amount of payment and the limit value are very soft factors, which can influence the optimisation calculation heavily.

5.1.1.2 Minimisation of the Influence in a Target Area

The goal of the optimisation of the conductor arrangement is therefore defined as to minimise the influence of the low-frequency electric and magnetic field in a certain target area.

The most obvious objective function would be then to minimise the influence of the low-frequency electric and magnetic field in a certain target area. The influence can be expressed either as magnetic flux density B , electric field strength E or a weighted combination of these two values (5.2).

$$f = wf_1 B + wf_2 E \quad (5.2)$$

wf_1, wf_2 weighting factors

An obvious way to choose the weighting factors is to use the inverse of limits (thresholds) given by the local standardisations, regulations or other required specifications B_{thre} and E_{thre} , leading to (5.3).

$$f = \frac{B}{B_{thre}} + \frac{E}{E_{thre}} \quad (5.3)$$

E.g. Salameh et al. chose in [8] for their optimisation an objective function with a B_{thre} of 0.4 μT and an E_{thre} of 5 kV/m. This approach might be useful for exposure minimisation near overhead lines outside buildings. Due to shielding effects it is not useful to weight the electric field strength for exposure minimisation inside buildings. There it might be more effective to give the reference values of the electric field strength as a constraint directly under the line (considering harmonics) and consider only the magnetic flux density in the target area.

Further it has to be decided, if the goal is to minimise either

- the maximum influence,
- the average influence,
- a weighted average of influence
- the median, quantiles or other statistic variables of the influence

in a specific target area.

E.g Celozzi et al. [14] used the average value of the magnetic flux density in the target (a building) for their optimisation.

In fig. 5.1 some general aspects of choosing a target area for the optimisation are shown. Subfig. a) demonstrates a typical target area below an overhead line, where e.g. the maximum or the average value of the magnetic field below the line should be minimised. In b) the same for underground cables or electrified railways in tunnels is illustrated. It should be mentioned, that the target area can also transform into a straight line, e.g. typically chosen as a path 1 m above ground. Subfig. c) shows how target areas can be defined for more distant areas on one side of the field source. In d) it is shown how target areas can be defined, if there are sensible areas on both sides of the field source. Some more fancy target area are shown in e) and f). The target area in e) might be e.g. a playground and a building near and below an OHL, in subfigure f) the field source is optimised in a way, that the surrounding in all directions is handled equally, which can be interesting e.g. for a cable in the center of a building.

It is not possible to give a general recommendation, how a target area should be chosen. It depends strongly on preconditions as there are protection target, standards, type of field source and other constraints.

5.1.1.3 Minimisation of an Area With Specific Influence

Another method is to minimise the area around the field source, with values higher than the specific influence limit. Practically this can be done for example by minimising the distance from the field source to the isoline with the specific influence limit. This method is variable on the selection of the limit value (type and amount). In fig. 5.2 the distance to an isoline in two ways is demonstrated. d_{i1} is the maximum distance to the specified limit level and d_{i2} the distance to the isoline at a height h .

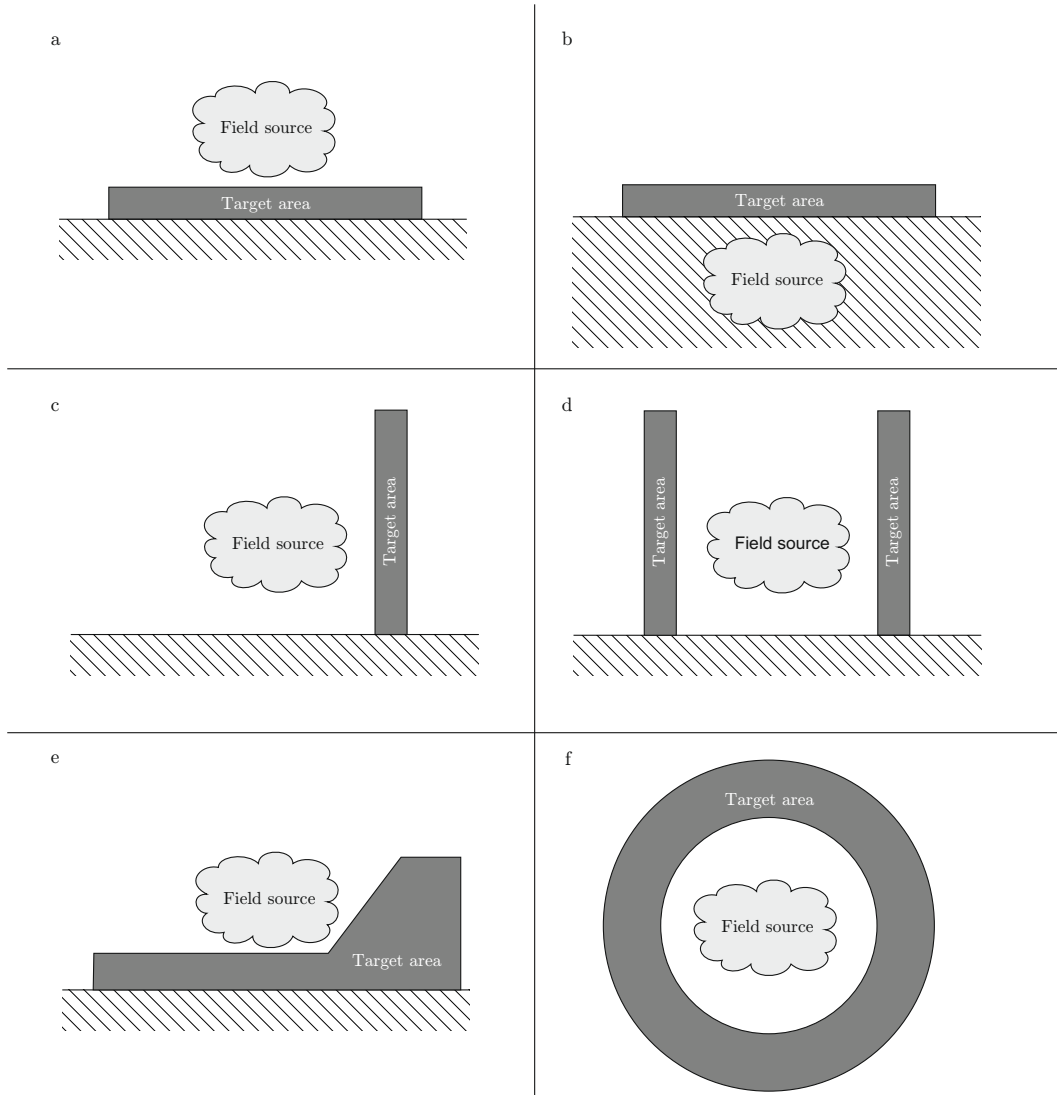


Figure 5.1: General sketch of possible target areas near a field sources (overhead and underground) and distance to an isoline

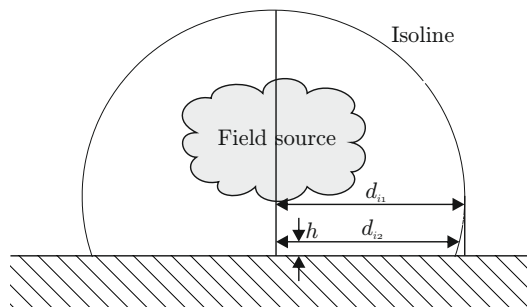


Figure 5.2: General sketch for defining the distance to an isoline

5.1.1.4 Minimisation of Visibility

In case of high voltage OHLs the visibility, which depends - not only, but mainly - on the height of the towers is also a very important factor for people in the surrounding. The optimisation problem can therefore be defined in a way, that the goal is to minimise the height of the tower in such a way, that the electric and magnetic fields, now defined as congestions, do not exceed a certain value.

5.1.2 Variables

The variables x of the optimisation problem of a conductor arrangement are the positions of the conductors. In a 2D-model for each conductor which can be manipulated in its position, there are two variables, the height and the horizontal position. Therefore the optimisation problem of a three-phase single circuit optimisation problem has 6 variables. The more variables, the more difficult for the optimisation algorithm it is to converge to the optimum solution within the search space. The variables can be reduced, when some of the conductors are considered to be fix. Another option is to consider symmetry, as it is the case e.g. for a symmetrical double OHL as given in fig. 3.3. Then, the number of variables can be reduced to the half.

5.1.3 Congestions

Congestions complete the optimisation problem and effect the results mainly. Because the congestions are highly dependent on the optimisation goal, e.g. the chosen objective function and the field source, here only some examples are given, the congestions are described more in detail later on.

E.g. for an OHL, one congestion might be that the minimum distance between 2 conductors should not be less than a certain value and the height above ground should be higher than a certain safety value. For UGLs on the other hand, the insulation and also thermal aspects can be formulated as congestions.

Further the congestions can restrict the area either where the conductors are allowed, or where they are not allowed. For railways it is useful to define areas, where the conductors are allowed, because for example the cross section of the train or areas accessible to public must be free of conductors. Limit values, given by standards and regulation can be other congestions. Here, the area, where this values have to be fulfilled, can be chosen independent from the target area for the optimisation problem. For example, one congestion might be, that the electric field strength in all areas one meter above ground must not exceed the reference values. Another example might be, that the magnetic field

strength is minimised in an area of children playgrounds. Then an additional congestion might be, that the exposure ratios for cardiac pacemaker should not exceed the value 1 in all accessible areas.

5.2 Application of Conductor Arrangement Optimisation in Matlab

The conductor arrangement optimisation problem can be classified into a non-linear optimisation problem with non-linear constraints. This type of problem can be solved using iterative or heuristic methods. A prominent representative of iterative methods is for example Newton's method, a typical representative of heuristic methods is a genetic algorithm. For the optimisations in this thesis the optimisation function 'fmincon' of the optimisation toolbox of MATLAB® was used. This function is an easy-to-use iterative function for finding a minimum of a constrained non-linear multi variable function. As an alternative a genetic algorithm could have been used, which was applied for a similar problem for high voltage lines in [14]. For comparison also in this thesis, a genetic algorithm, the 'ga' algorithm from Matlab, was used. A genetic algorithm has theoretically the advantage, that the solution space is scanned more thoroughly and a global minimum is typically found reliably. The disadvantage is, that the accuracy of the result increases only slowly with the number of samples. In contrast, the iterative 'fmincon'-algorithm might be stuck in a local minimum and is less reliable for discontinuous functions. But, a local minimum can be found more exactly with the same computation time.

For demonstration, the conductor arrangement optimisation for double circuit OHL (symmetrical model) was optimised comparable with the iterative 'fmincon'-algorithm and the genetic 'ga'-algorithm. Although the computing time with the 'ga'-algorithm was 5 times higher than for one and the same problem with the 'fmincon'-algorithm, 'fmincon' found a much better solution. E.g. the best result of minimising the maximum magnetic flux density for 'ga' was 7.28 μT while the 'fmincon'-algorithm results in 3.20 μT .

The above described disadvantage for of getting stuck into a local minimum for iterative algorithms can be anticipated by choosing randomly a certain set of start configurations. This can automatically be done with the Matlab functions 'MultiStart' and 'GlobalSearch'. As described in the manual of MATLAB® [51] the main difference between 'MultiStart' and 'GlobalSearch' is, that 'GlobalSearch' uses a scatter-search mechanism to generate start points, while 'MultiStart's uses uniformly distributed start points within bounds (as for example the conductor areas given the return conductor and feeder position optimisation) or user defined starting points. Further 'MultiStart' runs all (predefined) start configuration, while 'GlobalSearch' rejects those starting points where improvements are unlikely.

The experience with conductor position optimisation showed, that the 'GlobalSearch'

found typically faster (with less trial points) an optimum configuration. On the other hand, the 'MultiStart' algorithm has the advantage, that the results from former optimisation routines can be used as start configuration, which improves the runtime duration, especially, if only little parameter adaptations are done (e.g. changing the minimum distance between two conductors in a small range).

All in all, both algorithms 'MultiStart' and 'GlobalSearch', are used in such a way, that an optimum configuration, in a reasonable short time, is reached.

5.3 Models and Constraints for Three-Phase Systems

5.3.1 Model and Constraints for Single Circuit Lines

In this section the model and constraints of a conductor arrangement for single circuit lines (OHLs and UGLs) are discussed in detail.

The optimisation is done with regard to minimise the influence of a line, using different characteristics of influence (E , B , ER_{cpm} and eq. (5.2)), different target areas and different congestions. Therefore the most general 2D-model with three positions for the phase conductors (P1, P2, P3) which are defined with their x - and y -coordinates in a chosen coordinate system is used. Optional also earth wires can be part of the electrical system.

Only due to appropriate chosen constraints, the results of the optimisation will get useful. In the following, the constraints for single circuit OHL according to fig. 5.6 are defined.

1. minimal distance between conductors $d_{ik,min}$ to ensure appropriate insulation
2. minimal overhead clearance or rather the minimum distance between earth and lowest conductor at maximum sag $h_{l,min}$. This value might be given in the sense of electrical parameters (flash over) or geographically given (e.g. through a crossing street, an object below the line)
3. maximal height $h_{u,max}$ of the tower or the maximal height of the uppermost conductor, as a measure of the visibility of the overhead line
4. maximal width w_{max} of the OHL considering the space demand
5. in order to minimise the risk of direct lightning, the angle between an existing earth wire and phase conductors (the shielding angle) ϑ_{EW} has to be smaller than a certain value $\vartheta_{EW,max}$

6. reference values of the electrical field strength and of the magnetic flux density at ground level must not be exceeded at any point which is open to public (e.g in an area between 0 and 2 m above ground) ($ER_E < 1$, $ER_B < 1$) for worst case. Optionally a further congestion might ensure, that the interference of people with cardiac pacemaker will not take place, by checking if $ER_{cpm} < 1$ (for details about the combined evaluation of E and B field see sec. 2.2.4)

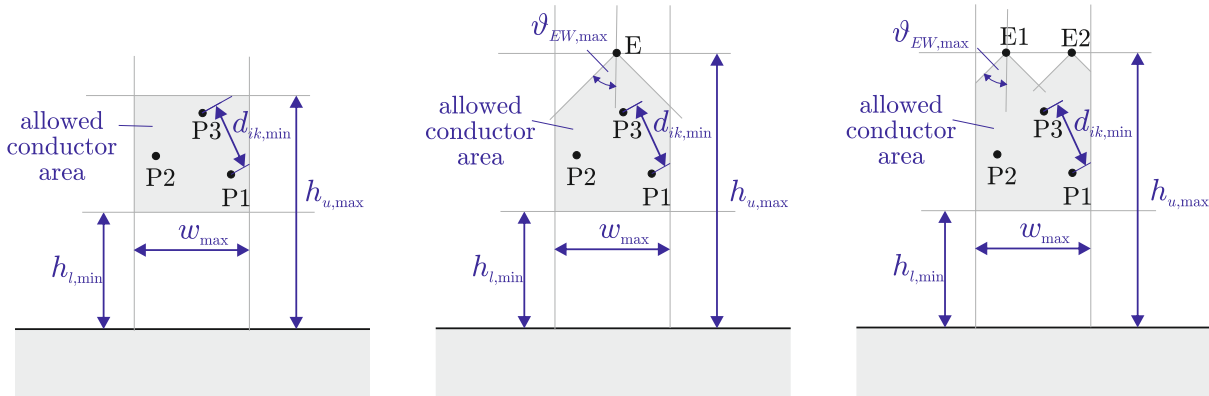


Figure 5.3: Models for single circuit OHLs for conductor arrangement optimisation with certain constraints

It is obvious that through the choice of this constraints, the optimisation result will be influenced significantly. Further, if the geometrical constraints are given very tough, it can be seen in fig. 5.3, that the area, where the conductors are allowed can get quite small, and so does the freedom of degree for the optimisation algorithm. As a consequence, the result of the objective function will be greater than from an optimisation with a greater degree of freedom. Further it might happen, that no set of parameters can be found, which satisfied all constraints.

To define reasonable geometrical constraints, especially the minimum distance between conductors, one option is to look into given standards for minimum distances. For example in ÖVE/ÖNORM EN 50341 [1] the minimum distance for OHLs exceeding AC 45 kV are given. These values are listed in tab. 5.1. It has to be mentioned, that ice and wind loads, sag etc. must be considered additionally to this values. For an evaluation of actual necessary distances the geometry of the tower and the environmental parameters have to be known, which is a disadvantage for an optimisation algorithm.

Another option is to analyse existing towers, assuming, that the actual minimum distances of these lines are already optimised values considering ice and wind loads and other practical constraints. This is done for double circuit OHLs in sec. 5.3.2. For simplification and generalisation, for a single circuit OHL a minimum distance between

Table 5.1: Minimum distances phase to earth D_{el} and phase to phase D_{pp} according to [1]

nominal voltage U_N (kV)	highest operation voltage U_S (kV)	D_{el} (m)	D_{pp} (m)
45	52	0.6	0.7
50, 60, 63, 66	72.5	0.7	0.8
70	82.5	0.75	0.85
90	100	0.9	1.05
110	123	1	1.15
132	145	1.2	1.4
150	170	1.3	1.5
220, 225	245	1.7	2
275	300	2.1	2.4
380, 420	420	2.8	3.2
480	525	3.5	4
700	765	4.9	5.6

conductors of $d_{ik,min} = 6$ m for 400 kV are analysed. It has to be mentioned, that the distances to elements of the towers or other conducting materials has to be considered additionally. This distances are considered also in the next section 5.3.2, and are here left out for a more general analysis.

For single circuit UGLs the general model with its constraints looks very similar (fig. 5.4) to the model of the single circuit OHL without earth wire. The vertical constraints are adopted towards $h_{u,min}$ for the minimum depth of the uppermost conductor which is a factor for reliability and safety and $h_{l,max}$ for the maximum depth of the lowest conductor which is a measure for the depth of the cable trench and therefore a factor of cost and thermal conductivity. The minimum distances between the conductors $d_{ik,min}$ are smaller compared to OHL conductor configuration and depend on the thermal conductivity of the surrounding. Further no electrical field will be caused above ground level.

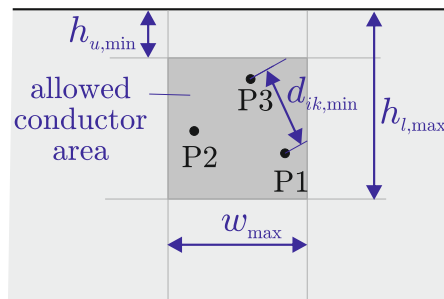


Figure 5.4: Models for a single circuit UGL for conductor arrangement optimisation with certain constraints

5.3.2 Model and Constraints for Double Circuit Overhead Lines

In fig. 5.5 different models are given for double circuit OHLs. The asymmetrical tower model is the most general model. There, each of the 7 conductors (2x3 phase conductors and one earth wire) can be positioned separately, having 2 variables each (an horizontal coordinate x and vertical coordinate y relative to the tower axis). There, the result might be an asymmetrical tower, with it's disadvantage in sense of real application. By constricting the horizontal coordinates being only negative for one circuit, and positive for the second circuit, it can be made sure, that the two circuits are not mixed up, which should be avoided, e.g in sense of reliability and maintenance reasons. The other model is the symmetrical model, which concurs with the image of the 3-level-tower from fig. 3.3. It is the most general symmetrical model, because it can be transformed into the 2-level tower by setting variable $d = 0$ m and to the 1-level tower by additive stating $e = 0$ m.

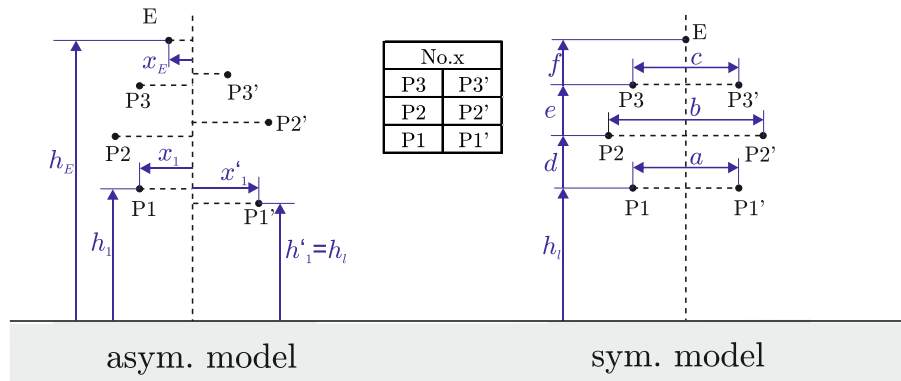


Figure 5.5: Asymmetrical and symmetrical model for conductor arrangement optimisation of double circuit OHLs

The allocation of the phases to given conductor positions has a great influence on the electric and magnetic field as is described in detail in sec. 3.2. In opposition to the asymmetrical model, for the symmetrical model the phase position becomes an additional variable. Due to the simultaneous positioning of circuit 1 and circuit 2, not all phase positions can be resulted in the optimisation procedure. Therefore for each phase position of tab. 3.5 the optimisation algorithm has to be run through.

The cross section orthogonal to the conductors can be defined either, at a tower or at the deepest point between two towers. The advantage of defining it in the middle of the span according to sec. 3.1 is, that typically the highest field values for the hole OHL can be evaluated directly (worst case). It is assumed, that the sags of all conductors are equal. This will ensure, that the relative positions between the conductors remain constant along the line.

Table 5.2: Conductor positions/distances of double circuit OHLs from Austrian with a single earthwire

voltage level tower type		110 kV			220 kV		380 kV	
		1-level	2-level	3-level	2-level	3-level	2-level	3-level
$h_{u,max} - h_{l,min}$ in m	min	5.0	8.7	10.3	13.0	18.4	18.9	24.0
	max	8.4	11.2	16.3	23.2	23.3	22.5	30.9
$d_{ik,min}$ in m	min	3.4	3.6	3.4	5.0	6.3	5.3	7.9
	max	4.2	3.8	6.7	6.0	7.3	6.6	9.8
$\Delta x_{t,min}$ in m	min	2.9	2.6	2.2	5.0	5.0	7.0	6.4
	max	3.2	3.4	3.3	7.4	5.5	7.6	7.5
$(\vartheta_{EW,max})$ in °	min	53.9	34.8	28.2	36.3	30.5	36.3	29.3
	max	63.4	44.1	45.9	49.8	42.3	45.1	49.1
Δx_{level} in m ¹⁾	min	3.4	3.6	-	5.0	-	5.3	-
	max	4.2	3.8	-	6.0	-	6.6	-
Δh_{level} in m ²⁾	min	-	4.0	3.2	6.5	6.1	9.0	7.2
	max	-	4.3	6.5	9.5	7.0	11.5	9.5

¹⁾ horizontal distance between conductors of the same level

²⁾ vertical distance between tower level

5.4 Conductor Arrangement Optimisation of Single Circuit Lines

5.4.1 Optimisation Results for Single Circuit OHLs Without Earth Wires

In this section the optimisation results for a single circuit 110 kV OHL without any earth wire are discussed. Therefore a reference configuration for all congestions for the corresponding model of fig. 5.3 is chosen quite moderately for a 110 kV OHL in tab. 5.3. The objective function $f(x)$ for the reference configuration is therefore the maximum magnetic flux density in an area ± 25 m from the line axis 1 m above ground. The goal is to position the conductors in such a way, that this maximum magnetic flux density is minimised. Most of the congestions are geometrical congestions, like the maximum height of the uppermost conductor $h_{u,max}$. Additionally, it is ensured with additional congestions, that the reference values for electric field strength and magnetic flux density at 1 m above ground do not exceed the reference values. Therefore the reference values for general public according to ICNIRP 1998 [31] ($B_{L,50\text{Hz}}=100 \mu\text{T}$, $E_{L,50\text{Hz}}=10 \text{ kV/m}$) and typical harmonics ($k_{H,I} = 1.2$ and $k_{H,U} = 1.2$) are considered. In the following figures always on the left side, the set of positions of the conductors which would lead

Table 5.3: Reference configuration of the optimisation problem of a single circuit OHL

model	OHL tower type current $I^{(1)}$ voltage $U^{(1)}$	single circuit 600 A $123/\sqrt{3}$ kV
geometric congestions	$d_{ik,min}$	5 m
	$h_{u,max}$	20 m
	$h_{l,min}$	8 m
	w_{max}	15 m
other congestions objective function	$\max(ER_B(h = 1 \text{ m})) \leq$	1
	$\max(ER_E(h = 1 \text{ m})) \leq$	1
	target area	$h=1 \text{ m}, x=-25\dots+25 \text{ m}$
	objective to minimise	$\max(B(\text{target area}))$

to the minimum objective functions are given. The thick black line indicates the ground level. The legend tells, which congestions parameter is varied, all other parameters are constant as given in tab. 5.3. On the right hand side of the figure, the value of the objective function is given, for the reference objective function and target area it is the maximum magnetic flux density 1 m above ground.

The results for varying maximum width of the conductor configuration w_{max} (fig. 5.7) show, that as long as it is not possible to set two conductors in a horizontal line ($w_{max} < d_{ik,min} = 5 \text{ m}$) a vertical triangle would lead to the lowest magnetic flux densities. That means, that for narrow traces of a line, the configuration similar to the 3-level-tower as shown in fig. 3.2 (p. 52) are the best solutions. For wider traces, an equilateral triangle form heading with one vertex to the bottom, would be for that reference configuration the best case.

The results for varying maximum height $h_{u,max}$ of the conductor configuration are given in fig. 5.8.

It can be seen, that for very low vertical space $h_{u,max} - h_{l,min}$ the horizontal configuration at the highest allowed location (at $h_{u,max}$) will lead to the lowest maximum magnetic flux density 1 m above ground. In this example between $h_{u,max} = 15 \text{ m}$ and $h_{u,max} = 17 \text{ m}$ the optimal configuration changes to a triangle form. That means, that for a certain $h_{u,max}$ the configuration with one conductor lower than the maximum allowed height would lead to smaller maximum magnetic field than the configuration with all conductors in a horizontal line at the top. The horizontal deflection of the conductor arrangement for e.g. for $h_{u,max} = 17 \text{ m}$ does not impact the maximum magnetic flux density at 1 m ground.

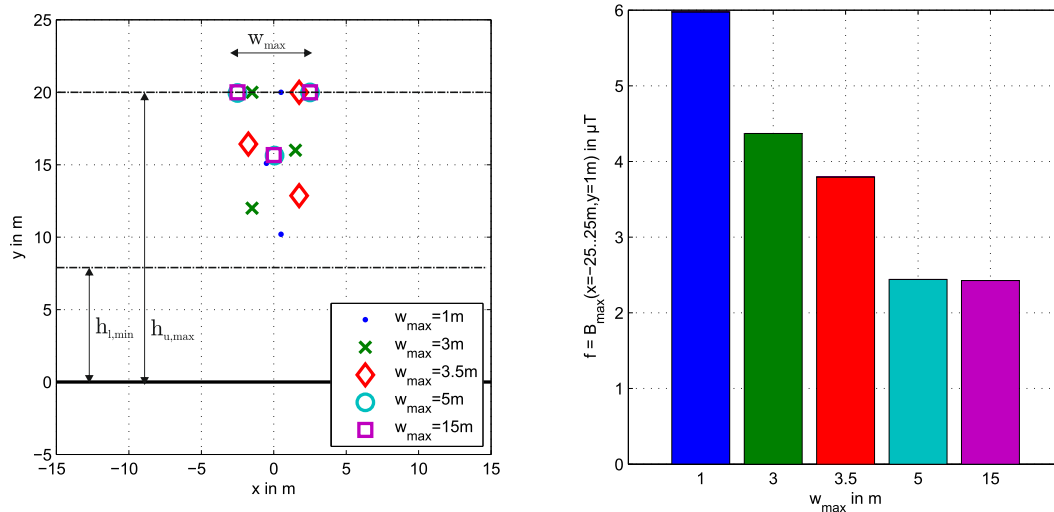


Figure 5.7: Results of the optimisation for varying maximum width w_{max} of the conductor configuration

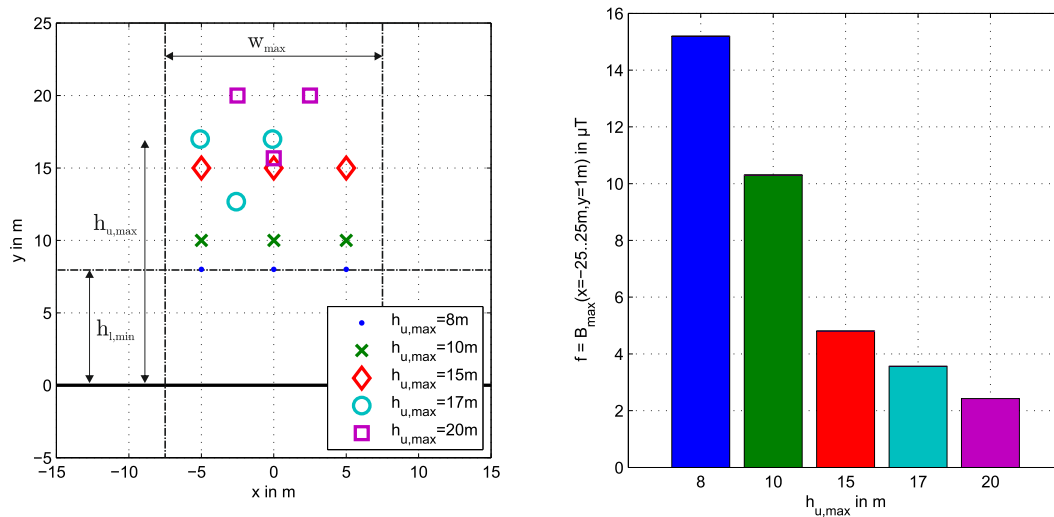


Figure 5.8: Results of the optimisation for varying maximum height $h_{u,max}$ of the conductor configuration

In the following fig. 5.9, the same optimisation is done as in fig. 5.8 but with the objective to minimise the maximum electric field strength 1 m above ground. Compared to the optimisation in respect to minimise the maximum magnetic flux density, here the configuration starts for lower $h_{u,max}$ with a triangle shape. But the equilateral triangle as it is reached for higher $h_{u,max}$ when minimising magnetic flux density, would not lead to the optimum in respect to electric field strength. As a conclusion it can be seen, that it makes a big difference, when minimising the electric field instead of the magnetic field, which means, that there is no optimum which fulfils both conditions.

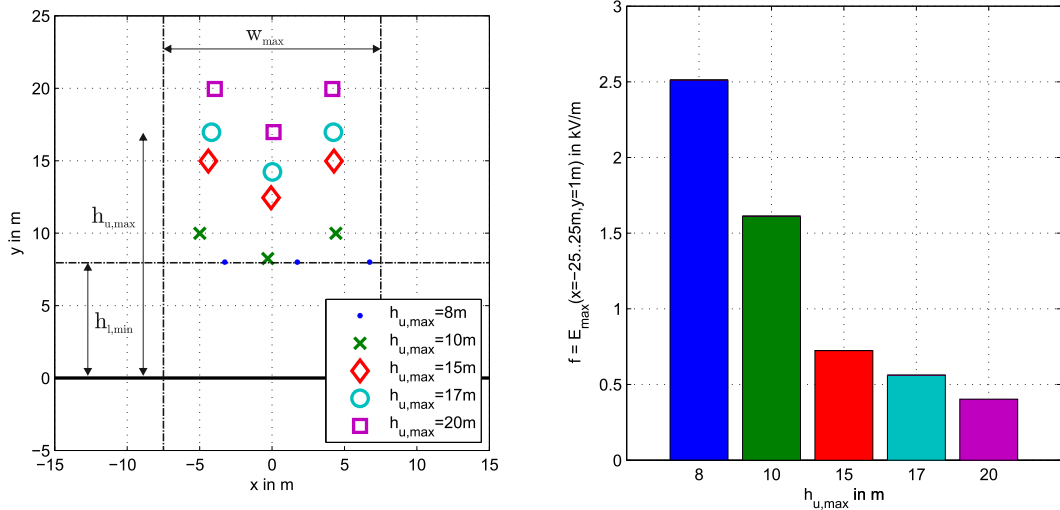


Figure 5.9: Results of the optimisation in respect to minimise the electric field strength for varying maximum height $h_{u,max}$ of the conductor configuration

Other objective functions and target areas are discussed more in detail for double circuit OHLs in section 5.5.

5.4.2 Optimisation Results for Single Circuit OHLs With One Earth Wires

For an OHL with a single earth wire, taking a shielding angle of $\vartheta_{EW} = 40^\circ$ into account, the resulting configurations of the conductors are shown again for varying w_{max} and $h_{u,max}$. Compared to tab. 5.3 the reference parameter $h_{u,max}$ is manipulated toward $h_{u,max} = 25$ m, in order to enable even for a small w_{max} a result which fulfils all congestions.

It can be seen, that again the phase conductors for not very strict congestions are forming towards an equilateral triangle, but with the earth wires at the top. Therefore the hole conductor configuration is forming a rhombus.

5.4.3 Optimisation Results for Single Circuit OHLs With Two Earth Wires

In the following the optimisation algorithm is extended toward two earth wires. An additional condition for the earth wires was, that the needed to be symmetrical to the line axis, in order to have only two instead of four variables for the earth wires, and further that they are on the top of the tower.

The results for that optimisation can be found in fig. 5.12 and 5.13. The distance

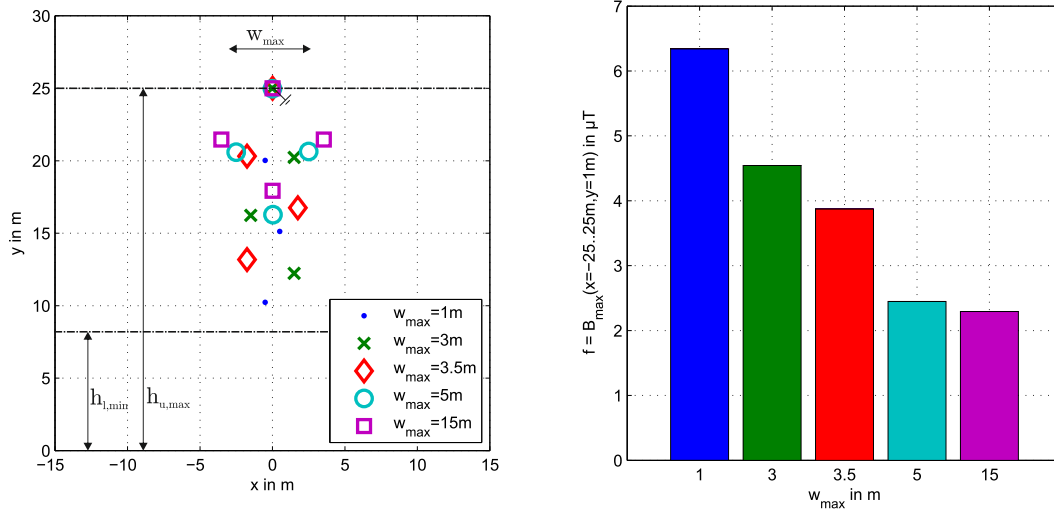


Figure 5.10: Results of the optimisation with a single earth wire for varying maximum width w_{max} of the conductor configuration

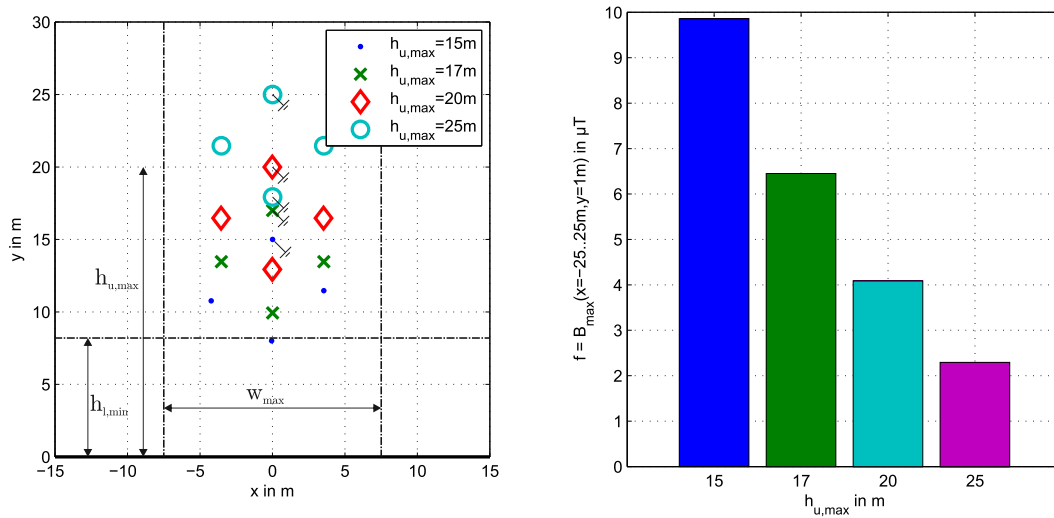


Figure 5.11: Results of the optimisation with a single earth wire for varying maximum height $h_{u,max}$ of the conductor configuration

between both earth wires was allowed to be zero. Hence, in some cases, the earth wires overlap each other (leading to only one earth conductor) and only 4 conductors can be found in fig. 5.12 for $w_{max}=3$ m and $w_{max}=3.5$ m.

The optimal configuration for moderate congestions again becomes a triangle shape, but with the earth wire in its extensions. Compared to the single earth wire optimisation, it can be seen that the objective function with the double earth wire configuration with same w_{max} or $h_{u,max}$ have lower field levels. Therefore it can be concluded, that an installation of a second earth wire has advantage in sense of maximum magnetic flux

density, if choosing the same maximum height and maximum weight of the tower, as well as the same shielding angle ϑ_{max} .

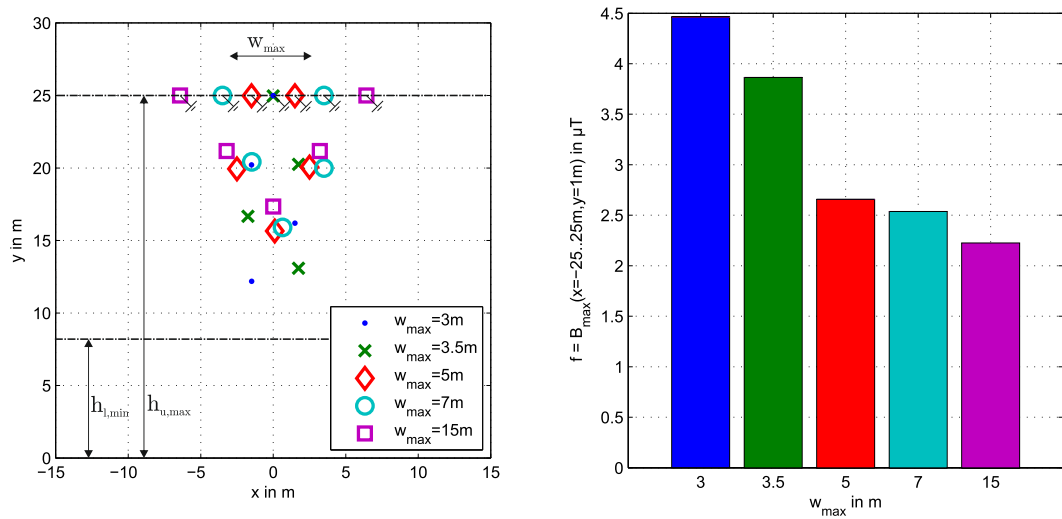


Figure 5.12: Results of the optimisation with 2 earth wires for varying maximum width w_{max} of the conductor configuration

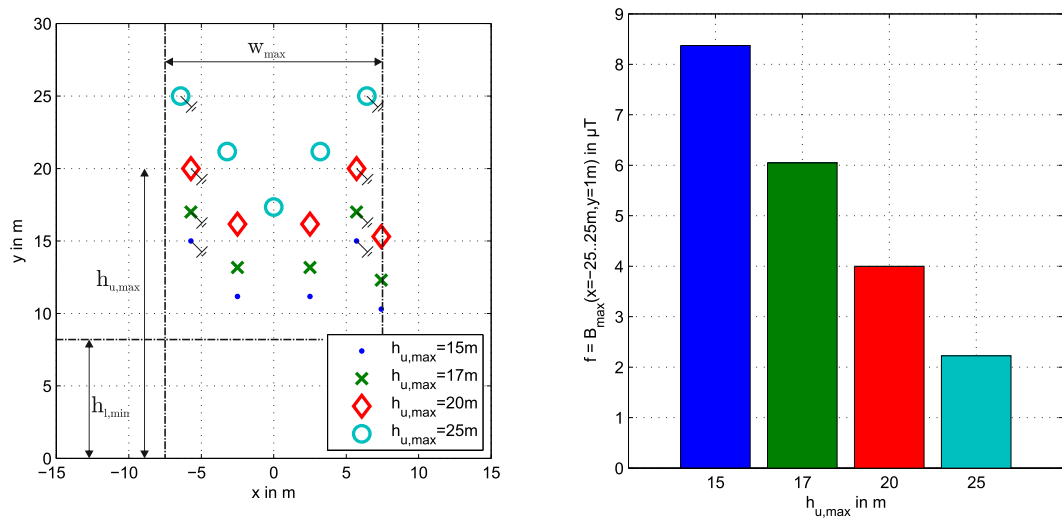


Figure 5.13: Results of the optimisation with 2 earth wires for varying maximum height $h_{u,max}$ of the conductor configuration

5.4.4 Optimisation of the Height of a Single Circuit OHL

In the following, a single circuit OHL should be optimised in sense of visibility. Because mainly the height of a tower affects the visibility, the height of the uppermost conductor $h_{u,max}$ will be the measure to optimise. The question to be answered another way around with that optimisation is, which height of a tower is necessary to comply with certain field limits in a specified target area under the condition, that the conductors can be varied. The exposure limit might be on one hand, e.g. the reference values according to ICNIRP [31, 33], but also some other arbitrary values, e.g. 1 μT in a specified target area. Because then the specific level of the magnetic flux density the tower type is optimised, the current of the circuit is significant for that optimisation. Therefore the current is assumed with an appropriate value of 600 A for a 110 kV line.

Table 5.4: Configuration to minimise the height of a single circuit OHL

model	OHL tower type current $I^{(1)}$ voltage $U^{(1)}$	single circuit 600 A $123/\sqrt{3}$ kV
geometric congestions	$d_{ik,min}$ $h_{l,min}$ w_{max}	5 m 2 m 15 m
other congestions	$\max(ER_B(h = 1 \text{ m})) \leq$ $\max(ER_E(h = 1 \text{ m})) \leq$ target area $\max(B(\text{target area})) \leq$	1 1 $h=0..2 \text{ m}, x=-\pm 20 \text{ m}$ 1 μT
objective function	objective to minimise	$h_{u,max}$

In fig. 5.14 the resulting conductor configurations and tower heights for different values of congesting magnetic flux densities in an area 20 m away from the line axis are summarised.

In the following fig. 5.15 another possibility for determining the necessary height of a conductor configuration is given. There instead of the congesting B -value at a distance of 20 m from the line axis, the maximum exposure ratios for CPMs (ER_{cpm}) at 2 m above ground are taken into account. That is done, in analogy to e.g. sec. 3.9 for four different CPM types.

This type of analysis can be extended also to other or additional with other parameters. So it might be interesting to constrict the magnetic flux density in one target area, while in another target area the electric field strength should be below a certain value.

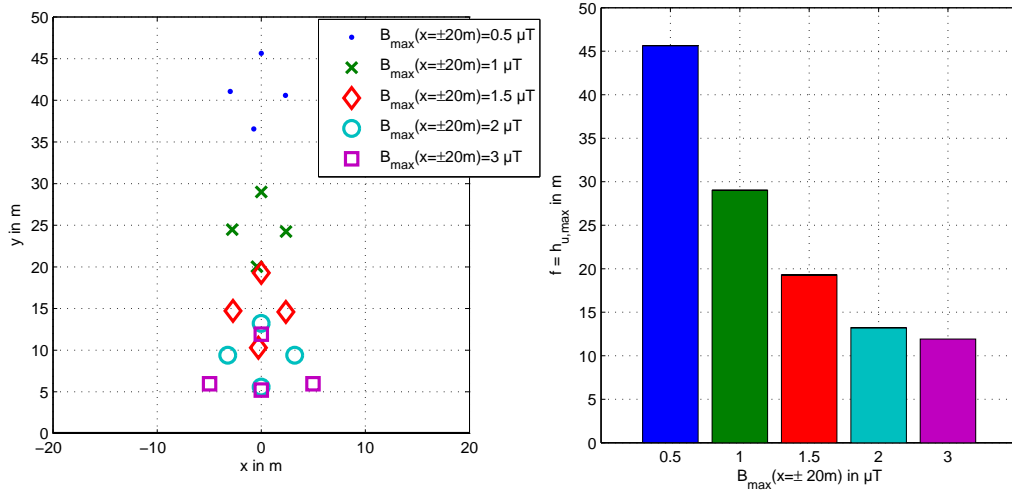


Figure 5.14: Results of the optimisation in order to minimise the height of the tower of an OHL with a single earth wire, varying congesting maximum flux density in a target area 20 m away from the line axis

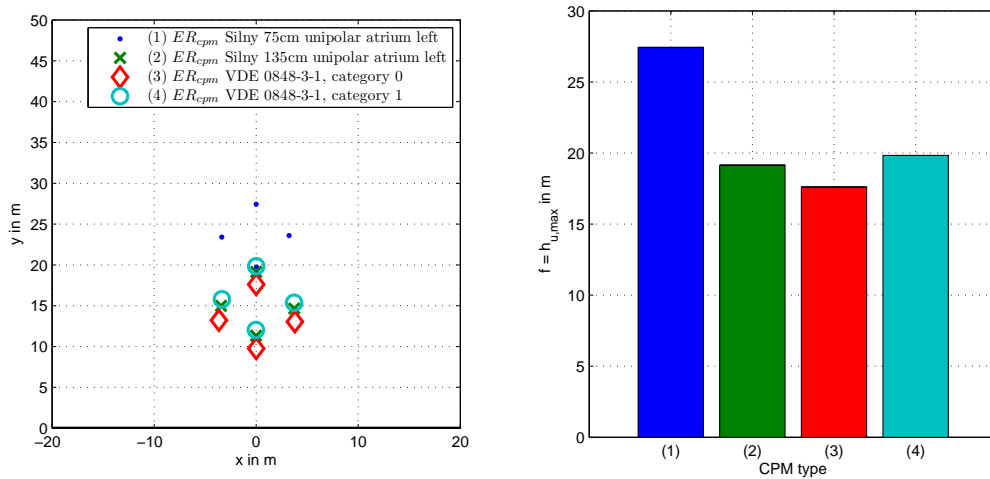


Figure 5.15: Results of the optimisation in order to minimise the height of the tower of an OHL with a single earth wire, varying types of CPM, in order to fulfil $ER_{cpm} \leq 1$ in 2 m above ground

5.4.5 Optimisation Results for Single Circuit UGLs

The same as in section 5.4.1 is done in this section for a 110 kV UGL. The reference configuration therefore is given in tab. 5.5. Compared to OHLs, the allowed distance between the conductors can be chosen much smaller, here for example with 1 m, which is quite big for a 110 kV cable.

Because cables do not cause any electric field strengths on ground level, again the maximum magnetic flux density at 1 m above ground is the measure for the optimisation

Table 5.5: Reference configuration of the optimisation problem of a single circuit OHL

model	UGL type current $I^{(1)}$	single circuit	
		600	A
geometric congestions	$d_{ik,min}$	1	m
	$h_{l,max}$	-2.5	m
	$h_{u,min}$	-0.5	m
	w_{max}	3	m
other congestions objective function	$\max(ER_B(h = 1 \text{ m})) \leq$	1	
	$\max(ER_E(h = 1 \text{ m})) \leq$	1	
	target area	$h=1 \text{ m}, x=-25\dots+25 \text{ m}$	
	objective to minimise	$\max(B(\text{target area}))$	

algorithm.

In fig. 5.16 the results for maximum width of the cable tray w_{max} and in fig. 5.17 the ones for maximum depth of the cable $h_{l,max}$ are presented.

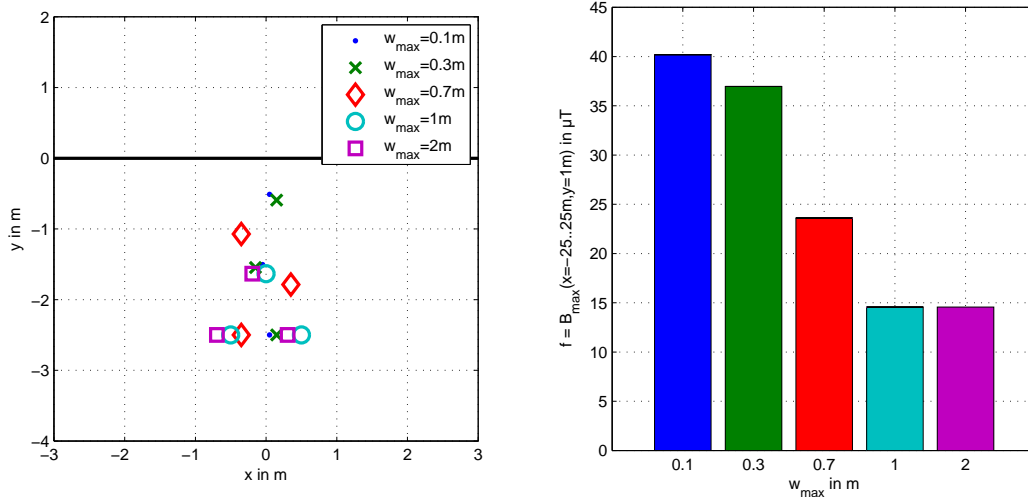


Figure 5.16: Results of the optimisation for varying maximum width of the conductor configuration w_{max} for an UGL

Again, the width of the conductor arrangement for e.g $w_{max} = 2 \text{ m}$ in fig. 5.16 does not impact the maximum magnetic flux density at 1 m above ground further than $w_{max} = 1 \text{ m}$. Therefore, the values of the objective function are equal for $w_{max} = 1 \text{ m}$ and $w_{max} = 2 \text{ m}$. That further means, that greater values of w_{max} than 1 m, would not lead to better results in respect of magnetic flux densities above ground.

Further it is significant, that the triangle form, if it is possible due to given congestions, would lead again to the lowest maximum magnetic flux density at 1 m above ground. Only very close to the conductors, e.g. when the distances to the field points are \geq

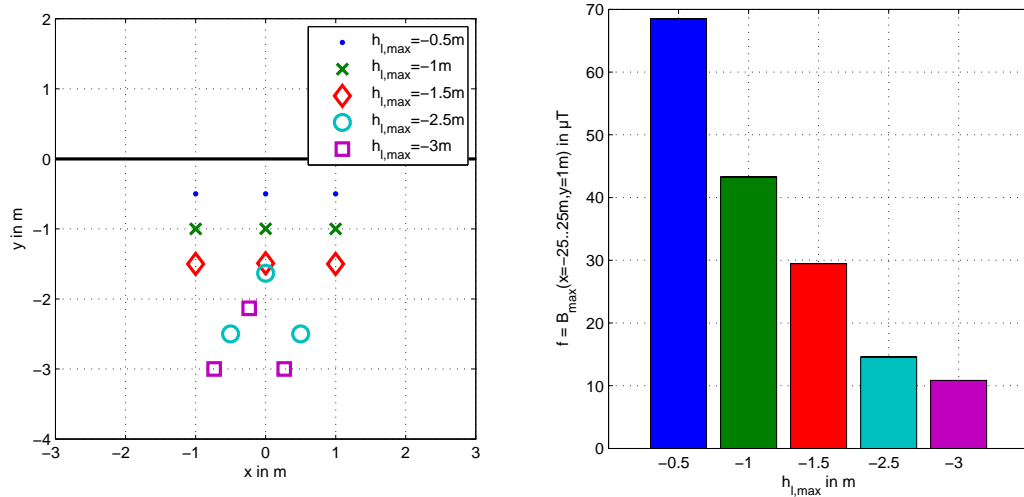


Figure 5.17: Results of the optimisation for varying maximum depth of the cable tray $h_{l,max}$ for a UGL

2.5 m, as it is for a $h_{l,max}=-1.5$ m in fig. 5.17 the horizontal configuration is advantageous compared to the triangle form - but only for points very close to the conductor arrangement.

5.5 Conductor Arrangement Optimisation of Double Circuit Overhead Lines

In the following the optimisation of conductor arrangements for double circuit OHLs with a single earth wire according to the models given in section 5.3.2 are discussed in detail. The optimisation is done according to minimise the influence of the overhead line, using different characteristics of the influence (E , B , ER_{cpm} and eq. (5.2)), different target areas and different congestions.

5.5.1 Reference Configuration

The chosen reference parameters, where all variations are developed are given in table 5.6.

The currents and voltages are considered to be symmetrical, in the sense of symmetrical components. That means, that only the positive sequence system is present. Further both circuits are considered to be equally loaded (value and phase angle of the positive sequence systems of both circuits are identical).

For the symmetrical model the optimisation is always done with all possible phase

Table 5.6: Reference configuration of the optimisation problem

model	OHL tower type current $I^{(1)}$ per circuit voltage $U^{(1)}$	symmetric	
		2300 A	$420/\sqrt{3}$ kV
geometric congestions	$d_{ik,min}$	6	m
	$\Delta x_{t,min}$	7	m
	$\vartheta_{EW,max}$	40	m
	$h_{u,max}$	40	m
	$h_{l,min}$	8	m
	w_{max}	30	m
other congestions	$\max(ER_B(h = 1 \text{ m})) \leq$	1	
	$\max(ER_E(h = 1 \text{ m})) \leq$	1	
objective function	target area objective to minimise	$h=1 \text{ m}, x=-25\dots+25 \text{ m}$ $\max(B(\text{target area}))$	

positions (see sec. 3.2), and only the best result (the configuration with the lowest resulting objective function) is selected. As before, for very strict congestion parameters, it might happen, that the algorithm doesn't find an appropriate configuration, which fulfils all congestions. Therefore, the congestions in tab. 5.6 are chosen in a way, that at least one phase position would be able to comply with all congestions.

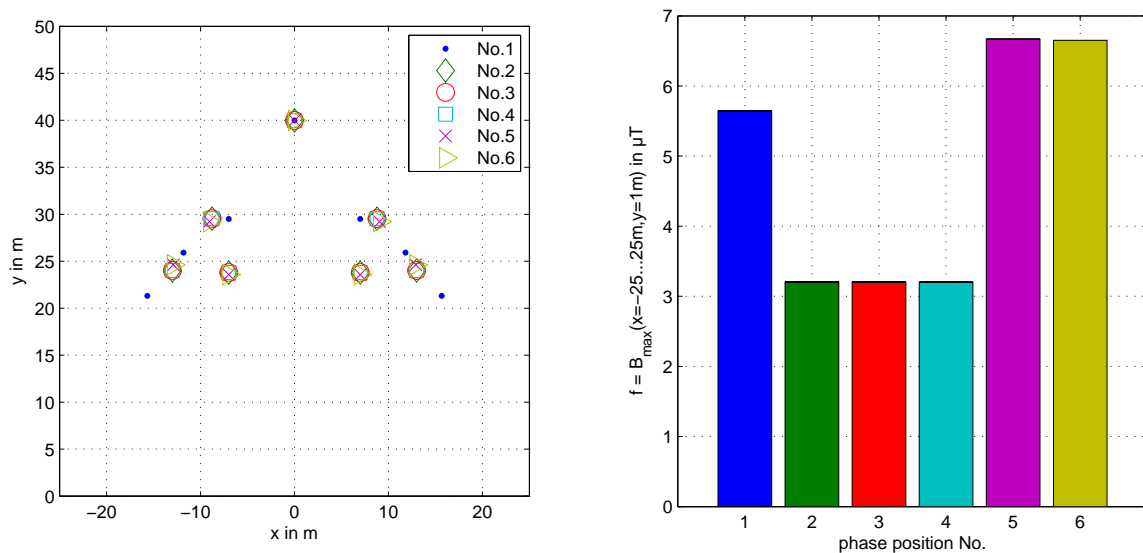


Figure 5.18: Results of the optimisation with the reference configuration of a double circuit OHL

In fig. 5.18 on the left side, the resulting conductor arrangements for the optimisation with parameters, as described in tab. 5.6, are shown. The results of the objective function (maximum magnetic flux density at 1 m above ground) are presented on the

right hand side. For the start configurations of the optimisation algorithm the phase positions are varied (No. 1 to No. 6), and the geometrical model parameters d and e (distances between two levels of the tower) are allowed to be also negative. Significant is, that the results (conductor positions and objective function) for No. 2, No. 3 and No. 4 are identical. Therefrom potentially one would conclude, that the magnetic flux density of these phase positions would be the same, which would be contradictory to section 3.2. In fact, due to the freedom that the vertical parameters d and e might become negative, also from starting configuration No. 2 and No. 4 phase position No. 3 can be achieved. For better illustration this transformation is displayed in fig. 5.19.

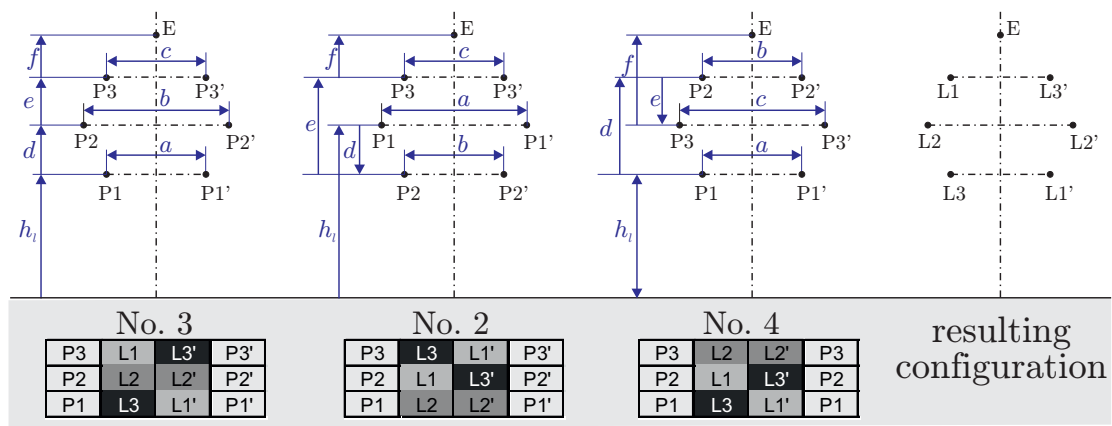


Figure 5.19: Transformation from phase position No. 2 and No. 4 to actual phase position No. 3 with negative vertical parameters d (for No. 2) or e (for No. 3)

The resulting configuration for the optimisation No. 2, No. 3 and No. 4 is therefrom phase position No. 3 (η).

The resulting conductor arrangement for start configurations with No. 5 and No. 6 is very similar to that from No. 2, No. 3 and No. 4, only the result of the objective function (B_{max} in 1 m above ground) is much higher. The only outlier in sense of the resulting conductor arrangement is the result of the optimisation for phase position No. 1, which results in a completely different conductor arrangement. In the following, only the best results from all possible phase positions are given.

5.5.2 Variation of the Optimisation Model

The next step is to look at results for different models, especially the 1-level-, 2-level-, 3-level- and asymmetrical model. For the 1-level-model the congestions w_{max} need to be changed from $w_{max}=30$ m to $w_{max}=50$ m, otherwise no solution would have been possible. The asymmetrical model becomes apparent to be most difficult to evaluate,

because instead of 7 parameters (a, b, c, d, e, f, h) 14 variables (7 conductors with each 2 coordinates) have to be handled. Due to the great number of 14 variables, it is more likely to get stuck in local optima. Therefore a much greater number of start configurations has to be run through in order to get the global optimum. For the chosen reference objective function, the result of the asymmetrical model is again a symmetrical tower, in fact exactly the same as achieved with the symmetrical model. For other objective functions, with e.g. target areas of one side of the tower only, the result of symmetric model and asymmetric model might be different.

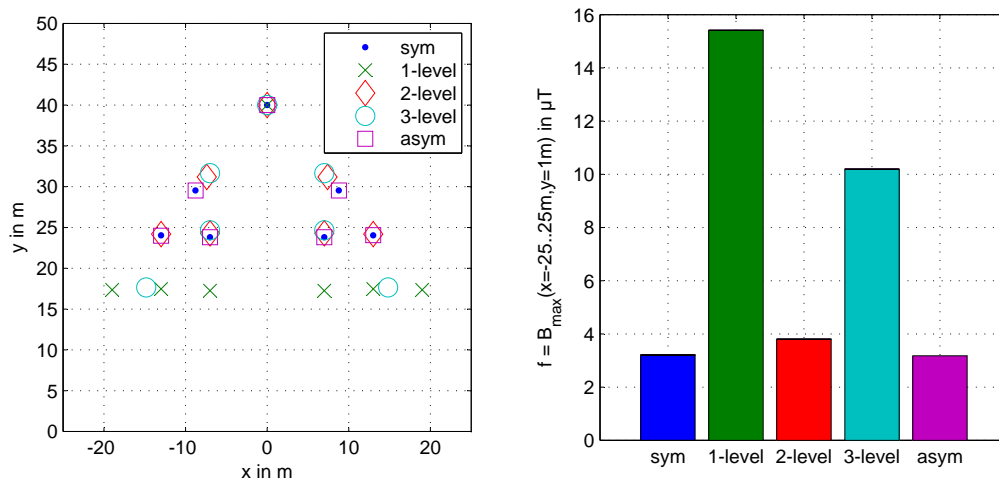


Figure 5.20: Results of the optimisation for different model types of double circuit OHLs

5.5.3 Variation of the Geometric Congestion Parameters

In fig. 5.21 the minimum distance $d_{ik,min}$ between two conductors is varied between 5 m and 7 m (6 m is the reference configuration). It can be seen, that naturally with higher minimum distance between the conductors also the result of the objective function is increasing. The conductor configuration itself looks always very similar, only a bit stretched.

In fig. 5.22 the maximum height of the uppermost conductor $h_{u,max}$ is varied between 30 m to 50 m (40 m is the reference configuration). It can be seen, that naturally with higher allowed height, the conductors are positioned higher and the objective function is increasing. Further, the triangles built by the conductors on the left and right side of the tower are rotated a bit. Therefrom it can be seen, that the optimisation in sense of the maximum magnetic flux density at the maximum sag would lead to other results than an optimisation directly at the point of suspension.

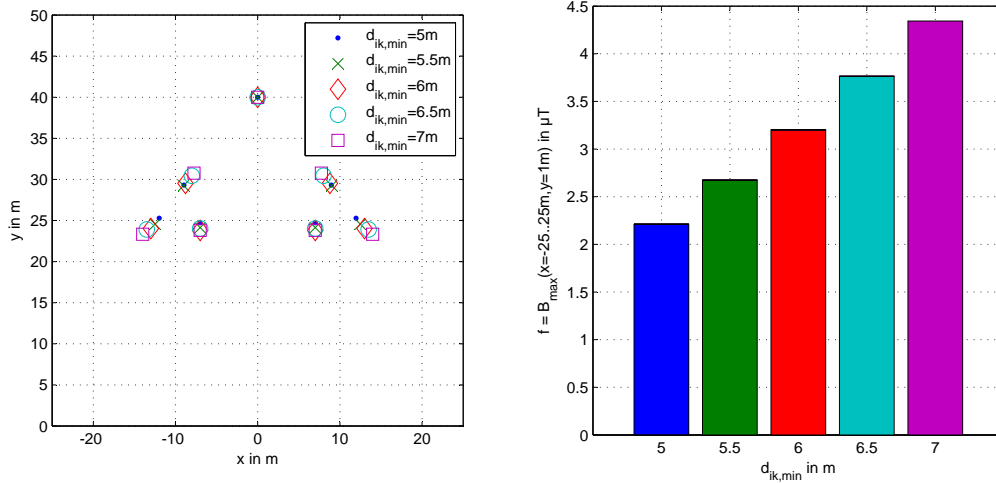


Figure 5.21: Results of the double circuit OHL optimisation for different $d_{ik,min}$

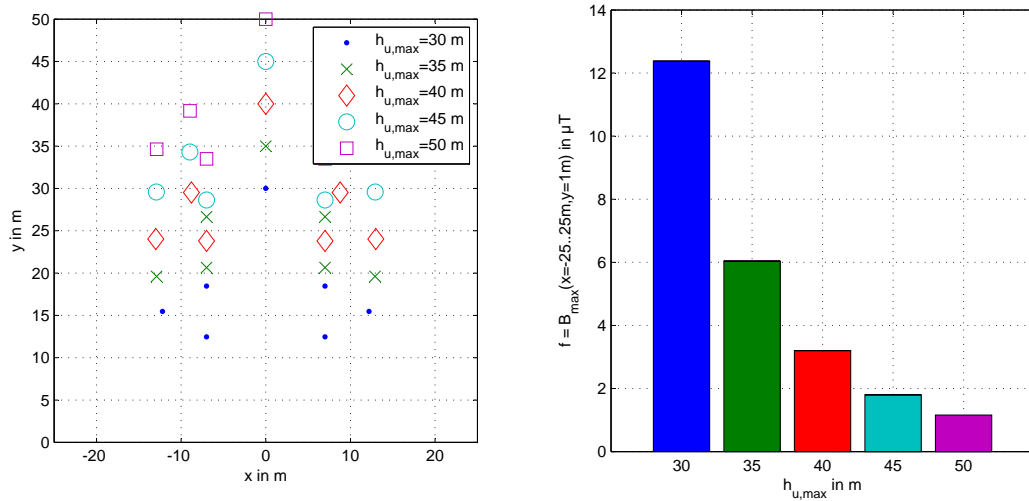


Figure 5.22: Results of the double circuit OHL optimisation for different $h_{u,max}$

For a variation of the ϑ_{max} , given in fig. 5.23, similar results can be extracted. The bigger the allowed shielding angle is, the higher the conductors can be allocated, and the result of the objective function (B_{max}) decreases. Therefrom it can be seen, that it makes sense to question the determination of a shielding angle in order to minimise magnetic fields but without changing other constraints as height of the tower or the width of the trace. Further improving would be achieved by switching to a model with two earth wires, as it was analysed for a single circuit OHL (sec. 5.4.3).

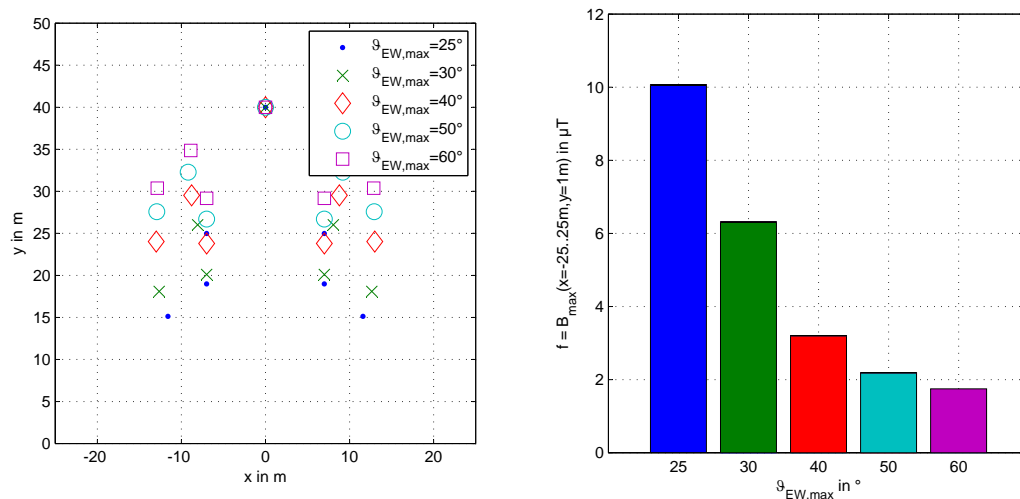


Figure 5.23: Results of the double circuit OHL optimisation for different ϑ_{max}

5.5.4 Variation of the Objective Function

As it could already be seen for the single circuit optimisation in section 5.4.1, the results of an optimisation according to minimise the maximum electric field strength differ from the results for minimisation of the maximum magnetic flux density in the same target area. In tab. 5.7 and fig. 5.24, the results of several objective functions for the reference configurations of a double circuit OHL are compared. The chosen objective functions can be found at the top of tab. 5.7. The target area for all objective functions is constant (1 m above ground, ± 25 m from the line axis), but for each function (except f_2) it is distinguished if either the maximum value (max) or the mean value (mean) of the function within the target area is taken into account. The objective functions f_1 and f_2 are examples for optimisation functions combining electric field strength and magnetic flux density (see bottom of tab. 5.7). The function f_1 represents a weighting according to ICNIRP 1998, general public exposure. In function f_2 the value for magnetic flux density is reduced, because the weight of electric field strength is higher with the reference levels according to ICNIRP than the actual values below an OHL than the weight of the magnetic flux density.

The best configurations of the optimisations are again actually phase position No. 3 (η). It can be seen, that the conductors of function $\max(f_1)$ and $\max(f_2)$ lay between the conductors with $\max(E)$ and $\max(B)$, while the conductor positions of $\max(f_1)$ are closer to $\max(E)$, and the positions of $\max(f_2)$ closer to $\max(B)$.

Table 5.7: Comparison of different objective functions for OHL

best result with conductors optimised for objective function						
$\max(B)$ μT	$\text{mean}(B)$ μT	$\max(E)$ kV/m	$\text{mean}(E)$ kV/m	$\max(f_1)$ -	$\text{mean}(f_1)$ -	$\max(f_2)$ -
3.202	3.029	0.715	0.616	0.176	0.154	0.309

Conductors optimised for	Deviation of objective function to best result in %						
	$\max(B)$	$\text{mean}(B)$	$\max(E)$	$\text{mean}(E)$	$\max(f_1)$	$\text{mean}(f_1)$	$\max(f_2)$
$\max(B)$	0.0	0.5	40.3	12.9	31.4	9.8	14.3
$\text{mean}(B)$	2.3	0.0	50.6	21.5	40.8	16.6	21.9
$\max(E)$	38.9	22.2	0.0	8.9	0.0	10.9	11.5
$\text{mean}(E)$	6.4	2.9	16.9	0.0	11.1	0.0	0.7
$\max(f_1)$	38.9	22.2	0.0	8.9	0.0	10.9	11.5
$\text{mean}(f_1)$	6.4	2.9	16.9	0.0	11.1	0.0	0.8
$\max(f_2)$	17.8	9.5	10.5	1.9	6.3	2.8	0.0

$$f_1 = \frac{E}{5\text{kV/m}} + \frac{B}{100\mu\text{T}}, \quad f_2 = \frac{E}{5\text{kV/m}} + \frac{B}{20\mu\text{T}}$$

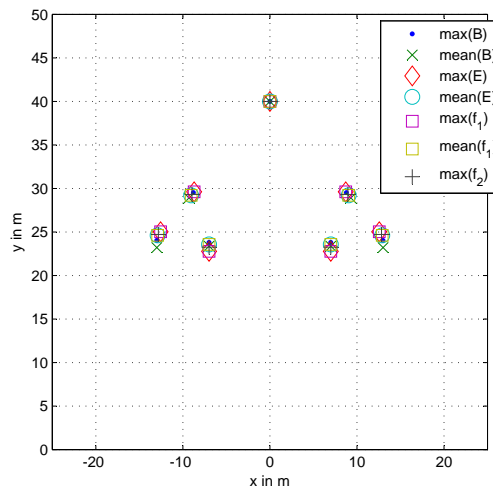


Figure 5.24: Results of the double circuit OHL optimisation for different objective functions

5.5.5 Variation of the Target Area

In this section the target area of the objective function is varied. Here the target area exists of only one point for each optimisation, at a height $y = 10$ m and a variable distance from the line axis x . The point is only on one side of the line axis.

For the symmetrical model the resulting conductor arrangements are shown in fig. 5.25.

For $x=60\dots100$ m the arrangements are very similar and therefore only one of them (for $x=90$ m) is drawn. It can be seen also in tab. 5.8, that between the optimisation for a point at $x=40$ m and the optimisation for a point at $x=90$ m the deviation in the magnetic flux density is smaller than 1 % and therefore negligible. On the other hand, the conductor arrangement for an optimisation with target area at $x=90$ m causes a magnetic flux density at $x=10$ m which is 4 times (+300%) higher than the conductor arrangement optimised for that target area.

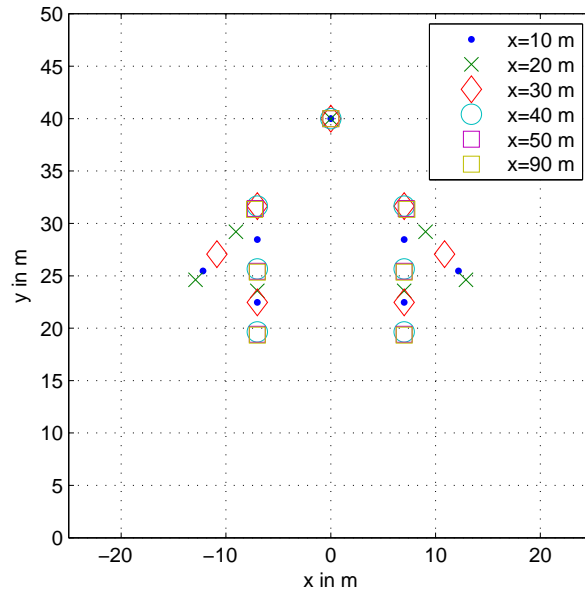


Figure 5.25: Results of the double circuit OHL optimisation for different target areas in the form of points at a height $y = 10$ m and in a distance x from the line axis

In fig. 5.26, similar to the figures in sec. 3.2, the areas, where a conductor configuration would lead to the minimum magnetic flux density compared to configurations, optimised for another point, are coloured corresponding to the conductor positions in fig. 5.25. Additionally the analysed target areas (here only points) are marked with black circles.

Table 5.8: Comparison of results for different target areas

best result with conductors optimised for target area in μT :						
	$x = 10 \text{ m}$	$x = 20 \text{ m}$	$x = 30 \text{ m}$	$x = 40 \text{ m}$	$x = 50 \text{ m}$	$x = 90 \text{ m}$
	10.358	7.245	3.481	1.781	0.981	0.190

Conductors optimised for	Deviation of B at the target area to best result in %					
	$x = 10 \text{ m}$	$x = 20 \text{ m}$	$x = 30 \text{ m}$	$x = 40 \text{ m}$	$x = 50 \text{ m}$	$x = 90 \text{ m}$
$x = 10 \text{ m}$	0.0	25.2	61.6	98.5	142.7	325.5
$x = 20 \text{ m}$	14.6	0.0	7.4	19.3	38.0	130.4
$x = 30 \text{ m}$	43.3	3.1	0.0	1.4	7.6	44.9
$x = 40 \text{ m}$	106.1	19.9	4.9	0.0	0.2	0.9
$x = 50 \text{ m}$	111.9	21.5	5.4	0.1	0.0	0.1
$x = 90 \text{ m}$	114.0	22.1	5.6	0.2	0.0	0.0

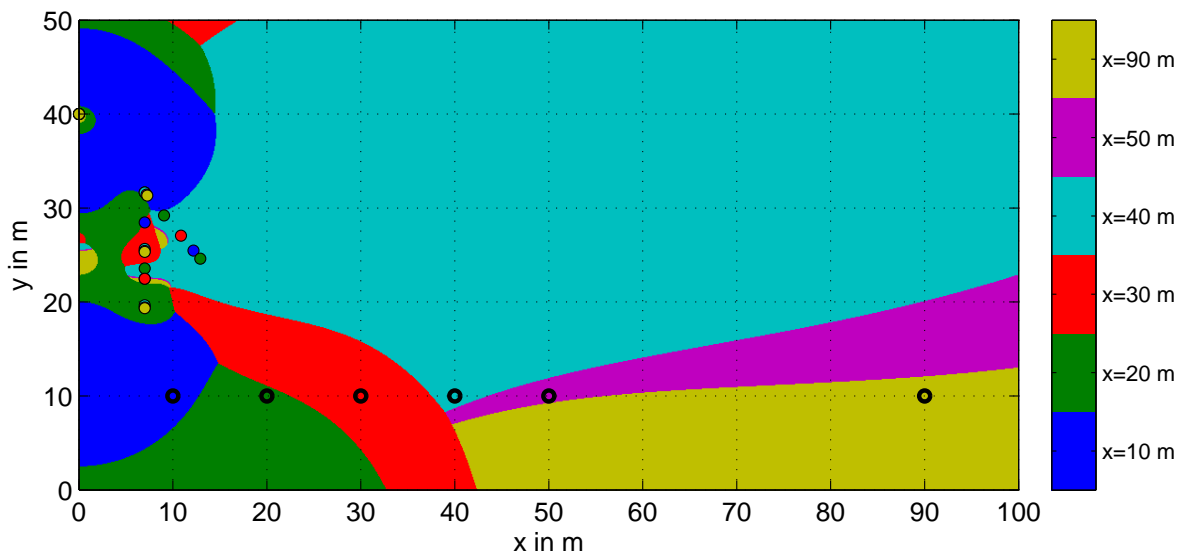


Figure 5.26: Areas, where the resulting conductor arrangements for minimum magnetic flux density in a point at height $y = 10 \text{ m}$ in a distance x from the line axis will lead to the lowest magnetic flux density compared to other resulting conductor arrangements

5.6 Optimisation of Electrical Railway Systems

5.6.1 Model and Constraints for Electrical Railway Systems

In analogy to OHLs and UGLs for electrical railways the positions of return conductor and feeder are optimised in order to minimise the magnetic flux density in the surrounding. Only return conductor and feeders are optimised, because messenger, contact wire

and the rails are given due to the traction system, and cannot be varied. In fig. 5.27 the model for the optimisation is given.

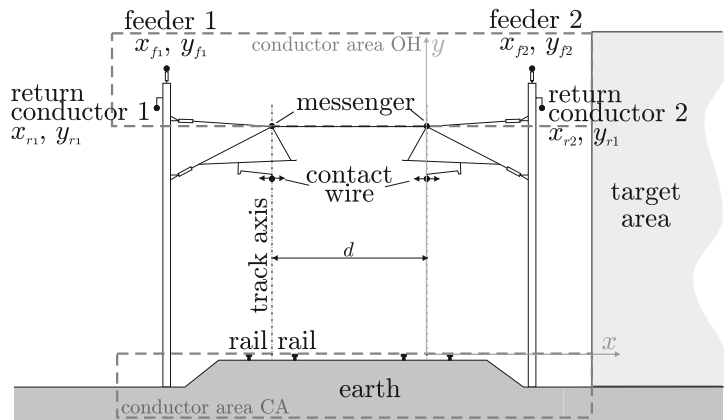


Figure 5.27: Cross section of a typical Austrian double track railway system, exemplary with a target area, where the objective function has to be minimised and the conductor areas, where feeders (coordinates x_f, y_f) and return conductors (x_r, y_r) are allowed (dashed rectangles)

The messenger (height $y = 7.1$ m) and the rails ($y = 0$ m, track gauge = 1.4 m) are assumed to be at a fixed position. As analysed in section 4.3, the horizontal position of the contact wire varies ± 0.4 m from the rail axis due to the applied zigzag while the height is fixed with $y = 5.5$ m. The traction current is chosen constant with 1000 A per track. For the calculation of the currents in the conductors the average position of the contact wire, which is at the rail axis, is sufficient, while for the calculation of the magnetic and electric field, this variation of the position should be considered. For the optimisation, the position of the contact wire is fixed at the centred position, but in an analysis afterwards, the effect of the zigzag is analysed again. For a multiple track system further the distance between the rail axes has to be assumed. For the following example a typical value of $d = 5.0$ m is chosen. The position(s) of the feeder(s) and the return conductor(s) in that model can be varied in certain areas, which will allow a practical implementation (see dashed rectangles labelled 'conductor area' in fig. 5.27). Therefore, the following congestions for positioning the conductors for an optimisation algorithm can be stated:

- allowed horizontal positions of feeder(s) and return conductor(s) are in an area $\Delta x = \pm 5$ m from rail axis (for double track systems ± 5 m from each rail axis),
- allowed vertical positions for underground cables (CA) are $y = -2 \dots 0$ m or for overhead wires (OH) $y = 7.1 \dots 10$ m.

Due to the between an underground area and an overhead area, the following four different cases are investigated (OH...overhead, CA...cable):

- case 1: return conductor and feeder overhead (OH OH)
- case 2: return conductor and feeder as cables below earth (CA CA)
- case 3: return conductor overhead, feeder as a cable (OH CA)
- case 4: return conductor as a cable, feeder overhead (CA OH)

All of these positions are technically applicable, although the feeder realised as a cable has the practical disadvantage of the more difficult connections to contact wire and messenger.

In analogy to OHLs, uninsulated lines must have a minimum distance to each other in order to prevent flash overs. The minimum distance between two conductors has to be at least a certain value a_{min} which is here chosen with 1 m. For generalisation the same minimum distance was implemented for the underground cables, although cables could be put closer together.

5.6.2 Conductor Arrangement Optimisation for Electrical Railway Systems

In this section the coordinates of feeders and return conductors for a single and a double track system are searched. The goal again is to minimise the maximum magnetic flux density, now in three different target areas, all with a height and width of 10 m, in different distances to the rail axis. The target area 1 starts at a distance of 5 m from the axis, target area 2 at 15 m and for a distant field investigation target area 3 starts at 100 m (for example see fig. 5.28).

The results of the optimisation for the single railway track are shown in tab. 5.9, results for the double track system in tab. 5.10. In order to get a value of the efficiency of the optimisation, the maximum flux densities within the target areas are compared with the value of the original configuration as shown in fig. 5.27. The results show, that the best configuration for all target areas would be the case with the feeders realised as a cable and the return conductors above earth with a reduction rate compared to the original configuration up to 37.4% for a single track and 65.6% for a double track system. But also the configuration with both conductors overhead could be optimised with a reduction rate up to 31.7% or 64.1%.

The optimisation is done for a centred contact wire, but the influence on B_{max} of the zigzag of the contact wire with the maximum horizontal deflection can be seen in the

Table 5.9: Results for the optimisation of a single railway system

	case	return c. area	feeder area	return c.		feeder		B _{max}			reduction compared to original
				x _{r1}	y _{r1}	x _{f1}	y _{f1}	center	zigzag left	zigzag right	
				m	m	m	m	μT	μT	μT	
target area 1 x=5...15m y=0...10m	-	OH	OH	-3.50	7.65	-3.20	8.75	24.21	23.38	25.21	original
	1	OH	OH	2.39	7.10	-5.00	10.00	16.53	15.85	17.45	-31.71
	2	CA	CA	-2.60	-0.07	4.05	-1.99	19.69	20.09	20.57	-18.69
	3	OH	CA	1.68	7.10	-5.00	-2.00	15.15	14.41	16.05	-37.41
	4	CA	OH	-4.89	0.00	-5.00	10.00	26.44	25.63	27.41	9.20
target area 2 x=15...25m y=0...10m	-	OH	OH	-3.50	7.65	-3.20	8.75	7.18	7.08	7.29	original
	1	OH	OH	5.00	7.81	-5.00	7.11	5.51	5.43	5.61	-23.24
	2	CA	CA	4.36	0.00	-5.00	-2.00	6.52	6.43	6.61	-9.21
	3	OH	CA	5.00	7.10	-5.00	-2.00	5.08	5.00	5.18	-29.18
	4	CA	OH	3.66	0.00	-5.00	7.10	7.53	7.44	7.62	4.87
target area 3 x=100...110m y=0...10m	-	OH	OH	-3.50	7.65	-3.20	8.75	1.03	1.02	1.03	original
	1	OH	OH	-1.00	7.10	-2.00	7.10	0.98	0.98	0.98	-4.39
	2	CA	CA	5.00	0.00	0.00	-0.70	1.04	1.04	1.05	1.69
	3	OH	CA	1.00	7.10	-1.70	0.00	0.98	0.98	0.98	-4.64
	4	CA	OH	5.00	0.00	-5.00	7.10	1.08	1.07	1.08	5.06

Table 5.10: Results for the optimisation of a double track system

	case	return c. area	feeder area	return c. 1		return c. 2		feeder 1		feeder 2		B _{max}			reduction compared to original
				x _{r1}	y _{r1}	x _{r2}	y _{r2}	x _{f1}	y _{f1}	x _{f2}	y _{f2}	center	zigzag left	zigzag right	
				m	m	m	m	m	m	m	m	μT	μT	μT	
target area 1 x=5...15m y=0...10m	-	OH	OH	-8.50	7.65	3.50	7.65	-8.20	8.75	3.20	8.75	43.89	43.86	43.89	original
	1	OH	OH	0.75	7.78	1.49	7.10	-9.97	9.95	-9.97	8.31	15.75	16.01	16.59	-64.10
	2	CA	CA	-2.31	-0.01	-7.40	-0.02	-9.96	-1.98	4.89	-2.00	24.24	24.77	25.23	-44.77
	3	OH	CA	1.00	7.10	-1.00	7.10	-10.00	-2.00	-10.00	-1.00	15.11	14.47	15.95	-65.56
	4	CA	OH	-6.85	0.00	-9.10	0.00	-10.00	10.00	-10.00	7.10	34.51	33.48	35.74	-21.36
target area 2 x=15...25m y=0...10m	-	OH	OH	-8.50	7.65	3.50	7.65	-8.20	8.75	3.20	8.75	9.68	9.55	9.82	original
	1	OH	OH	4.78	7.82	4.77	9.16	-9.80	7.67	-9.78	9.74	5.40	5.34	5.52	-44.26
	2	CA	CA	4.63	0.00	3.45	0.00	5.00	-2.00	-10.00	-2.00	8.55	8.42	8.67	-11.73
	3	OH	CA	3.50	7.10	4.52	7.10	-9.99	-0.08	-9.99	-1.20	5.11	5.03	5.20	-47.26
	4	CA	OH	-2.35	0.00	2.59	0.00	-10.00	7.10	-10.00	8.10	10.40	10.28	10.52	7.38
target area 3 x=100...110m y=0...10m	-	OH	OH	-8.50	7.65	3.50	7.65	-8.20	8.75	3.20	8.75	1.44	1.43	1.44	original
	1	OH	OH	-2.50	7.97	-1.00	7.10	-2.00	7.10	-3.00	7.10	1.30	1.30	1.31	-9.29
	2	CA	CA	5.00	0.00	-9.40	0.00	-10.00	-0.80	-8.47	-0.37	1.43	1.43	1.44	-0.15
	3	OH	CA	-1.00	7.10	1.00	7.10	-5.00	-0.70	-6.70	0.00	1.30	1.30	1.31	-9.13
	4	CA	OH	5.00	-2.00	5.00	0.00	-9.00	7.10	-10.00	7.10	1.53	1.52	1.53	6.31

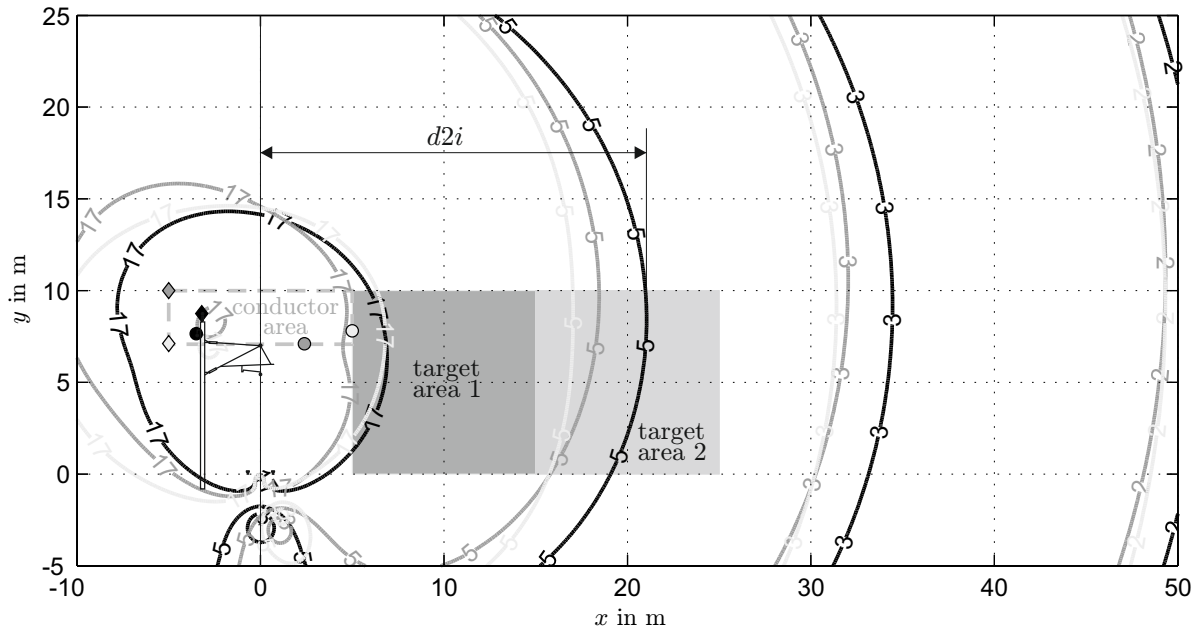


Figure 5.28: Isofluxlines in μT for a single track system for three different line configurations: black...original, gray...results for optimisation case 1-area 1, light gray...case 1-area 2; the positions of the return conductors are marked with a circle, the feeders with a diamond, $d2i$...distance to isoline

columns 'zigzag left' ($x_{\text{deflect}} = -0.4 \text{ m}$) and 'zigzag right' ($x_{\text{deflect}} = +0.4 \text{ m}$). For the target area very close to the rail axis (target area 1 and 2) the deviation of B_{max} is up to $\pm 6\%$ compared to a centred contact wire.

In fig. 5.28 several isofluxlines (17, 5, 3 and 2 μT) for the original configuration (black) as well as for the resulting conductor positions of the optimisation for case 1 (both conductors overhead) for target area 1 (gray) and 2 (light gray) are shown. The positions of the return conductors are marked with circles, the positions of the feeders with diamonds. It can be seen, that the magnetic flux density, caused by the configuration optimised for target area 2 (light gray) causes higher magnetic flux densities in target area 1 than the configuration optimised for target area 1 (gray) and vice versa. From this it follows, that the result of an optimisation for one specific target area, might not be the optimal solution for another target area. Further can be seen from fig. 5.28, that on the left side of the rail axis ($x < 0 \text{ m}$) the magnetic flux densities of the optimised systems are higher than from the original configuration (the isolines of the value 17 μT are more extended on the left side). This negative effect has to be taken into account and it is obvious, that a general solution for minimising the field in several target areas simultaneously is quite impossible.

The following can be summarised from the railway system optimisation: It is shown with the examples for a single track and a double track system, that there is a great potential

for the reduction of the magnetic and/or the electric field in the vicinity of railway systems through optimisation of the positions of both, feeder and return conductor. For the example of a double track system the reduction of the maximum magnetic flux density in a target area close to the railway system was up to 65% compared to the original configuration.

The problems in the selection and the realisation of alternative practical installations achieved from the optimisation algorithm are:

- strong dependency on the target area, so that a general solution is hardly possible
- possible need of additional towers, trenches or cable troughs due to the alternative and maybe more spacious location of the optimised conductors
- more difficult connections of feeders to messengers and contact wires in case of realisation the feeder as a cable
- possible increase of the field outside the target area, especially on the opposite side of the rail axis

For a specific reduction problem, where a given target area, optimisation function and possible areas for the position of the conductors are known, also the change of the current distribution between active and passive conductors and earth due to location-dependent geological conditions, position of equipotential bondings and earthing systems as well as additional conductors like pipelines as shown in [23] have to be considered.

6

Chapter 6

Conclusion

In chapter 1 of this thesis, the introduction and motivation of the work, as well as the previous literature are given.

In chapter 2 general aspects about exposure evaluation in sense of electric and magnetic fields of electrical power systems are discussed. The principal evaluation of electric and magnetic fields, the calculation of impedances to get the corresponding currents and further the current standards and guidelines for exposure evaluation are described.

In chapter 3 the main parameter for the evaluation of electric and magnetic fields of three-phase systems are analysed. On the base of existing conductor configurations first the allocation of the phases on given conductor positions is analysed. For a symmetrical three-phase line with only one circuit the six possible phase configurations have no effect in sense of RMS- and peak-value of a field, only the rotation of the electric or magnetic field vectors and a phase shift can be noticed. For multi circuit lines, a simultaneous exchanging of all phases of all circuits has the same effect. For a double circuit line with 36 options to allocate the phase on given conductor positions, six cases remain, which have different electric and magnetic field characteristics. A worst case scenario is evaluated from these six phase positions and it is further analysed, where each phase position has its advantages and disadvantages in sense of field exposure. The conclusion therefore is, that the phase positions have a significant influence on both, the electric and the magnetic field, and that there is no optimal phase position for all exposure cases (electric and magnetic field, near and distant areas).

Further the phase positions are analysed for a double circuit underground cable and a triple circuit underground cable systems. For the triple circuit underground line, 36 cases of positioning the phases have to be analysed.

In a next step the influence of the earth wire for OHLs is analysed. Depending on the position of the earth wire, tower configuration, phase position and the other parameters, the earth wires changes the magnetic fields in a range of up to 0.4 μT per kA compared to a line without any earth wire. The electric field strength on ground level is also influenced by an earth wire of up to ± 100 V/m for a 380 kV OHL.

From the analysis of the effect of the sag it can be concluded, that a two dimensional calculation in the middle of the span is appropriate and only small deviations (0.1 μT per kA) have to be taken into account. For evaluations near the towers the deviation is higher, and the conductor height has to be adapted to a lower level in order to get lower deviations.

For multiple circuit lines the effect of phase shifts and unbalances (different symmetrical loadings) on the magnetic flux is further analysed. The conclusion there-from is, that a phase position, which is the preferable phase position for parallel operation mode (both circuits equally loaded) might be disadvantageous, if both circuits are symmetrical but completely independent. A comfortable way to evaluate the worst case magnetic flux density of such a line is, to evaluate the RMS-values of each circuit separately and add them up afterwards. Thereby, the phase cancellation is not considered, which is the worst case. The overestimation due to this proceeding depends on the phase position, the range of possible phase shift between the circuits and on the number of entities. Even for a parallel double circuit line at least three cases have to be analysed in order to find the worst case electric field strength and magnetic flux density (both circuits in operation, and 2 cases where only one circuit is in operation). Unbalances in voltage and current within a three-phase circuit are further analysed. There it is shown, that e.g. for compensated networks, a displacement voltage of only 4% of the positive sequence system at normal operation increases the maximum electrical field strength of up to 18% compared without zero sequence component. But mainly the electric field strength in compensated networks is influenced by single phase faults, which can last between some seconds until some hours. An evaluation with symmetrical components has the advantage, that the worst case is evaluated with less steps, by determining the electric field strength for each symmetrical component of the voltage and adding them as RMS-values. The method of symmetrical components is further used to consider harmonics in three-phase systems with harmonic factors.

An implementation of exposure ratios for cardiac pacemakers on the base of actual standards and publications is achieved. For selected OHLs and railway systems the application as well as the impact on the field evaluation could be shown. It is significant, that very sensitive types of cardiac pacemakers might be interfered although the electric field strength and the magnetic flux density comply with the reference values according to ICNIRP.

In chapter 4 the exposure evaluation for electrical railway systems is discussed in detail. For the evaluation of worst case magnetic fields in the vicinity of electrical railways it could be shown, that the current distribution has a main impact on the magnetic field.

The current distribution is on one hand determined with the earth return impedances. On the other hand, current distributions from measurements found in literature and general considerations concerning the effect of booster transformers are taken into account. From that, a worst case scenario and typical magnetic flux densities are determined. The influence of the zigzag of the contact wire can be estimated with about 2.3 μT for 1000 A traction current per track, which amounts to about 3% of the flux densities with centred contact wires. For a worst case evaluation only the extreme positions (most left and right deflection) of the conductor have to be analysed.

In chapter 5 the goal is to create and implement models to optimise the conductor arrangement of overhead lines, underground cables and electrical railways. The premise is, that due to optimal positioning of the conductors, the magnetic and electric field are reduced compared to actual applied configurations. First, general aspects of mitigating electric and or magnetic fields in the vicinity of an electrical power system are formulated. For a single circuit OHL, double circuit OHL, single circuit UGL and an electric railway system models are developed with the focus to get applicable conductor applications. For these models several passages of corresponding optimisation algorithm are performed, analysing the behaviour with several objective functions, target areas and congestions. It is shown, that the optimisation leads to quite applicable configurations, but general statements for three-phase systems, like the conductors should be always in a triangle form, cannot be concluded, because the actual configuration depends very strongly on the constraints defined. Anyhow, this models can be applied to any exposure case.

A big obstacle in the practical application will be, that the conductor arrangement can be only optimised for one specific exposure situation. That means that the choice of the objective function and the congestions can be very sophisticated and has to be achieved with great care.

Bibliography

- [1] ÖVE/ÖNORM EN 50341 Freileitungen über AC 45 kV, Std. ÖVE/ÖNORM EN 50 341, Rev. 2002-09-01.
- [2] ÖVE B1 Beeinflussung von Fernmeldeanlagen durch Wechselspannungsanlagen mit Nennspannungen über 1kV, Std., 1976.
- [3] *Safety in electrical, magnetic and electromagnetic fields - Part 3-1: Protection of persons with active implants in the frequency range 0 Hz to 300 GHz*, Std. DIN VDE 0848-3-1; VDE 0848-3-1:2002-05, Rev. draft, 05 2002.
- [4] *Vornorm ÖVE/ÖNORM E8850 Elektrische, magnetische und elektromagnetische Felder im Frequenzbereich von 0 Hz bis 300 GHz - Beschränkung der Exposition von Personen*, Std. ÖVE/ÖNORM E88 850, 02 2006.
- [5] *ÖVE/ÖNORM E8007 Starkstromanlagen in Krankenhäusern und medizinisch genutzten Räumen außerhalb von Krankenhäusern*, Std. ÖVE/ÖNORM E8007, 12 2007.
- [6] A. Abart and E. Schmutzner, *MF-Calc-railway-the formula background of calculation*, 2007.
- [7] M. Aigner, “Einfluss der Stromoberschwingungen im magnetischen Feld unter Berücksichtigung aktueller Ergebnisse im Bereich von Zellmodellen,” Master’s thesis, University of Technology Graz, 2009.
- [8] M. S. H. Al Salameh and M. A. S. Hassouna, “Arranging Overhead Power Transmission Line Conductors Using Swarm Intelligence Technique to Minimize Electromagnetic Fields,” *Progress In Electromagnetics Research*, vol. 26, pp. 213–236, 2010.
- [9] M. Albano, R. Benato, and R. Turri, “Predictive analysis of environmental magnetic fields generated by multiple power lines,” in *Proc. IEEE Bologna Power Tech*, vol. 2, Jun. 23–26, 2003, p. 6pp.

- [10] P. Bauhofer, *Felder von Hochspannungs-Freileitungen*. Verband der Elektrizitätswerke Österreichs, 1994.
- [11] H. Biesenack, E. Braun, G. George, G. Hofmann, A. Schmieder, and A. Stephan, *Energieversorgung elektrischer Bahnen*, 1st ed. Teubner, 2006.
- [12] A. Canova, F. Freschi, and M. Tartaglia, “Multiobjective optimization of parallel cable layout,” *Magnetics, IEEE Transactions on*, vol. 43, no. 10, pp. 3914–3920, oct. 2007.
- [13] J. Carson, “Wave propagation in overhead wires with ground return,” *Bell System Technical Journal*, vol. 5, pp. 539–554, 1926.
- [14] S. Celozzi and F. Garzia, “Active shielding for power-frequency magnetic field reduction using genetic algorithms optimisation,” *Science, Measurement and Technology, IEE Proceedings*, vol. 151, no. 1, pp. 2–7, Jan. 2004.
- [15] W. G. C. Cigré, “Mitigation techniques of power frequency magnetic fields originated from electric power systems,” *Cigré Technical Brochure*, vol. 373, p. 166, 2009.
- [16] Cigré WG36.01, “Electric and magnetic fields produced by transmission systems—description of phenomena practical guide for calculation,” 1980.
- [17] E. Council, “Council recommendation of 12 July 1999 on the limitation of exposure of the general public to electromagnetic fields (0 Hz to 300 GHz),” *Official Journal of the European Communities*, vol. L199, pp. 59–70, 1999.
- [18] P. Cruz Romero, C. Izquierdo, and M. Burgos, “Optimum passive shields for mitigation of power lines magnetic field,” *IEEE Transactions on Power Delivery*, vol. 18, no. 4, pp. 1357–1362, Oct. 2003.
- [19] P. Cruz Romero, J. Santos, J. del Pino Lopez, A. de la Villa Jaen, and J. Ramos, “A comparative analysis of passive loop-based magnetic field mitigation of overhead lines,” *IEEE Transactions on Power Delivery*, vol. 22, no. 3, pp. 1773–1781, July 2007.
- [20] J. C. del Pino Lopez and P. Cruz Romero, “The effectiveness of compensated passive loops for mitigating underground power cable magnetic fields,” *IEEE Transactions on Power Delivery*, vol. 26, no. 2, pp. 674–683, April 2011.

- [21] W. Fricke, "Netzfrequente magnetische felder von hochspannungskabelanlagen," *Elektrizitätswirtschaft, Jg 97(1998), Heft 26*, vol. 26, pp. 39–43, 1998.
- [22] K. Friedl and E. Schmutzner, "Impact of the phase positions on the electric and magnetic field of high-voltage overhead lines," in *Electricity Distribution-Part 1, 2009. CIRED 2009. 20th International Conference and Exhibition on*. IET, 2009, pp. 1–4.
- [23] K. Friedl, E. Schmutzner, and L. Fickert, "Berechnung des magnetischen Feldes in der Umgebung von elektrischen Bahnanlagen in Abhängigkeit der Stromaufteilung auf Schienen, Rückleiter und Erdreich," *e & i Elektrotechnik und Informationstechnik*, vol. 126, no. 6, pp. 227–233, Jun. 2009. [Online]. Available: <http://dx.doi.org/10.1007/s00502-009-0646-0>
- [24] K. Friedl, "3d-berechnung magnetischer felder in hochspannungsschaltanlagen," Master's thesis, TU Wien, 2005.
- [25] K. Friedl, M. Aigner, and Ernst, "Impact of phase positions of overhead lines on electromagnetic fields," in *Proceedings on 2nd International Youth Conference on Energetics 2009*, 2009.
- [26] K. Friedl, H. Renner, E. Schmutzner, and A. Abart, "Harmonic factor evaluation for electric and magnetic fields using symmetrical components," in *Electricity Distribution-Part 1, 2011. CIRED 2011. 21th International Conference and Exhibition on*. IET, 2011, pp. 1–4.
- [27] K. Friedl, E. Schmutzner, and L. Fickert, "Effect of the new ICNIRP guidelines on exposure evaluation of electrical power systems," in *Proceedings on 3rd International Youth Conference on Energetics 2011*, 2011, pp. 1–5.
- [28] W. Hadrian, "Die magnetischen Störfelder des elektrischen Bahnbetriebes," *e & i Elektrotechnik und Informationstechnik*, vol. 123, no. 1-2, pp. 46–49, 2006.
- [29] G. Hosemann, *Elektrische Energietechnik: Band 3: Netze*, G. Hosemann, Ed. Springer, 2000.
- [30] I. Ibrahim, A. Farag, I. Said, H. Hussain, and N. Rahman, "Magnetic field reduction principles and options of primary overhead distribution lines," in *Applied Electromagnetics, 2005. APACE 2005. Asia-Pacific Conference on*, Dec. 2005, pp. 5 pp.–.

- [31] ICNIRP, “Guidelines for limiting exposure to time-varying electric, magnetic, and electromagnetic fields (up to 300 GHz),” *Health Phys*, vol. 74, no. 4, pp. 494–522, 1998.
- [32] —, “Guidance on determining compliance of exposure to pulsed and complex non-sinusoidal waveforms below 100 kHz with ICNIRP guidelines,” *Health Phys*, vol. 84, pp. 383–387, 2003.
- [33] —, “Guidelines for limiting exposure to time-varying electric and magnetic fields (1Hz to 100 kHz),” *Health Phys*, vol. 99(6), pp. 818–836, 2010.
- [34] IEC, *IEC 61000-4-8:2009 Electromagnetic compatibility (EMC) - Part 4-8: Testing and measurement techniques - Power frequency magnetic field immunity test*, Std. IEC 61 000-4-8:2009, Rev. ed2.0, 09 2009.
- [35] IEEE, *IEEEStdC95.6 Standard for Safety Levels With Respect to Human Exposure to Electromagnetic Fields, 0-3 kHz*, IEE Std. IEEE Std C95.6-2002, 2002.
- [36] K. Jokela, “Restricting exposure to pulsed and broadband magnetic fields,” *Health Phys*, vol. 79, pp. 373–388, 2000.
- [37] W. Kaune and L. Zaffanella, “Analysis of magnetic fields produced far from electric power lines,” *IEEE Transactions on Power Delivery*, vol. 7, no. 4, pp. 2082–2091, Oct 1992.
- [38] F. Kießling, P. Nefzger, and U. Kaintzyk, *Freileitungen: Planung, Berechnung, Ausführung;[nach EN 50341]; mit 163 Tabellen*, 5th ed. Springer, 2001.
- [39] H. Koch and H. Schüppler, “Einfluß des Schienenwiderstands auf elektrische Ströme im Gleisnetz,” *Signal und Schiene*, vol. 2/3/4, pp. 56–57,100–102,143–146, 1988.
- [40] M. Lehmann and H. Neumann, “Netzberechnung mit knotenspannungsanalyse unter einbeziehung der magnetischen kopplung,” *eb Elektrische Bahnen*, vol. 8-9, pp. 416–420, 2008.
- [41] M. Lörtscher and E. Lörtscher, “Niederfrequente elektromagnetische felder in führerständen von triebfahrzeugen der sbb,” *eb Elektrische Bahnen*, vol. 8-9, pp. 354–368, 2004.
- [42] G. Lucca and M. Moro, “Environmental 50hz magnetic field produced by a railway line equipped with autotransformers,” in *Electromagnetic Compatibility - EMC Europe, 2008 International Symposium on*, sept. 2008, pp. 1 –6.

- [43] G. Lucca, M. Moro, A. Pagani, and L. Zucchelli, "Measurement of magnetic field produced by the 25kv-50hz italian high speed railway line," in *Power Electronics, Electrical Drives, Automation and Motion, 2006. SPEEDAM 2006. International Symposium on*, 23-26 2006, pp. 1101 –1105.
- [44] A. Mamishev, R. Nevels, and B. Russell, "Effects of conductor sag on spatial distribution of power line magnetic field," *IEEE Transactions on Power Delivery*, vol. 11, no. 3, pp. 1571 –1576, jul 1996.
- [45] A. Mariscotti, "Distribution of the traction return current in ac and dc electric railway systems," *IEEE Transactions on Power Delivery*, vol. 18, no. 4, pp. 1422–1432, 2003.
- [46] A. Mariscotti and P. Pozzobon, "Measurement of the internal impedance of traction rails at 50 hz," *Proceedings of the 16th IEEE Technology Conference, 1999. IMTC/99*, vol. 49, no. 2, pp. 294–299, 2000.
- [47] —, "Low-frequency magnetic field in dc railway substations," *IEEE Transactions on Vehicular Technology*, vol. 53, no. 1, pp. 192–198, 2004.
- [48] —, "Resistance and internal inductance of traction rails at power frequency: a survey," *IEEE Transactions on Vehicular Technology*, vol. 53, no. 4, pp. 1069–1075, 2004.
- [49] A. Mariscotti, P. Pozzobon, and M. Vanti, "Simplified modeling of 2 nbsp; times; nbsp; 25-kv at railway system for the solution of low frequency and large-scale problems," *IEEE Transactions on Power Delivery*, vol. 22, no. 1, pp. 296 –301, jan. 2007.
- [50] K. G. Markwardt, *Power Supply for Electric Railways (russian)*. Moskovskiiinstitut inzhenerov zheleznodorozhnogo transporta, 1982.
- [51] *Help of Matlab - The Language of Technical Computing*, R2010a ed., The Math-Works.
- [52] G. Mazzanti, "The role played by current phase shift on magnetic field established by ac double-circuit overhead transmission lines-part i: static analysis," *IEEE Transactions on Power Delivery*, vol. 21, no. 2, pp. 939–948, Apr. 2006.
- [53] —, "The role played by current phase shift on magnetic field established by double-circuit overhead transmission lines-part ii: dynamic analysis," *IEEE Transactions on Power Delivery*, vol. 21, no. 2, pp. 949–958, Apr. 2006.

- [54] C. Obkircher, “Ausbaugrenzen gelöscht betriebener Netze,” Ph.D. dissertation, Graz University of Technology, 2008.
- [55] D. Oeding and B. R. Oswald, *Elektrische Kraftwerke und Netze*, 6th ed. Springer, 2004.
- [56] R. Oswald, “Vergleichende Studie zu Stromübertragungstechniken im Höchstspannungsnetz,” ForWind, Zentrum für Windenergieforschung, Tech. Rep., 2005.
- [57] F. Pollaczek, “Über das Feld einer unendlich langen wechselstromdurchflossenen Einfachleitung,” *Elektr. Nachrichten-Technik*, vol. 3, no. 9, pp. 339–359, 1926.
- [58] N. Örländer, S. Berlinjn, and K. A. Halsan, “Design and installation of a new 420kV tower type for minimal magnetic field,” in *International colloquium on Power Frequency Electromagnetic Fields ELF EMF*, 2009, p. Paper 36.
- [59] E. Salinas, “Standard, new and future trends on mitigation techniques for elf magnetic,” in *2nd International Conference on EMF-ELF, Paris, March 24th & 25th, 2011*, Cigre, Ed., 2011, pp. D–0–05.
- [60] E. Schmautzer, K. Friedl, and M. Aigner, “Quick and efficient method for low-frequency emf evaluation of electric power system considering multiple sources with different frequencies and harmonics,” in *Proc. 20th International Conference and Exhibition on Electricity Distribution*, Jun. 8–11, 2009, pp. 1–4.
- [61] E. Schmautzer, J. Silny, K. Friedl, L. Fickert, M. Aigner, A. Gaun, G. Rechberger, and A. Abart, *Elektromagnetische Felder im Bereich elektrifizierter Bahnanlagen und ihre gesundheitlichen Risiken*. Verlag der Technischen Universität Graz, 2011.
- [62] Österreichisches Elektrotechnisches Komitees - OEK, “Fachinformation: Personen mit aktiven Implantaten in elektrischen, magnetischen und elektromagnetischen Feldern,” 04 2009.
- [63] D. Tsanakas, G. Filippopoulos, J. Voyazakis, and G. Kouvarakis, “Compact and optimum phase conductor arrangement for the reduction of electric and magnetic fields,” in *CIGRE Report Session 2000*, vol. 36, no. 103. cigrè, 2000.
- [64] *ÖVE-EN 1 Teil 3 (§ 41) Errichtung von Starkstromanlagen mit Nennspannungen bis 1000 V und \approx 500 V, Beschaffenheit, Bemessung und Verlegung von Leitungen und Kabeln, Bemessung von Leitungen und Kabeln in mechanischer und elektrischer Hinsicht, Überstromschutz*, ÖVE Std., 1995.

- [65] Y.-J. Wang and J.-H. Wang, “Modeling of frequency-dependent impedance of the third rail used in traction power systems,” *IEEE Transactions on Power Delivery*, vol. 15, no. 2, pp. 750–755, apr 2000.
- [66] G. Zimmert, “Auswertungen der Messungen zu den Impedanzen und Rückstromverhältnissen der Strecke Magdeburg-Marienborn in der Zeit vom 26.04. ...12.05.1993,” Deutsche Reichsbahn, Zentralstelle Elektrotechnik, Tech. Rep., 1993.
- [67] A. Zynovchenko, *Ausbreitung von Stromüberschwingungen und Resonanzerscheinungen im Fahrleitungsnetz*. Cuvillier Verlag, 10 2007.
- [68] A. Zynovchenko, J. Xie, S. J. Ulm, and F. Klier, “Impedances of contact lines and propagation of current harmonics,” *eb Elektrische Bahnen*, vol. 5, pp. 222–227, 2006.